AN ABSTRACT OF THE THESIS OF

JOHN TICHAUER KIWI (Name of student) for the DOCTOR OF PHILOSOPHY (Degree)

in CHEMISTRY (Major) presented on June 30, 1971 (Date)

Title: STRUCTURE AND RADIOLYSIS OF CONCENTRATED NITRATE SOLUTIONS

Redacted for Privacy

Abstract approved: Dr. Malcolm Daniels

Studies of the structure of the concentrated nitrate solutions have been carried out to determine the hydration and ion complex behaviour of $LiNO_3$, KNO_3, $NaNO_3$, $CsNO_3$, $Ca(NO_3)_2$, $(CH_3)_4NNO_3$ and NH_4NO_3. Near infrared absorption spectroscopy has been carried out over a wide concentration range for each of these solutes. Proton nuclear magnetic resonances have been measured over a range of temperatures for different concentrations of each solute. The hydration values obtained for a given concentration of a specific salt do not generally agree when determined by these two different methods.

Generally the values for the hydration parameter obtained by near infuared are smaller than the values obtained by nuclear magnetic resonance for the same molarity of nitrate. Hydration values for $LiNO_3$ solutions vary from a maximum of 2.38 for a 1M $LiNO_3$ solution to 1.11 for a 8.78 solution when near infrared spectroscopy

is used. But when nuclear magnetic resononce is ued the hydration parameters vary between 4. 9 for a 1M $LiNO_3$ solution to a value of 1. 1 for a 8. 78 M$LiNO_3$ solution. These observations are summarized in the following table for the remaining nitrates studied.

Molarity range of Nitrate	Hydration (near-infrared)	Hydration (nuclear magnetic resonance)
$NaNO_3$ (0. 5M-7. 85M)	4. 12 - 2. 25	6. 4 - 1. 8
KNO_3 (0. 5M-2. 98M)	6. 02 - 2. 92	7. 7 - 1. 4
$CsNO_3$ (0. 56M-1. 12M)	3. 90 - 3. 58	1. 7 - 2. 1
$Ca(NO_3)_2$ (1. 0M-11. 0M)	2. 55 - 1. 14	7. 8 - 2. 5
$(CH_3)_4NNO_3$ (1. 0M-3. 89M)	3. 15 - 0. 91	6. 4 - 2. 0

An assignment for the cationic and anionic hydration is reported, assuming that only the NO_3^- group hydrates in the $(CH_3)_4NNO_3$ salt. Ultraviolet spectral studies of these salts have been carried out and a two band resolution has been attempted in the 300 mμ band, assigning one band to the hydrated NO_3^- ion and the other to an cation-anion ion-pair with specific optical properties. Added salt studies on $LiNO_3$ and $Ca(NO_3)_2$ solutions reveal and ion-pairing effect when high concentration of cation is added and in the case of $Ca(NO_3)_2$ an association constant has been evaluated. A modified Job type of study has been carried out on 5 M nitrate solutions and an association

constant for the solutions has been obtained. Solvent studies have been undertaken to study the variation of the ultraviolet spectra of 10^{-1} M nitrate solutions as a function of dielectric constant and dipolar moment of the solvent.

Concentrated solutions of lithium, potassium, sodium, caesium and calcium nitrate have been irradiated in a Co^{60} γ source. The values of $G(NO_2^-)$, $G(H_2O_2)$, $G(O_2)$ and $G(H_2)$ are reported as a function of concentration. The gas values are tentative in nature due to the difficulties experienced in the experiments. In spite of this fact an interpretation of the products of radiolysis has been carried out based on the electronic fractionation model for the absorption of energy.

Structure and Radiolysis of Concentrated Nitrate Solutions

by

John Tichauer Kiwi

A THESIS

submitted to

Oregon State University

in partial fulfillment of
the requirements for the
degree of

Doctor of Philosophy

June 1972

APPROVED:

Redacted for Privacy

Associate Professor of Chemistry
in charge of major

Redacted for Privacy

Chairman of Department of Chemistry

Redacted for Privacy

Dean of the Graduate School

Date thesis is presented June 30, 1971

Typed by Opal Grossnicklaus for John Tichauer Kiwi

Dedication

To my mother and father

ACKNOWLEDGMENTS

The author wishes to express appreciation to:

Dr. Malcolm Daniels for his guidance throughout the course of this work.

The Fullbright Commission for the travel grant that made possible my trip to the United States. The United States Atomic Energy Commission for the three year research fellowship that financed my work in the first stages.

My family who supported me fully during the last year towards my doctorate.

My friends, colleagues and professors whose advice helped me in the completion of this work.

TABLE OF CONTENTS

I. INTRODUCTION 1

II. INFRARED STUDIES IN THE HYDRATION OF NITRATES 6

Introduction 6
Experimental Section 12
Description of a Typical Difference Spectra 13
Theoretical Considerations for the N.I.R. Method 15
Calculation and Results of the Hydration Spectral Studies 17
$LiNO_3$ Solutions 17
$NaNO_3$ Solutions 20
KNO_3 Solutions 22
$CsNO_3$ Solutions 24
$Ca(NO_3)_2$ Solutions 26
$(CH_3)_4NNO_3$ Solutions 26
NH_4NO_3 Solutions 30
General Discussion and Tentative Assignment of Cationic and Anionic Hydration for: 30
$LiNO_3$ Solutions 35
$NaNO_3$ Solutions 35
KNO_3 Solutions 35
$CsNO_3$ Solutions 35
$Ca(NO_3)_2$ Solutions 35
$(CH_3)_4NNO_3$ Solutions 70
NH_4NO_3 Solutions 73
Discussion of Results of Separated Cationic and Anionic Hydration Bands 75

III. NUCLEAR MAGNETIC RESONANCE STUDIES OF CONCENTRATED NITRATE SOLUTIONS 85

Introduction 85
Experimental Part 87
Correction Factor for the Observed Shifts 96
Intrinsec Magnetic Susceptibility Measurements 100
Hydration Results for: 109
$LiNO_3$ Solutions 114
$NaNO_3$ Solutions 118
KNO_3 Solutions 120

$CsNO_3$ Solutions 121
$Ca(NO_3)_2$ Solutions 123
$(CH_3)_4NNO_3$ Solutions 125
Previous Work on Nitrate Solutions 126
Discussion 130

IV. SPECTRAL STUDIES OF NITRATE SOLUTIONS 135

Pure Salt Spectra 135
Introduction 135
Experimental Part 139
Results and Discussion for the Pure Spectra of:
$LiNO_3$ Solutions 141
$NaNO_3$ Solutions 151
KNO_3 Solutions 154
$CsNO_3$ Solutions 154
$Ca(NO_3)_2$ Solutions 156
$(CH_3)_4NNO_3$ Solutions 159
Tentative Assignment of Nitrate Resolved Spectra for the Nitrate Solution 161
Added Salt Studies 172
Study of Nitrate Solutions Using the Method of Continuous Variations 190
Study of Nitrate Solutions by Variation of the Solvent 197
Spectral Studies of Nitrates in Mixed Solvents 203

V. RADIOLYSIS OF CONCENTRATED NITRATE SOLUTIONS 211

Introduction 211
Experimental Part 214
Dosimetry 214
Determination of Nitrite Yields 218
Determination of Hydrogen Peroxide Yields 219
Determination of Oxygen and Hydrogen Yields 221
Results 228
Discussion 246

BIBLIOGRAPHY 251

LIST OF FIGURES

Figure		Page
2-1	Ionic hydration model.	10
2-2	Resolution of a difference absorbance spectra.	14
2-3	Difference absorbance spectra $LiNO_3$.	18
2-4	Difference absorbance spectra $NaNO_3$.	21
2-5	Difference absorbance spectra KNO_3.	23
2-6a	Difference absorbance spectra of $CsNO_3$.	25
2-6b	Difference absorbance spectra of $Ca(NO_3)_2$.	28
2-7	Difference absorbance spectra of $(CH_3)_4NNO_3$.	29
2-8	Difference absorbance spectra of NH_4NO_3.	31
2-9	Hydration number of the salts vs. concentration.	34
2-10	Hydration number of the cation vs. concentration.	38
2-11a, b, c	McCabe and Fisher hydration spectra of sodium salts.	41
2-12	McCabe and Fisher hydration spectra of chlorides.	41
2-13 a, b	Hydration difference spectra cations.	44
2-14	Hydration spectra 3 M KCl.	45
2-15	Hydration spectra 3 M NaCl.	45
2-16	$LiNO_3$ Hydration spectra.	47
2-17	$LiNO_3$ Hydration spectra.	48
2-18	$NaNO_3$ Hydration spectra.	49
2-19	$NaNO_3$ Hydration spectra.	50

Figure		Page
2-20	KNO_3 Hydration spectra.	51
2-21	$CsNO_3$ Hydration spectra.	52
2-22	$Ca(NO_3)_2$ Hydration spectra.	53
2-23	$Ca(NO_3)_2$ Hydration spectra.	54
2-24	$(CH_3)_4NNO_3$ Hydration spectra.	55
2-25	NH_4NO_3 Hydration spectra.	56
2-26	3 M Hydration spectra of nitrates.	76
2-27	3 M Hydration spectra of nitrates.	77
2-28	Cation hydrate absorbance for KNO_3 solutions.	81
3-1	Diagram of the Varian probe assembly.	90
3-2	Thermostat attachment Varian probe assembly.	90
3-3	Coaxial tubing system.	91
3-4a,b	1 M $NaNO_3$ 10° C signals.	93
3-5	Sample tube containing a cylindrical and spherical reference tube.	98
3-6	Cyclohexane water spectrogram 40° C.	102
3-7	Signal shift for water in the 10-70° C range.	115
3-8	Hindman shifts for nitrates as a function of concentration.	128
3-9	Plot of shifts vs. molarity at 20° C for $NaNO_3$, $LiNO_3$, and $Ca(NO_3)_2$ solutions.	129
4-1	Pure salt spectra $LiNO_3$ of solutions.	142
4-2	ε and f vs. concentration plot in $LiNO_3$ solutions.	146

Figure		Page
4-3	λ_{max} vs. concentration for $LiNO_3$ solutions.	147
4-4	Determination of λ_{max} in $LiNO_3$ 7 M solution.	149
4-5	Separation and symmetry of bands in the 300 mμ transition.	150
4-6	Pure salt spectra of $NaNO_3$ solutions.	152
4-7	Pure salt spectra of KNO_3 solutions.	156
4-8	Pure salt spectra of $CsNO_3$ solutions.	157
4-9	Pure salt spectra $Ca(NO_3)_2$ solutions.	158
4-10	Pure salt spectra $(CH_3)_4NNO_3$ solutions.	160
4-11	Tentative resolution of the 300 mμ band.	164
4-12	Resolved 300 mμ band in 10^{-2} M $LiNO_3$ solution.	166
4-13	Added salt spectra in $LiNO_3$ 10^{-1} M solution.	175
4-14	Added salt spectra in $NaNO_3$ 10^{-1} M solution.	177
4-15	Added salt spectra in $NaNO_3$ solution.	178
4-16	Added salt spectra in KNO_3 solution.	180
4-17	Added salt spectra in KNO_3 solution.	181
4-18	Added salt spectra in $Ca(NO_3)_2$ solution.	182
4-19	Added salt spectra in $Ca(NO_3)_2$ solution.	183
4-20	Association constant determination in $Ca(NO_3)_2$ at 32000 cm^{-1}. Low molarities of $CaCl_2$ added.	186
4-21	Association constant determination in $Ca(NO_3)_2$ at 34500 cm^{-1}. Low molarities of $CaCl_2$ added.	187
4-22	Association constant determination in $Ca(NO_3)_2$ at 32000 cm^{-1}. High molarities of $CaCl_2$ added.	188

Figure		Page
4-23	Association constant determination in $Ca(NO_3)_2$ at 34500 cm^{-1}. High molarities $CaCl_2$ added.	189
4-24	Job plot of $LiNO_3$ solution at 290 mμ.	193
4-25	Inverse Job plot for $LiNO_3$, $NaNO_3$, KNO_3, and $Ca(NO_3)_2$ solutions.	194
4-26	Spectra of 10^{-1} M $LiNO_3$ in several solvents.	199
4-27	Spectra of 10^{-1} M $LiNO_3$ in several solvents.	200
4-28	λ_{max} vs. dipole moment of solvent for 10^{-1} M $LiNO_3$ in 1.00 [cm] cell.	202
4-29	λ_{max} vs. dielectric constant of solvents for 10^{-1} M $LiNO_3$ in 1.00 [cm] cell.	204
4-30	$LiNO_3$ 10^{-1} M spectra in H_2O - dioxane solvent system.	206
4-31	$NaNO_3$ 10^{-1} M spectra in H_2O - DMF solvent system.	210
5-1	Electronic fractionation model for $NaNO_3$.	212
5-2a,b	Irradiation cells for Co^{60} γ source.	215
5-3	Dosimetry Co^{60} γ source.	217
5-4	Calibration curve for H_2O_2 determination in KNO_3 solutions.	220
5-5	Injector device for degassed solutions.	222
5-6a,b	Gas collection system in vacuum line.	223
5-7	Typical mass spectrometric scan.	227
5-8	Products of the radiolysis of $LiNO_3$ solutions.	234
5-9	Products of the radiolysis of $NaNO_3$ solution.	235
5-10	Products of the radiolysis of KNO_3 solutions.	236

Figure		Page
5-11	Products of the radiolysis of $CsNO_3$ solutions.	237
5-12	Products of the radiolysis of $Ca(NO_3)_2$ solutions.	238
5-13	Electronic fractionation model of $LiNO_3$ solutions.	243
5-14	Electronic fractionation model for KNO_3 solutions.	244
5-15	Electronic fractionation model for $Ca(NO_3)_2$ solutions.	245

LIST OF TABLES

Table		Page
2-1	Partial motal volumes and intrinsec volume of ions.	8
2-2	Near infrared water absorption spectrum.	13
2-3	Hydration values for $LiNO_3$ solutions.	20
2-4	Hydration values for $NaNO_3$ solutions.	22
2-5	Hydration values for KNO_3 solutions.	24
2-6	Hydration values for $CsNO_3$ solutions.	24
2-7	Hydration values for $Ca(NO_3)_2$ solutions.	26
2-8	Density of $(CH_3)_4NNO_3$ solutions.	27
2-9	Hydration values for $(CH_3)_4NNO_3$ solutions.	27
2-10	Hydration values for NH_4NO_3 solutions.	30
2-11	Hydration parameters for NH_4NO_3, $NaNO_3$, $Ca(NO_3)_2$, $LiNO_3$ solutions.	32
2-12	Hydration of $LiNO_3$, $NaNO_3$, KNO_3, $CsNO_3$, $(CH_3)_4NNO_3$ and NH_4NO_3 at infinite dilution.	35
2-13a	Individual hydration values of ions.	36
2-13b	Extrapolated hydration values of ions.	37
2-14	Hydration difference spectra 3 M chloride solutions (KCl-CsCl).	43
2-15	Hydration difference spectra 3 M chloride solutions (NaCl-RbCl).	43
2-16	$LiNO_3$ 1.0 M hydration spectrum.	57
2-17	$LiNO_3$ 2.0 M hydration spectrum.	57

Table		Page
2-18a	$LiNO_3$ 3.0 M hydration spectrum.	58
2-18b	$LiNO_3$ 4.0 M hydration spectrum.	58
2-19	$LiNO_3$ 5.0 M hydration spectrum.	59
2-20	$LiNO_3$ 7.0 M hydration spectrum.	59
2-21	$LiNO_3$ 8.78 M hydration spectrum.	59
2-22	$NaNO_3$ 0.5 M hydration spectrum.	60
2-23	$NaNO_3$ 1.0 M hydration spectrum.	60
2-24	$NaNO_3$ 2.5 M hydration spectrum.	61
2-25	$NaNO_3$ 3.25 M hydration spectrum.	61
2-26	$NaNO_3$ 4.0 M hydration spectrum.	62
2-27	$NaNO_3$ 6.0 M hydration spectrum.	62
2-28	7.85 M $NaNO_3$ hydration spectrum.	63
2-29	0.5 M KNO_3 hydration spectrum.	64
2-30	1.0 M KNO_3 hydration spectrum.	64
2-31	2.0 M KNO_3 hydration spectrum.	65
2-33	2.98 M KNO_3 hydration spectrum.	65
2-34	0.56 M $CsNO_3$ hydration spectrum.	66
2-35	0.8 M $CsNO_3$ hydration spectrum.	66
2-36	1.12 M $CsNO_3$ hydration spectrum.	66
2-37	0.5 M $Ca(NO_3)_2$ hydration spectrum.	67
2-38	1.5 M $Ca(NO_3)_2$ hydration spectrum.	67
2-39	2.0 M $Ca(NO_3)_2$ hydration spectrum.	68

Table		Page
2-40	2.5 M $Ca(NO_3)_2$ hydration spectrum.	68
2-41	3.5 M $Ca(NO_3)_2$ hydration spectrum.	69
2-42	4.22 M $Ca(NO_3)_2$ hydration spectrum.	69
2-43	5.50 M $Ca(NO_3)_2$ hydration spectrum.	69
2-44	0.50 M $(CH_3)_4NNO_3$ hydration spectrum.	70
2-45	1.0 M $(CH_3)_4$ NNO_3 hydration spectrum.	70
2-46	2.0 M $(CH_3)_4NNO_3$ hydration spectrum.	71
2-47	3.0 M $(CH_3)_4NNO_3$ hydration spectrum.	71
2-48	3.89 M $(CH_3)_4NNO_3$ hydration spectrum.	72
2-49	0.5 M NH_4NO_3 hydration spectrum.	73
2-50	2.0 M NH_4NO_3 hydration spectrum.	73
2-51	4.0 M NH_4NO_3 hydration spectrum.	73
2-52	6.0 M NH_4NO_3 hydration spectrum.	74
2-53	8.0 M NH_4NO_3 hydration spectrum.	74
2-54	10.0 M NH_4NO_3 hydration spectrum.	74
2-55	Difference hydration spectra of 3 M $NaNO_3$-$LiNO_3$ solution.	78
2-56	Difference hydration spectra of 3 M KNO_3-$Ca(NO_3)_2$.	78
2-57	Difference hydration spectra of 4 M nitrate solutions.	79
3-1	Magnetic susceptibility of cyclohexane.	103
3-2	Magnetic susceptibility of $LiNO_3$ solutions.	105
3-3	Magnetic susceptibilities $NaNO_3$ solutions.	106

Table		Page
3-4	Magnetic susceptibilities KNO_3 solutions.	106
3-5	Magnetic susceptibilities $CsNO_3$ solutions.	107
3-6	Magnetic susceptibilities $Ca(NO_3)_2$ solutions.	107
3-7	Magnetic susceptibilities $(CH_3)_4NNO_3$ solutions.	108
3-8	Magnetic susceptibilities reported by Klemm (1941) and found in this work.	109
3-9	Shifts of peak signals of water in the 10° -70° C range.	113
3-10	Shifts as a function of temperature (10-70° C) for $LiNO_3$ solutions.	117
3-11	Shifts as a function of temperature (10-70° C) for $LiNO_3$ solutions.	117
3-12	Hydration values for $LiNO_3$ solutions.	118
3-13	Shifts as a function of temperature (10-70°C) for $NaNO_3$ solutions.	119
3-14	Shifts as a function of temperature (10-70°C) for $NaNO_3$ solutions.	119
3-15	Hydration values for $NaNO_3$ solutions.	120
3-16	Shifts as a function of temperature (10-70° C) for KNO_3.	121
3-17	Hydration values for KNO_3 solutions.	122
3-18	Shifts as a function of temperature (10-70° C) for $CsNO_3$ solutions.	122
3-19	Hydration values for $CsNO_3$ solutions.	123
3-20	Shifts as a function of temperature (10-70° C) for $Ca(NO_3)_2$ solutions.	124

Table		Page
3-21	Shifts as a function of temperature (10-70° C) for $Ca(NO_3)_2$ solutions.	125
3-22	Hydration values for $Ca(NO_3)_2$ solutions.	125
3-23	Shifts as a function of temperature (10-70° C) for $(CH_3)_4NNO_3$ solutions.	125
3-24	Hydration values for $(CH_3)_4NNO_3$ solutions.	126
3-25	Tentative assignment of anionic and cationic hydration by means of $(CH_3)_4NNO_3$.	133
4-1	Kangro's association values for $LiNO_3$ solutions.	143
4-2	Spectral data for $LiNO_3$ solutions.	144
4-3	Spectral data for $NaNO_3$ solutions.	153
4-4	Kangro's association values for $NaNO_3$ solutions.	153
4-5	Spectral data for KNO_3 solutions.	154
4-6	Spectral data for $CsNO_3$ solutions.	155
4-7	Spectral data for $Ca(NO_3)_2$ solutions.	159
4-8	Spectral data for $(CH_3)_4NNO_3$ solutions.	159
4-9	Spectral resolution of the $LiNO_3$ 300 mμ band.	168
4-10	Spectral resolution of the $NaNO_3$ 300 mμ band.	168
4-11	Spectral resolution of KNO_3 300 mμ band.	169
4-12	Spectral resolution of the $CsNO_3$ 300 mμ band.	169
4-13	Spectral resolution of $Ca(NO_3)_2$ 300 mμ band.	170
4-14	Spectral resolution of $(CH_3)_4NNO_3$ 300 mμ band.	170
4-15	Boston and Smith (1961) parameters for molten nitrates of the first group.	172

Table		Page
4-16	Data for the association constant for $LiNO_3$ by Job's method.	192
4-17	Data for the association constant for $NaNO_3$ by Job's method.	195
4-18	Data for the association constant for KNO_3 by Job's method.	195
4-19	Data for the association constant for $Ca(NO_3)_2$ by Job's method.	196
4-20	Spectral data for 10^{-1} M nitrate in different solvents.	198
4-21	Dielectric constant of the water-dioxane solutions.	205
4-22	Spectral data of the $LiNO_3$-water-dioxane system.	205
4-23	Spectral data of the $NaNO_3$-water-dioxane system.	207
4-24	Spectral data of the KNO_3-water-dioxane system.	208
4-25	Spectral data for the $Ca(NO_3)_2 \cdot 4H_2O$ dioxane-water system.	208
4-26	Spectral data for $(CH_3)_4NNO_3$ in water-dioxane mixture.	209
4-27	KNO_3-DMF-H_2O system.	209
5-1	Dose rate Co^{60} γ source (January 18, 1971)	216
5-2	Experimental data for the radiolysis of $LiNO_3$ solutions.	229
5-3	Experimental data for the radiolysis of $NaNO_3$ solutions.	230
5-4	Experimental data for the radiolysis of KNO_3 solutions.	230
5-5	Experimental data for the radiolysis of $CsNO_3$ solutions.	231

Table		Page
5-6	Experimental data for the radiolysis of $Ca(NO_3)_2$ solutions.	232
5-7	Calculated data for the energy fractionation model of $LiNO_3$ solutions.	240
5-8	Calculated data for the energy fractionation model of KNO_3 solutions.	241
5-9	Calculated data for the energy fractionation model of $Ca(NO_3)_2$ solutions.	242
5-10	Values of $G(NO_2^-)$ and $G(O_2)$ for the "direct" and "indirect" effect in nitrate solutions.	248
5-11	Values for the "direct" and "indirect" effect for H_2O_2 formation.	249

STRUCTURE AND RADIOLYSIS OF NITRATE SOLUTIONS

I INTRODUCTION

Interest in the chemical behaviour of aqueous nitrate solutions undergoing radiolysis derives both from the use of such solutions in handling high radioactive materials and from inconsistent results of published studies on the system. Plutonium is produced in thermal power reactors as a by-product and is recovered in the fuel reprocessing operations. Nitric acid and nitrate salts are involved in the handling, storing and shipping of plutonium. The radiolysis of nitrates is closely related to what happens in plutonium nitrate solution Pu being the source of radiation. Nitrite is produced in radiolysis and enters into oxidation-reduction reactions with Pu. Hydrogen peroxide, also a radiolysis product, is an oxidizing and reducing agent with active cations like thorium and uranium.

The status of the present knowledge on the radiolysis of nitrate solutions can be summarized as follows: The major products of radiolysis are nitrite and oxygen. There is some agreement on the mechanism of nitrite production at low concentration but the overall mechanism is not well understood.

At higher nitrate ion concentration there appears to be mechanisms other than those of the indirect radiolysis involving some sort of direct absorption of energy from the radiation beam by the nitrate

ion. There is not general agreement on either the mechanism for this direct effect or on the relative contribution of this effect to the total radiolysis reaction.

Data from various investigators are often in disagreement and have led to differing conclusions, e.g., that large yields of chemically activated excited water are produced by radiolysis as postulated by Sworski (1965). Kabachki (1958) suggested that the increase of nitrite yield with nitrate concentration occurs in a way that it may be due to a reaction of H atoms with nitrate ions. Later Daniels and Wigg (1967) ascribed this effect mainly to an $e^-_{(aq)}$ type of interaction. What is clear though from data published so far is that H_2, O_2, H_2O_2, NO_2^- are the only significant products of radiolysis.

To clarify the radiolysis of nitrate solutions, it is necessary to measure the yield of all the products of radiolysis: $G(H_2)$, $G(O_2)$, $G(NO_2^-)$, and $G(H_2O_2)$ since these G values are needed in neutral solutions for $LiNO_3$, $NaNO_3$, KNO_3, $CsNO_3$, $Ca(NO_3)_2$, in the whole concentration range.

The nature of the precursors of the $G(H_2)$ yield is an unresolved problem in water radiolysis and our measurements combined with $G(NO_2^-)$ yield should help clarify the origin of the primary species involved. $G(H_2O_2)$ and $G(O_2)$ values at higher concentrations of the different nitrates employed will serve as a basis to look for an explanation of these yields using various theoretical approaches such as

a) electronic fractionation of incident energy, b) mass absorption coefficient of the species involved, and c) using the (H_2O^*) postulated in radiolysis of H_2O when trying to explain the G values observed in radiolysis of nitrates.

Another aspect that has become of particular importance is the clarification of the association of species, hydration of ions and the intimate physical structure of the ionic solutions of nitrates, specially at concentrations above 10^{-2} M. Also, as we do not know the exact nature of the species the knowledge of the activity coefficients of the aggregates formed is not possible at this stage. In our studies to determine hydration of the nitrate solutions we may assume that the water in the first hydration shell is immobilized near nitrate ion and is involved with this ion in the low lying n-π^* electronic transition observed. We seek to interpret the u.v. spectra as a function of hydration as the concentration of nitrate and of the cation is varied.

Since an uncertainty exists in the ionic radii of ions in solutions, the assignment of coordinated water molecules to cation and anion as adjacent molecules to these species becomes arbitrary. The determination of an hydration number which is operationally useful and that is suitable to our purposes becomes important to interpret the results of nitrate radiolysis. We will employ methods that account for hydration and do not depend on an assigned value for the radii of ions in solutions.

Recent work on hydration of electrolytes is based mainly on: (A) X-ray diffraction which gives water-to-ion distances and coordination modes of ions. (B) Infrared and Raman spectra which report vibrational changes of water due to the presence of an electrolyte. (C) Nuclear magnetic resonance (N.M.R.) which gives an insight into changes in the electron distribution around the nuclei of the solvent molecules when electrolytes are present and on the average exchange rate of the water molecules into the coordination shell. (D) Partial vapor pressure of electrolyte solutions, and (E) Values reported from transference data of concentrated solutions. Our approach will be to carry out ultraviolet infrared, and N.M.R experiments and compare the results obtained with the values reported in the literature by transference and vapor pressure for association and hydration of cation and anion in nitrate solutions.

Despite the general accepted theory that ions are hydrated in solution, strong disagreement between authors arises as soon as quantitative treatments of hydration are attempted. The problem seems to be due to the fact that with each different physical method employed, a different property of the solution is measured when trying to determine hydration.

Current investigations are advancing our knowledge about the intimate structure of liquid water. A renewed interest in this subject has led to the interpretation based on a certain number of "unbonded"

gaslike molecules in liquid water and new ways to look into its water structure, breakdown of the structure in the presence of electrolytes, and hydrogen bonding with solutes. The methods that have been used in studying liquid water are beginning to be applied in the study of electrolyte solutions, but even for the simplest electrolytes there still remain significant discrepancies between the various experimental observations.

By comparing the results in the radiolysis of our five nitrate solutions, we may seek to account for them on the basis of cation-anion interaction in concentrated solutions, e.g., comparing yield of different products at a same concentration of nitrate, or comparing the role of cations in radiolysis that may be responsible for these various yields. The way in which the energy intake of the cation during radiation takes place and its solvent interaction is not exactly known at the present stage in nitrate radiolysis.

Absorption of energy during radiation that could be ascribed to the individual constituents of a mixture on a theoretical or empirical basis is a current topic of much interest among radiation chemists. But a consistent way to correlate energy intake, concentration and pH, and account for the final products observed is far from being a resolved problem in radiation chemistry.

II INFRARED STUDIES IN THE HYDRATION OF NITRATES

Introduction

The infrared and Raman spectra of liquid water in the OH stretching region result from a superposition of three main components, mainly ν_1, ν_2, and $2\nu_3$ i.e., symmetric stretching, antisymmetric stretching and first overtone of the antisymmetric stretching mode. The 1.45-μ band of water assigned (Herzberg, 1945) to $\nu_1 + \nu_3$ was chosen for this investigation.

It was shown by Suhrmann and Breyer (1933) that the near infrared (N.I.R.) bands of water are characteristically changed by the presence of dissolved electrolytes. This technique has been used repeatedly to obtain information about the structure of water in electrolyte solutions.

The 1.45-μ band has an absorption that depends on temperature and dissolved solute (Klotz, 1965). The present work is an extension of the measurements carried out by McCabe and Fisher (1970) where difference spectra of aqueous solutions of some alkali-halides measured vs. water were resolved into two components, one representing the hydration of the solute, and the other, the volume of the free water present.

Such an approach to the establishment of hydration parameters for a given salt may help to overcome our limited knowledge in the structure of solutions. We do not know the exact radius of an ion when

passing from solid crystalline state to the dissolved state, so that the Pauling and Goldschmidt interionic crystalline distances are only approximately extrapolated to give radii of ions in solution (Latimer et al., 1939; Verwey, 1942). Interactions of ions with water are not simply to calculate due to the uncertainty in true ionic radii, in the coordination number of ions and the orientation of the water molecules in the coordination shell.

Of the numerous methods that have been suggested to obtain individual partial ionic volumes (Mukerjee, 1966) only a few are actually independent of the knowledge of the true radii of the ions. Padova (1964) has shown that the apparent molar volume of a hydrated ion is given by

$$\phi_v = V_{in} + nv_o^h \qquad (1)$$

where h is the hydration number and v_o^h the molar volume of water in the hydration shell different from that of ordinary water. V_{in} is the intrinsic volume of the electrolyte and ϕ_v is the partial molar volume of the solute.

In dealing with changes in volume during hydration a process takes place of the type

$$M^o_{aq} + A^o_{aq} \longrightarrow M^+_{aq} + A^-_{aq} \qquad (2)$$

and the corresponding electrostriction is defined as

$$V_{el} = V_{in} - \phi_v \qquad (3)$$

where V_{in} the intrinsic molar volume of the electrolyte can be identified with the actual volume occupied by the unhydrated ions in solution. ϕ_v is the partial molar of the solute. Therefore, by definition, the dimensions of the ion are considered unchanged during the charging process and the electrostriction is attributed to the change in the solvent. The intrinsic volume of electrolytes can be obtained experimentally from the concentration dependence of the compressibility of the solution (Padova, 1964; Tamura and Sasaki, 1963).

Table 2-1 presents absolute partial molal volumes and intrinsec volumes of ions. The absolute values of V_{in} are probably not known to much better than 2 ml/g-ion because of the large experimental errors involved. This table is due to Padova (1964). Values are at 25° C in cc/g-ion. $\overline{V}^o$ is the partial molal volume at infinite dilution in ml/g-ion.

Table 2-1

Ions	V_{in} experimental[a]	V_{in} experimental[b]	V_{in} calculated[b]	$\overline{V}^o$ experimental[b]	$\overline{V}^o$ experimental[c]
H^+	0	0	0	-5.5	-5.4
Li^+	2.0	4.9	2.7	-6.6	-11.2
Na^+	6.4	8.4	5.8	-7.0	-7.4
K^+	15.3	15.3	11.3	3.3	3.4
Cs^+	25.5	27.1	21.4	15.6	15.5

[a] Padova (1964

[b] Conway et al. (1965)

[c] Zana and Yeager (1967)

According to this view, ions are spheres in a structureless solvent and V_{in} would simply be $\frac{4}{3}\pi r^3 N$ where r is the crystallographic radius and N the number of solute particles present. What is not taken into account in this treatment is that the finite size of the solvent molecules causes the presence of a certain amount of free space between the ions and the solvent molecules.

A Born-Haber cycle for the hydrations of ions which describes the energetics of the coordination process (Russell et al., 1965) fails to assign specific hydration for cation and anion because direct measurements of the energies of all steps is not possible. A statistical mechanical analysis of solutions is too complicated to calculate the intermediate quantities that fit a final result obtained by experiment.

Nitrates do not have a significant absorption in the 1.45μ region of the spectrum. These observations have been verified by a) Irish and Walrafen (1967), b) Goulden and Manning (1967), c) Gmelin (1966), d) Mellor (1967) and e) Irish (1969).

The strong ion-dipole interactions cause a local collapse of the open structure of water; the water molecules in the coordination shell are more closely packed than they are in ordinary water and an overall shrinkage of the solvent is observed. Electrolytes are denser and less compressible than pure water.

Padova's work (1964) assumes that the water molecules in the structure broken region Figure 2-1 have the same compressibility as pure water. Nothing is known with certainty

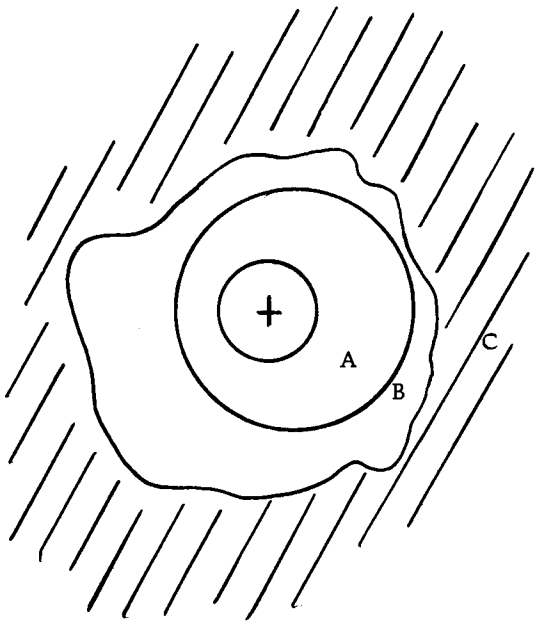

A) region of immobilization of water molecules
B) region of structure breaking
C) structurally "normal" or bulk water

Figure 2-1

about the compressibility of the structure-broken region and a full understanding of this region is not possible at present. This model for ionic hydration is due to Frank and Wen (1957).

In this type of treatment it is necessary to clarify the meaning of the term "hydration number" being used here. It is the best known hydration parameter but examiniation of reviews by Bockris and Conway (1959) and Journet and Vadon (1955) showed that we need to define an hydration number that is useful for our purposes. Knowledge of absolute solvation numbers is of great importance in several ways. Such values are necessary to further the model of an ionic solution and for many detailed purposes involving the theory of reactions in solution.

The hydration number — in its most general definition — is an empirical parameter which gives the effective number of water molecules that have undergon some constant critical change in property related to a suitable definition of hydration. The hydration number in equation (3) refers to the effective number of water molecules that are in physical contact with the ions and, as such, are incompressible. This hydration parameter attributes to a few water molecules the total change in compressibility of the solvent around the isolated ion.

Goto (1964) works out the basis of Padova's treatment employed

later by McCabe and Fisher (1970) to determine hydration numbers. In the earliest concepts of ionic solvation, ions were regared as chemically bound to water molecules, forming hydrates in aqueous solution. This concept was supported by observations upon the sudden changes of conductivity, cryoscopic constants, etc., with solution composition which are regarded as corresponding to the formation and decomposition of various definite hydrates. The object of the present work, therefore, is more closely to define the term "solvation number" and to attempt, from a critical discussion of the results of the literature, to find some order in the apparent chaos of conflicting results existing there.

Experimental Section

Nitrates of Li, Na, K, Cs, Ca were analytical reagent grade and were recrystallized in triple distilled water. Spectra were obtained using a Schimadzu Model MPS-50L multipurpose recording spectrophotometer. Silica cells 0.100 [cm] path length were used. Path lengths were checked as described by Vandebelt and Spulock (1955) using standard alkaline solution of K_2CrO_4 of known ε value.

In each experiment, the sample cell contained an aqueous salt solution and the reference cell contained water alone. Cells were thermostated 15 minutes at 25° C before taking each reading. The temperature attained was 25 ± 0.2° C.

Description of a Typical Difference Spectrum

In Figure 2-2 is shown the determination of the hydration and excluded volume spectrum for an 8 M solution $NaNO_3$. The absorption for pure water is labeled H_2O and the values are given in Table 2-2.

Table 2-2

λ [mμ]	A	λ [mμ]	A
1175	0.07	1475	1.25
1275	0.07	1500	0.93
1325	0.18	1525	0.70
1350	0.18	1515	0.42
1375	0.28	1625	0.37

The spectrum of water itself was taken against a silica-air cell. The precision of the absorbance measurements is approximately ±1%.

In Figure 2-2 curve A is the difference spectrum of 8 M $NaNO_3$ measured vs. water. It represents the absorption due to various forms of water. The salt does not absorb in this region. This absorption is due to the unbound (free) and bound (hydration water) in 8 M $NaNO_3$. This difference spectrum is arbitrarily divided into two components. The difference spectrum as such is negative because the reference cell absorption is greater than the sample cell absorption at all wavelengths.

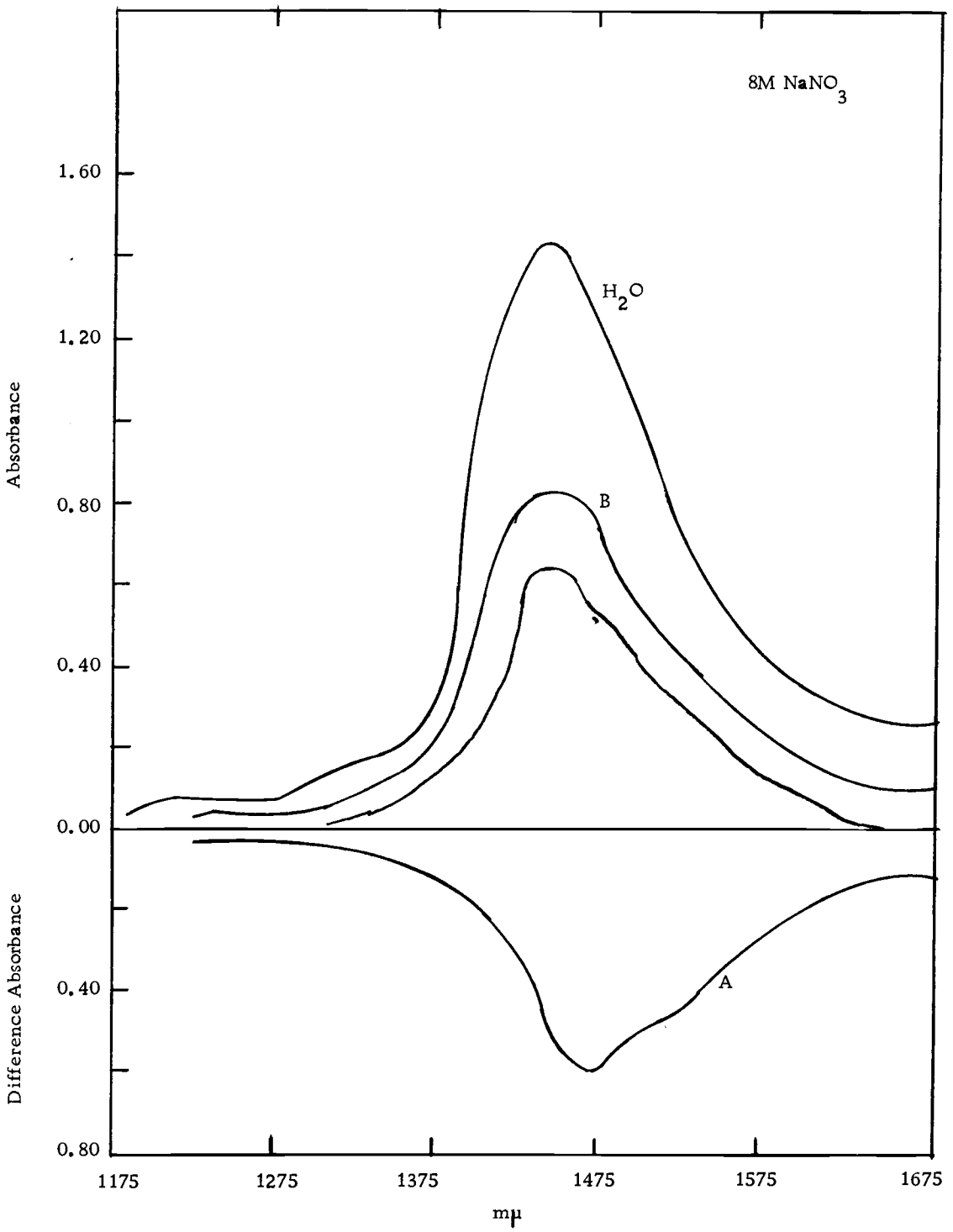
8M NaNO3
H2O
B
A
Absorbance
Difference Absorbance
1.60
1.20
0.80
0.40
0.00
0.40
0.80
1175
1275
1375
1475
1575
1675
mμ

Figure 2-2

The next step is to isolate a "normalized" water spectrum. This is shown in Figure 2-2 by curve B. The physical meaning of such a "normalized spectrum" is the absorbance ascribed to a type of water that is in the same physical state as the pure water depicted in the H_2O curve. This represents the unbound water in the salt solution with the same structure as pure water. The criteria for choosing the value of the normalizing factor is the minimum of the water absorption band which is located at 1675 mμ. The criteria adopted minimizes the unbound or free water and consequently maximizes the other component, namely the hydration spectra C, representing the bound water or water of hydration.

In Figure 2-2 the normalization factor is given by the ratio 0.16 (due to 8 M $NaNO_3$) and 0.26 due to water absorption at 1675 mμ. McNabe and Fisher (1970) also point out that this factor so chosen must meet the criterion that all the negative contribution of the difference spectrum is cancelled out. To determine the hydration spectrum C, curve A and B have to be added. Spectrum C so obtained must be positive at all wavelengths.

Theoretical Considerations of This Method

We have already seen by equation (3) that $V_{el} = V_{in} - \phi_v$ where V_{el}, the electrostriction volume is the reduction in the volume of the solvent due to the interaction ion-solvent. The meaning of V_{in}

and ϕ_v have been seen before. Rearranging equation (3)

$$\phi_v = V_{in} - V_{el} \tag{9}$$

If nV_h is the hydration volume (solute plus solvent interacting with solute) where n are the number of moles of solute solvated and V_h the volume of solvent interacting with solute, then equation (9) becomes

$$V_{excl} = V_{in} + nV_h \tag{10}$$

then V_{excl} being the molar excluded volume of the hydrated solute. Next it is desired to calculate nV_o where V_o is the molar volume of H_2O at a given temperature and pressure. From the way we have defined the terms used

$$nV_o = nV_h + V_{el} \tag{11}$$

From equation (3) and (10)

$$V_{excl} - \phi_v = (V_{in}+nV_h) - (V_{in}-V_{el}) = nV_h + V_{el} \tag{12}$$

From (11) and (12)

$$nV_o = V_{excl} - \phi_v \tag{13}$$

Padova (1964) worked out an expression for ϕ_v (the partial molar volume of the solute) in terms of readily observable quantities is

$$\phi_v = 10^3 \frac{(d_o - d)}{Cd_o} + \frac{M}{d_o} \tag{14}$$

In equation (14) C is the molar concentration of the solute, d_o is the density of the solvent, d is the density of the solution, M_o molecular weight of solvent and M the molecular weight of the solute. From equation (13) and (14)

$$\phi_s = \phi_v + nV_o \tag{15}$$

and

$$nV_o = \frac{nM}{d_o} \tag{16}$$

Calculation and Results of the Hydration Spectral Studies

$LiNO_3$ Solutions

The difference absorbance spectrum of $LiNO_3$ are presented in Figure 2-3. From Figure 2-3 it becomes clear that such a spectrum does not exist for solutions below concentrations of 1 M. (Note the inversion below the zero reference line). Since the normalization is done at the minimum of the water band, both V_{excl} and nV_o, which were calculated by this procedure, must be considered as minimum values and hence V_{excl} and nV_o are listed in the following pages as V_{excl} and nV_o but represent values for $(V_{excl})_{min}$ and $(nV_o)_{min}$.

A typical calculation is presented for a solution 1 M $LiNO_3$. The molar excluded volume, V_{excl}, can be calculated from curve B and curve H_2O. If the magnitude of the curve H_2O represents

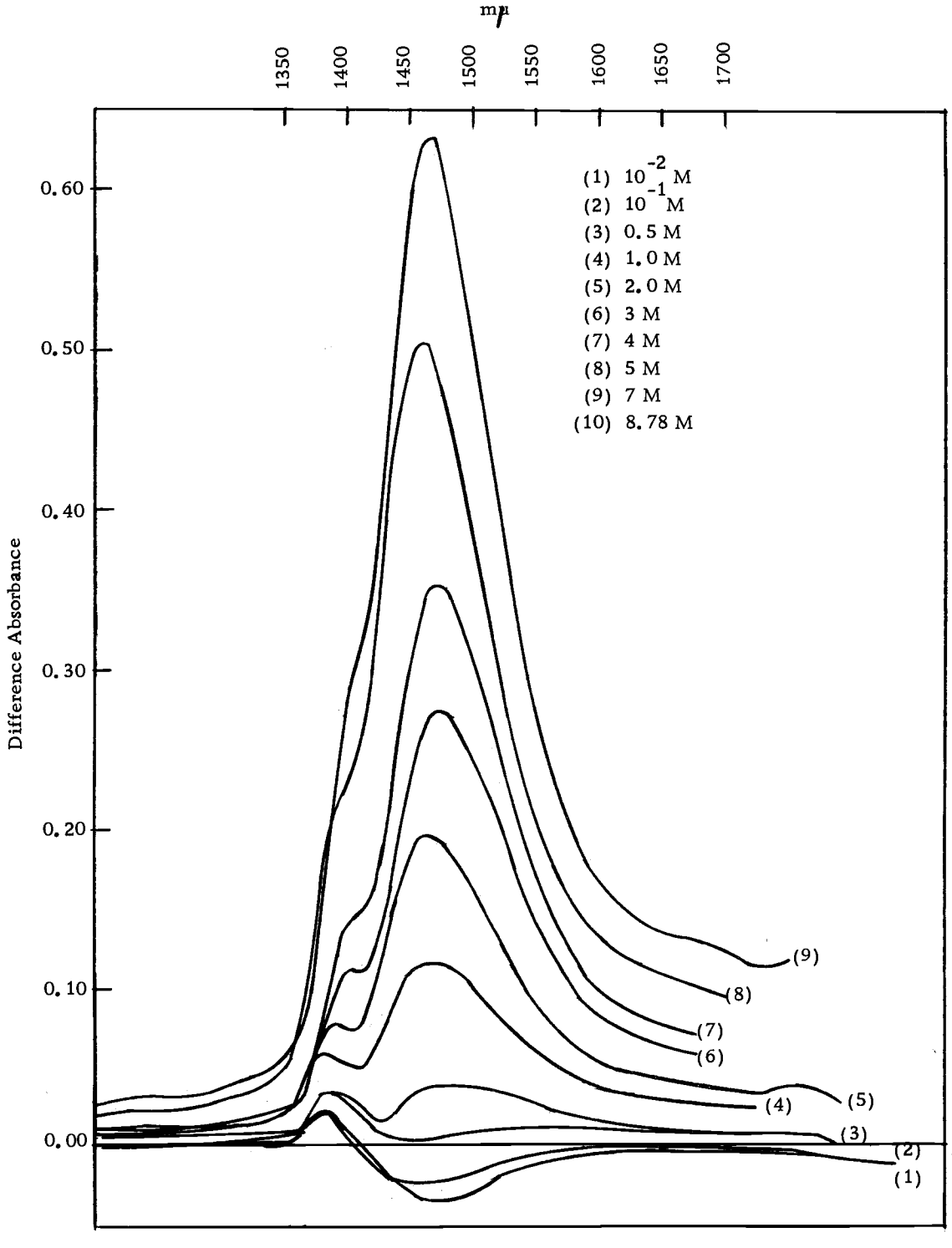

Figure 2-3. Difference Absorbance Spectra $LiNO_3$.

the total volume of the solution, then the ratio of the magnitudes of curve B to curve H_2O taken at any frequency, is equal to the fractional volume (FV) which is occupied by the hydrated solute. The molar excluded volume, V_{excl}, is defined experimentally in relation to this fractional volume, namely

$$V_{excl} = \frac{1000\,(FV)}{C} \tag{17}$$

In the 1 M $LiNO_3$ solution we have $(FV)\,\frac{0.020}{0.0260} = 0.076923$ that represents the "normalization" factor. V_{excl} then is:

$$V_{excl} = \frac{1000 \cdot 0.076923}{1.0} = 76.923 \text{ ml/mol}$$

$$\phi_v = \frac{10^3(d_o - d)}{Cd_o} + Md_o = \frac{10^3(1.003-1.037)}{1.003} + 69.156 = 35.258 \text{ ml/mol}$$

$$(nV_o) = V_{excl} - \phi_v = 76.923 - 35.258 = 41.665$$

$$n = \frac{(nV_o)d_o}{M} = \frac{41.665 \cdot 1.033}{18.015} = 2.38 \text{ mol } H_2O/\text{mol}$$

A complete table of results is presented in Table 2-3.

Table 2-3

$LiNO_3$

Molarity $LiNO_3$	Density g/ml 20°C	Moles H_2O/lt solution	χ_{salt} [a]	χ_{H_2O} [b]	(FV) [c]	V_{excl} ml/mol	ϕ_v ml/mol	n [d]
1	1.0371	53.731	0.0183	0.9817	0.077	76.923	35.258	2.38
2	1.0760	52.070	0.0370	0.9630	0.144	72.000	32.765	2.17
3	1.1129	50.299	0.0563	0.9437	0.200	66.667	32.600	1.91
4	1.1539	48.745	0.0758	0.9241	0.231	62.500	31.519	1.77
5	1.1881	46.805	0.0965	0.9035	0.307	61.520	32.267	1.61
7	1.2610	43.203	0.1394	0.8606	0.423	60.440	32.404	1.32
8.78	1.3250	39.943	0.1802	0.8198	0.461	52.505	32.591	1.11

a Molar fraction salt, b Molar fraction water, c Fractional volume, d mol H_2O/mol salt

Note that we have a regular decrease in the difference absorbance spectra as we go to lower concentrations.

$NaNO_3$ Solutions

The difference absorbance spectra are presented in Figure 2-4. The normalization factor is taken at 1675 mμ. Note that the trend is the same as in case of the $LiNO_3$ solutions decreasing the height of spectra as we go down in concentration. Note that no workable spectra according to the criteria adopted in the present treatment for solutions below 0.5 M is possible because the spectra is below the base line. The results for $NaNO_3$ solutions are shown in Table 2-4.

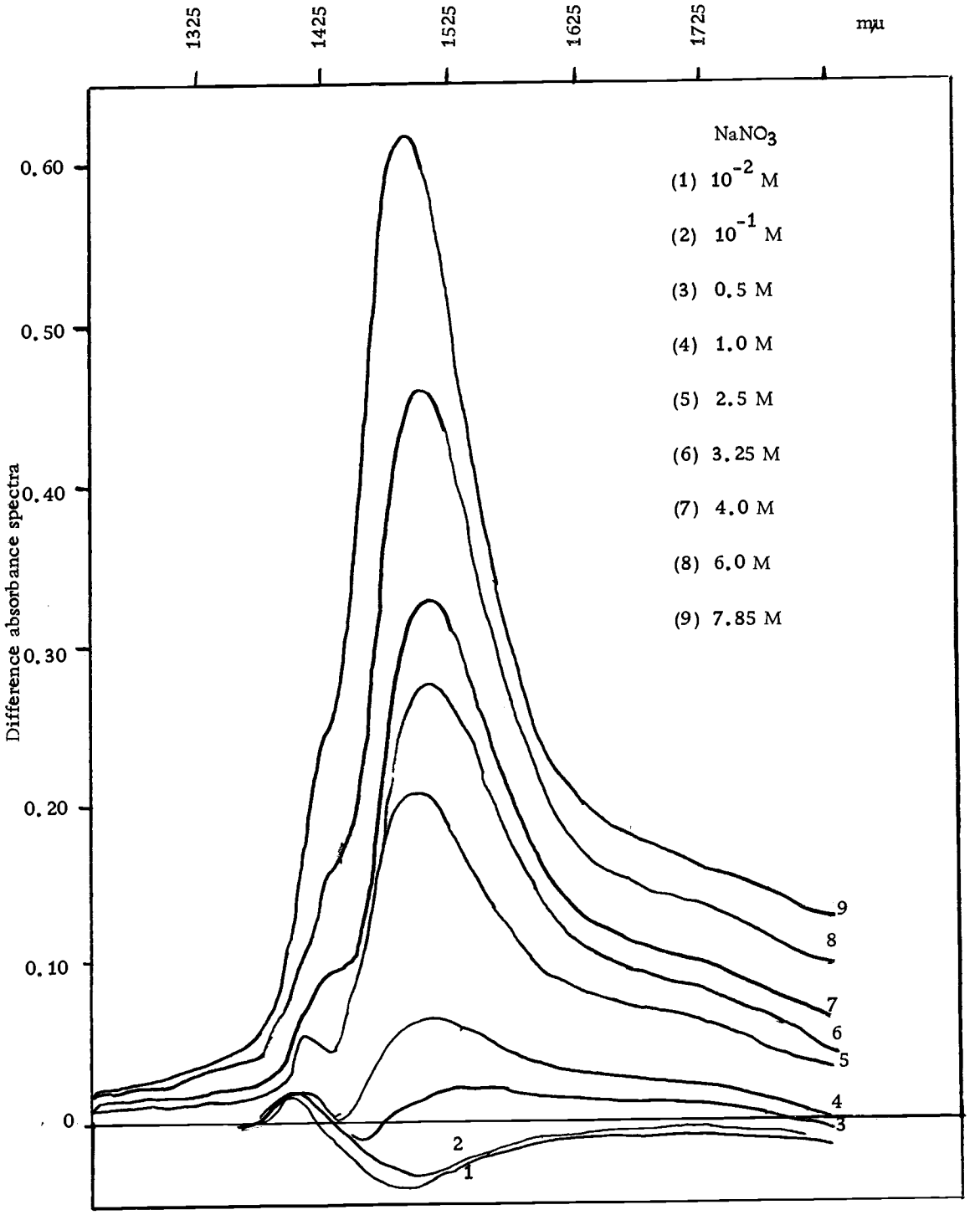
1325
1425
1525
1625
1725
mμ
NaNO3
(1) 10-2 M
(2) 10-1 M
(3) 0.5 M
(4) 1.0 M
(5) 2.5 M
(6) 3.25 M
(7) 4.0 M
(8) 6.0 M
(9) 7.85 M
Difference absorbance spectra
0.60
0.50
0.40
0.30
0.20
0.10
0
1
2
3
4
5
6
7
8
9

Figure 2-4

Table 2-4

Molarity $NaNO_3$	Density g/ml 20°C	Moles H_2O/ solution	χ_{salt} [a]	χ_{H_2O} [b]	(FV) [c]	V_{excl} ml/mol	ϕ_v ml/mol	n [d]
0.5	1.0249	54.535	0.0091	0.9909	0.057	115.38	41.376	4.12
1	1.0519	53.675	0.0183	0.9817	0.107	107.80	36.391	3.93
2.5	1.1281	50.817	0.0469	0.9531	0.257	102.80	35.394	3.75
3.25	1.1679	49.499	0.0616	0.9384	0.315	96.92	34.627	3.47
4	1.2038	47.959	0.0769	0.9230	0.365	91.25	35.145	3.12
6	1.3041	44.075	0.1198	0.8801	0.500	83.33	35.228	2.68
7.85	1.3910	40.177	0.1634	0.8365	0.596	75.92	35.943	2.25

[a] Molar fraction salt

[b] Molar fraction water

[c] Fractional volume

[d] mol H_2O/mol salt

KNO_3 Solutions

Difference spectral studies of KNO_3 solutions are presented in Figure 2-5. The normalization factor is taken at 1675 mμ. The decreasing trend in the height of the curves is similar to the one observed in $LiNO_3$ and $NaNO_3$ solutions. Spectra of 10^{-1} and 10^{-2} M solutions have no physical meaning according to the method employed. The results for KNO_3 solutions are shown in Table 2-5.

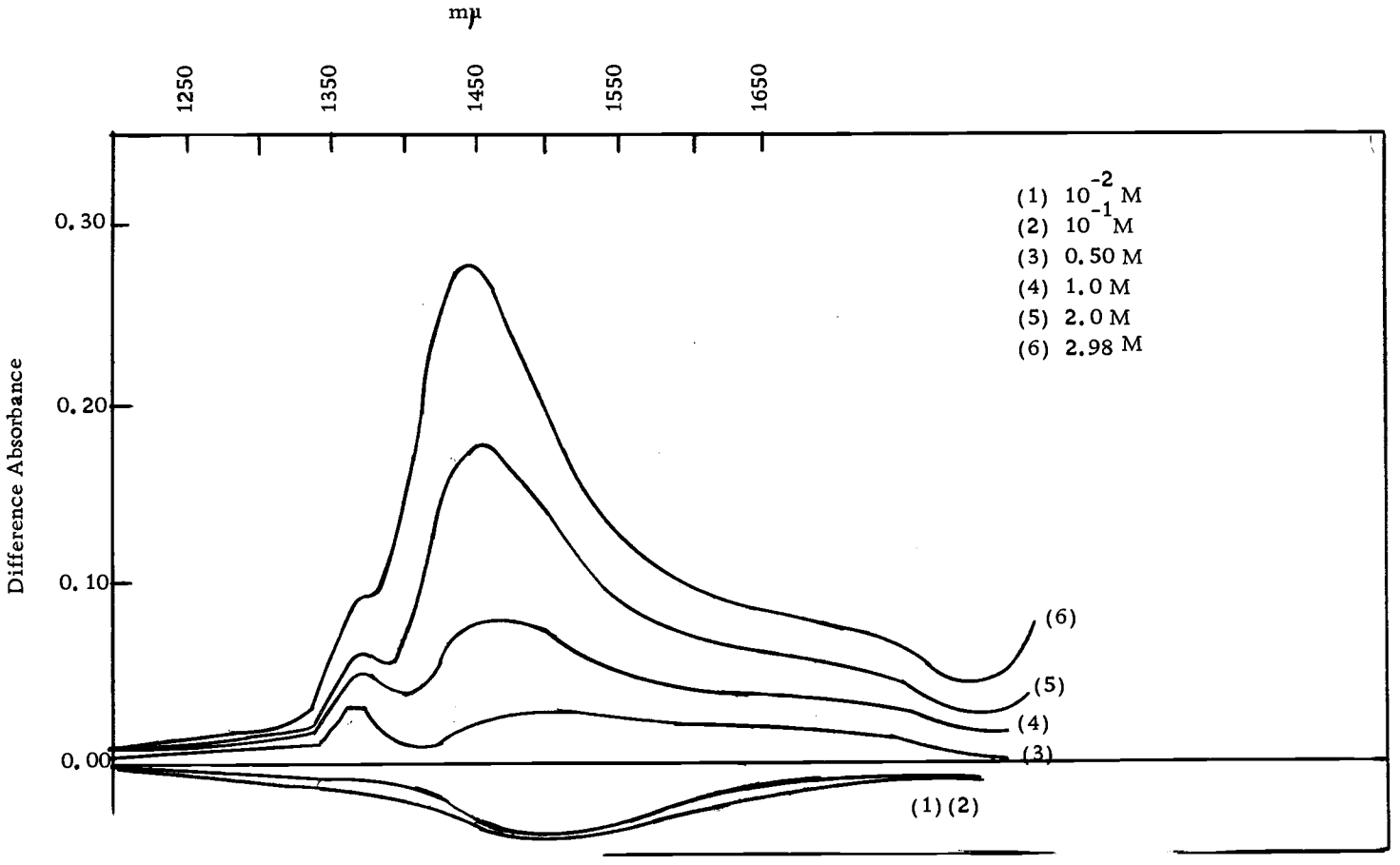

Figure 2-5. Difference Absorbance Spectra KNO_3.

Table 2-5

M	Density g/ml 20°C	Moles H_2O/ solution	χ_{salt} [a]	χ_{H_2O} [b]	(FV)[c]	V_{excl} ml/mol	ϕ_v ml/mol	n[d]
0.5	1.0283	54.143	0.0091	0.9908	0.081	108.447	51.553	6.02
1	1.0582	53.169	0.0185	0.9815	0.146	146.15	46.572	5.54
2	1.1121	51.054	0.0377	0.9623	0.230	115.38	47.076	3.80
2.98	1.1632	47.274	0.0593	0.9407	0.303	100.67	48.218	2.92

a Molar fraction salt, b Molar fraction of water, c Fractional volume, d mol H_2O/mol salt

$CsNO_3$ Solutions

The difference spectral studies of $CsNO_3$ solutions are presented in Figure 2-6a. The normalization factor is taken at 1675 mμ. The decreasing trend in the height of the spectra is similar to the ones observed in $LiNO_3$, $NaNO_3$ and KNO_3 solutions. The results for $CsNO_3$ are presented in Table 2-6.

Table 2-6

$CsNO_3$ M	Density g/ml 20°C	Moles H_2O/ solution	χ_{salt} [a]	χ_{H_2O} [b]	(FV)[c]	V_{excl} ml/mol	ϕ_v m/mol	n[d]
0.56	1.0750	53.611	0.0103	0.9896	0.077	137.32	67.310	3.90
0.84	1.1339	53.856	0.0154	0.9846	0.107	128.09	61.250	3.72
1.12	1.1869	53.792	0.0204	0.9796	0.109	96.09	31.700	3.58

a Molar fraction salt, b Molar fraction of water, c Fractional volume, d mol H_2O/mol salt

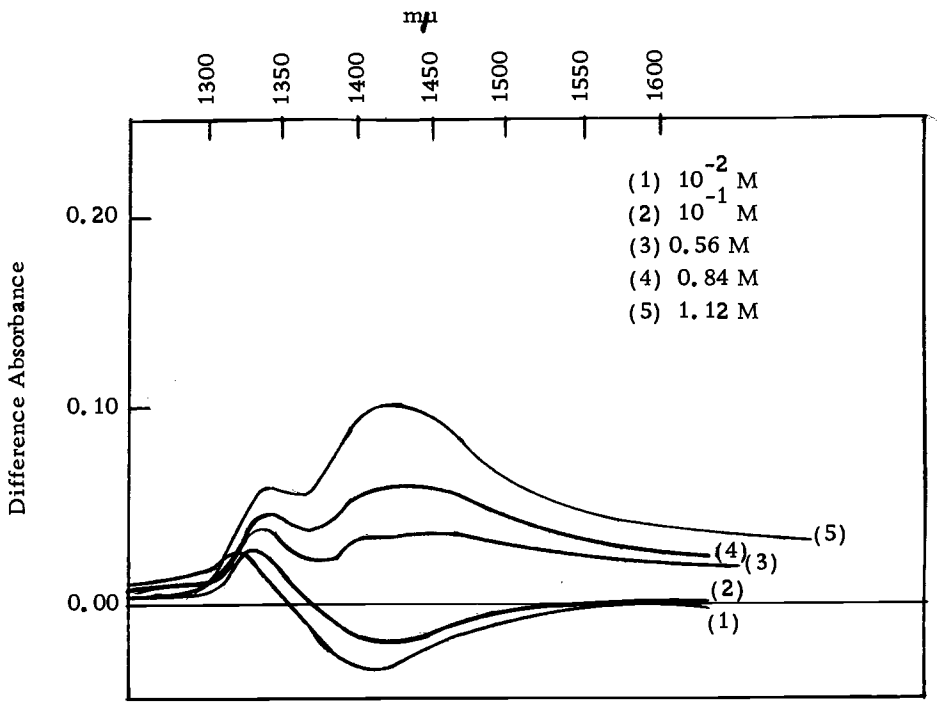

Figure 2-6a. Difference Absorbance Spectra $CsNO_3$.

$Ca(NO_3)_2$ Solutions

The same pattern for the difference absorbance spectra of $Ca(NO_3)_2$ solutions is observed as in the other inorganic solutions previously described. The spectra is shown in Figure 2-6b. The calculated results based on these observations are presented in Table 2-7.

Table 2-7

M $[Ca^{++}]$	Density g/ml 20°C	Moles H_2O/ solution	χ_{salt} [a]	χ_{H_2O} [b]	(FV) [c]	V_{excl} ml/mol	ϕ_v ml/mol	n [d]
0.5	1.0629	54.452	0.0091	0.9909	0.038	90.769	90.769	2.55
1.5	1.1739	51.509	0.0283	0.9717	0.133	88.974	88.974	2.17
2.0	1.2250	49.778	0.0386	0.9613	0.177	88.452	88.462	1.92
2.5	1.2751	48.013	0.0495	0.9505	0.215	86.154	88.154	1.67
3.5	1.3839	44.960	0.0722	0.9278	0.292	83.516	83.516	1.52
4.22	1.4529	42.240	0.0908	0.9091	0.346	78.381	78.381	1.33
5.50	1.6039	40.936	0.1184	0.8816	0.388	70.629	70.629	1.14

a Molar fraction salt, b Molar fraction of water, c Fractional volume, d mol H_2O/mol salt

$(CH_3)_4NNO_3$ Solutions

The spectra of these solutions is presented in Figure 2-7. It is noticed that at 1675 mμ where usually the normalization factor was calculated, the spectra has zero height so that no normalization factor can be calculated as in the case of the other inorganic nitrates. The normalization was done at 1450 mμ and physically it means that

the hydration water found (due to the calculations carried out as in the case of the inorganic salts) is not a maximum value but possibly a close approximation to it. In the calculation of the ϕ_v (apparent molar volume of the solute) the density values of $(CH_3)_4NNO_3$ reported by Hertz (1971) were used and are given in Table 2-8.

Table 2-8

$(CH_3)_4NNO_3$ [M]	Density [g/ml 25°]
0.8115	1.1050
1.7425	1.1085
2.3702	1.1128
2.8986	1.1193
3.3555	1.1280
3.7561	1.1374

The calculated results are presented in Table 2-9 for $(CH_3)_4NNO_3$ solutions of different concentrations.

Table 2-9

M	Density g/ml 20°C	Moles H_2O/ solution	χ_{salt} [a]	χ_{H_2O} [b]	(FV) [c]	V_{excl} ml/mol	ϕ_v ml/mol	n [d]
1	1.1051	52.722	0.0186	0.9814	0.091	91.500	34.880	3.15
2	1.1090	45.277	0.0423	0.9577	0.225	112.500	83.728	1.61
3	1.1211	39.500	0.0706	0.9294	0.347	115.270	97.355	1.00
3.89 (sat)	1.1412	33.888	0.1030	0.8970	0.457	117.670	101.204	0.91

[a] Molar fraction salt

[b] Molar fraction of water

[c] Fractional volume

[d] mol H_2O/mol salt

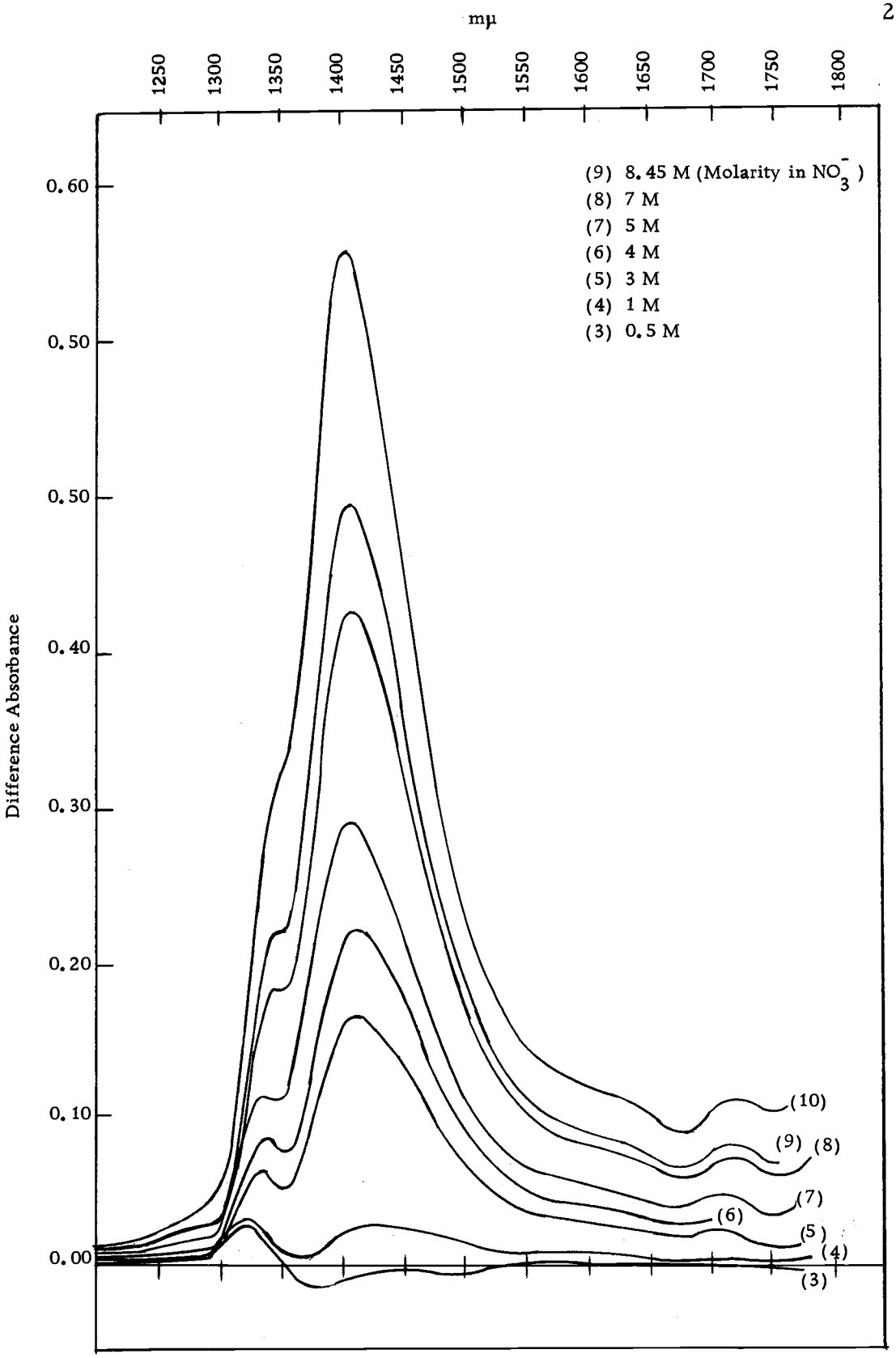

Figure 2-6b. Difference Absorbance Spectra $Ca(NO_3)_2$.

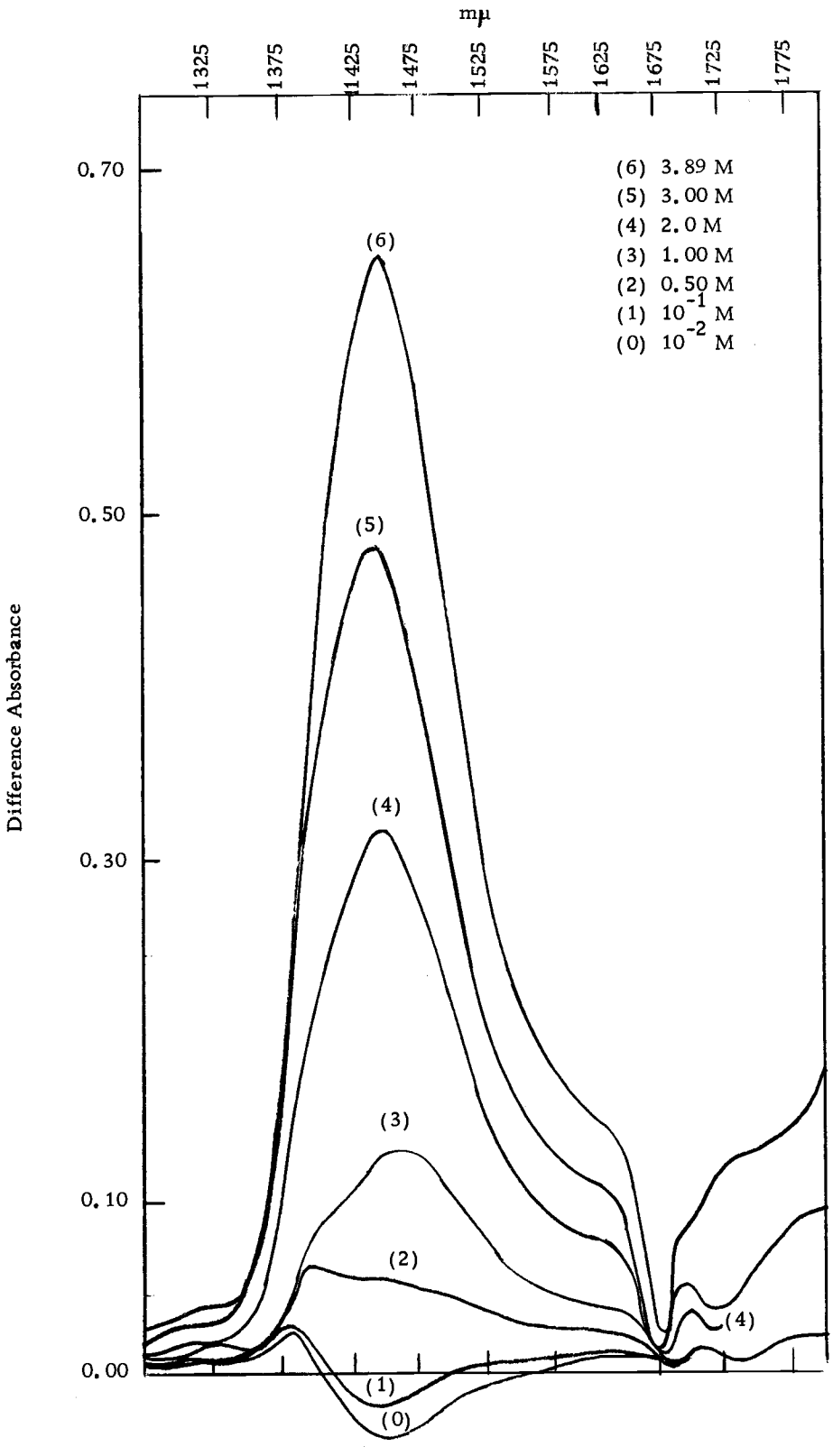

Figure 2-7 Difference Absorbance Spectra $(CH_3)_4NNO_3$.

NH_4NO_3 Solutions

The spectra of these solutions is shown in Figure 2-8. The normalization is done at 1450 mμ and the physical meaning of this fact has been already stated for the $(CH_3)_4NNO_3$ case. The shape of these spectra indicate a more regular peak at all molarities than the nitrates previously studied. The spectra present two isosbestic points 1500 mμ and at 1700 mμ and a minimum at 1560 mμ. In Table 2-10 are cited the calculated values for NH_4NO_3.

Table 2-10

M	Density g/ml 20°C	Moles H_2O/lt solution	χ_{salt} [a]	χ_{H_2O} [b]	(FV) [c]	V_{excl} ml/mol	ϕ_v ml/mol	n [d]
0.5	1.0131	54.010	0.0091	0.9908	0.056	112.000	60.041	2.73
2	1.0599	49.958	0.0382	0.9615	0.152	75.758	51.865	1.33
4	1.1190	44.388	0.0820	0.9173	0.272	68.182	52.124	0.89
6	1.1771	38.722	0.1342	0.8658	0.386	64.394	51.367	0.72
8	1.2340	35.573	0.1836	0.8164	0.500	62.500	51.500	0.61
10	1.2869	27.033	0.2700	0.7300	0.598	59.648	52.863	0.55

a Molar fraction salt, b Molar fraction water, c Fractional volume, d mol H_2O/mol salt

General Discussion and Tentative Assignment of Cationic and Anionic Hydration

Four determinations of hydration have been carried out directly on concentrated solutions of nitrates. Kappusami (1969) using an approach by classical thermodynamics based on densities, ultrasonic velocity of water and solvent compressibility data, arrives

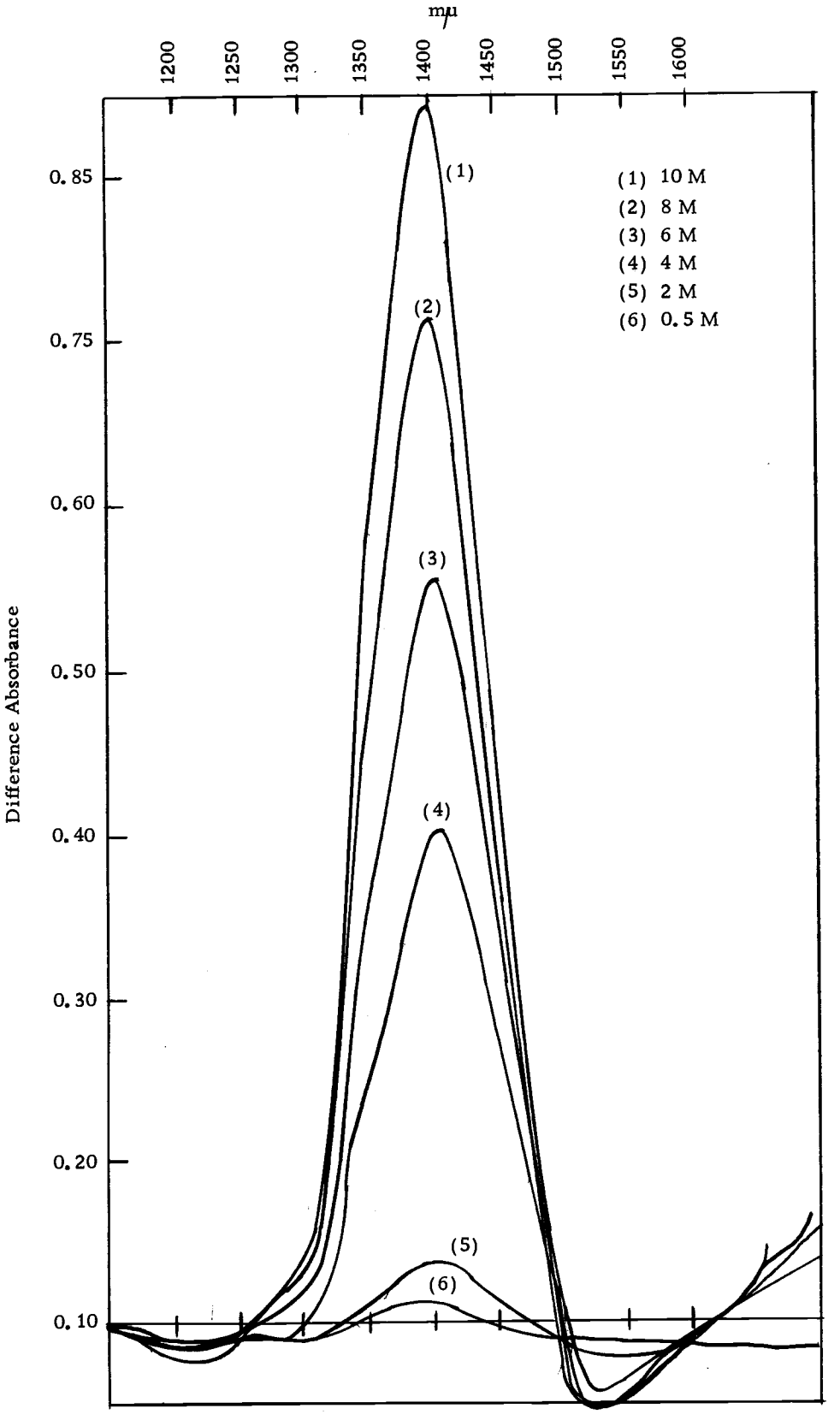

Figure 2-8. Difference Absorbance Spectra NH_4NNO_3.

at hydration numbers for NH_4NO_3. Troshin (1965) obtained data from the transfer number of Li in concentrated solutions of lithium nitrate. By means of this transfer number and the viscosity of Li ions in solutions of $LiNO_3$ at high concentrations he obtained the hydration of ions of Li in these solutions. The results are consistently higher than the one we arrived at by our method. Vogrin et al. (1971) and Malinonski and Knapp (1966) have used the N.M.R. technique to determine the hydration of concentrated solution of nitrates. In Table 2-11 these values are given, namely:

Table 2-11

M	nNH_4NO_3 [a]	$nNaNO_3$ [b]	$nCa(NO_3)_2$ [b]	$nLiNO_3$ [c]
1	3.5	3.6 ± 1.5		
2	3.2	3.2 ± 0.5		2.8
3	2.9	3.3 ± 0.2	7.8 ± 0.2	2.7
4	2.7	2.9 ± 0.1		2.5
6	2.1			2.2
8	1.7			1.8
10	1.3			1.6

n hydration, a Kappusami (1969), b Vogrin et al (1971), c Troshin (1965)

From Figure 2-3 in $LiNO_3$ solutions for a 0.5 M concentration no hydration determination by this method is possible since no difference spectra was obtained. No hydration for a 0.5 M $Ca(NO_3)_2$ solution [in NO_3^-] is possible for the same reason (Figure 2-6). The spectra of $(CH_3)_4NNO_3$ (Figure 2-7) present at the minimum of the 1.46 μ

band a regular decrease in magnitude as it is the in all the other salts. At the present time no explanation is known for this fact.

A plot of the hydration vs. concentration of these nitrate solutions would give an hypothetical hydration number of infinite dilution and the slope of the lines may show the particular cation-anion interaction in each particular case. This is shown in Figure 2-9. To obtain slopes for KNO_3, $(CH_3)_4NNO_3$ and NH_4NO_3 salts are not possible from this plot. The slopes of $NaNO_3$, $Ca(NO_3)_2$ and $LiNO_3$ solutions have a close value and thus may indicate a similar type of interaction cation-anion as we go up in concentration. The slope of $CsNO_3$ as well as the KNO_3 for is bigger as concentrations between 1 and 3M and thus seems due to the fact that we are close to saturation concentrations for this salts. Extrapolation to zero concentration does not reveal any particular trend which may be related to e.g., heat of hydration of the salt, or crystalline radius of the cation. There are no experimental values in the literature to compare an hydration at infinite dilution with the values extrapolated from Figure 2-9 and shown in Table 2-12. The values for the hydration of salts reported in the literature are usually obtained by adding a differential hydration of cation and anion and thus may not be meaningful for comparison purposes.

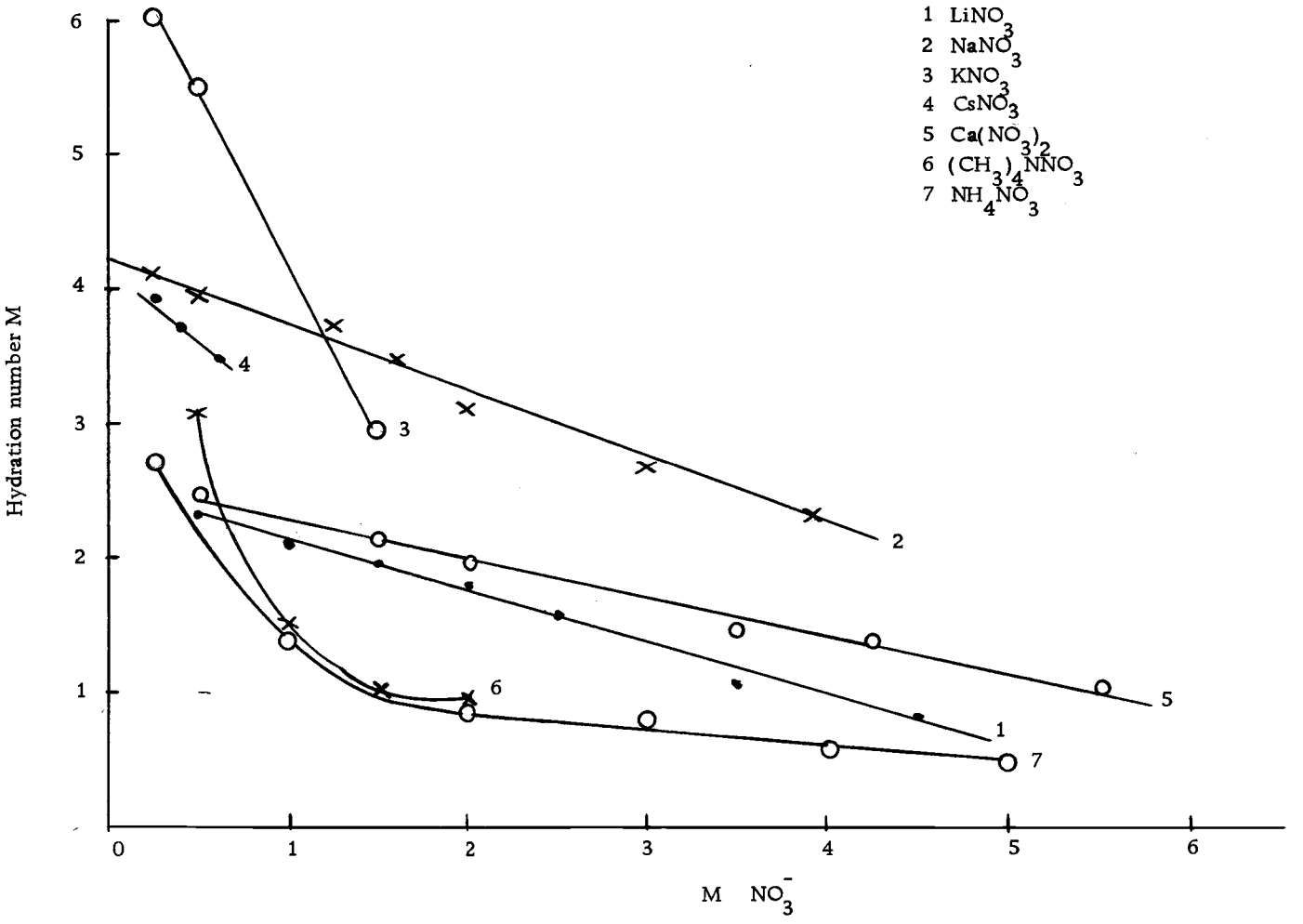
1 LiNO3
2 NaNO3
3 KNO3
4 CsNO3
5 Ca(NO3)2
6 (CH3)4NNO3
7 NH4NO3
Hydration number M
M NO3-
0
1
2
3
4
5
6

Figure 2-9

Table 2-12

Salt	Hydration at infinite dilution
$LiNO_3$	2.4
$NaNO_3$	4.3
KNO_3	6.4
$CsNO_3$	4.5
$Ca(NO_3)_2$	2.7
$(CH_3)_4NNO_3$	-
NH_4NO_3	3.3

It is our intention to separate the hydration of the cation and of the anion by means of $(CH_3)_4NNO_3$. As a first approximation it is assumed that all hydration is in the anion. Gluekauf (1955) employed for the first time the assumption to assign a differential hydration for cation and anion.

Studies in the past ten years have shown alkyl ammonium cations do not interact with the anion and very little with the solvent present. It is generally believed that as the size of cation increases or the solution gets more concentrated the polar character necessary for an hydration process decreases. Robinson and Stokes (1955) stated that it is generally acceptable that these salts have little electrostatic interaction with water. Zundel (1969) verifies this assumption by use of infrared investigations with polyelectrolyte membranes. Studies carried out in alkyl ammonium halides (Wen and Saito, 1965; Redlich, 1964) have shown that a) the alkyl group completely saturates the N^+ center, the external surface of N^+ ion

being mainly the organic part, b) large cations do not displace water from a solvated anion or form strong bonds with water in aqueous solution, c) R_4N^+ cation is coordinately saturated and is incapable of forming more bonds.

The limit of solubility of $(CH_3)_4NNO_3$ is 3.89 M and for the purpose of separating the hydration of anion and cation this will set a restriction at concentrations above this value. Larger chain alkyl ammonium nitrates do not exhibit higher solubility, so this problem could not be obviated (Hertz, 1964). The individual ion hydration values so separated are shown in Table 2-13a.

Table 2-13a

KNO_3			$LiNO_3$			$NaNO_3$		
M	n_{K^+}	$n_{NO_3^-}$	M	n_{Li^+}	$n_{NO_3^-}$	M	n_{Na^+}	$n_{NO_3^-}$
1	2.39	3.15	1	-	-			
2	2.19	1.61	2	0.56	1.61	1	0.78	3.15
2.98(sat)	1.92	1.00	3	0.91	1.00	2.5	2.60	1.15
			4	0.86	0.91	3.25	2.52	0.95
						4	2.24	0.88

$CsNO_3$			$Ca(NO_3)_2$		
M	N_{Cs^+}	$n_{NO_3^-}$	$M[NO_3^-]$	$n_{Ca^{++}}$	$n_{NO_3^-}$
0.84	0.22	3.50	1	--	--
1.12	0.68	2.90	3	1.17	1.00
			4	1.01	0.91

In Figure 2-10 is shown the hydration of cations extrapolated to infinite dilution. A note of caution is necessary here, since the extrapolation is based on two or three points in some cases, making this assignment only tentative. The extrapolated values are shown in Table 2-13b and compared with values found in the literature.

Table 2-13b

Cation	Extrapolated hydration number at infinite dilution, this work	Literature
Li^+	0.55	2.5-7 [a, b]
Na^+	--	2.0-7 [a, b]
K^+	2.6	1.0-7 [a, b]
Cs^+	--	1.0-6 [c, d]
Ca^{++}	1.65	4.3 [e]

[a] Bockris (1964)

[b] Malinowski (1971)

[c] Hindman (1962)

[d] Cotton and Wilkinson (1966)

[e] Swift and Sayre (1966)

The values reported for the hydration of the NO_3^- are 0 by Hindmann (1962) and 0.5 by Vogrin et al. (1971) both using N.M.R. technique. By inspection of values in Table 2-13, the extrapolated value at infinite dilution for the hydration of the NO_3^- ion due to the different nitrates, approaches asymptotically infinity and no such value can be reported in this fashion. It has been used in the calculation of ϕ_v (apparent molar volume) the values reported by

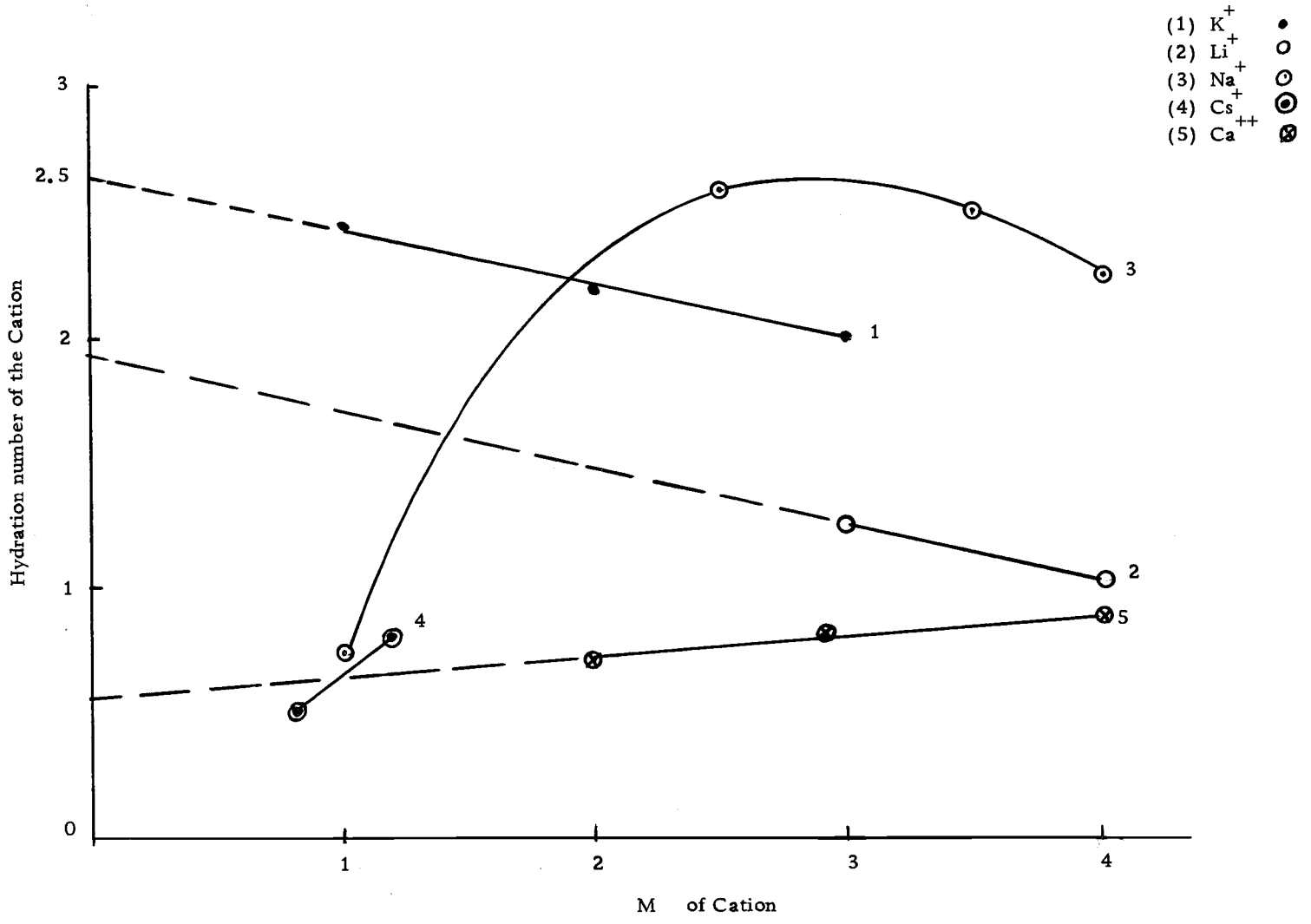
(1) K^+
(2) Li^+
(3) Na^+
(4) Cs^+
(5) Ca^{++}
Hydration number of the Cation
3
2.5
2
1
0
1
2
3
4
M of Cation

Figure 2-10

G. Hertz (1971). No value for a 0.5 M concentration is given there and in spite of having obtained a difference spectrum for this molarity in Figure 2-7. No hydration number for this molarity is possible because the density for such a molarity is not known.

Different workers have different ideas about the interaction of R_4N^+ and surrounding water. Franks (1968) has the view that concentration and temperature studies of R_4NNO_3 salts suggest maybe electrostatic pair hydration in solution of these salts. Prue (1966) has the idea that a simple competition model in which a large cation is unable to displace water from the hydration shell of the anion accounts for experimental data in these solutions. Mak and Roth (1968) think that the weak electrostatic attraction between cation and anion is due to the fact that tetrahedral four H bonded water conserves this structure when surrounding the R_4N^+ ion and is responsible for the anomalous behaviour of this ion. The lack of more basic information about $(CH_3)_4NNO_3$ may explain in part why sometimes we are able to use its hydration to separate cation and anion hydration in inorganic nitrates and sometimes not as shown in our results of individual nitrates already given. Using our data we have been able to separate the hydration of cation of anion up to molarities of 4 M. At still higher molarities, short-range forces of the Van der Waals type become important, and solutions begin to resemble the state of a molten salt. When concentrations of 3 or 4 M are reached,

there are barely enough solvent molecules to surround the ions so that competition between ions for the solvent molecules exists. The conditions under which the ion solvent interactions arise are therefore quite different from those effective at lower concentrations. That the least association occurs in $(CH_3)_4N^+NO_3^-$ and not higher alkyl ammonium nitrates is assumed here as an extrapolation of Wirth's (1967) work on alkyl ammonium halides where increasing molecular association for these halides takes place as the alkyl group gets larger. Associations steps postulated should not hide the fact that we do not know the species present nor the physical structure of the solvent. We have also inability to make well founded statements about activity coefficients of aggregates formed.

McCabe and Fisher (1970) plot the hydration spectra for 3 M NaI 3 M Na Br and 3 M NaCl shown in Figure 2-11a. Then they subtract the hydration spectra of 3 M NaCl from 3 M Na and obtain an "hydration difference" spectra shown in Figure 2-11b. This hydration difference spectra is fitted by a Gaussian curve with a maximum at 1.42 μ and a half band width of about 15 mμ. In Figure 2-11c McCabe ascribed this Gaussian to the hydration of the iodide anion when fitting a 3 M NaI hydration spectra since it was possible with the Gaussian found in Figure 2-11b. A second Gaussian found by subtraction of the 3 M Na I hydration spectra was ascribed to the hydration component of the Na^+ cation hydrate present. To study

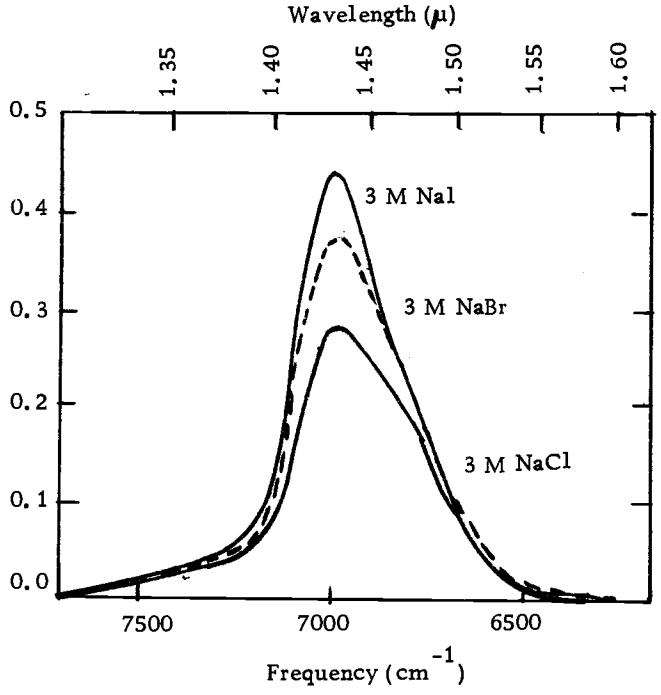

Figure 2-11a

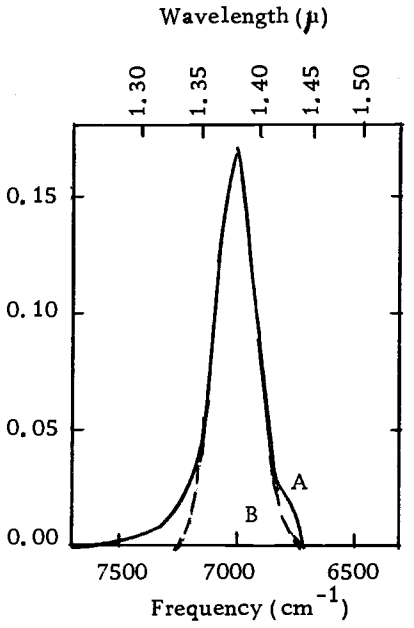

Figure 2-11b

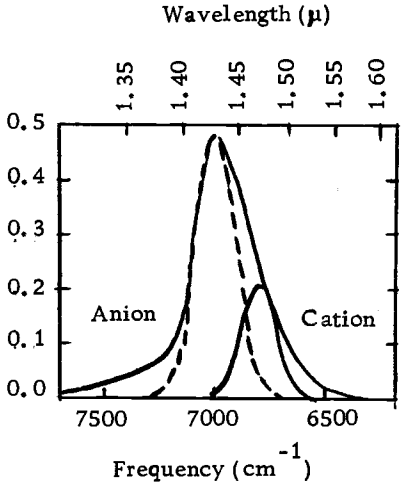

Figure 2-11c

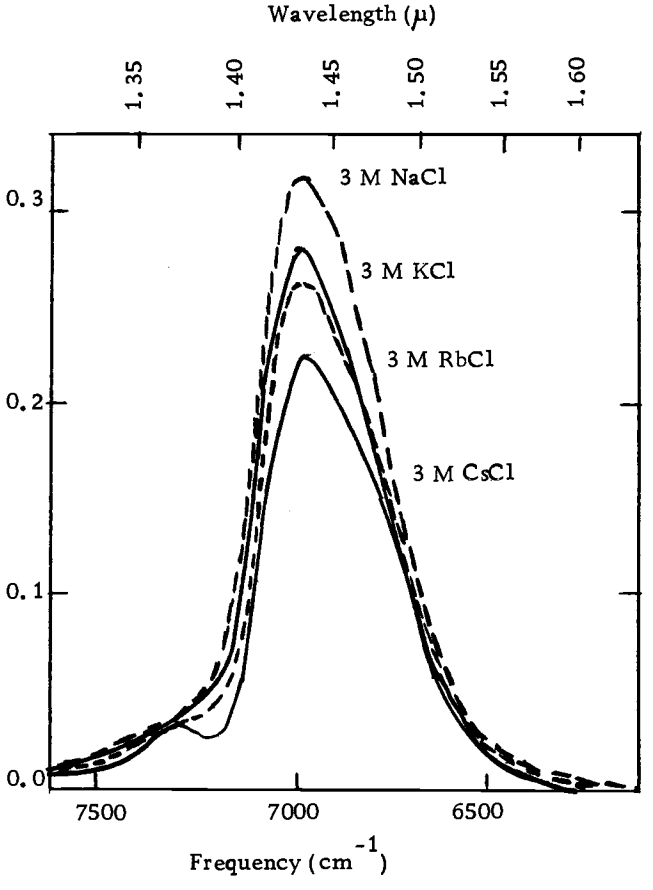

Figure 2-12

the hydration spectra of the cation (which is our interest since the nitrates observed differ in the cation present) the hydration difference spectra have been worked out from Figure 2-12. In Figure 2-13 for the 3 M NaCl-RbCl and KCl-CsCl solutions. The data are presented in Tables 2-14, 15. It is observed, that the position of the maximum of the "difference hydration spectra" this time due to cation absorption is 1.42 μ, that is, the converse assignment that McCabe and Fisher (1970) suggests in their paper. A Gaussian at this position with an half band width of 37 mμ in Figure 2-14 and an 32 mμ in Figure 2-13b would represent the cationic absorption in the hydration spectrum. A Gaussian with λ_o = 1425 mμ, a half band width of 32 mμ and height of OD = 0.06 in Figure 2-14 should fit the hydration of the Cl^- ion by subtraction of the 3 M KCl and 3 M NaCl from the K^+ and Na^+ hydration respectively. This is shown in Figure 2-14 and 2-15. The Cl^- anionic hydration spectrum of 3 M KCl has a maximum of 1435 mμ and $\Delta\lambda_{\frac{1}{2}}$ of 35 mμ. The Cl^- anionic hydration in the 3 M NaCl case has also a maxima at 1435 mμ and a $\Delta\lambda_{\frac{1}{2}}$ of 35 mμ. The anionic hydration is so characterized by a band with a specific position for the maxima and half band width. The values of $\Delta\lambda_{\frac{1}{2}}/A_{max}$ are different for 3 M NaCl and 3 M KCl but we attribute this to the interaction cation-anion and the fact that the hydration spectra of neither cation or anion are pure Gaussians but only approximate ones. The hydration spectra of the different nitrates

Table 2-14

Hydration Difference Spectra of 3M Chloride Solutions (McCabe and Fisher, 1970) Fig. 4

λ [mμ]	Hydration Spectra 3 M KCl	Hydration Spectra 3 M CsCl	Hydration Difference Spectra 3 M KCl-3 M CsCl
1325	0.02	0.01	0.01
1350	0.03	0.02	0.01
1375	0.04	0.03	0.01
1400	0.08	0.04	0.04
1425	0.27	0.21	0.06
1450	0.25	0.20	0.05
1475	0.17	0.15	0.02
1500	0.08	0.07	0.01
1525	0.03	0.03	0.00
1550	0.01	0.01	0.00
1575	0.00	0.00	0.00
1600	0.00	0.00	0.00

Table 2-15

Hydration Difference Spectra of 3 M Chloride Solutions (McCabe and Fisher, 1970) Fig. 4

λ [mμ]	Hydration Spectra 3 M NaCl	Hydration Spectra 3 M RbCl	Hydration Difference Spectra 3 M NaCl-3 M RbCl
1325	0.01	0.01	0.01
1350	0.02	0.02	0.01
1375	0.04	0.03	0.01
1400	0.11	0.06	0.05
1425	0.31	0.25	0.06
1450	0.29	0.24	0.05
1475	0.20	0.16	0.04
1500	0.09	0.08	0.01
1525	0.03	0.02	0.01
1550	0.02	0.01	0.01
1575	0.01	0.00	0.00
1600	0.00	0.00	0.00

Hydration Difference Spectra Cations
(McCabe and Fisher (1970) Figure 4.

(2)-13a)

3 M $NaCl^-$ - 3 M RbCl

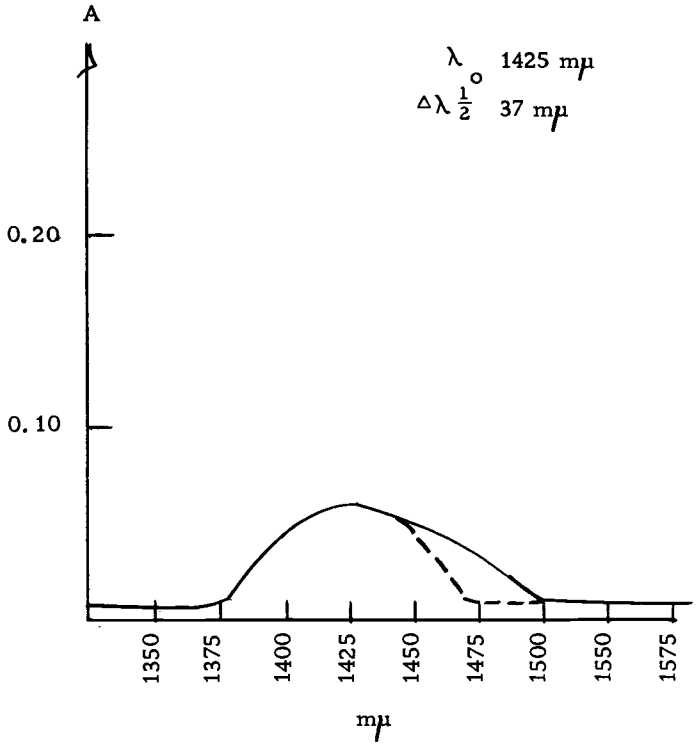

(2)-13b)

3 M K KCl - 3 M CsCl

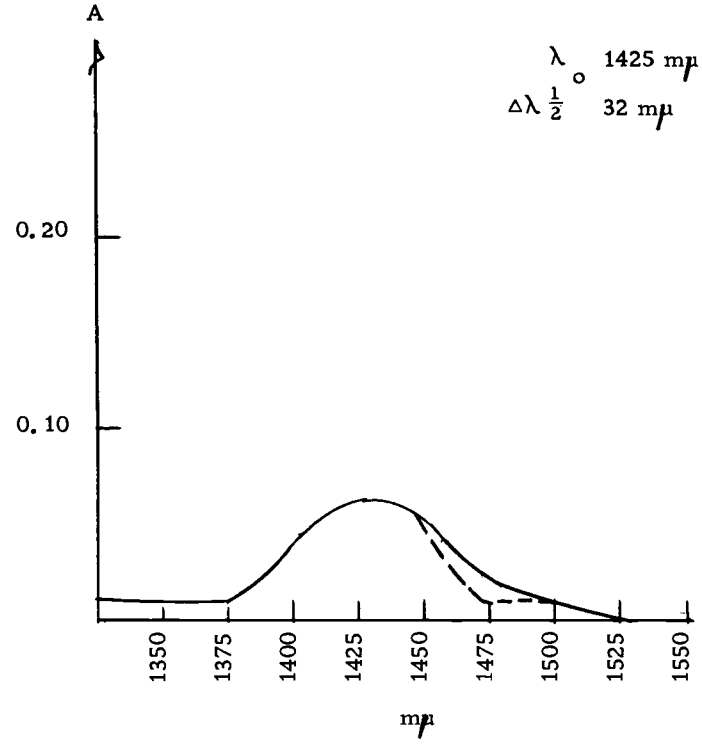

Figure 2-13

Hydration Spectra 3 M KCl
(McNabe and Fisher, 1970)

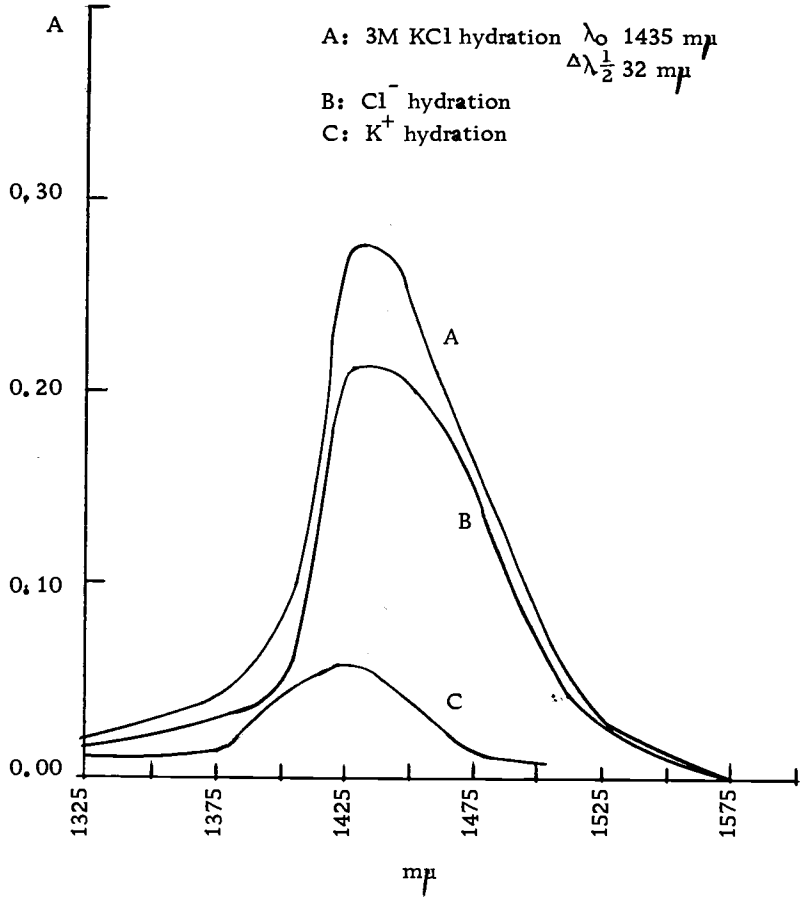

Figure 2-14

Hydration Spectra 3 M NaCl
(McNabe and Fisher, 1970)

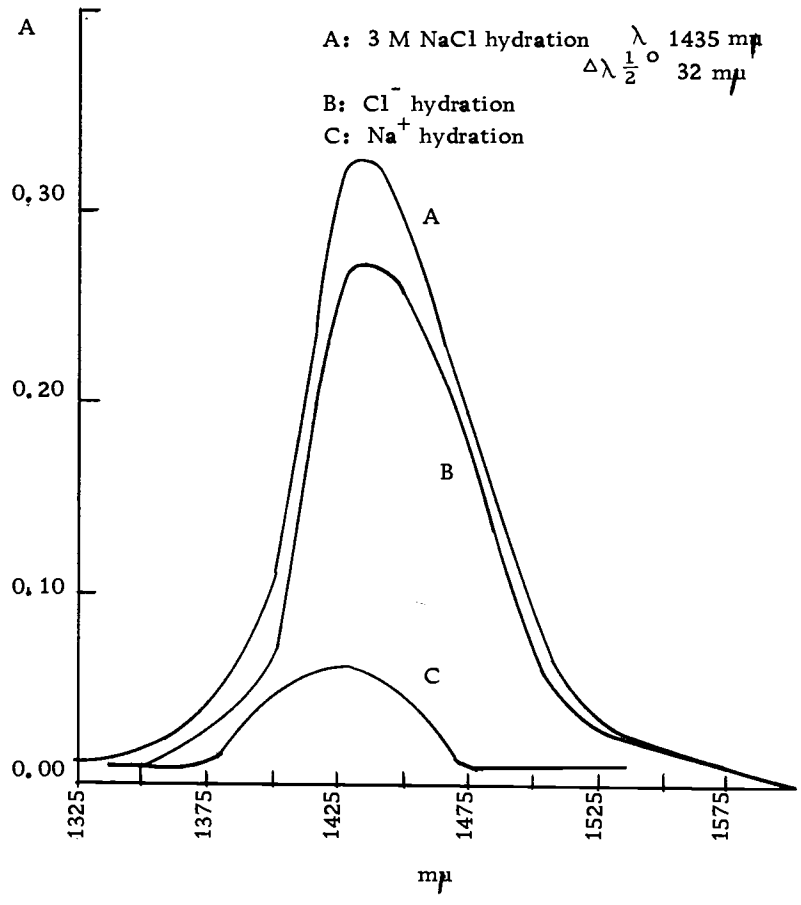

Figure 2-15

have been determined in the same way shown in Figure 2-2 for an 8 M $NaNO_3$ solution.

The $LiNO_3$ solutions are shown in Figures 2-16 and 2-17. The pertinent data are presented in Tables 2-16 through 2-21. The maximum is around 1430 mμ for all spectra and the tail in the right hand side diminishes as we go up in concentration. In Figures 2-18 and 2-19 are presented the hydration spectra of $NaNO_3$ solutions. The values are reported in Tables 2-22 through 2-28. The trend in the shape and the peak is the same as observed in the $LiNO_3$ solutions. The hydration spectra of the KNO_3 solution is shown in Figure 2-20. The values are reported in Tables 2-29 through 2-33. In Figure 2-21 hydration spectra of $CsNO_3$ solutions are shown. The values are reported in Tables 2-34 through 2-36. In Figures 2-22 and 2-23 are shown the hydration spectra of $Ca(NO_3)_2$. The values are reported in Tables 2-37 through 2-43. The hydration spectra of $(CH_3)_4NNO_3$, which have a different shape to the inorganic nitrates, are presented in Figure 2-24. The values are reported in Tables 2-44 through 2-48. The hydration spectra of NH_4NO_3 are to be found in Figure 2-25. The values are reported in Tables 2-49 through 2-54.

The hydration spectra reported by McCabe and Fisher (1970) in Figure 2-11b are for "anion hydration" with a maxima at 1.43 μ and a half band width of 23 mμ. This Gaussian represent an iodide-hydrate in the 3 M NaI hydration spectra (Figure 2-11). A small

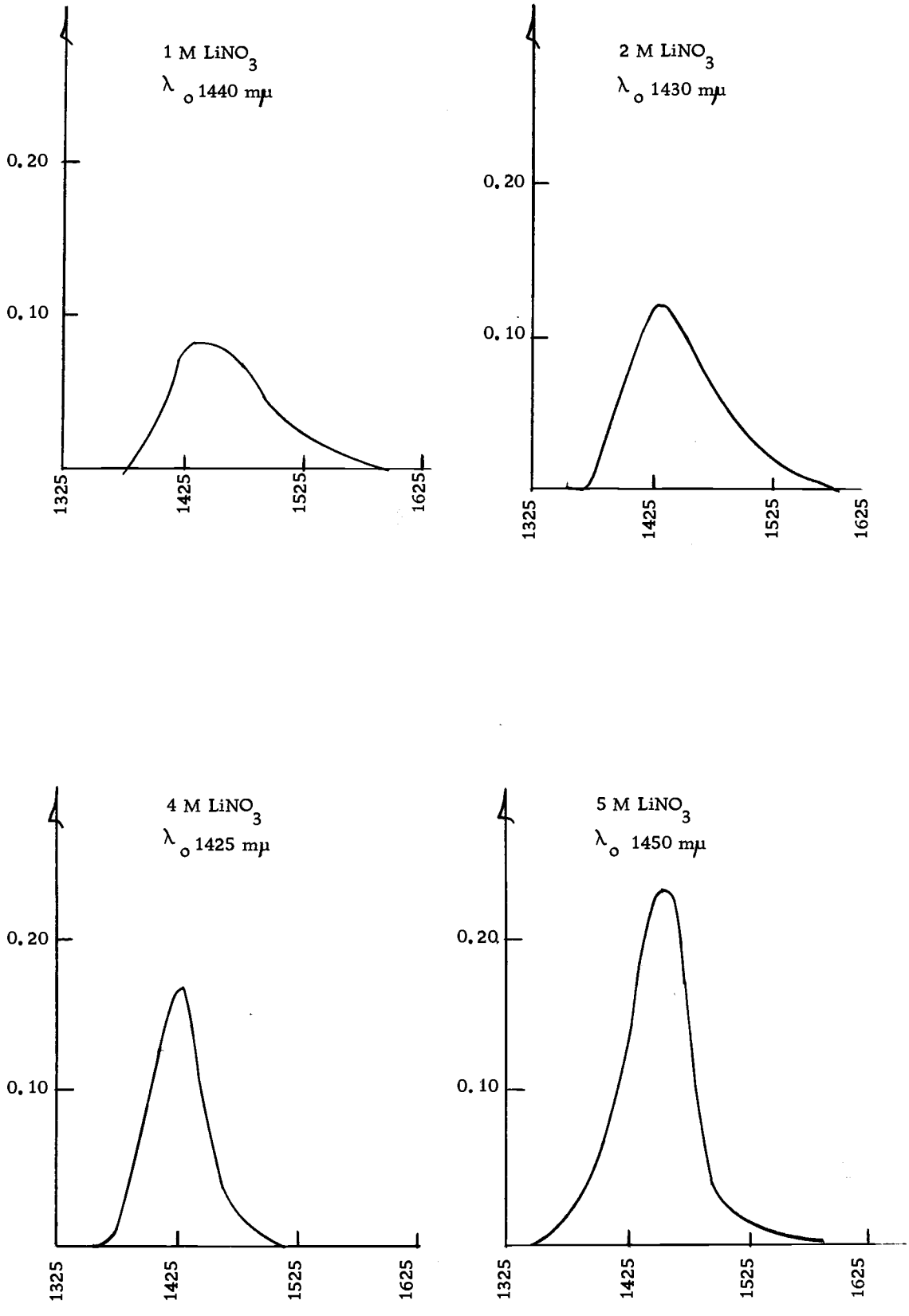
1 M LiNO3
λ o 1440 mμ
0.20
0.10
1325
1425
1525
1625
2 M LiNO3
λ o 1430 mμ
0.20
0.10
1325
1425
1525
1625
4 M LiNO3
λ o 1425 mμ
0.20
0.10
1325
1425
1525
1625
5 M LiNO3
λ o 1450 mμ
0.20
0.10
1325
1425
1525
1625

Figure 2-16

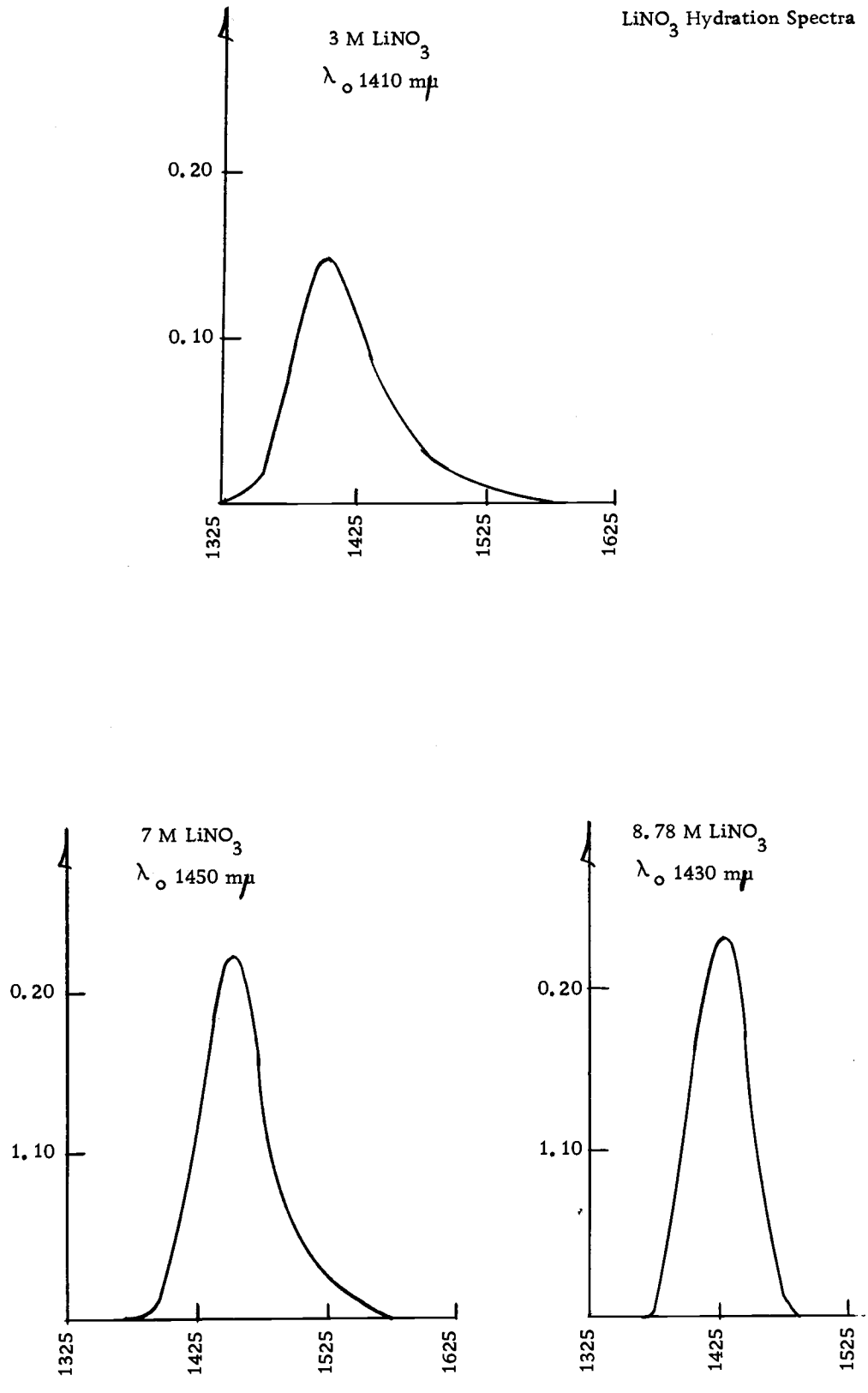
LiNO3 Hydration Spectra
3 M LiNO3
λo 1410 mμ
0.20
0.10
1325
1425
1525
1625
7 M LiNO3
λo 1450 mμ
0.20
1.10
1325
1425
1525
1625
8.78 M LiNO3
λo 1430 mμ
0.20
1.10
1325
1425
1525

Figure 2-17

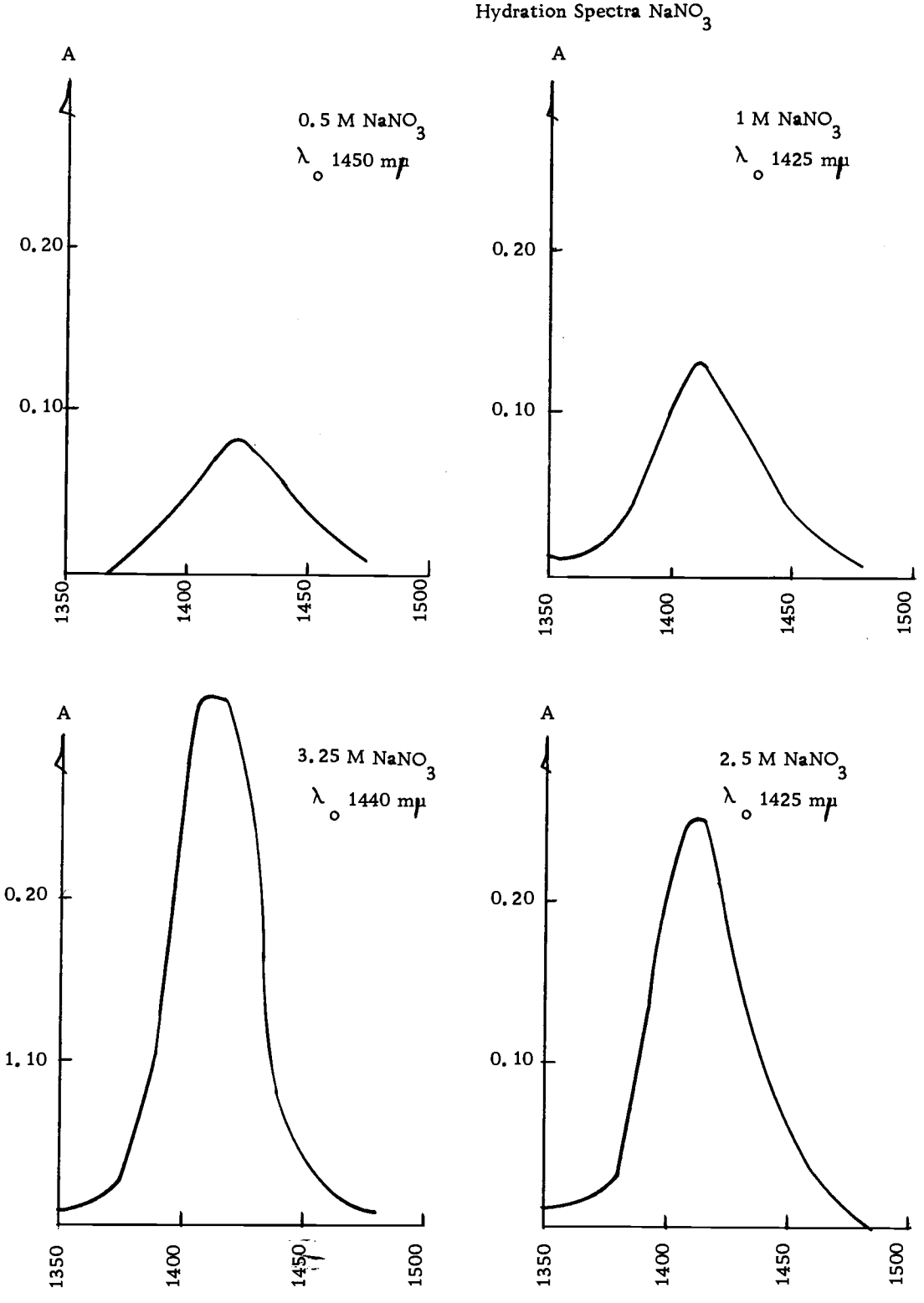
Hydration Spectra $NaNO_3$
A
0.5 M $NaNO_3$
λ_o 1450 mμ
0.20
0.10
1350
1400
1450
1500
A
1 M $NaNO_3$
λ_o 1425 mμ
0.20
0.10
1350
1400
1450
1500
A
3.25 M $NaNO_3$
λ_o 1440 mμ
0.20
1.10
1350
1400
1450
1500
A
2.5 M $NaNO_3$
λ_o 1425 mμ
0.20
0.10
1350
1400
1450
1500

Figure 2-18

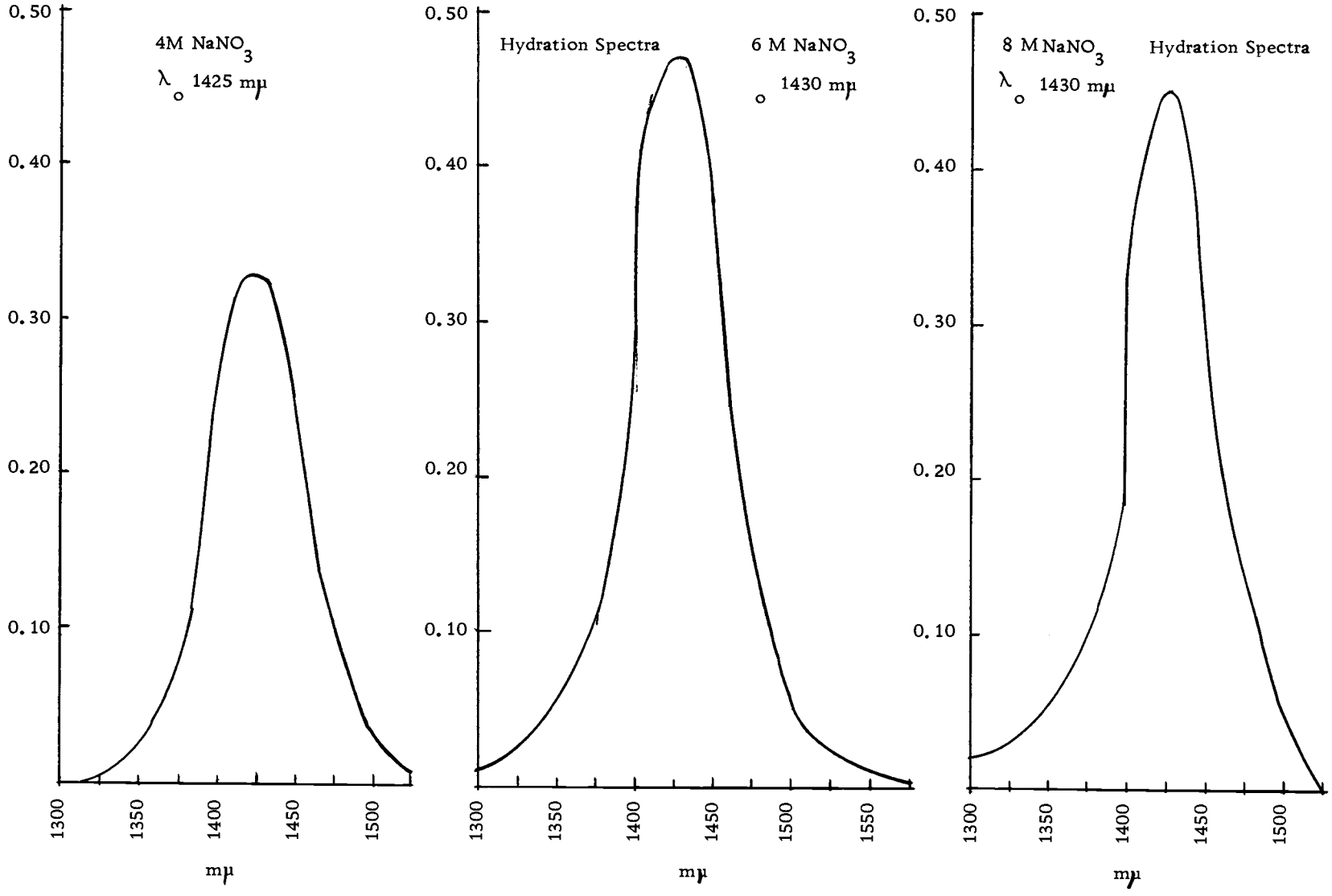
0.50
0.40
0.30
0.20
0.10
4M NaNO3
λo 1425 mμ
1300
1350
1400
1450
1500
mμ
Hydration Spectra
6 M NaNO3
λo 1430 mμ
1550
8 M NaNO3
Hydration Spectra
λo 1430 mμ

Figure 2-19

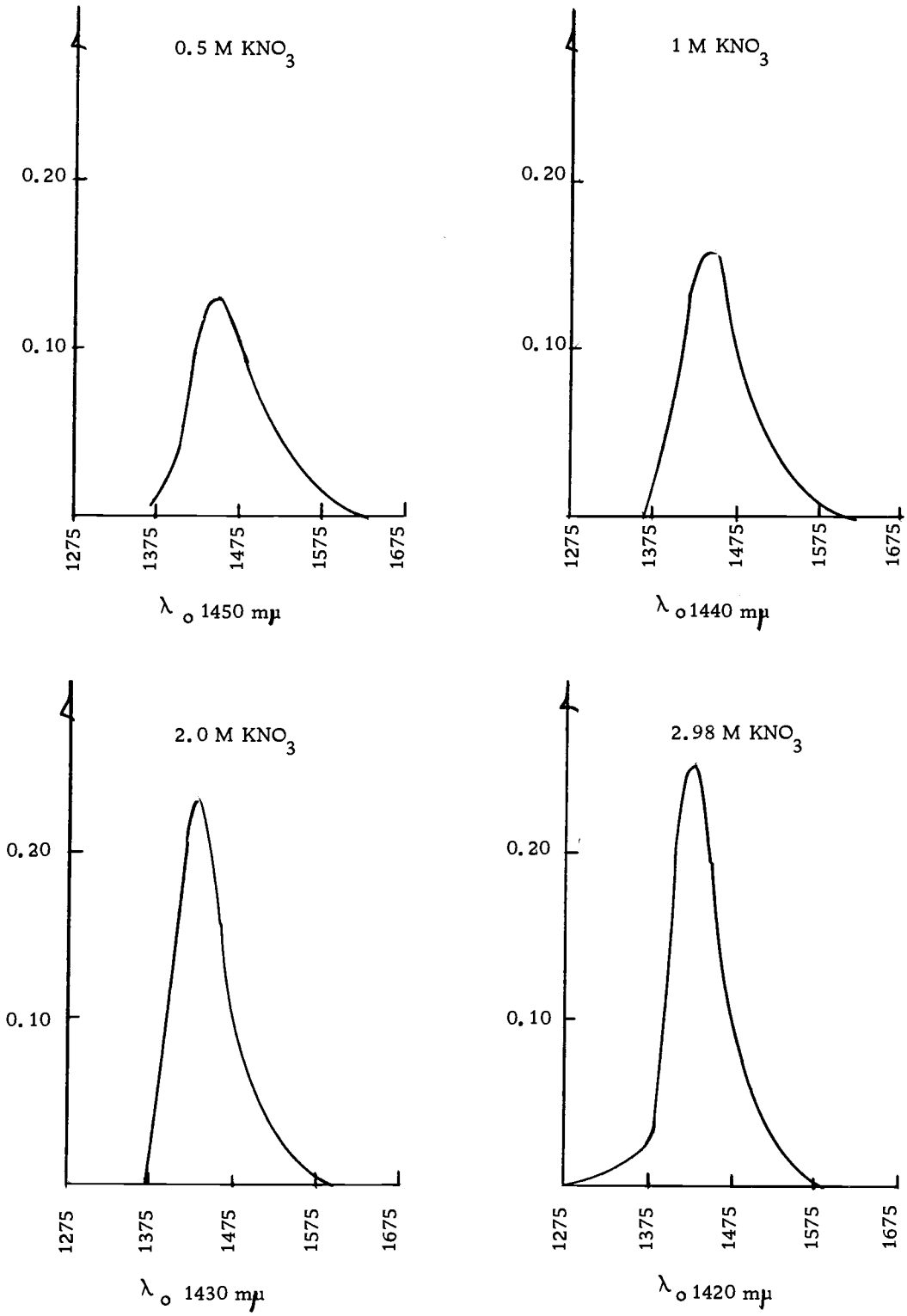

Figure 2-20. Hydration Spectra KNO_3.

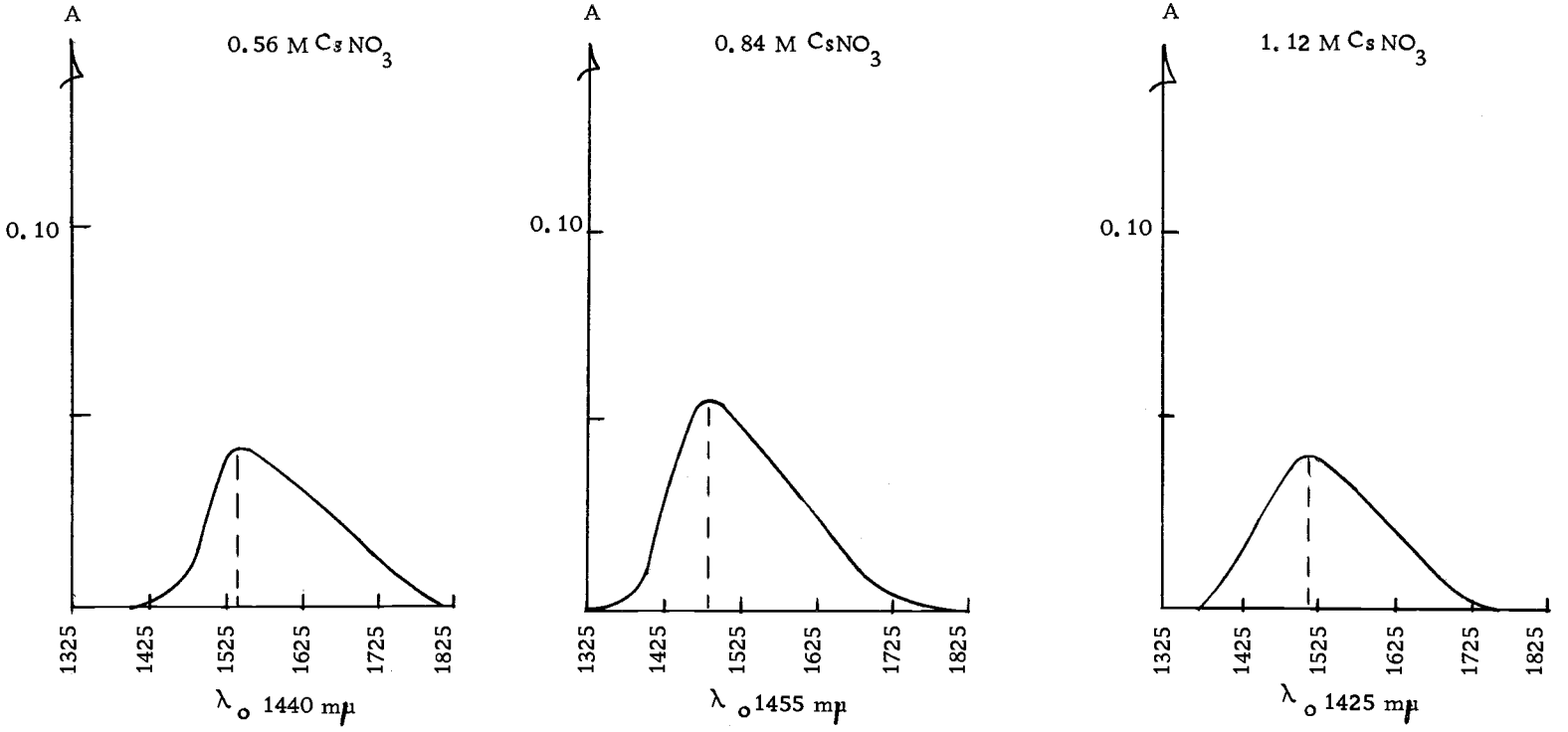

Figure 2-21. $CsNO_3$ Hydration Spectra.

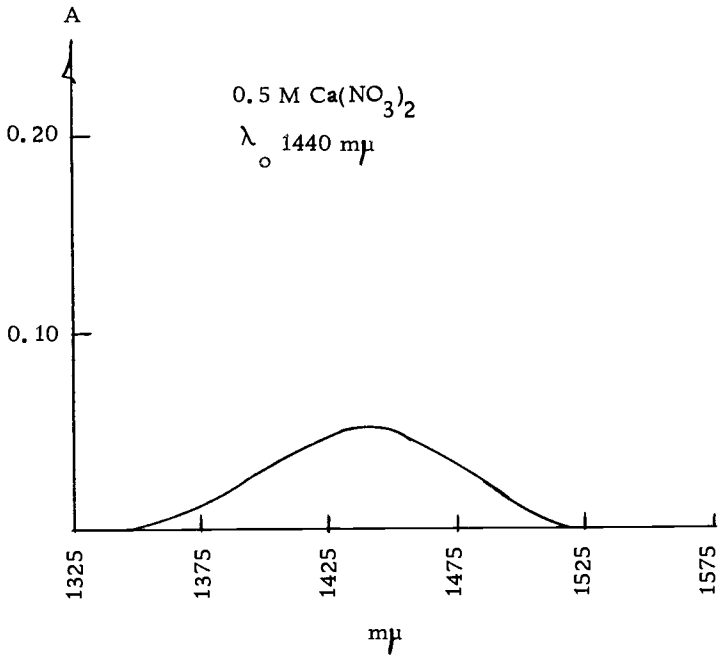
A
0.5 M Ca(NO3)2
λo 1440 mμ
0.20
0.10
1325
1375
1425
1475
1525
1575
mμ

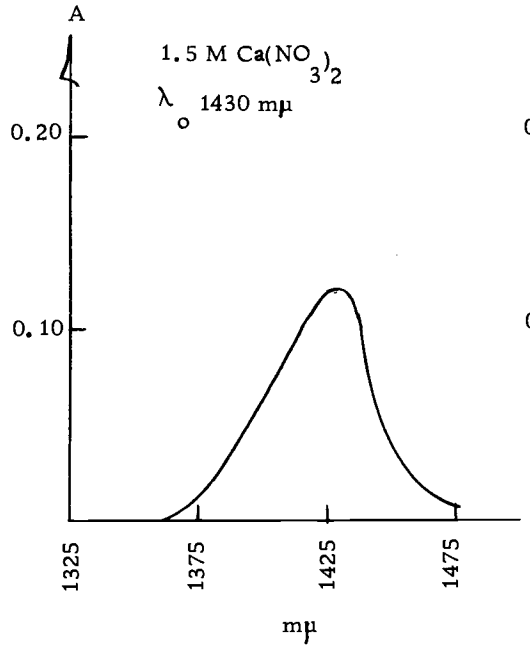
A
1.5 M Ca(NO3)2
λo 1430 mμ
0.20
0.10
1325
1375
1425
1475
mμ

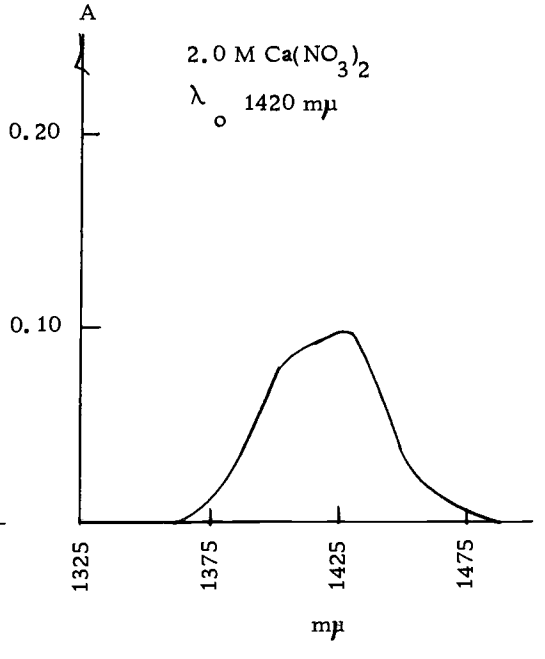
A
2.0 M Ca(NO3)2
λo 1420 mμ
0.20
0.10
1325
1375
1425
1475
mμ

Figure 2-22

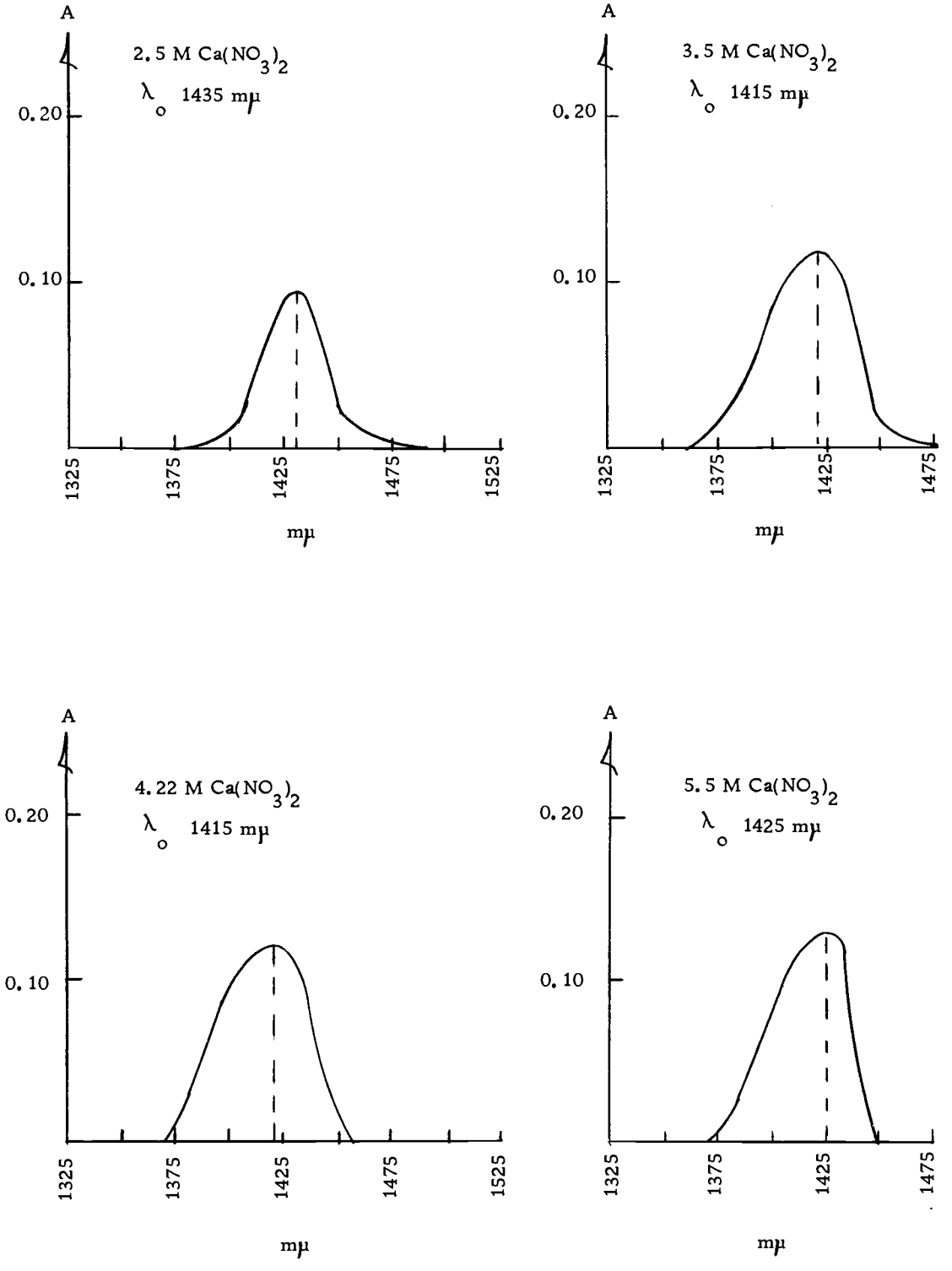

Figure 2-23. Hydration Spectra $Ca(NO_3)_2$.

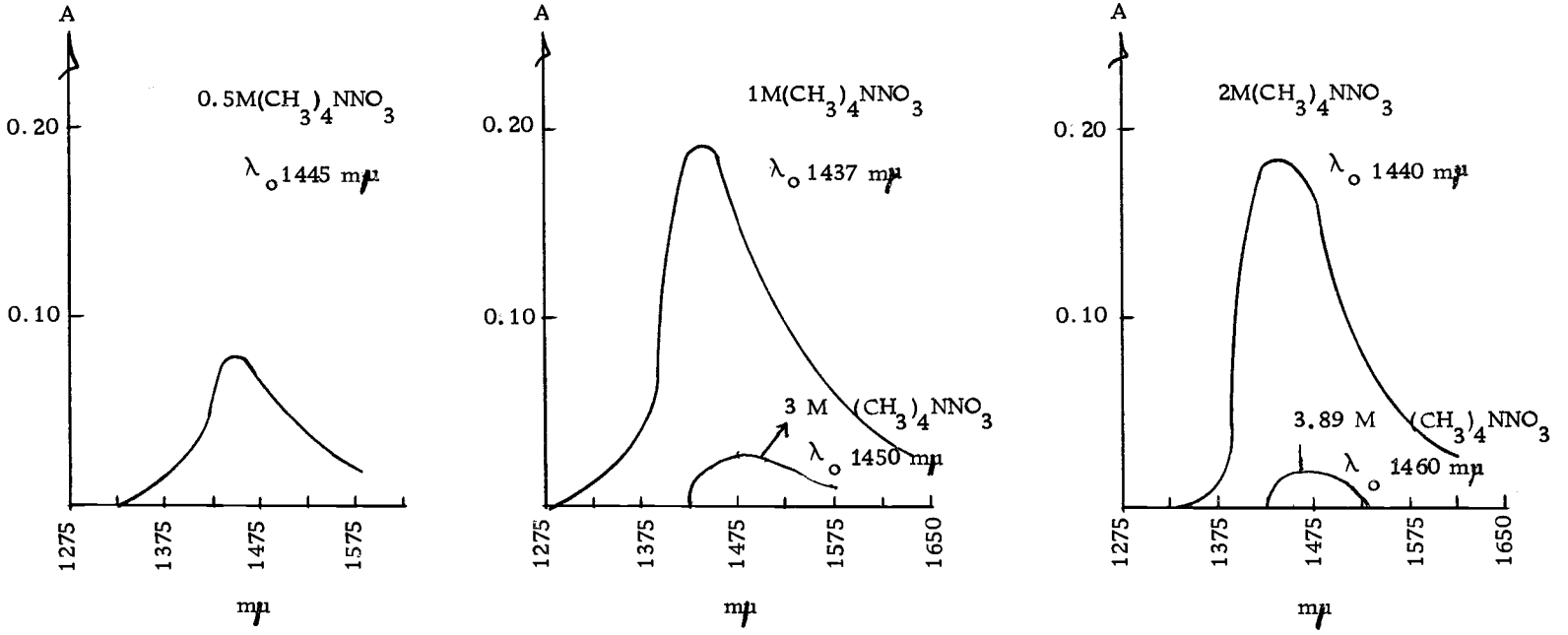

Figure 2 - 24. $(CH_3)_4NNO_3$ hydration spectra.

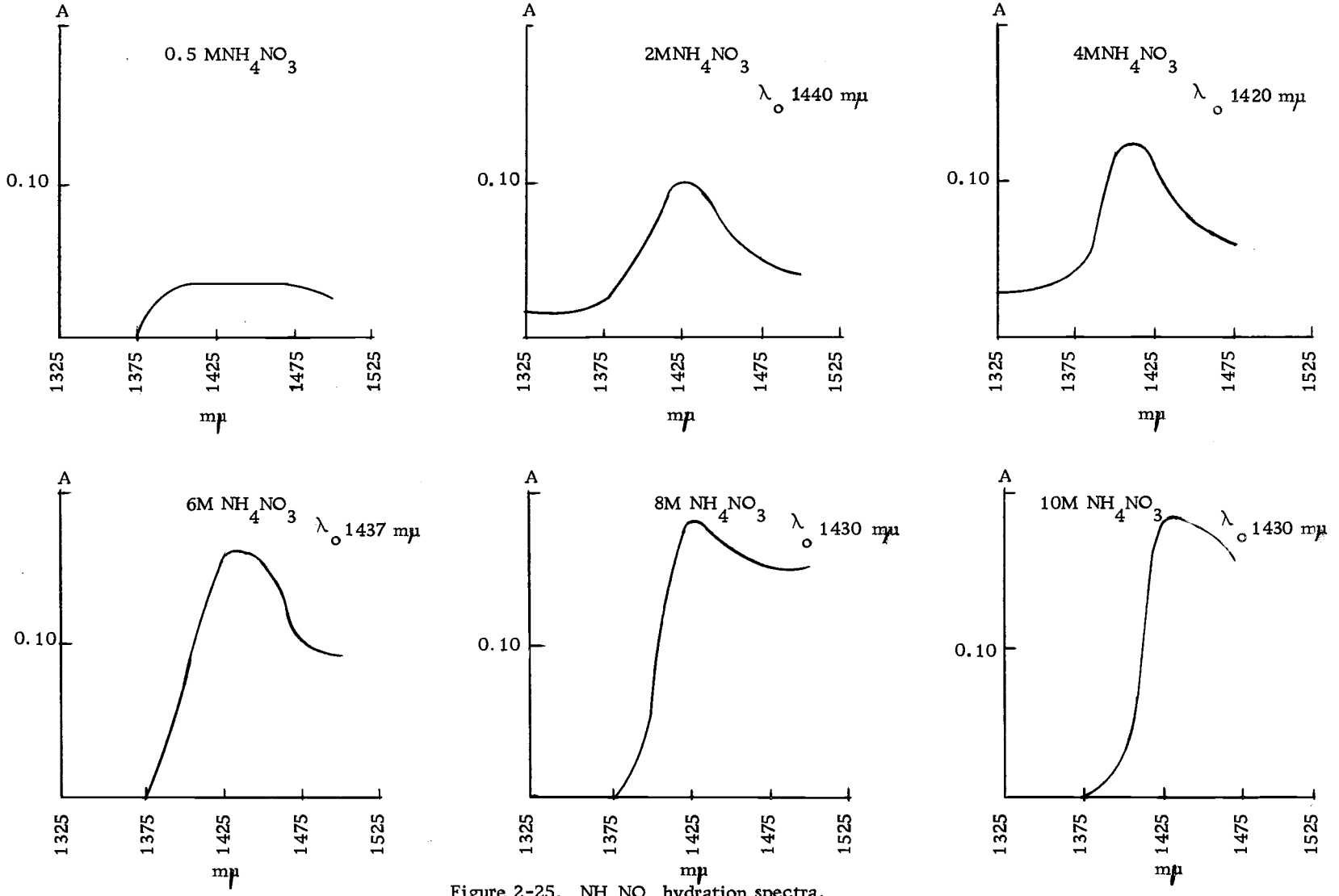

Figure 2-25. NH_4NO_3 hydration spectra.

Table 2-16
$LiNO_3$ 1.0 M Hydration Spectra

λ [mμ]	Spectra H_2O[a]	Spectra B (0.077 · a)	Spectra A	Spectra C = B - A
1325	0.12	0.01	0.01	0.00
1375	0.27	0.02	0.02	0.00
1400	0.83	0.06	0.03	0.03
1425	1.30	0.10	0.02	0.08
1450	1.43	0.11	0.03	0.08
1475	1.25	0.10	0.04	0.06
1500	0.93	0.07	0.04	0.03
1525	0.70	0.05	0.03	0.02
1575	0.42	0.03	0.02	0.01
1625	0.32	0.02	0.01	0.01
1675	0.26	0.02	0.00	0.00

Table 2-17
2 M $LiNO_3$ Hydration Spectra

λ mμ	Spectra H_2O[a]	Spectra B (0.144 · a)	Spectra A	Spectra C = B - A
1325	0.12	0.02	0.02	0.00
1375	0.27	0.04	0.04	0.00
1400	0.83	0.12	0.05	0.07
1425	1.30	0.19	0.07	0.12
1450	1.43	0.21	0.11	0.10
1475	1.25	0.18	0.12	0.06
1500	0.93	0.13	0.10	0.03
1525	0.70	0.10	0.08	0.02
1575	0.42	0.06	0.05	0.01
1625	0.32	0.04	0.04	0.00
1675	0.26	0.03	0.03	0.00

Table 2-18a
3 M $LiNO_3$ Hyrdration Spectra

λ [mμ]	Spectra H_2O[a]	Spectra B (0.200 · a)	Spectra A	Spectra C = B - A
1325	0.12	0.02	0.02	0.00
1375	0.27	0.05	0.00	0.00
1400	0.83	0.17	0.08	0.09
1425	1.30	0.26	0.11	0.15
1450	1.43	0.29	0.18	0.11
1475	1.25	0.25	0.19	0.06
1500	0.93	0.19	0.16	0.03
1525	0.70	0.14	0.12	0.02
1575	0.42	0.08	0.07	0.01
1625	0.32	0.06	0.05	0.01
1675	0.26	0.05	0.05	0.00

Table 2-18b
4 M $LiNO_3$ Hydration Spectra

λ [mμ]	Spectra H_2O[a]	Spectra B (0.231 · a)	Spectra A	Spectra C = B - A
1325	0.12	0.03	0.03	0.00
1375	0.27	0.06	0.05	0.01
1400	0.83	0.19	0.11	0.08
1425	1.30	0.30	0.13	0.17
1450	1.43	0.33	0.24	0.09
1475	1.25	0.29	0.27	0.01
1500	0.93	0.22	0.23	0.00
1525	0.70	0.19	0.19	0.00
1575	0.42	0.07	0.07	0.00
1625	0.32	0.07	0.07	0.00
1675	0.26	0.06	0.06	0.00

Table 2-19

5 M $LiNO_3$ Hydration Spectra

λ [mμ]	Spectra H_2O[a]	Spectra B (0.307 · a)	Spectra A	Spectra C = B - A
1325	0.12	0.04	0.04	0.00
1375	0.27	0.08	0.06	0.02
1400	0.83	0.25	0.11	0.14
1425	1.30	0.40	0.17	0.23
1450	1.43	0.44	0.30	0.14
1475	1.25	0.38	0.35	0.13
1500	0.93	0.29	0.29	0.00
1525	0.70	0.21	0.21	0.00
1575	0.47	0.13	0.13	0.00
1625	0.32	0.09	0.09	0.00
1675	0.26	0.07	0.07	0.00

Table 2-20

7 M $LiNO_3$ Hydration Spectra

λ [mμ]	Spectra H_2O[a]	Spectra B (0.423 · a)	Spectra A	Spectra C = B - A
1325	0.12	0.05	0.05	0.00
1375	0.77	0.11	0.10	0.01
1400	0.83	0.35	0.23	0.12
1475	1.30	0.55	0.33	0.22
1450	1.43	0.60	0.49	0.11
1475	1.25	0.53	0.48	0.05
1500	0.93	0.40	0.38	0.02
1525	0.70	0.29	0.28	0.01
1575	0.42	0.18	0.18	0.00
1625	0.32	0.13	0.13	0.00
1675	0.26	0.11	0.11	0.00

Table 2-21

8.78 M $LiNO_3$ Hydration Spectra

λ [mμ]	Spectra H_2O[a]	Spectra B (0.461· a)	Spectra A	Spectra C = B - A
1325	0.12	0.04	0.04	0.00
1375	0.27	0.12	0.12	0.00
1400	0.83	0.38	0.28	0.10
1425	1.30	0.60	0.37	0.23
1450	1.43	0.66	0.55	0.11
1475	1.25	0.58	0.58	0.00

Table 2-22
0.5 M $NaNO_3$ Hydration Spectra

λ [mμ]	Spectra H_2O[a]	Spectra B (0.057 · a)	Spectra A	Spectra C = B - A
1300	0.08	0.00	0.00	0.00
1350	0.17	0.01	0.00	0.01
1400	0.93	0.05	0.00	0.05
1425	1.30	0.07	0.00	0.07
1450	1.43	0.08	0.00	0.08
1475	1.25	0.07	0.01	0.06
1500	0.93	0.05	0.02	0.03
1525	0.70	0.03	0.01	0.02
1575	0.42	0.02	0.01	0.01
1625	0.32	0.02	0.02	0.00
1675	0.26	0.01	0.01	0.00

Table 2-23
1 M $NaNO_3$ Hydration Spectra

λ mμ	Spectra H_2O[a]	Spectra B (0.107 · a)	Spectra A	Spectra C = B - A
1300	0.08	0.01	0.00	0.01
1350	0.17	0.02	0.00	0.02
1400	0.93	0.10	0.00	0.10
1425	1.30	0.14	0.01	0.13
1450	1.43	0.15	0.05	0.10
1475	1.25	0.13	0.06	0.07
1500	0.93	0.10	0.06	0.04
1525	0.70	0.07	0.05	0.02
1575	0.42	0.07	0.03	0.01
1625	0.32	0.03	0.03	0.00
1675	0.26	0.02	0.02	0.00

Table 2-24
2.5 M $NaNO_3$ Hydration Spectra

λ [mμ]	Spectra H_2O[a]	Spectra B (0.257 · a)	Spectra A	Spectra C = B - A
1300	0.08	0.02	0.01	0.01
1350	0.17	0.04	0.02	0.02
1400	0.93	0.24	0.04	0.20
1425	1.30	0.33	0.08	0.25
1450	1.43	0.37	0.18	0.19
1475	1.25	0.32	0.21	0.11
1500	0.93	0.24	0.18	0.06
1.525	0.70	0.18	0.14	0.04
1.575	0.42	0.10	0.09	0.01
1.625	0.32	0.08	0.08	0.00
1.675	0.26	0.07	0.07	0.00

Table 2-25
3.25 M $NaNO_3$ Hydration Spectra

λ [mμ]	Spectra H_2O[a]	Spectra B (0.315 · a)	Spectra A	Spectra C = B - A
1300	0.08	0.03	0.02	0.01
1350	0.17	0.05	0.03	0.02
1400	0.93	0.29	0.07	0.22
1425	1.30	0.41	0.11	0.30
1450	1.43	0.45	0.18	0.26
1475	1.25	0.39	0.27	0.08
1500	0.93	0.29	0.25	0.04
1525	0.70	0.22	0.20	0.02
1575	0.42	0.13	0.12	0.01
1625	0.32	0.10	0.10	0.00
1675	0.26	0.08	0.08	0.00

Table 2-26
4 M $NaNO_3$ Hydration Spectra

λ [mμ]	Spectra H_2O[a]	Spectra B (0.365)	Spectra A	Spectra C = B - A
1300	0.08	0.03	0.03	0.00
1350	0.17	0.05	0.03	0.02
1400	0.93	0.34	0.09	0.25
1425	1.30	0.41	0.11	0.33
1450	1.43	0.45	0.23	0.22
1475	1.25	0.40	0.33	0.11
1500	0.93	0.34	0.31	0.03
1525	0.70	0.26	0.25	0.01
1575	0.42	0.15	0.16	0.00
1625	0.32	0.12	0.12	0.00
1675	0.26	0.09	0.10	0.00

Table 2-27
6 M $NaNO_3$ Hydration Spectra

λ mμ	Spectra H_2O[a]	Spectra B (0.500 · a)	Spectra A	Spectra C = B - A
1300	0.08	0.04	0.03	0.01
1350	0.17	0.09	0.04	0.05
1400	0.93	0.46	0.14	0.32
1425	1.30	0.65	0.18	0.47
1450	1.43	0.72	0.34	0.38
1475	1.25	0.62	0.45	0.17
1500	0.93	0.46	0.42	0.04
1525	0.70	0.35	0.34	0.02
1575	0.42	0.21	0.21	0.00
1625	0.32	0.16	0.16	0.00
1675	0.26	0.13	0.14	0.00

Table 2-28
7.85 M $NaNO_3$ Hydration Spectra

λ [mμ]	Spectra H_2O[a]	Spectra B (0.596 · a)	Spectra A	Spectra C = B - A
1300	0.08	0.05	0.03	0.02
1350	0.17	0.10	0.05	0.05
1400	0.93	0.55	0.23	0.22
1425	1.30	0.78	0.33	0.45
1450	1.43	0.85	0.57	0.28
1475	1.25	0.75	0.60	0.15
1500	0.93	0.55	0.51	0.04
1525	0.70	0.47	0.49	0.00
1575	0.42	0.25	0.24	0.00
1625	0.32	0.19	0.18	0.00
1675	0.26	0.15	0.16	0.00

Table 2-29
Hydration Spectra 0.5 M KNO_3

λ mμ	Spectra H_2O[a]	Spectra B (0.081 · a)	Spectra A	Spectra C = B - A
1275	0.07	0.01	0.00	0.00
1325	0.12	0.01	0.01	0.00
1375	0.27	0.04	0.03	0.00
1400	0.83	0.07	0.04	0.03
1425	1.30	0.12	0.02	0.10
1450	1.43	0.14	0.01	0.13
1475	1.25	0.12	0.02	0.10
1500	0.93	0.09	0.02	0.07
1525	0.70	0.07	0.03	0.04
1575	0.42	0.03	0.02	0.00
1625	0.32	0.02	0.02	0.00
1685	0.26	0.02	0.02	0.00

Table 2-30
1.0 M KNO_3 Hydration Spectra

λ mμ	Spectra H_2O	Spectra B (0.146· a)	Spectra A	Spectra C = B - A
1.275	0.07	0.01	0.01	0.00
1.325	0.12	0.02	0.02	0.00
1375	0.27	0.04	0.03	0.01
1400	0.83	0.12	0.05	0.07
1425	1.30	0.19	0.04	0.15
1450	1.43	0.21	0.06	0.15
1475	1.25	0.18	0.08	0.10
1500	0.93	0.14	0.08	0.06
1525	0.70	0.10	0.07	0.03
1575	0.42	0.06	0.05	0.01
1625	0.32	0.04	0.04	0.00
1675	0.26	0.07	0.04	0.00

Table 2-31
Hydration Spectra 2.0 M KNO_3

λ mμ	Spectra H_2O[a]	Spectra B (0.230· a)	Spectra A	Spectra C = B - A
1275	0.07	0.02	0.02	0.00
1325	0.12	0.03	0.02	0.01
1375	0.27	0.06	0.05	0.01
1400	0.83	0.19	0.06	0.13
1425	1.30	0.30	0.07	0.23
1450	1.43	0.33	0.15	0.18
1475	1.25	0.29	0.18	0.11
1500	0.93	0.21	0.17	0.04
1525	0.70	0.16	0.14	0.02
1575	0.42	0.10	0.09	0.01
1625	0.32	0.07	0.07	0.00
1675	0.26	0.06	0.06	0.00

Table 2-33
2.98 M Hydration Spectra KNO_3

λ mμ	Spectra H_2O[a]	Spectra B (0.303 · a)	Spectra A	Spectra C = B - A
1275	0.07	0.02	0.00	0.00
1325	0.12	0.04	0.02	0.01
1375	0.27	0.08	0.07	0.01
1400	0.83	0.25	0.09	0.16
1425	1.30	0.40	0.15	0.25
1450	1.43	0.43	0.25	0.18
1475	1.25	0.38	0.27	0.11
1500	0.93	0.28	0.24	0.04
1525	0.70	0.21	0.19	0.02
1575	0.42	0.13	0.12	0.01
1625	0.32	0.10	0.19	0.01
1675	0.26	0.08	0.08	0.00

Table 2-34
Hydration Spectra 0.56 M $CsNO_3$

$\lambda_{m\mu}$	Spectra H_2O[a]	Spectra B (0.077 · a)	Spectra A	Spectra C = B - A
1325	0.12	0.01	0.01	0.00
1375	0.27	0.02	0.02	0.00
1400	0.83	0.06	0.03	0.03
1425	1.30	0.10	0.02	0.08
1450	1.43	0.11	0.03	0.07
1475	1.25	0.10	0.03	0.07
1500	0.93	0.07	0.03	0.04
1525	0.70	0.05	0.03	0.02
1575	0.42	0.03	0.02	0.01

Table 2-35
$CsNO_3$ 0.84 M Hydration Spectra

$\lambda_{m\mu}$	Spectra H_2O[a]	Spectra B (0.107 · a)	Spectra A	Spectra C = B - A
1325	0.12	0.01	0.01	0.00
1375	0.27	0.03	0.03	0.00
1400	0.83	0.09	0.04	0.05
1425	1.30	0.14	0.03	0.11
1450	1.43	0.15	0.06	0.09
1475	1.25	0.13	0.06	0.07
1500	0.93	0.10	0.06	0.04
1525	0.70	0.07	0.05	0.02
1575	0.42	0.04	0.04	0.00

Table 2-36
1.12 M $CsNO_3$ Hydration Spectra

$\lambda_{m\mu}$	Spectra H_2O[a]	Spectra B (0.109)	Spectra A	Spectra C = A - B
1325	0.12	0.01	0.01	0.00
1375	0.27	0.03	0.03	0.00
1400	0.83	0.09	0.06	0.03
1425	1.30	0.14	0.06	0.08
1450	1.43	0.16	0.10	0.06
1475	1.25	0.14	0.10	0.04
1500	0.93	0.10	0.09	0.01
1525	0.70	0.08	0.08	0.00
1575	0.42	0.05	0.05	0.00

Table 2-37
0.5 M $Ca(NO_3)_2$ Hydration Spectra

λ [mμ]	Spectra H_2O[a]	Spectra B (0.038 · a)	Spectra A	Spectra C = B - A
1325	0.12	0.01	0.00	0.00
1375	0.27	0.01	0.00	0.01
1425	1.30	0.05	0.00	0.05
1450	1.43	0.05	0.00	0.05
1475	1.25	0.05	0.02	0.03
1500	0.93	0.04	0.03	0.01
1525	0.70	0.03	0.03	0.00
1575	0.42	0.02	0.02	0.00
1625	0.32	0.01	0.01	0.00
1675	0.26	0.01	0.00	0.00

Table 2-38
1.5 M $Ca(NO_3)_2$ Hydration Spectra

λ [mμ]	Spectra H_2O[a]	Spectra B (0.133 · a)	Spectra A	Spectra C = B - A
1325	0.12	0.02	0.02	0.00
1375	0.27	0.06	0.05	0.01
1425	1.30	0.17	0.09	0.08
1450	1.43	0.19	0.16	0.03
1475	1.25	0.17	0.16	0.01
1500	0.93	0.12	0.13	0.00
1525	0.70	0.09	0.09	0.00
1575	0.42	0.05	0.04	0.00
1625	0.32	0.04	0.03	0.00
1675	0.26	0.03	0.02	0.00

Table 2-39
2.0 $Ca(NO_3)_2$ Hydration Spectra

λ [mμ]	Spectra H_2O[a]	Spectra B (0.177 · a)	Spectra A	Spectra C = B - A
1325	0.12	0.02	0.02	0.00
1375	0.27	0.05	0.05	0.01
1400	0.93	0.16	0.08	0.08
1425	1.30	0.23	0.13	0.10
1450	1.43	0.25	0.22	0.03
1475	1.25	0.22	0.21	0.01
1500	0.93	0.16	0.17	0.00
1525	0.70	0.12	0.13	0.00
1575	0.42	0.07	0.06	0.00
1625	0.32	0.05	0.04	0.00
1675	0.26	0.04	0.04	0.00

Table 2-40
2.5 M $Ca(NO_3)_2$ Hydration Spectra

λ [mμ]	Spectra H_2O[a]	Spectra B (0.215·a)	Spectra A	Spectra C = (B-A)
1325	0.12	0.03	0.03	0.00
1375	0.27	0.08	0.08	0.00
1400	0.93	0.19	0.11	0.01
1425	1.30	0.28	0.19	0.09
1450	1.43	0.30	0.28	0.02
1475	1.25	0.27	0.27	0.00
1500	0.93	0.20	0.20	0.00
1525	0.42	0.09	0.08	0.00
1625	0.32	0.07	0.06	0.00
1675	0.26	0.06	0.05	0.00

Table 2-41
3.5 M $Ca(NO_3)_2$ Hydration Spectra

λ [mμ]	Spectra H_2O[a]	Spectra B (0.292 · a)	Spectra A	Spectra C=B-A
1325	0.12	0.03	0.03	0.00
1375	0.27	0.08	0.08	0.00
1400	0.93	0.26	0.18	0.08
1425	1.30	0.39	0.27	0.12
1450	1.43	0.42	0.41	0.01
1475	1.25	0.39	0.40	0.00
1500	0.93	0.29	0.31	0.00
1525	0.70	0.23	0.23	0.00

Table 2-42
4.22 M $Ca(NO_3)_2$ Hydration Spectra

λ [mμ]	Spectra H_2O[a]	Spectra B (0.346 a)	Spectra A	Spectra C=B-A
1325	0.12	0.04	0.04	0.00
1375	0.27	0.09	0.10	0.00
1400	0.93	0.32	0.22	0.10
1425	1.30	0.45	0.33	0.12
1450	1.43	0.49	0.49	0.00
1475	1.25	0.43	0.43	0.00
1500	0.93	0.32	0.35	0.00
1525	0.70	0.24	0.24	0.00

Table 2-43
5.50 M $Ca(NO_3)_2$ Hydration Spectra

λ [mμ]	Spectra H_2O[a]	Spectra B (0.445 a)	Spectra A	Spectra C=B-A
1325	0.12	0.05	0.05	0.00
1375	0.27	0.12	0.12	0.00
1400	0.93	0.41	0.32	0.09
1425	1.30	0.58	0.45	0.13
1450	1.43	0.66	0.65	0.01
1475	1.25	0.56	0.58	0.00
1500	0.93	0.41	0.45	0.00
1525	0.70	0.32	0.33	0.00

Table 2-44
0.5 M $(CH_3)_4 NNO_3$ Hydration Spectra

λ [mμ]	Spectra H_2O[a]	Spectra B (0.091 · a)	Spectra A	Spectra C = B - A
1275	0.07	0.01	0.01	0.00
1325	0.12	0.01	0.01	0.00
1375	0.27	0.02	0.02	0.01
1400	0.83	0.08	0.05	0.03
1425	1.30	0.12	0.05	0.07
1450	1.43	0.13	0.05	0.08
1475	1.25	0.11	0.04	0.07
1500	0.93	0.08	0.03	0.05
1525	0.70	0.06	0.03	0.03
1575	0.42	0.04	0.02	0.02
1625	0.32	0.03	0.01	0.02
1650	0.29	0.02	0.00	0.02

Table 2-45
1 M $(CH_3)_4 NNO_3$ Hydration Spectra

λ mμ	Spectra H_2O[a]	Spectra B (0.225 · a)	Spectra A	Spectra C = B - A
1275	0.07	0.02	0.01	0.01
1325	0.12	0.03	0.01	0.02
1375	0.27	0.06	0.03	0.03
1400	0.83	0.19	0.08	0.11
1425	1.30	0.29	0.10	0.19
1450	1.43	0.32	0.13	0.19
1475	1.25	0.28	0.13	0.15
1500	0.93	0.21	0.10	0.11
1525	0.70	0.16	0.08	0.08
1575	0.42	0.09	0.04	0.05
1625	0.32	0.07	0.04	0.03
1650	0.29	0.06	0.00	0.06

Table 2-46
2 M $(CH_3)_4$ NNO_3 Hydration Spectra

m	Spectra H_2O[a]	Spectra B (0.347 a)	Spectra A	Spectra C = B - A
1275	0.07	0.02	0.01	0.00
1325	0.12	0.04	0.02	0.00
1375	0.27	0.09	0.08	0.01
1400	0.83	0.29	0.21	0.08
1425	1.30	0.45	0.28	0.17
1450	1.43	0.49	0.3]	0.17
1475	1.25	0.43	0.28	0.15
1500	0.93	0.32	0.21	0.11
1525	0.70	0.24	0.15	0.09
1575	0.42	0.14	0.09	0.05
1625	0.32	0.11	0.07	0.04
1650	0.29	0.10	0.01	0.09

Table 2-47
$(CH_3)_4$ NNO_3 3 M Hydration Spectra

m	Spectra H_2O[a]	Spectra B (0.347 • a)	Spectra A	Spectra C = B - A
1275	0.07	0.02	0.02	0.00
1325	0.12	0.04	0.04	0.00
1375	0.27	0.09	0.12	0.00
1400	0.83	0.29	0.33	0.00
1425	1.30	0.46	0.45	0.01
1450	1.43	0.51	0.48	0.03
1475	1.25	0.44	0.40	0.03
1500	0.93	0.32	0.30	0.02
1525	0.70	0.24	0.22	0.02
1575	0.42	0.14	0.13	0.01
1625	0.32	0.11	0.09	0.02
1650	0.29	0.10	0.02	0.08

Table 2-48
3.89 M $(CH_3)_4 NNO_3$ Hydration Spectra

λ [mμ]	Spectra H_2O[a]	Spectra B (0.457 · a)	Spectra A	Spectra C = B - A
1275	0.07	0.03	0.03	0.00
1325	0.12	0.05	0.05	0.00
1375	0.27	0.12	0.12	0.00
1400	0.83	0.38	0.38	0.00
1425	1.30	0.59	0.58	0.01
1450	1.43	0.66	0.64	0.02
1475	1.25	0.58	0.56	0.02
1500	0.93	0.43	0.42	0.01
1525	0.70	0.32	0.39	0.01
1575	0.42	0.17	0.17	0.00

Table 2-49
0.5 M NH_4NO_3 Hydration Spectra

m	Spectra H_2O[a]	Spectra B (a 0.056)	Spectra A	Spectra C = B - A
1325	0.12	0.01	0.00	0.00
1375	0.27	0.01	0.01	0.00
1400	0.83	0.05	0.02	0.03
1425	1.30	0.07	0.04	0.03
1450	1.43	0.08	0.05	0.03
1475	1.25	0.07	0.04	0.03
1500	0.93	0.05	0.03	0.02
1550	0.52	0.03	0.00	0.03

Table 2-50
2 M NH_4NO_3 Hydration Spectra

[m]	Spectra H_2O[a]	Spectra B (a 0.152)	Spectra A	Spectra C = B - A
1325	0.12	0.02	0.00	0.02
1375	0.27	0.04	0.02	0.02
1400	0.83	0.12	0.06	0.06
1425	1.30	0.20	0.10	0.10
1450	1.43	0.22	0.15	0.07
1475	1.25	0.19	0.14	0.05
1500	0.93	0.14	0.09	0.05
1550	0.52	0.08	0.00	0.08

Table 2-51
4 M NH_4NO_3 Hydration Spectra

m	Spectra H_2O[a]	Spectra B (a • 0.272)	Spectra A	Spectra C = B - A
1325	0.12	0.03	0.00	0.03
1375	0.27	0.07	0.05	0.04
1400	0.83	0.28	0.16	0.12
1425	1.30	0.35	0.24	0.11
1450	1.43	0.38	0.31	0.07
1475	1.25	0.33	0.27	0.06
1500	0.93	0.25	0.18	0.07
1550	0.52	0.14	0.00	0.14

Table 2-52
NH_4NO_3 6 M Hydration Spectra

λ [mμ]	Spectra H_2O[a]	Spectra B (0.386 · a)	Spectra A	Spectra C = B - A
1325	0.12	0.05	0.00	0.05
1375	0.27	0.11	0.10	0.01
1400	0.83	0.32	0.25	0.07
1425	1.30	0.51	0.45	0.16
1450	1.43	0.56	0.41	0.15
1475	1.25	0.48	0.38	0.10
1500	0.93	0.36	0.26	0.09
1550	0.52	0.20	0.00	0.20

Table 2-53
NH_4NO_3 8 M Hydration Spectra

λ mμ	Spectra H_2O[a]	Spectra B (0.500 · a)	Spectra A	Spectra C = B - A
1325	0.12	0.06	0.02	0.04
1375	0.27	0.13	0.13	0.00
1400	0.83	0.41	0.36	0.05
1425	1.30	0.65	0.47	0.18
1450	1.43	0.72	0.56	0.16
1475	1.25	0.62	0.47	0.15
1500	0.93	0.46	0.29	0.17
1550	0.52	0.26	0.00	0.26

Table 2-54
10 M NH_4NO_3 Hydration Spectra

λ mμ	Spectra H_2O[a]	Spectra B (0.598 · a)	Spectra A	Spectra C = B - A
1325	0.12	0.07	0.02	0.05
1375	0.27	0.16	0.16	0.00
1400	0.83	0.50	0.48	0.02
1425	1.30	0.78	0.60	0.18
1450	1.43	0.85	0.68	0.17
1475	1.25	0.75	0.50	0.15
1500	0.93	0.56	0.35	0.21
1550	0.52	0.31	0.00	0.31

cation spectrum for the Na^+ hydrate is shown at the right hand side in this figure. In Figure 2-26 there are shown hydration spectra of 3 M nitrate solution of different cations. Since the contribution of the NO_3^- to the spectra cancels out the cation hydrate absorption presumably is located at 1435 mμ in all cases. The hydration difference spectra that gives the cation hydrate band has a maxima at 1435 mμ and a $\Delta\lambda_{\frac{1}{2}}$ of 40 mμ. As seen in Figure 2-26 the hydration difference spectra are different when the pair KNO_3-$Ca(NO_3)_2$ or $NaNO_3$-$LiNO_3$ are considered. These curves could be used to fit the hydration spectra of 3 M $LiNO_3$, $NaNO_3$ and KNO_3 solutions and obtain a nitrate band, but not in the case of $Ca(NO_3)_2$. The reason is not clear at the present time. The $Ca(NO_3)_2$ case present hydration numbers (Table 2-7) in our work that are smaller than the ones reported in the literature for the Ca^{+2} ion alone (Swift and Sayre, 1966). Another reason may be the ion-pairing effect that leads to a formation of $CaNO_3^+$ as reported by Irish and Walrafen (1968) in Raman studies of $Ca(NO_3)_2$ solution. This ion pair may then form a species with definite optical absorption properties causing the decrease of the hydration spectra of $Ca(NO_3)_2$ salts. The values for Figure 2-26 are in Tables 2-55 and 2-56. In Figure 2-27 the same treatment is shown for 4 M nitrate solutions. Results are similar to the 3 M nitrate case and the validity of this approach seems to hold them at different concentrations. The values are reported in Table 2-57.

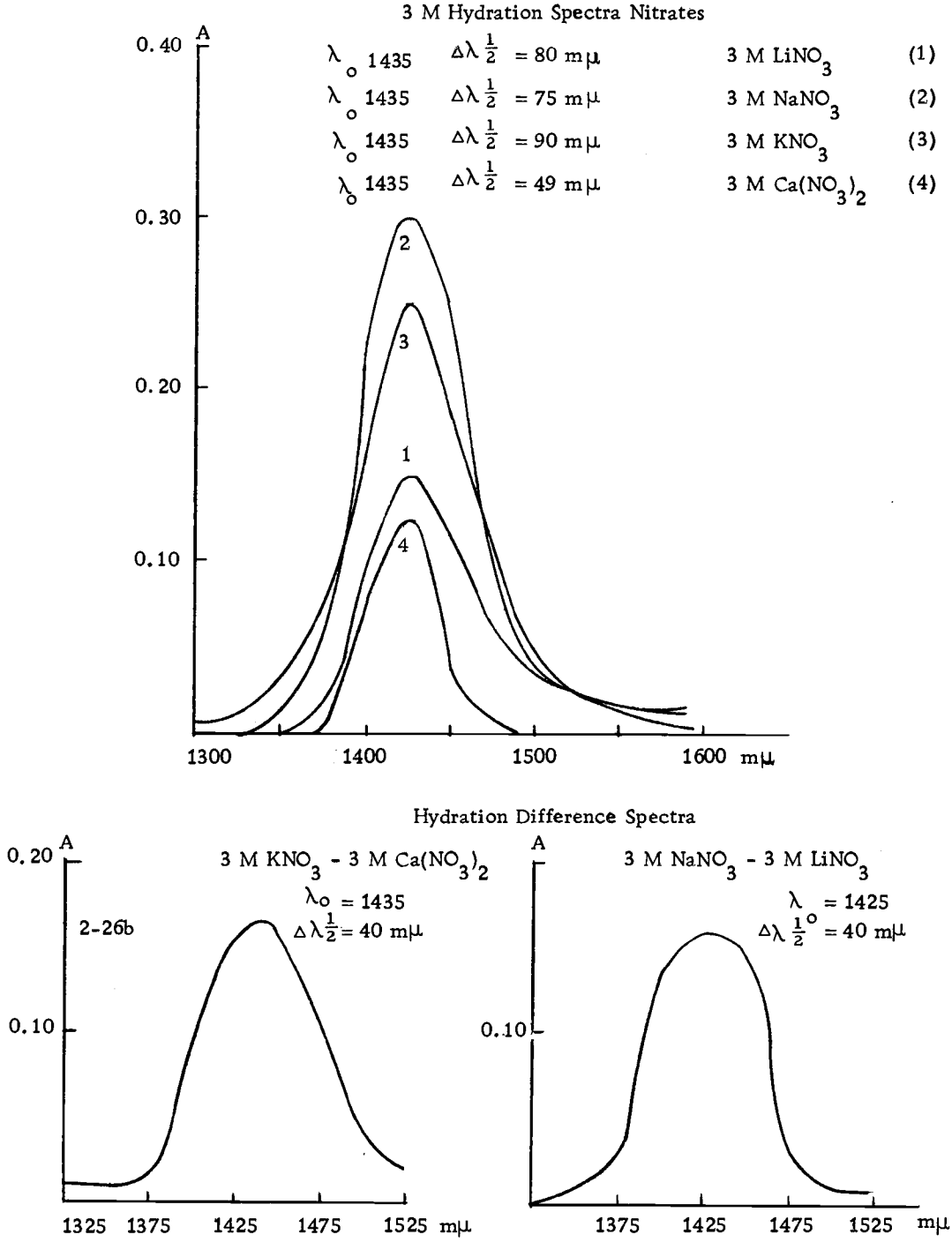

Figure 2-26. 3M hydration spectra nitrates.

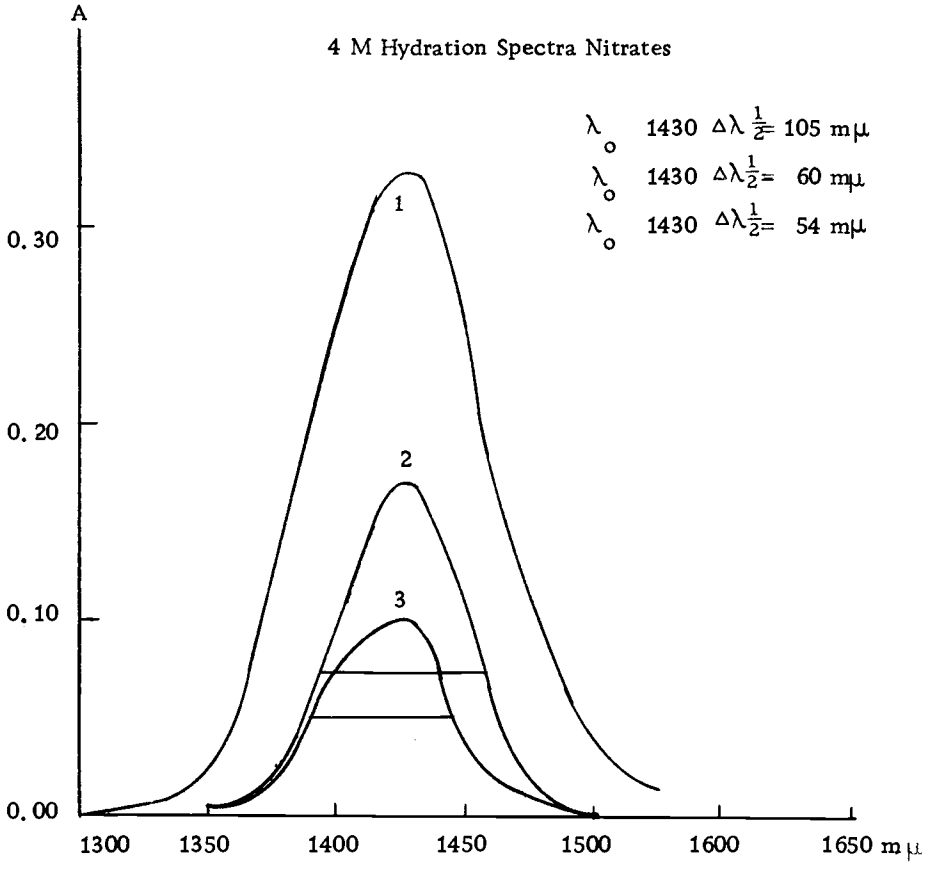
A
4 M Hydration Spectra Nitrates
λo 1430 Δλ½ = 105 mμ 4 M NaNO3 (1)
λo 1430 Δλ½ = 60 mμ 4MLiNO3 (2)
λo 1430 Δλ½ = 54 mμ 4MCa(NO3)2 (3)
0.30
0.20
0.10
0.00
1
2
3
1300
1350
1400
1450
1500
1600
1650 mμ

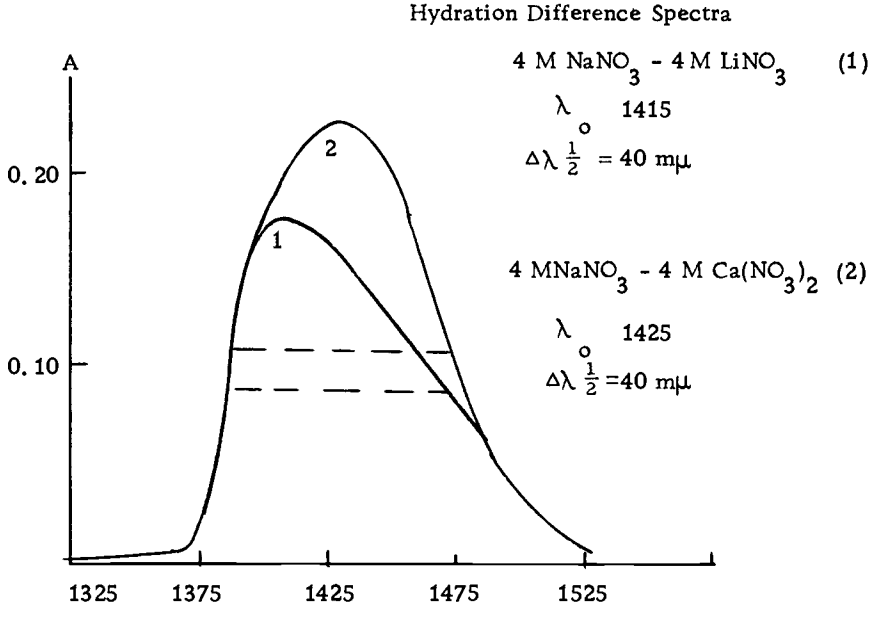
Hydration Difference Spectra
A
4 M NaNO3 - 4 M LiNO3 (1)
λo 1415
Δλ½ = 40 mμ
4 MNaNO3 - 4 M Ca(NO3)2 (2)
λo 1425
Δλ½ = 40 mμ
0.20
0.10
1
2
1325
1375
1425
1475
1525

Figure 2-27

Table 2-55
Difference Hydration Spectra of 3 M $NaNO_3$ - 3 M $LiNO_3$

λ [mμ]	Hydration Spectra 3 M $NaNO_3$	Hydration Spectra 3 M $LiNO_3$	Difference Hydration Spectra 3 M $NaNO_3$ - 3 M $LiNO_3$
1325	0.01	0.00	0.01
1375	0.02	0.00	0.02
1400	0.22	0.10	0.13
1425	0.30	0.15	0.15
1425	0.26	0.11	0.15
1450	0.08	0.06	0.02
1475	0.04	0.03	0.01
1500	0.02	0.02	0.00
1525	0.01	0.01	0.00

Table 2-56
Difference Hydration Spectra of 3 M KNO_3 and 3 M $Ca(NO_3)_2$ in $[NO_3^-]$

λ [mμ]	Hydration Spectra 3 M KNO_3	Hydration Spectra 3 M $Ca(NO_3)_2$	Difference Hydration Spectra 3 M KNO_3 - 3 M $Ca(NO_3)_2$
1325	0.01	0.00	0.01
1375	0.01	0.00	0.01
1400	0.16	0.07	0.09
1425	0.25	0.12	0.13
1450	0.18	0.03	0.16
1475	0.11	0.01	0.10
1500	0.04	0.01	0.03
1525	0.02	0.00	0.02

Table 2-57
Difference Hydration Spectra of 4 M Nitrate Solutions

λ mμ	(A) Hydration Spectra 4 M $LiNO_3$	(B) Hydration Spectra 4 M $NaNO_3$	(C) Hydration Spectra 4 M $Ca(NO_3)_2$	Spectra (B) - (A)	Spectra (B) - (C)
1325	0.00	0.00	0.00	0.00	0.00
1375	0.01	0.02	0.01	0.01	0.01
1400	0.08	0.25	0.08	0.17	0.17
1425	0.17	0.33	0.10	0.16	0.23
1450	0.09	0.22	0.03	0.13	0.19
1475	0.01	0.11	0.01	0.10	0.10
1500	0.00	0.03	0.00	0.03	0.03
1525	0.00	0.01	0.00	0.01	0.01
1575	0.00	0.00	0.00	0.00	0.00

Figure 2-28 is an attempt to apply the cation hydrate obtained in Figure 2-26 b) to separate a cationic and anionic hydration for the four concentrations studied of KNO_3. This is not possible according to McCabe and Fisher's (1970) view that absorption peaks representing single homogeneous molecular species could be compared and consequently ascribed to the same species if the position of the absorption maximum λ_o and the half band width $\Delta\lambda_{\frac{1}{2}}$ are the same.

Although we have applied this criterion it must be pointed out that Gaussians representing a single absorption species generally characterized by a) the absorption maximum and b) the $A_{max}/\Delta\lambda_{\frac{1}{2}}$ value being A_{max} the maximum absorbance. The cation hydrate from Figure 2-26 b) has been used in the fit of KNO_3 solution (Figure 2-28) applying absorption parameters for this cationic species $\lambda_o = 1435\ m\mu$ and $\Delta\lambda_{\frac{1}{2}} = 40\ m\mu$. The position of the cation hydrate absorbance is shown in Figure 2-28 and the half band width was assigned from left to right. In the fit of McCabe and Fisher (1970) (Figure 2-11), the Gaussians for anion and cation hydration do not perfectly match the whole curve and this fact may be due to overlap of the other water bands in the N.I.R. region. It is interesting to note at this point, that generally Gaussians are described by a distribution function that relies on $A_{max}/\lambda\ \Delta_{\frac{1}{2}}$ values. A possible two Gaussian resolution may lead to values for cationic and anionic hydration, since V_{excl} is calculated and the total number of solute and water present are

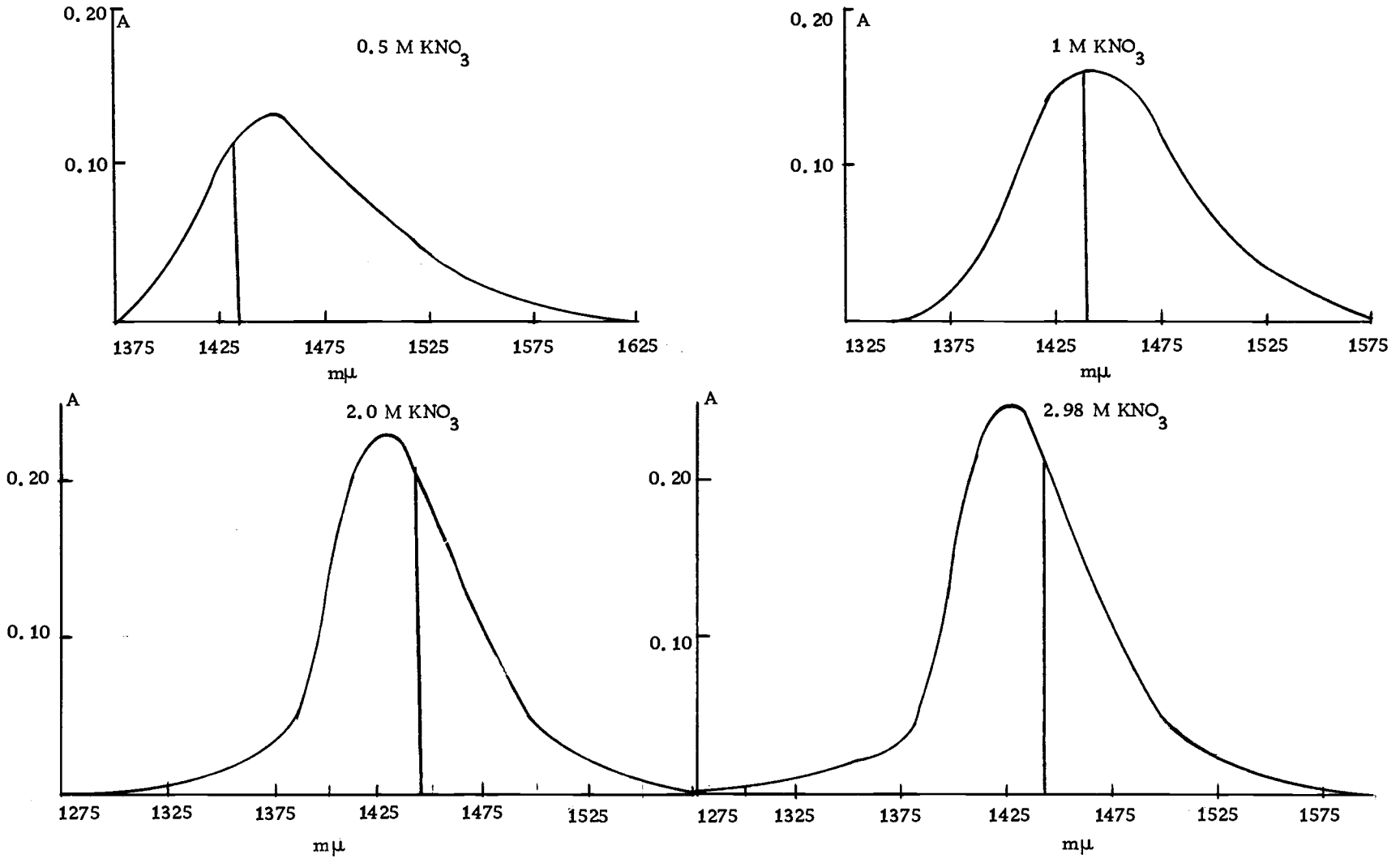
0.20
A
0.5 M KNO3
0.10
1375
1425
1475
1525
1575
1625
mμ
0.20
A
1 M KNO3
0.10
1325
1375
1425
1475
1525
1575
mμ
A
2.0 M KNO3
0.20
0.10
1275
1325
1375
1425
1475
1525
mμ
A
2.98 M KNO3
0.20
0.10
1275
1325
1375
1425
1475
1525
1575
mμ

Figure 2-28

known. One of the problems is the ignorance about the values of the molar absorption coefficients for cationic and anionic hydration in the spectra found. The different position of the peaks in Figure 2-28 may be due to the different interaction cation-anion at different concentration of salt. If only ion dipole interactions are considered, the shape of the water molecule will presumably allow the oxygen to come closer to the cation than to the anion. Therefore we expect that $M^{+}\cdots O\begin{smallmatrix}H\\H\end{smallmatrix}$ distances would be somewhat smaller than $NO_3^{-}\cdots\begin{smallmatrix}H\\H\end{smallmatrix}O$ for ions of identical dimensions. The hydration spectra of NH_4NO_3 solutions are very different from other inorganic nitrates (Figure 2-25). The difference absorbance spectra (Figure 2-8) suggest that it could be a pure component since it is more regular than the spectra of inorganic nitrates. Hindman (1962) ascribed no hydration to the NH_4^+ ion in solution. The shape of our spectra suggests possibilities which we have no means to check now, such as: a) NH_4^+ hydrates in a different way than other cations, b) First shell hydration water is not present and loose bound water has different optical properties than the water in the first shell, c) Solutions present a solvated ion-pair with a definite optical absorption.

The structure of water surrounding a ion is very important when considering the hydration of ions. McCabe and Fisher (1970) thought to have found two independent methods to determine hydration namely the volume excluded method and the integrated absorption

method. It is our opinion that the second method is not independent of the first one. That the electrostriction factor (factor of V_{el}) varies with concentration, as well as the difference absorbance spectra, is a meaningful experimental result. The weakness of any treatment that includes compressibility measurements to determine hydration is that they suppose the water of the first hydration shell to be incompressible and ascribe the compressibility to the loosely bound or free water. Future work with solutions at different temperatures is necessary to determine the hydration as a function of temperature. It has to be noted however, that the water itself changes absorbance as a function of temperature observed by Klotz (1965).

In this chapter we have started finding values for parameters like a) V_{excl} (that is the volume of water present that does not participate in the hydration) in the salts under consideration b) The total hydration number. These values have been compared with the literature and the available results show internal consistency of the method employed.

Cationic and anionic hydration has been separated with partial success by means of $(CH_3)_4 NNO_3$ ascribing all the hydration to the anion. The assumption that only water interacts with NO_3^- ion and therefore only hydration of this ion is to be found, is in agreement with the current literature but there is not much experimental

evidence given to back this assumption. The cationic and anionic separation worked out in this way has been shown in Table 2-13 and has only an approximate character. The Gaussian resolution of the hydration spectrum as suggested by McCabe and Fisher (1970) has not been successful in separating cationic and anionic hydration (based on an hydration difference spectra) in the nitrate solutions studied. An assignment of Gaussians based on other type of assumptions of the hydration spectra may succeed in resolving this spectra into components.

It must be concluded that satisfactory quantitative description of the intermolecular nature of water does not yet exist and until such is available, discussions of aqueous mixtures will tend to be semi-empirical. The physical properties of the solvent media employed are in many cases unknown or imperfectly understood. Nevertheless a large volume of data exists concerning the behaviour of ions in aqueous solutions. The results obtained in our studies will be compared with the values obtained using N.M.R. spectroscopy in the next chapter.

III NUCLEAR MAGNETIC RESONANCE STUDIES OF CONCENTRATED NITRATE SOLUTIONS

Introduction

An atom placed in a magnetic field acquires a magnetic moment due to the field applied. The shell electrons constitute effective currents around nucleus which produce a secondary magnetic field which screens nucleus present. Induced currents are proportional to the applied magnetic field H_o and the magnitude of the secondary field will also be proportional to H_o.

The magnetic field at the position of the nucleus is then

$$H = H_o(1 - \sigma)$$

σ is called the screening constant and it depends on the electronic environment of nucleus; it is dimensionless and independent of H_o.

For structural studies a given nucleus may give resonances in different parts of the spectrum due to chemically different position. This displacement is called chemical shift δ. The magnitude for different shifts of different solutions in a same magnetic field is due to changes in temperature, solvent and concentration of the solutions used.

If a substance with magnetization I (magnetic moment per unit volume) is placed in a magnetic field of strength H, the magnetic

induction, β, is given in c.g.s. Gaussian units by

$$\beta = H + 4\pi I$$

which can be rewritten:

$$\beta = H + 4\pi \chi_v H$$

where χ_v is the volume susceptibility, a dimensionless quantity.

The specific susceptibility, χ, is defined by

$$\chi = \frac{\chi_v}{d}$$

where d is the density of the sample in grams/ml. The molecular susceptibility χ_M is

$$\chi_M = M\chi = \frac{M\chi_v}{d}$$

where M is the molecular weight of the substance in grams. If a substance with diamagnetic susceptibility χ_M is placed in a field H the interaction energy is $\frac{1}{2}\chi_M H^2$.

In certain systems in which the molecules are associated by relatively strong bonds, proton exchange effects may be observed. The proton may be regarded as alternating between the structures XH. . . . . Y and X. . . . .HY. When this exchange occurs relatively infrequently, two separate signals are observed in the N.M.R. spectrum; they correspond to the different environment of the proton at the two different sites X and Y. By increasing the temperature, the

two separate signals due to these states can be made to coalesce into a single sharp signal. When a proton is placed in a magnetic field, it occupies one of the two possible energy levels depending on whether its magnetic moment points in the direction of the field or in the opposite direction.

Experimental Part

The magnetic field in the Varian high-resolution nuclear magnetic resonance spectrometer is 23.500 Gauss. The resonance measurements were carried out at 100 MHz. A magnetic field of high homogeneity is required for it. The volume of the sample is reduced to lower the inhomogeneity of the magnetic field, since no field is totally homogeneous. The smallest volume is determined by that which can give a substantial amount of signal strength needed to record the shift, and at the same time make the inhomogeneity a minimum.

A diagram of our apparatus is shown in Figure 3-1. In Figure 3-2 the cooling system is shown. Nitrogen gas is used to cool or heat the spinning sample. The heat exchanger acts on the N_2 gas if temperatures of 35°C and up are needed. In box (1) (Figure 3-2) the nitrogen is cooled by means of a mixture of acetone and ice if work is carried out at temperatures below 35°C.

Chemical shifts are measured in δ (ppm) but they correspond

to a fraction of milligauss. We have a chemical shift e. g.; of 250 Hz and an applied field of 100 Mc/sec.

$$\delta = \frac{250}{100 \cdot 10^6} = 2.5\ 10^{-6} \text{ or } 2.5 \text{ ppm}$$

In a field of 23. 500 Gauss, the milligauss value corresponding to this chemical shift

$$\frac{x}{23.500} = \frac{250}{100\ 10^6} \qquad x = 0.59 \text{ milligauss.}$$

Since we are concerned with small shifts a high resolution apparatus is necessary. To insure that the temperature in the sample is the same as that of the thermocouple ethylene-glycol is used. The shift of this substance as function of temperature is known. Samples are equilibrated several minutes before each reading. The sample is maintained within $\pm 1^{o}C$ of the desired temperature.

The chemical shift was measured with respect to cyclohexane from 10^{o} to $70^{o}C$ in 10 degrees intervals. As a reference for proton shifts cyclohexane has the advantage of having a well defined single resonance line, a boiling point of $78.5^{o}C$ and all protons present are equivalent. The sample is spinning during our measurements to give homogeneity to the magnetic field experienced by the nuclei due to this mechanical motion of the sample. A typical value is four revolutions/second.

By the sample holder or probe it is meant the assembly which

carries the air turbine for sample spinning, the receiver coil, the linear sweep coils and the pre-amplifier. The sample holder is mounted on a manipulator (usually plastic) to enable the best position in the magnetic field to be found. The body has to be rigid and has to provide accurate location of the receiver coil. Our machine has a crossed coil probe (See Figure 3-1 and 3-2).

In the nitrate samples we have to use external referencing. This is most convenient carried out with the aid of precision coaxial tubing. Such an arrangement is shown in Figure 3-3. Usually the reference is contained in the central capillary and the sample in the surrounding annulus. Coaxial tube arrangements are employed when the sample tube is rotated. Rotation of the system about its axis averages the field experienced by the annular liquid, resulting in a single signal. The component glass tubes must be free of imperfections; if not slight signal broadening causes slight signal shifts. Wilmad coaxial high resolution N.M.R. tubes are used. The width used to record the spectrograms is 250 cycles and since the scan velocity employed is 250 seconds the sweeping velocity is 1 cycle/second. Peaks obtained are Lorentzian in shape. This indicates (Hallyday et al., 1969) that the measured chemical shift is an averaged value of chemical shifts in all ionic environments. It is assumed that the ionic shift, in the limit of zero salt concentration, is determined by a sum of binary interactions of the ion with solvent

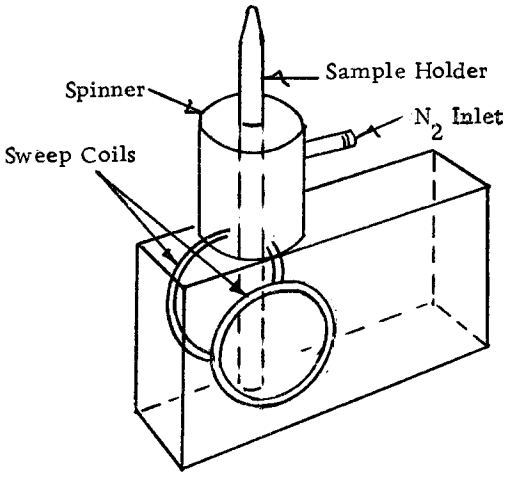

Figure 3-1. Schematic diagram of the Varian probe assembly.

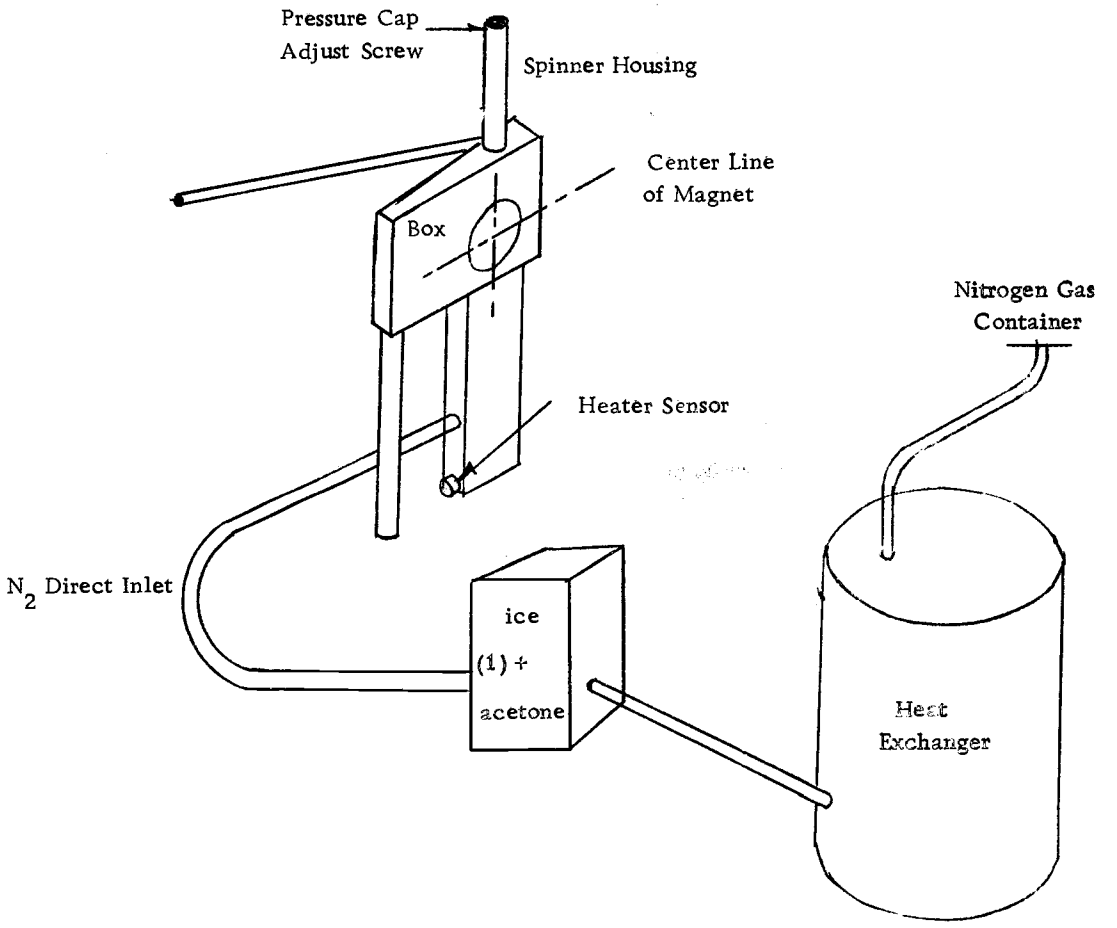

Figure 3-2

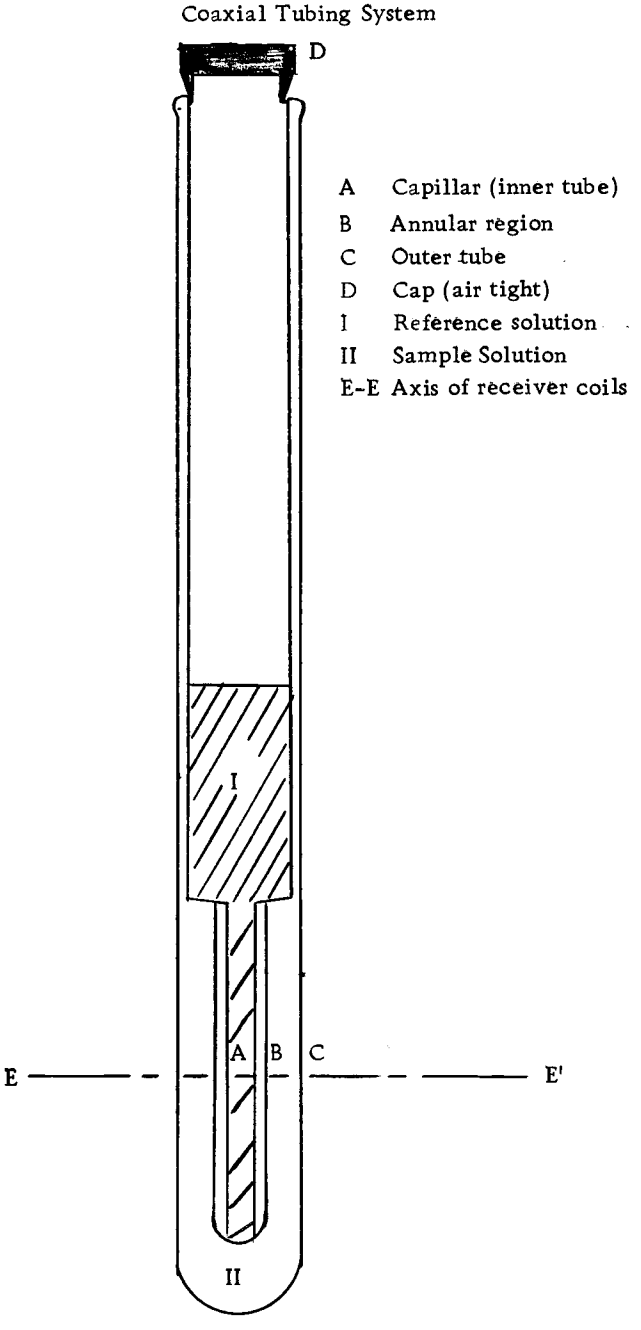
Coaxial Tubing System
D
A Capillar (inner tube)
B Annular region
C Outer tube
D Cap (air tight)
I Reference solution
II Sample Solution
E-E Axis of receiver coils
I
A
B
C
E
E'
II

Figure 3-3

molecules in the solvatation region. Shifts of our concentrated nitrate solutions are to lower field values since the shielding of protons is bigger in cyclohexane than in our aqueous solutions.

In our bands we have observed a certain width that at this point has no reasonable explanation. In these measurements we aim for the optimum homogeneity for the field applied at the position of the reference. Since the position of the lock is the same as for the sample it should reflect, maximum homogeneity for the sample. The instrument is provided with a screen to detect the optimum homogeneity applied to the sample. The magnetic field applied is adjusted varying the radio-frequency, sweeping time and the velocity of the spinning used. Then the signal on the screen is the sharpest possible and this means the magnetic field in the sample has a maximum homogeneity. Proceeding in this fashion, signals with unsymmetrical distribution in the N.M.R. peaks are obtained as shown in Figure 3-4a. But if the criterion of attaining the sharpest signal on the screen is disregarded, and instead the spinning velocity, radiofrequency and sweep time is adjusted to obtain the most symmetrical peak in the N.M.R. spectrogram, then a peak is obtained like the one shown in Fibure 3-4b. The reason for this phenomena is not known and it is in disagreement with the instructions to operate the N.M.R. machine.

Broadening of lines is observed in some N.M.R. peaks. Dyer

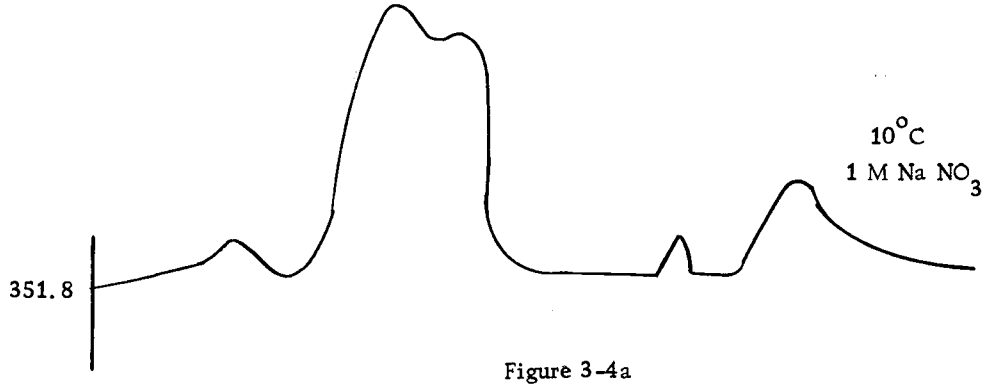

Figure 3-4a

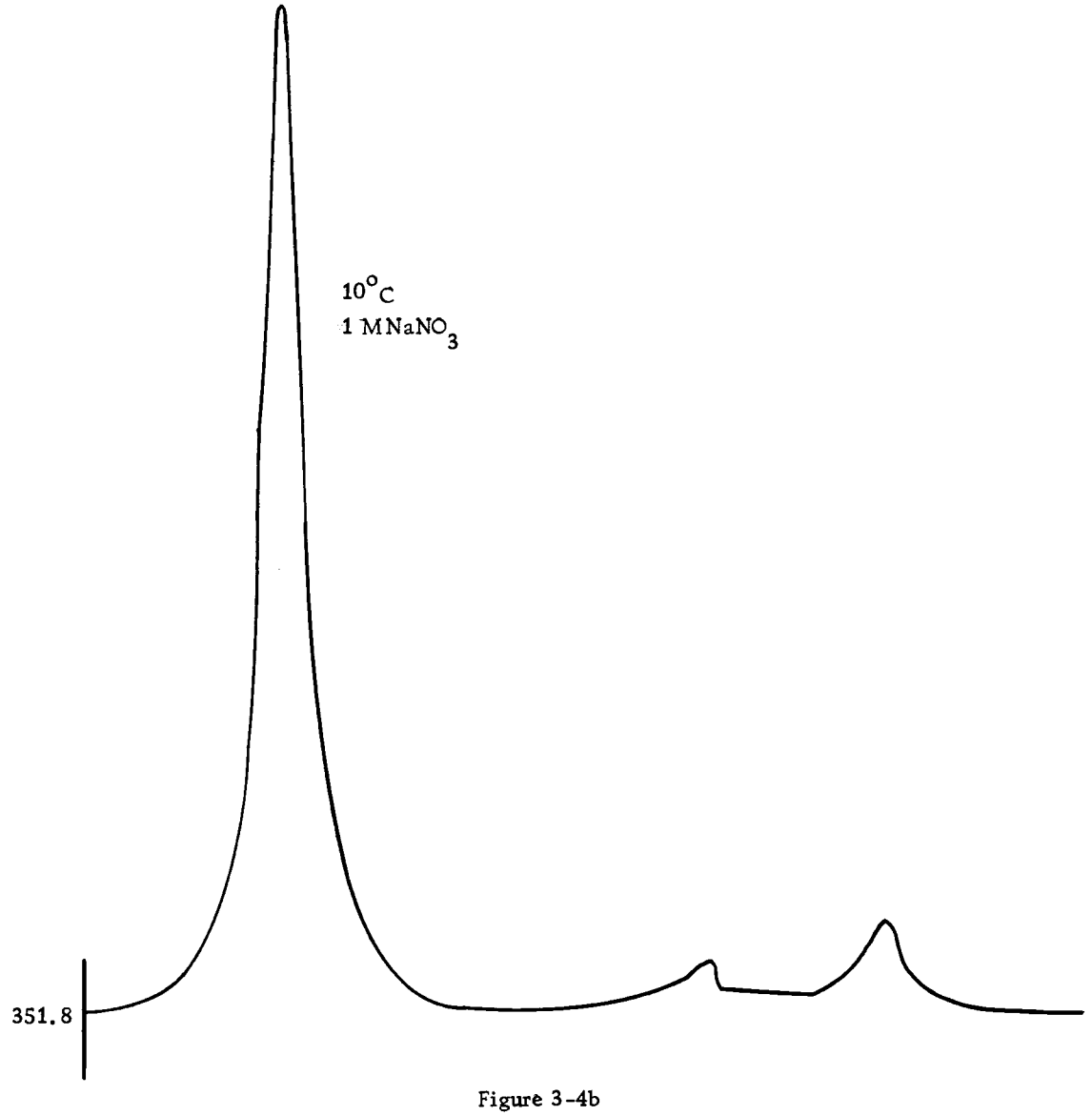

Figure 3-4b

(1965) explains that the broadening is due to two factors. a) Some broadening may result from the presence of paramagnetic ions in the sample b) In nitrates, the nitrogen nucleus is present, which has an electric quadrupole moment. A consequence of this is that the absorption bands for H nuclei attached directly to N atoms are generally broadened due to quadrupolar relaxation effects. Inert solvent studies like CH_3CN may throw some light on the formation of H bonds in the NH systems. The magnitude of the electric quadrupole moment is a measure of the non-spherical nature of the electric charge distribution of the nucleus. Degassing of the samples produces a decrease of about $0.005 \cdot 10^{-6}$ cgs units in the value of χ_v in diverse samples (Frei and Bernstein, 1962) mainly due to the elimination of oxygen present.

Other investigators in the N.M.R. field feel that broadening of the resonance line is due to the viscosity of solution. This is in agreement with the commonly accepted view that hydrogen bond breakage is known to be consistent with the decrease observed in the viscosity of water as temperature rises. The viscosity of a liquid is a measure of its resistance to flow. Since flow takes place by displacements of the equilibrium positions of molecules, studies of viscosities can yield some information on the nature of these displacements. Self-diffusion coefficients and viscosity values should in the future be related to shifts in the spectrograms obtained and

may explain the magnitude and direction of the shift observed in the peaks (Wang and Edelman, 1953). It also may be thought that a saturation effect is responsible for this line broadening. The effect of absorption of energy of an oscillating magnetic field sometimes will be to reduce the excess population of the upper state and so reduce the probability of further absorption. The magnitude of such an effect will increase with the amplitude of the oscillating field and is referred to as saturation. Considerations of this sort make it advisable to avoid saturation effects if possible by employing sufficiently small radiofrequency fields. The weak field can be obtained by modulating the main magnetic field at a frequency large compared with the line width, using an audiofrequency oscillator capable of giving a small amplitude. In our work measurments have been taken at 0.001 rf, which is a low of rf. value. Values over 0.01 are considered as high rf. and give saturation problems.

Generally it is considered that side bands are introduced here by precision and inhomogeneity of the sample coaxial tube while spinning as shown in Figure 3-4. These side bands appear mostly at 10 or more cycles to the sides of the main signal. Contrary to this widespread interpretation Spanier, Vladimiroff and Malinowski (1966) reported that these side bands are due to the geometry of the coaxial system and are not caused by imperfections in the cells as it is generally believed.

The lower limit of concentration for which a sharp resonance signal can be detected in the coaxial system arrangement is less than one half percent of solute. This means approximately a 0.25 M concentration in our nitrate solutions.

Correction Factor for the Observed Shifts

In order that the final chemical shift values be independent of the magnetic effects of the medium in which they are measured, it is necessary to correct for the bulk diamagnetic susceptibility of the sample being measured. The interaction of magnetic fields and sample depend on the electrons of the sample (since shielding currents develop) so that we want the same field for samples that present different magnetic shielding.

In measurements where a coaxial system is used in the inner capillary we have cyclohexane and in the annular region is placed the salt solution. The outside solution is equivalent to a spherical surface which acts like a perfect Lorentzian cavity due to the fact that the cylinder employed has a considerable inner diameter. But in the capillary of the coaxial system the actual field experienced by individual molecules will depend on the magnetic polarization near the surface. Since we have to compare two Lorentzian cavities - and one of them in the system is not of this type - we have to apply some sort of correction. Therefore if both sample and reference

compounds were contained in spherical sample tubes then no correction for differences in diamagnetic susceptibilities would be necessary. Unfortunately good spherical containers are not easily like the one shown in Figure 3-5. External referencing is carried out conveniently with the aid of a precision coaxial tubing as shown in Figure 3-3. The reference is usually contained in the central capillary and the sample in the surrounding annulus. Since it is somewhat tedious to measure susceptibilities many investigators have either ignored any corrections (thereby invalidating their work) or have used internal standards, for which no susceptibility corrections have to be applied. Using a coaxial cell system as shown in Figure 3-3 correction measurements have been carried out. Corning Glass No. 7740 is the cell material. The theoretical feasibility of this method to measure susceptibilities was first reported by Reilley, McConnell and Meisenheimer (1955). Further development of the theory was given by Morin, Paulett and Hobbs (1956). The simple geometry of the system allows the calculation of the susceptibility corrections. The general solution of Laplace's equation for the case of symmetry along the z-axis. In this way the external field that the molecule experiences in both the capillary and the annulus can be readily calculated. The application of the bulk susceptibility corrections is particularly important for proton resonance measurements where the chemical shift is small. Zimmerman and Foster (1957) have

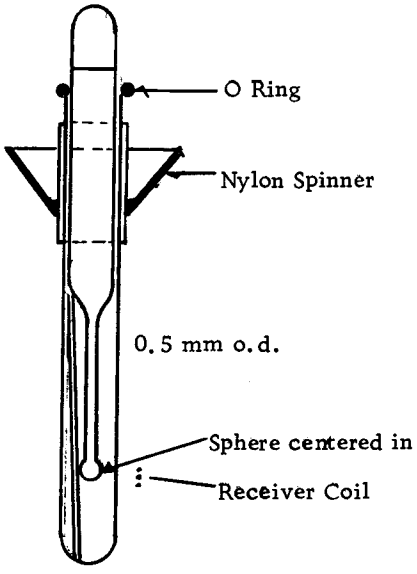

Figure 3-5. Sample tube containing a cylindrical and a spherical reference tube.

examined the general practicability of a coaxial system to determine magnetic susceptibilities. The problem consisted in that experimental data was not available for most of the solutions commonly used and a way had to be found to get this information. The mathematical treatment gets complicated by the fact that the magnetic susceptibility is a tensor and the component along each axis can be written as the sum of negative diamagnetic contribution and a smaller positive paramagnetic contribution for diamagnetic materials. With the spinning probe, the cavity field in the direction of the external field that a molecule experiences H, in both the capillary and the annulus is given by $H = H_o (1 - 2/3\ \pi\chi_v)$ where H_o is the external field and χ_v is the bulk magnetic susceptibility per ml of material in the capillary or in the annulus. Zimmerman and Foster (1957) have examined the practicability of such a method and they found, that if the sample is magnetically and electrically isotropic, then accurate and reproducible results can be obtained. From the experimental point of view it is advisable to have a small volume of solution since the longer the sample the greater the temperature gradient along it. It is also advisable not to have any dead space above a solution sample because changing the temperature will change the concentration.

Intrinsic Magnetic Susceptibility Measurements

The expression employed in our determination of magnetic susceptibilities of our solutions is

$$n = 4\pi\gamma(\chi_1-\chi_2)\left(\frac{a}{r}\right)^2 + (\chi_2-\chi_3)\left(\frac{b}{r}\right)^2 \qquad (1)$$

where n is the separation in c.p.s., γ is the fixed radiofrequency in this case 100 m Hz, a, b and r are the internal and external radii, respectively of the inner glass tube, r is the mean radius of the annulus.

χ_1, χ_2, χ_3 are the volume magnetic susceptibilities of (1) solution contained in the inner glass tube, (2) glass, and (3) the annular liquid.

To date the most current data for the magnetic susceptibility of glass have come from Paul Inglefield (1970) of Clark University. The volume magnetic susceptibility has been determined to be $\chi_v = -0.848 \pm .003 \times 10^{-6}$. When taking the corrections we have to maximize homogeneity when sample is spinning. Sample is stopped and spectrogram is taken. Adjustments are made on the coils that operate the magnet and that are located in the x and z directions. With the attainment of sharp, symmetrical signals (Douglass and Fratiello, 1963) susceptibilities can be measured with a precision of ±1%. We carry out determination of the volume susceptibility (χ_v)

of cyclohexane using equation (1).

The χ_v of cyclohexane at different temperatures is denoted by χ_1. The value of χ_2 (for the glass tube) is taken as $-0.848 \cdot 10^{-6}$ as reported by Inglefield (1970). The values of $(\frac{b}{r})$ and $(\frac{a}{r})$ are geometrical constant of the coaxial system. The value of n is in c.p.s. and is taken adjusting the sweeping velocity to 250 sec, the r.f. value to $5 \cdot 10^{-2}$ while spinning. We tune the machine for maximum homogeneity when the sample is spinning by regulating the coils that operate the magnet in the x and z directions to attain two symmetric peaks. Samples are rotated 180^{o} and the spectrum taken each time to insure the peaks are unaffected by manual rotation, since the peak separation depends on the position of the sample tube in the magnetic field, thereby introducing ambiguity into the susceptibility measurements (Douglass and Fratiello (1963). A spectrogram as shown in Figure 3-6 for cyclohexane is obtained. The average of four values at each temperature is taken since the field drifts during the measurement. Two values correspond to a sweep from left to right and to the inverse case. The value of the field drifts since in the outer tube we have water and in the inner cyclohexane being able only to optimize the constancy of the field on the water that acts as a lock here. The important thing is to get symmetric peaks since only in this way the precision of our measurements is about 1% as stated by Douglass and Fratiello (1967). Therefore the values for

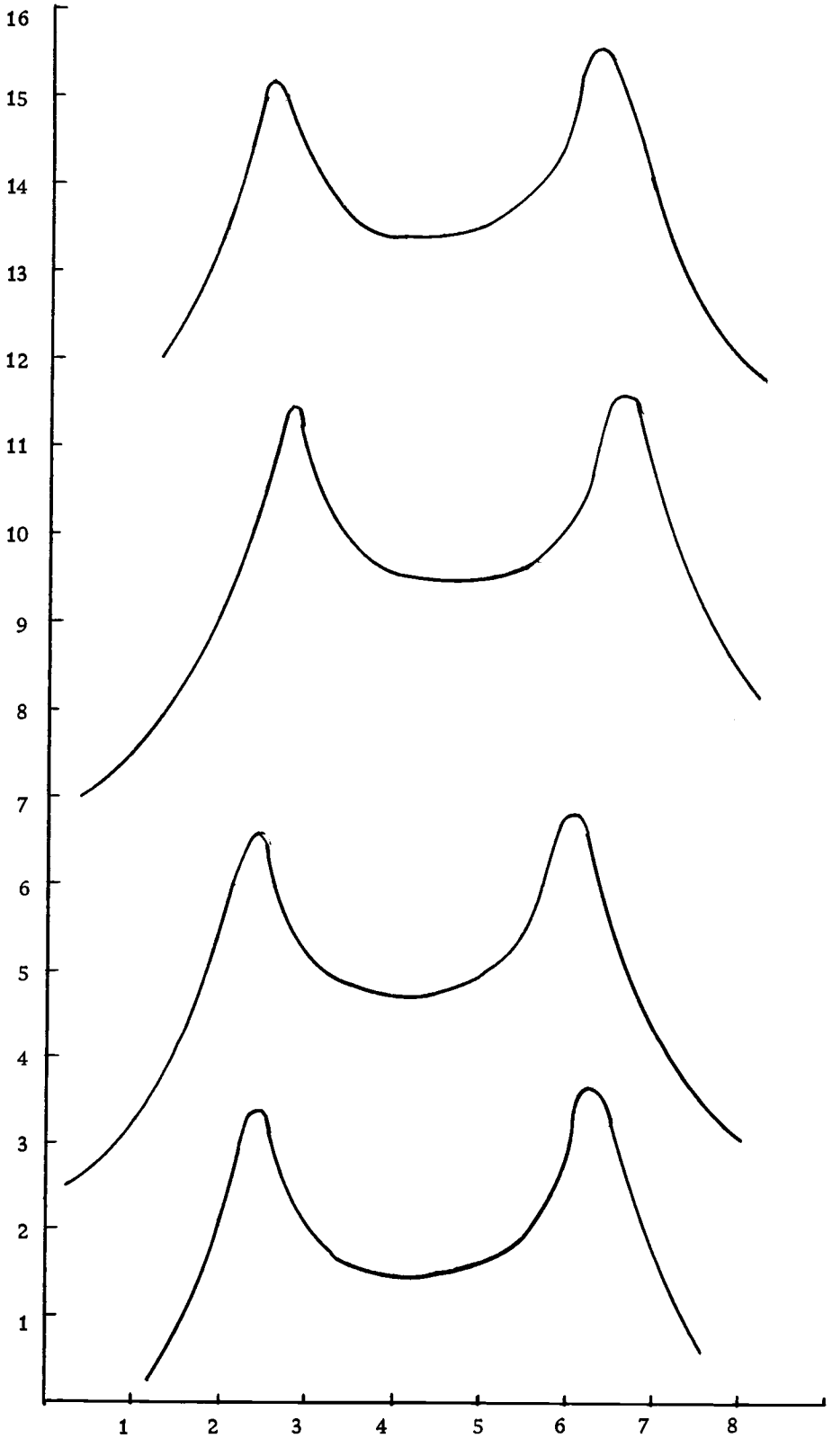

Figure 3-6. C_6H_{12}-H_2O System 40°C

χ_v of cyclohexane at different temperatures is given by:

$$\chi_{cyclohexane} = \chi_{glass} + \frac{\frac{n}{4\pi\gamma} - [\chi_{v\,glass} - \chi_{v\,H_2O}](\frac{b}{r})^2}{(\frac{a}{r})^2} \quad (2)$$

From equation (2) at each temperature the values of n and $\chi_v H_2O$ will be different. Fitting equation (2) with the values in the first of the columns to the left in Table 3-1, the experimental value for cyclohexane is reported in the second column and the calculated value is shown in the third column.

Table 3-1

T°C	$-\chi_{vH_2O} \cdot 10^6$ [a]	$-\chi_{v\,cyclohexane} \cdot 10^6$ [b]	$-\chi_{v\,cyclohexane} 10^6$ [c]
10	0.71942	0.635	0.637
20	0.72000	0.627	0.630
30	0.72085	0.610	0.623
40	0.72173	0.583	0.620
50	0.72238	0.547	0.602
60	0.72331	0.533	0.599
70	0.72439	0.525	0.592

[a] Cabrera and Fahlenbrach (1933) with $\chi_{v20°} = 0.720 \cdot 10^{-6}$ and density from I. C. T.

[b] This work

[c] Calculated from density measurements $\chi_v = \chi \cdot d$

For most materials the volume susceptibility χ_v is proportional to the density, suggesting that there is a basic susceptibility per

molecule. For diamagnetic substances, χ is usually approximately independent of temperature.

Since the density of a solution is a function of temperature it may seem that knowing χ and density of the solution at different temperatures will give us the χ_v values sought in the temperature range. The calculated values for χ_v of cyclohexane have been obtained by taking the reported value for χ (susceptibility/gram) of 20°C as $0.8100\ 10^{-6}$ c.g.s. for this material and applying the relation:

$$\chi_v = \chi \cdot d \qquad (\chi \text{ is susceptibility/gram})$$

in which the densities of cyclohexane at different temperatures were obtained from Timmerman's (1955).

Since the calculated values for χ_v of cyclohexane differ from the experimentally obtained, the first ones are regarded as approximate and the second values are used.

It is important to note that a spectrogram 250 cycles wide swept with a velocity of 250 seconds can be read in ppm with a precision of three decimals.

Solutions were not degassed during the correction measurements due to the fact that χ_v for water and cyclohexane are about $|0.6\ 10^{-6}|$ and the decrease of the value of susceptibility reported by Frei and Bernstein (1962) is about $|0.005\ 10^{-6}|$ so that errors

are small and of the same order of the error in the reading of the n (cps). The n values can be determined with a precision ± 0.2 Hz which in many solutions is 1% of the n (cps.) values obtained.

Magnetic Susceptibility $LiNO_3$ Solutions

To determine χ_v of $LiNO_3$ solutions at different temperatures, the electrolyte is located in the capillar and the cyclohexane in the annular region. Equation (2) is employed inserting the experimental values for χ_v of cyclohexane that have been already determined. The values of the shift and the χ_v of $LiNO_3$ at low concentration (0.5 M) is reported in Table 3-2. The same values are reported for concentrated solutions (8.78 M) and as it turns out only the third decimals varies.

Table 3-2

T°C	0.5 M $LiNO_3$		8.78 M $LiNO_3$	
	n (cps)	$-\chi_v \cdot 10^6$	n (cps)	$-\chi_v\ 10^6$
10	20.75	0.52482	24.12	0.52055
20	24.00	0.51913	25.12	0.51785
30	27.75	0.49766	26.95	0.49331
40	34.75	0.47116	33.12	0.47707
50	40.25	0.45985	35.75	0.46619
60	44.00	0.45078	39.62	0.45609
70	46.25	0.43880	42.75	0.44321

Magnetic Susceptibility $NaNO_3$ Solutions

The volume magnetic susceptibilities are determined as a function of temperature in the same way as the work for $LiNO_3$ was carried out.

Table 3-3

T°C	0.5 M $NaNO_3$		7.85 M $NaNO_3$	
	n (cps)	$-\chi_v 10^6$	n (cps)	$-\chi_v 10^6$
10	26.50	0.51012	30.37	0.50971
20	29.50	0.50321	33.25	0.50328
30	33.88	0.48410	36.87	0.48454
40	36.50	0.46015	41.25	0.45999
50	41.12	0.44893	47.25	0.44566
60	45.25	0.43406	50.50	0.43901
70	47.00	0.42649	53.87	0.42568

Magnetic Susceptibilities for KNO_3 Solutions

Table 3-4

T°C	0.5 M KNO_3		2.98 M $NaNO_3$	
	n(cps)	$-\chi_v 10^6$	n (cps)	$-\chi_v 10^6$
10	29.25	0.52039	26.00	0.51682
20	32.25	0.51395	29.50	0.50966
30	35.75	0.49062	32.25	0.48664
40	38.00	0.47796	39.50	0.47375
50	41.75	0.46314	39.50	0.46135
60	45.25	0.45511	42.00	0.45364
70	48.75	0.44589	45.75	0.43966

Magnetic Susceptibility for $CsNO_3$ Solutions

Table 3-5

T°C	$CsNO_3$ 0.1 M		$CsNO_3$ 1.12 M	
	n (cps)	$-\chi_v 10^6$	n (cps)	$-\chi_v 10^6$
10	28.62	-0.51029	22.00	0.5250
20	32.25	-0.50225	26.25	0.51480
30	36.00	-0.48262	31.75	-0.48360
40	37.75	-0.46856	35.25	-0.47282
50	41.00	-0.45883	40.35	0.46552
60	43.50	-0.45105	43.75	0.45062
70	46.25	-0.43640	47.00	0.43781

Magnetic Susceptibility for $Ca(NO_3)_2$ Solutions

Table 3-6

T°C	$Ca(NO_3)_2$ 0.5 M in $[NO_3^-]$		$Ca(NO_3)_2$ 9 M	
	n (cps)	$-\chi_v 10^6$	n (cps)	$-\chi_v 10^6$
10	24.75	0.51981	23.45	0.54112
20	28.00	0.51222	27.60	0.53817
30	31.80	0.48779	31.20	0.51735
40	37.75	0.46942	34.35	0.48128
50	41.20	0.45873	37.50	0.44098
60	44.40	0.44742	41.00	0.42889
70	47.00	0.43734	46.60	0.41755

Magnetic Susceptibilities for $(CH_3)_4 NNO_3$ Solutions

Table 3-7

T°C	$(CH_3)_4 NNO_3$ 0.5 M		$(CH_3)_4 NNO_3$ 3.89 M	
	n(cps)	$-\chi_v 10^6$	n (cps)	$-\chi_v 10^6$
10	23.12	0.52212	22.00	0.52394
20	26.62	0.51224	24.75	0.51784
30	29.87	0.49323	28.75	0.49275
40	31.75	0.47874	30.12	0.48155
50	35.62	0.46573	34.25	0.47043
60	39.75	0.45224	38.00	0.46052
70	44.75	0.43904	40.75	0.44593

The volume magnetic susceptibility value decreases as the temperature increases and this experimental observation is in agreement with the basic assumption that the volume magnetic susceptibility relate to susceptibility per gram of salt by the relation $\chi_v = \chi \cdot d$ being χ susceptibility per gram of salt and d the density of the solution.

These correction values deserve some comment. Selwood (1956) cites in page 78, the compilation for molar magnetic susceptibilities due to Klemm (1941). In Table 3-7 the diamagnetic susceptibility for nitrates is obtained by Widemann's additivity law. They are compared with our values:

Table 3-8

Salt	$-\chi_M \cdot 10^6$[a]	$-\chi_y 10^6$[a] 0.5M Solution (20°C)	$-\chi_y 10^6$[b] 0.5 M Solution (20°C)
$LiNO_3$	26.6	0.30	0.519
$NaNO_3$	25.0	0.30	0.503
KNO_3	33.0	0.32	0.514
$CsNO_3$	51.0	0.26	0.502
$Ca(NO_3)_2$	28.0	0.17	0.512
$(CH_3)_4NNO_3$	no data available		0.512

[a]Klemm (1941) [b]This work

The values reported in the literature for $\chi_{Ca^{++}}$ ion range from 4.5 to 18.5 as reported by Selwood (1956). Klemm has chosen a value of 8 and adding one of the possible theoretical values for NO_3^- namely 20 a total for $\chi_{Ca(NO_3)_2}$ is obtained as shown in Table 3-8. The influence of hydrate formation on ionic diamagnetism has been demonstrated by Rao (1934). Even when diamagnetic susceptibility corrections are applied, chemical shifts measured from an external reference will often contain an appreciable error because of the uncertainties involved in the correction procedure e.g., geometry of cells, positioning, field homogeneity and theoretical treatment of the data (Emsley, Feeney and Sutcliffe, 1967).

Hydration Results for Nitrate Solutions

To obtain the hydration parameter the treatment due to Creekmore and Reilley (1969) is used. This treatment is based on

Malinowski (1966) assumption that only the chemical shift of the bulk water is affected by the temperature changes. The chemical shift may be written as

$$\delta_{cor} = X_b \delta_b + X_s \delta_s \tag{3}$$

where δ_{cor} is the observed chemical shift corrected for bulk susceptibility effects, X_b and X_s are the mole fractions of bulk and solvation water, respectively, and δ_b and δ_s are the chemical shift of the bulk and solvatation water, respectively. Taking the derivative of equation δ_{cor} respect to temperature in equation (3)

$$\delta_{cor}/dT = X_b(d\delta_b/dT) + X_s\,(d\delta_s/dT) \tag{4}$$

Because

$$(d\delta_s/dT) = 0 \qquad d\delta_{cor}/dT = X_b(d\delta_b/dT) \tag{5}$$

Since bulk water should behave as pure water, then

$$d\delta_b/dT = d\delta_{H_2O}/dT \tag{6}$$

where $\delta\ H_2O$ is the susceptibility corrected shift for pure water. Hence,

$$\delta_{cor}/dT = (1-X_s)\, d\delta_{H_2O}/\delta T \tag{7}$$

Since X_s is $\frac{hm}{55.55}$ where h is the total effective hydration number and m the molality

$$h = \frac{55.55}{m} \cdot \frac{d\delta H_2O/\delta T - d\delta_{cor}/dT}{d\delta H_2O/dT} \qquad (8)$$

Experimentally, the chemical shift is measured by employing an external reference standard in a spinning coaxial-sample-tube arrangement. The N.M.R. spectrum contains two chemically shifted sharp absorption bands, one from the contents of each container. The separation between the two signals is linearly dependent upon the volume susceptibility of the sample contained in the conventional sample tube and is given by the expression

$$\delta_{cyl}(R) - \delta_{sph}(R) = [g(cyl) - g(sph)][\chi_v(R) - \chi_v(S)] \qquad (9)$$

where δ is the chemical shift in ppm, χ_v is the volume susceptibility in c.g.s. units and g is the geometrical constant which is dependent on the shape of the interface between sample and reference, but is independent of the shape of the outer tube. Considering a molecule in a diamagnetic medium and enclosing this molecule with a sphere small in dimensions compared with the size of the sample but large compared with the molecular dimensions, then the effective field experienced by a nucleus in the molecule will depend upon:

a) the external field H_o

b) the diamagnetic susceptibility of the medium outside the sphere

c) the shielding effect of the molecular electrons and intermolecular effects.

The medium outside the sphere can be regarded as continuous with a volume diamagnetic susceptibility χ; therefore the effective field at the molecule is given in the treatment of Pople, Bernstein and Schneider (1959) by

$$H_{eff} = H_o[1+(\frac{4\pi}{3} - \alpha)\chi] \qquad (10)$$

where α is a shape factor which is zero for a sphere and 2π for infinite cylinder. In a cylindrical tube the diamagnetic susceptibility of the medium gives a contribution of $(\frac{2\pi}{3})\chi$ to the shielding constant σ

$$\text{i.e.} \qquad \sigma_{obs} = \sigma_{mol} + \frac{2\pi}{3}\chi \qquad (11)$$

If the chemical shift is referred to an external reference compound, then the chemical shift δ is given by

$$\delta = \sigma - \sigma_R = \frac{H - H_R}{H_R}$$

where σ is the shielding constant of the molecule and σ_R that of the reference compound. The chemical shift δ_{obs} and the chemical shift corrected for the difference in a diamagnetic susceptibility are related by

$$\delta_{cor} = \delta_{obs} + \frac{2\pi}{3}(\chi_{ref} - \chi_{sample}) \qquad (12)$$

If magnetic moments and field strength are both measured in magnetic units, its magnitude is of the order of -10^{-6} for common materials. In order to measure a susceptibility of substance of the

order of 10^{-6} with an accuracy up to one percent by this method, it is necessary to measure a change in inductance, up to 10^{-8}. Since the change in the inductance is noted according to the disruption of resonance between two circuits, then for each measurement in our Varian N.M.R. spectrometer, the constancy of the oscillation frequency methods of measuring the susceptibility are applicable only to substances in which a dependance of the susceptibility itself on the frequency cannot be expected. As seen from equation (8) we have to take the shift of water as temperature changes which is the term $d\delta H_2O/dT$ in this equation. The data is shown in Table 3-9 and δ_{cor} is related to δ_{obs} by equation 3-12.

Table 3-9

T°C	δ_{obs} ppm	$-(\chi_{v\,C_6H_{12}}-\chi_{vH_2O})10^6$	$2/3\pi(\chi_{vC_6H_{12}}-\chi_{vH_2O})10^6$	δ_{cor} ppm
10	-3.723	0.0891	0.186	-3.537
20	-3.632	0.0905	0.189	-3.442
30	-3.555	0.1034	0.216	-3.339
40	-3.482	0.1128	0.236	-3.246
50	-3.391	0.1191	0.249	-3.142
60	-3.305	0.1200	0.251	-3.057
70	-3.222	0.1268	0.265	-2.957

Our data has been processed by means of a Hewlett-Packard 9100-A desk computer using a least square fit. The proton chemical shift for all aqueous solutions were measured relative to external

cyclohexane with a precision of ±0.2 Hz and the value of the slope is

$$\delta_{cor}/dT = 0.00969 \pm 0.00018 \text{ ppm/deg}$$

This value agrees well with that of other investigators who reported values 0.0095 (Schneider et al., 1958) and 0.00956 (Maliknowski et al., 1966) and 0.00958 (Reilley and Creekmore, 1969). Figure 3-7 shows the shift as function of temperature. The goodness of the fit is given by ±0.00018. This error term refers to the correlation factor for a straight live fit and the error in the value of $\chi_v C_6H_{12}$. They are added in a square root and this approach will be used consistently throughout this work to state the error. It means that if we want to state the error in the determination of H where quantities A and B are involved being a the error in A, and b the error in B, then the error h of H is given by:

$$\frac{h}{H} = \sqrt{\left(\frac{a}{H}\right)^2 + \left(\frac{b}{B}\right)^2}$$

The precision in δ_{cor} is only to the third decimals since δ_{obs} cannot be read (in ppm) in a better way from the experiments.

$LiNO_3$ Solutions

When the proton resides in an electrolyte solution its resonance position differs from that of pure water due to the effect of cation and anion present. The term δ_{cor}/dT changes for each molarity of

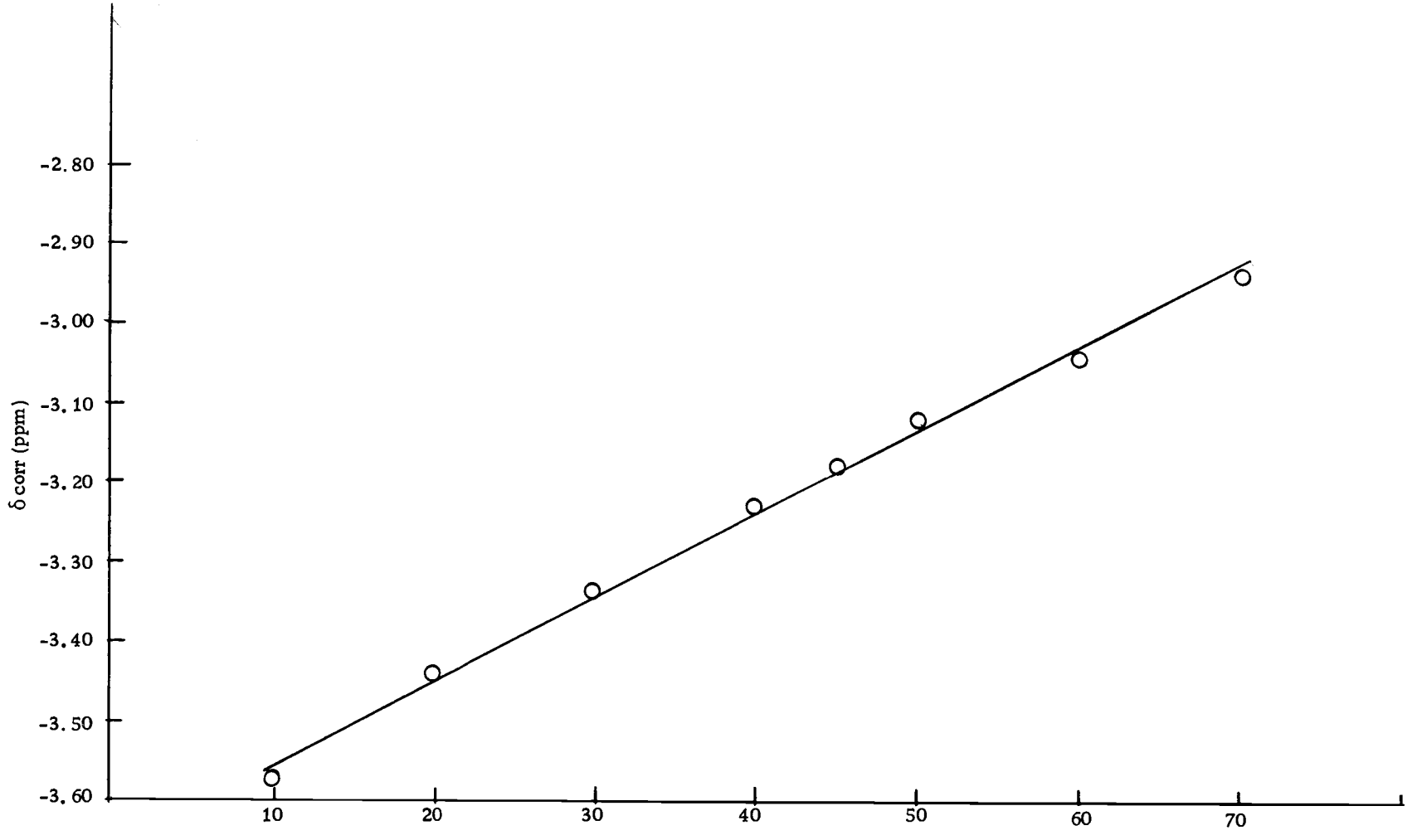

Figure 3-7. H_2O

$LiNO_3$. In the four lowest molarities the value of χ_v of 0.5 M $LiNO_3$ is used. In the four higher molarities the value of χ_v of 8.78 M is employed. It is done in this way due to the fact that as only three decimals are relevant in a correction factor (equation 12) and the values of χ_v at 0.5 M $LiNO_3$ and 8.78 M $LiNO_3$ being close, the interpolation in the values for intermediate molarities had negligible effect on the value of the hydration parameter (equation 8). The values for the observed and corrected shift for $LiNO_3$ solutions are presented in Tables 3-10 and 3-11.

Table 3-10

	1 M $LiNO_3$			2 M $LiNO_3$		3 M $LiNO_3$		4 M $LiNO_3$	
T°C	$-\delta^{b}_{obs}$	$-2/3\pi(\chi_{v_{C_6H_{12}}} - \chi_{v_{sample}})10^{6}$ [a]	$-\delta_{cor}$	$-\delta_{obs}$	$-\delta_{cor}$	$-\delta_{obs}$	$-\delta_{cor}$	$-\delta_{obs}$	$-\delta_{cor}$
10	3.676	0.236	3.912	3.607	3.893	3.605	3.841	3.531	3.767
20	3.605	0.228	3.833	3.534	3.762	3.520	3.748	3.429	3.649
30	3.528	0.241	3.769	3.455	3.696	3.425	3.666	3.391	3.632
40	3.414	0.228	3.646	3.391	3.619	3.377	3.605	3.333	3.561
50	3.350	0.178	3.528	3.315	3.493	3.321	3.499	3.272	3.450
60	3.290	0.167	3.457	3.251	3.418	3.259	3.421	3.212	3.379
70	3.230	0.178	3.408	3.192	3.370	3.180	3.358	3.158	3.336

[a] correction factor is the same for 1, 2, 3, 4 M $LiNO_3$ [b] δ_{obs} and δ_{cor} are in ppm.

Table 3-11

	5 M $LiNO_3$			6 M $LiNO_3$		7 M $LiNO_3$		8.78 M $LiNO_3$	
T°C	$-\delta^{b}_{obs}$	$-2/3\pi(\chi_{v_{C_6H_{12}}} - \chi_{v_{sample}})10^{6}$ [a]	$-\delta_{cor}$	$-\delta_{obs}$	$-\delta_{cor}$	$-\delta_{obs}$	$-\delta_{cor}$	$-\delta_{obs}$	$-\delta_{cor}$
10	3.535	0.247	3.782	3.515	3.751	3.490	3.737	3.375	3.622
20	3.440	0.245	3.665	3.153	3.692	3.417	3.662	3.335	3.580
30	3.370	0.258	3.628	3.392	3.664	3.340	3.598	3.290	3.548
40	3.299	0.230	3.529	3.352	3.636	3.279	3.509	3.233	3.463
50	3.231	0.180	3.411	3.260	3.564	3.219	3.399	3.174	3.354
60	3.181	0.165	3.346	3.197	3.509	3.162	3.327	3.118	3.283
70	3.027	0.178	3.702	3.149	3.478	3.087	3.265	3.021	3.199

[a] correction factor is the same for 5, 6, 7, 8.78 M $LiNO_3$ [b] δ_{obs} and δ_{cor} are in ppm.

A summary of the hydration values obtained is presented in Table 3-12. The hydration parameter is h.

Table 3-12
$LiNO_3$

Molality	Molarity	Temp range	δ_{cor}/dT	h
0.51	0.50	10-70°C	0.00879 ±0.00043	10.1 ±0.6
1.03	1.00	10-70°C	0.00880 ±0.00030	4.9 ±0.2
2.13	2.00	10-70°C	0.00880 ±0.00029	4.0 ±0.2
3.31	3.00	10-70°C	0.00825 ±0.00033	2.8 ±0.2
4.55	4.00	10-70°C	0.00720 ±0.00019	3.1 ±0.1
5.92	5.00	10-70°C	0.00679 ±0.00016	2.8 ±0.1
7.40	6.00	10-70°C	0.00659 ±0.00017	2.2 ±0.1
8.99	7.00	10-70°C	0.00816 ±0.00017	1.0 ±0.1
12.20	8.78	10-70°C	0.00735 ±0.00022	1.1 ±0.1

The values obtained for the hydration of $LiNO_3$ by the present method are very close to the values obtained by Troshin (1965) for molarities ranging between three and six molar solutions of $LiNO_3$. Troshin used data from the transfer number of Li in $LiNO_3$ solutions calculating the mobility of the ions in the solution.

$NaNO_3$ Solutions

In the case of $NaNO_3$ solutions results are shown in Tables 3-13, 14, 15. The correction factor obtained at 0.5 M $NaNO_3$ is used in 0.5 and 1 M. The correction factor obtained at 7.85 M is employed in solutions 6 and 7.85 M. An interpolated value for susceptibility corrections was applied in solutions 3.5 to 5 M $NaNO_3$. A summary of hydration values is presented in Table 3-15.

Table 3-13

	0.5 M $NaNO_3$			1 M $NaNO_3$		2.5 M $NaNO_3$			3.25 M $NaNO_3$	
T^oC	$-\delta_{obs}$	$-2/3\pi(\chi_{v_{C_6H_{12}}} - \chi_{v_{sample}})10^6$	$-\delta_{cor}$	$-\delta_{obs}$	$-\delta_{cor}$	$-\delta_{obs}$	$-2/3\pi(\chi_{v_{C_6H_{12}}} - \chi_{v\ sample}$	$-\delta_{cor}$	$-\delta_{obs}$	$-\delta_{cor}$
10	3.69	0.262	3.953	3.649	3.911	3.478	0.255	3.733	3.432	3.687
20	3.612	0.260	3.872	3.503	3.872	3.390	0.253	3.643	3.365	3.618
30	3.523	0.264	3.769	3.424	3.688	3.320	0.245	3.565	3.295	3.540
40	3.429	0.258	3.687	3.359	3.617	3.256	0.247	3.503	3.248	3.495
50	3.348	0.214	3.562	3.258	3.472	3.187	0.230	3.417	3.178	3.408
60	3.355	0.207	3.562	3.201	3.408	3.118	0.186	3.304	3.114	3.300
70	3.179	0.207	3.386	3.112	3.319	3.051	0.201	3.252	3.039	3.240

[a] δ_{obs} and δ_{cor} are in ppm.

Table 3-14

	4 M $NaNO_3$		5 M $NaNO_3$		6 M $NaNO_3$			7.85 M $NaNO_3$	
T^oC	$-\delta_{obs}$	$-\delta_{cor}$	$-\delta_{obs}$	$-\delta_{cor}$	$-\delta_{obs}$	$-2/3\pi(\chi_{v_{C_6H_{12}}} - \chi_{v_{sample}})10^6$	$-\delta_{cor}$	$-\delta_{obs}$	$-\delta_{cor}$
10	3.358	3.613	3.349	3.603	3.332	0.262	3.594	3.186	3.448
20	3.294	3.547	3.286	3.539	3.260	0.260	3.520	3.130	3.390
30	3.224	3.469	3.228	3.473	3.196	0.268	3.767	3.078	3.342
40	3.153	3.400	3.151	3.398	3.137	0.258	3.395	3.014	3.272
50	3.089	3.319	3.090	3.320	3.076	0.211	3.290	2.970	3.181
60	3.044	3.230	3.028	3.214	3.003	0.197	3.219	2.924	3.121
70	2.989	3.190	2.973	3.174	2.948	0.207	3.169	2.874	3.081

[a] δ_{obs} and δ_{cor} are in ppm.

Table 3-15
$NaNO_3$

Molality	Molarity	Temp Range	$-\delta_{cor}/dT$	h[a]
0.51	0.50	10-70°C	0.00912 ±0.00045	6.4 ±0.4
1.03	1.00	10-70°C	0.00890 ±0.00034	4.3 ±0.2
2.73	2.50	10-70°C	0.00810 ±0.00027	3.4 ±0.2
3.64	32.5	10-70°C	0.00753 ± 0.00025	3.4 ±0.1
4.49	4.00	10-70°C	0.00733 ±0.00023	3.0 ±0.1
6.04	5.00	10-70°	0.00747 ± 0.00020	2.1 ±0.1
7.55	6.00	10-70°C	0.00732 ±0.00021	1.8 ±0.1
10.84	7.85	10-70°C	0.00635 ±0.00019	1.8 ±0.1

[a] h: hydration parameter

For $NaNO_3$ the values obtained in the present work agree quite well with the value reported by Vogrin et al. (1970).

KNO_3 Solutions

Results for $NaNO_3$ solutions are shown in Tables 3-16 and 3-17. The correction factor obtained at 0.5 M is used in 0.5 M and 1 M solutions. The correction factor of a 2.98 M KNO_3 is employed to correct 2 M and 2.98 M solutions.

Table 3-16

T°C	0.5 M KNO_3 $-\delta^a_{obs}$	0.5 M KNO_3 $2/3\pi(\chi_{v_{C_6H_{12}}} - \chi_{v_{sample}})10^6$	0.5 M KNO_3 $-\delta_{cor}$	1 M KNO_3 $-\delta_{obs}$	1 M KNO_3 $-\delta_{cor}$	2 M KNO_3 $-\delta_{obs}$	2 M KNO_3 $2/3\pi(\chi_{v_{C_6H_{12}}} - \chi_{v_{sample}})10^6$	2 M KNO_3 $-\delta_{obs}$	2.98 M KNO_3 $-\delta_{obs}$	2.98 M KNO_3 $-\delta_{cor}$
10	3.684	0.240	3.924	3.668	3.908	3.526	0.247	3.773	3.450	3.697
20	3.600	0.243	3.843	3.569	3.812	3.435	0.245	3.680	3.357	3.602
30	3.510	0.249	3.759	3.465	3.714	3.343	0.257	3.600	3.281	3.538
40	3.420	0.220	3.640	3.405	3.625	3.296	0.228	3.524	3.232	3.460
50	3.328	0.235	3.563	3.300	3.535	3.219	0.180	3.399	3.149	3.329
60	3.245	0.220	3.465	3.213	3.443	3.149	0.165	3.307	3.072	3.237
70	3.176	0.225	3.901	3.157	3.382	3.062	0.177	3.234	3.009	3.187

[a] δ_{obs} and δ_{cor} are reported in ppm.

A summary for hydration values of KNO_3 solution is shown in Table 3-17.

Table 3-17

KNO_3

Molality	Molarity	Temp Range	δ_{cor}/d_T	h[a]
0.51	0.50	10-70°C	0.00025 ±0.00036	7.7 ±0.4
1.04	1.00	10-70°C	0.00910 ±0.00030	4.4 ±0.2
2.20	2.00	10-70°C	0.00900 ±0.00029	1.8 ±0.1
3.46	2.98	10-70°C	0.00882 ±0.00029	1.4 ±0.1

[a] h: hydration parameter

$CsNO_3$ Solutions

Results for $CsNO_3$ solutions are shown in Tables 3-18 and 3-19. The correction factor for the 0.56 M solution is an interpolated value between χ_v of 0.1 M and a 1.12 M solution of $CsNO_3$. The correction factor at 1.12 M is determined at that molarity.

Table 3-18

	0.56 M $CsNO_3$			1.12 M $CsNO_3$		
T°C	$-\delta^a_{obs}$	$2/3\pi(\chi_{v_{C_6H_{12}}} - \chi_{v_{sample}})10^6$	$-\delta_{cor}$	$-\delta_{obs}$	$2/3\pi(\chi_{v_{C_6H_{12}}} - \chi_{v_{sample}})10^6$	$-\delta_{cor}$
10	3.652	0.247	3.899	3.633	0.230	3.863
20	3.557	0.249	3.806	3.542	0.234	3.776
30	3.470	0.260	3.730	3.448	0.266	3.714
40	3.415	0.236	3.651	3.405	0.233	3.638
50	3.331	0.187	3.515	3.239	0.172	3.471
60	3.242	0.174	3.416	3.220	0.244	3.474
70	3.157	0.184	3.341	3.117	0.182	3.299

[a] δ_{obs} and δ_{cor} are reported in ppm.

A summary for hydration values is shown in Table 3-19.

Table 3-19
$CsNO_3$

Molality	Molarity	Temp Range	δ_{cor}/δ_T	h[a]
0.58	0.56	10-70°C	0.00953 ±0.00027	1.7 ±0.1
1.29	1.12	10-70°C	0.00919 ±0.00030	2.1 ±0.1

[a]h: hydration parameter.

$Ca(NO_3)_2$ Solutions

Results for $Ca(NO_3)_2$ solutions are shown in Tables 3-20, 21, 22. Correction susceptibilities determined at 1 M $Ca(NO_3)_2$ (in NO_3^- concentration) are used for molarities up to 5 M. At higher molarities the correction factor determined at 9 M $Ca(NO_3)_2$ (in NO_3^-) is employed.

A summary for hydration values are presented in Table 3-22.

The value reported by Vogrin et al. (1970) for only one concentration is close to the value we found for the same concentration. It is generally believed that doubly charged ions such as Ca^{++} are likely to affect the proton shifts of water molecules in the secondary layer (long range effect on bulk) because of the increased charge (Swift and Sayre, 1965).

Table 3-20

Molarities in Nitrate

T°C	1 M $(CaNO_3)_2$ $-\delta_{obs}$	$2/3\pi(\chi_{v_{C_6H_{12}}} - \chi_{v_{sample}})10^6$	$-\delta_{cor}$	3 M $(CaNO_3)_2$ $-\delta_{obs}$	$-\delta_{cor}$	4 M $Ca(NO_3)_2$ $-\delta_{obs}$	$-\delta_{cor}$	5 M $NaNO_3$ $-\delta_{obs}$	$-\delta_{cor}$
10	3.679	0.240	3.919	3.680	3.850	3.661	3.831	3.647	3.817
20	3.615	0.230	3.845	3.596	3.776	3.597	3.777	3.582	3.762
30	3.530	0.220	3.750	3.538	3.773	3.536	3.731	3.523	3.738
40	3.454	0.200	3.654	3.475	3.685	3.485	3.695	3.489	3.699
50	3.380	0.190	3.575	3.381	3.601	3.397	3.617	3.409	3.629
60	3.309	0.190	3.899	3.345	3.565	3.371	3.531	3.357	3.579
70	3.255	0.190	3.455	3.293	3.518	3.317	3.537	3.302	3.527

Table 3-21

T°C	7 M $(CaNO_3)_2$ $2/3\pi(\chi_{v_{C_6H_{12}}} - \chi_{sample})10^6$	$-\delta_{cor}$	$-\delta_{obs}$	9 M $Ca(NO_3)_2$ $-\delta_{cor}$	$-\delta_{obs}$	11 M $(CaNO_3)_2$ $-\delta_{cor}$	
10	3.642	0.180	3.812	3.610	3.790	3.605	3.785
20	3.586	0.186	3.766	3.577	3.752	3.565	3.751
30	3.527	0.194	3.722	3.505	3.699	3.515	3.709
40	3.484	0.213	3.694	3.483	3.696	3.477	3.690
50	3.431	0.222	3.651	3.474	3.696	3.433	3.655
60	3.381	0.218	3.609	3.400	3.618	3.394	3.612
70	3.326	0.225	3.546	3.355	3.518	3.375	3.600

[a] δ_{obs} and δ_{cor} are reported in ppm.

Table 3-22
$Ca(NO_3)_2$

Molality $[NO_3^-]$	Molarity $[NO_3^-]$	Temp Range	δ_{cor}/δ_T	h
1.11	1.00	10-70°C	0.00819 ±0.00031	7.8 ±0.3
3.24	3.00	10-70°C	0.00734 ±0.00025	7.3 ±0.3
4.44	4.00	10-70°C	0.00485 ±0.00015	6.3 ±0.2
6.53	5.00	10-70°C	0.00480 ±0.00018	4.3 ±0.2
7.42	7.00	10-70°C	0.00422 ±0.00010	4.1 ±0.1
12.50	9.00	10-70°C	0.00322 ±0.00011	3.0 ±0.1
14.92	11.00	10-70°C	0.00317 ±0.00006	2.5 ±0.1

$(CH_3)_4 NNO_3$ Solutions

Results for $(CH_3)_4 NNO_3$ are shown in Tables 3-23, 24. The correction factor for 1.10 M is the one obtained at 0.5 M. The correction for 2.42 and 3.89 M is determined at 3.89 M. Very little difference exist for these values even in the third decimal range as shown in Table 3-7.

Table 3-23

	1.10 M $(CH_3)_4 NNO_3$			2.42 M $(CH_3)_4 NNO_3$			3.89 M $(CH_3)_4 NNO_3$	
T°C	$-\delta_{obs}$	$2/3\pi(\chi_{v_{C_6H_{12}}} - \chi_{v_{salt}})10^6$	$-\delta_{cor}$	$-\delta_{obs}$	$2/3\pi(\chi_{v_{C_6H_{12}}} - \chi_{v_{salt}})$	$-\delta_{cor}$	$-\delta_{obs}$	$-\delta_{cor}$
10	3.408	0.236	3.645	3.221	0.232	3.454	3.198	3.430
20	3.315	0.240	3.556	3.228	0.224	3.453	3.117	3.331
30	3.221	0.245	3.466	3.132	0.245	3.377	3.009	3.254
40	3.182	0.213	3.395	3.085	0.213	3.298	2.979	3.192
50	3.127	0.169	3.296	3.053	0.161	3.214	2.954	3.115
60	3.028	0.184	3.213	2.994	0.151	3.146	2.898	3.050
70	2.938	0.180	3.139	2.907	0.166	3.073	2.807	2.973

The hydration values are shown in Table 3-24.

Table 3-24

Molality	Molarity	Temp Range	δ_{cor}/T	h[a]
1.15	1.10	10-70°C	0.00841 ±0.00021	6.4 ±0.2
2.77	2.42	10-70°C	0.00765 ±0.00017	4.2 ±0.2
6.00	3.89	10-70°C	0.00747 ±0.00016	2.0 ±0.1

[a]h: hydration parameter

Previous Work on Nitrate Solutions

The primary work of the proton resonances of aqueous electrolytes by Shoolery and Alder (1955) served to introduce two concepts in terms of which all subsequent measurements have been interpreted. Hydration of ions resulted in an increase in disorder in arrangement of water molecules with the breaking of hydrogen bonds and a consequent change to high field in proton chemical shift. For 1:1 electrolytes the structure breaking effect was dominant, the chemical shift increasing linearly with concentration. The data were interpreted by Shoolery and Alder in terms of the combined effect of a low-field shift for the protons of water molecules strongly bonded to ions, together with a high field shift due to the tendency of the ion to break up the hydrogen bonded structure of the water itself. Some broadening of peaks is discussed here in conjunction with relaxation mechanisms, and it was pointed out that the major contribution

to the line width was the viscosity of the solution.

As a result of Shoolery and Alder's work, Hindman (1962) studied the shifts of nitrates of NH_4NO_3, $LiNO_3$, $NaNO_3$, KNO_3 as a function of concentration 25 ±0.2°C. He works out expressions to calculate separately the hydration of cation and anion. He used cyclopentane as an external reference. Infinite dilution shifts (δ^o_{salt}) values were derived plotting δ_{obs} vs. m, the concentration in moles per 1000 grams water, as shown in Figure 3-8. Hindman (1962) thinks that the water molecules are reoriented by the ion and assigns to each ion a chemical shift value representing its contribution to the total shift of a given electrolyte. The shifts were also expressed in terms of individual ionic effects like Shoolery and Alder (1955). An effective hydration number for ions is so calculated namely for Li^+ 4.0 Na^+ 3.1, K^+ 2.1, Cs^+ 1.0, NO_3^- 0; for nitrates of the first group. Hindman does not believe in a tightly bound hydration shell as a consequence of his work, but the values obtained agree with the primary hydration estimates obtained from other types of measurements.

Fabricand and Goldberg (1961) estimate that breaking points appear when the shift is plotted against concentration of electrolytes when no more free water is present. In Figure 3-9 an inflection should take place when a linear dependence of shift against concentration disappears, indicating it is no more bulk water present.

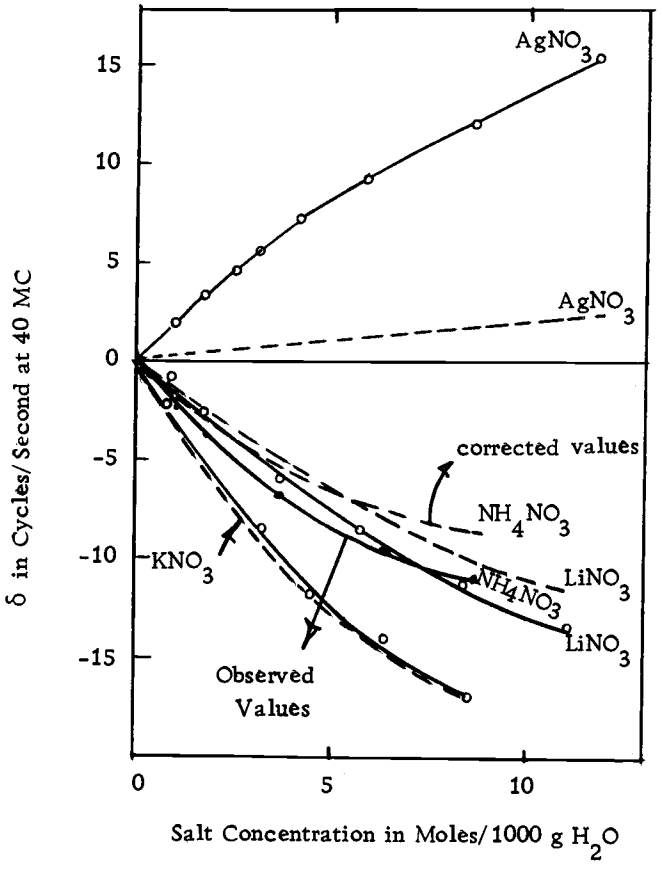

Figure 3-8. δ-concentration data for +1 nitrates.

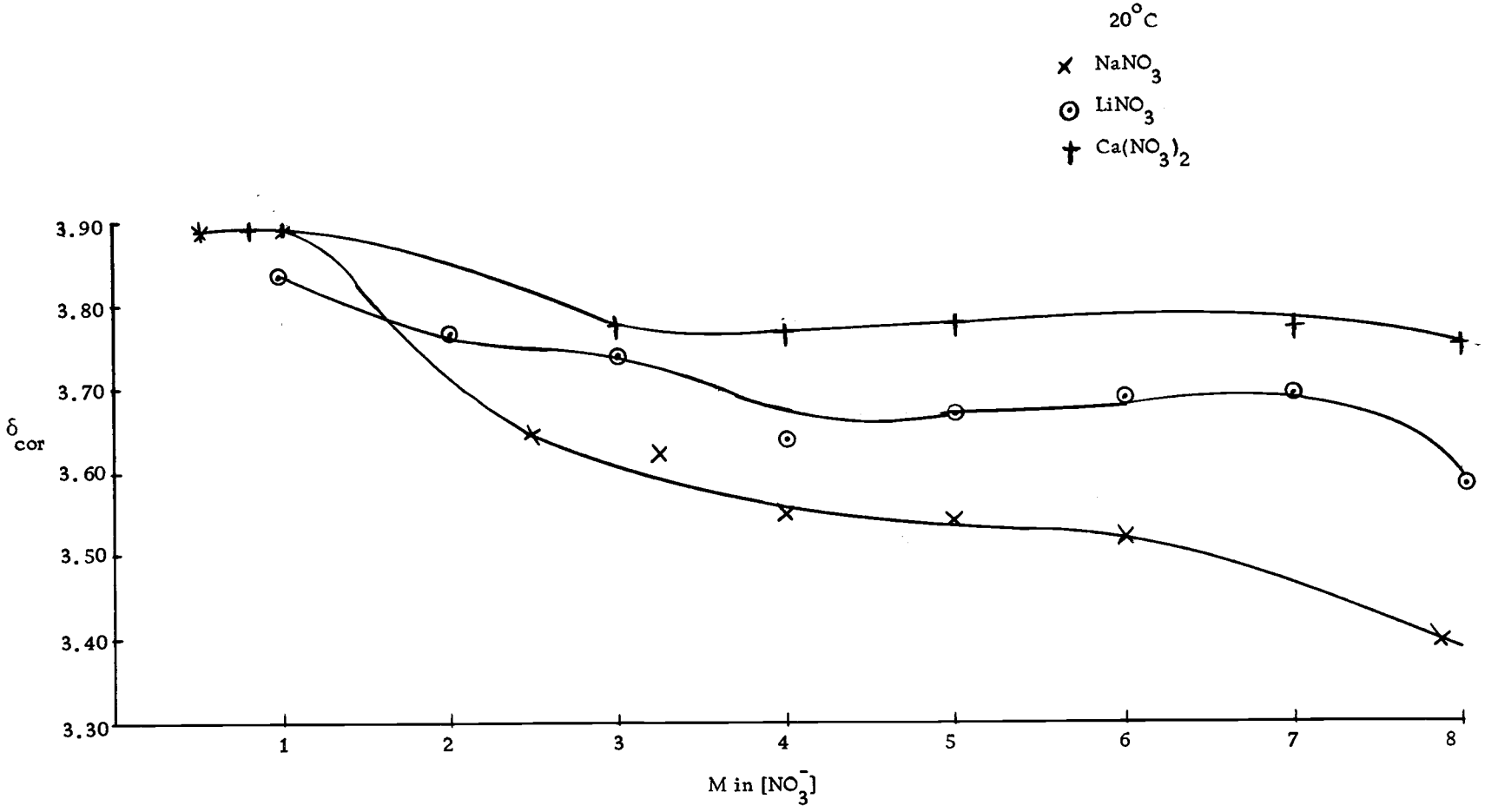
20°C
NaNO3
LiNO3
Ca(NO3)2
3.90
3.80
3.70
3.60
3.50
3.40
3.30
δcor
1
2
3
4
5
6
7
8
M in [NO3-]

Figure 3-9

It seems from these figures that several factors like viscosity, ion-pairing, hydrate formation take place as the concentration is increased and not a simple cation-anion repartition of bound water at higher concentrations. More work to explain the shape of the curves in Figure 3-9 remains a task of the future. Vogrin et al. (1971) works on some nitrates applying the N.M.R. technique in the same way it has been done here, and the values reported have been already compared to those reported in this work.

Discussion

The method we follow assumes that the proton resonance frequency of the water molecules in the hydration shell of the ions is independent of temperature. This may not be true in the structure broken region, but results by Malinowski, Knapp and Feuer (1966) using this approach is comparable to those obtained from thermodynamic properties (Conway and Bockris, 1954). For the N.M.R. studies applying different temperatures it is considered as a consequence of this model, that the proton shift of "normal" water is strongly dependent on temperature as it is in the case of pure water. Indeed, the linear shift caused by increasing temperature has been used to compare various structural models of water (Müller, 1965). When strong electrolytes are added to water, the proton shift is found to be strongly dependent upon the concentration. Our studies

follow the pattern established by Malinowski, Knapp and Feuer (1966) and Creekmore and Reilley (1969) and they considered the "first hydration shell" as consisting of the region of immobilized water and the structure broken region. The shift of shift observed therefore is a weighted average of some property of the hydration shell (hydrated forms and hydrogen bonding) and the bulk. In general ionic effects on the hydrogen nuclear shielding do not extend past the nearest neighbour water molecules. Hydrogen bonding arrangement of bulk water is destroyed progressively as we go up in temperature. The method assumes that the proton resonance frequency of the water molecules in the hydration sphere of the ions is independent of temperature. This may not be true for the proton water located in the structure broken region, but our results are comparable to those obtained from other measurements.

We do not get the same results for the hydration parameter using infrared and N.M.R. measurements because each method used to determine hydration serves to measure a different property of the substance. The number obtained in each case was difficult to interpret in terms of any fixed definition of hydration. Such a useful definition of hydration is difficult to obtain and it may vary from system to system. We are not only confronted with obtaining our spectra but also how to interpret it. The hydration number is therefore an empirical parameter which gives the "effective" number of

water molecules that have undergone some change in property, but the change observed is a change of "some" property of the solution under study. It is not known if h, the hydration parameter, is for water molecule interaction at close distance or also includes weaker effects on more distant water molecules.

It has been argued for some time that a sharpening of proton resonance lines occurs when the temperature is raised because they disrupt molecular aggregates whatever they are (Emsley et al., 1967). No regular sharpening was observed in the spectra of electrolytes as the temperature is raised in the peaks under study.

Since solutions containing solely cations or solely anions cannot be prepared we assign an average shift δ_h to the proton in its hydrated forms. The average time a proton resides in either water or in an ionic atmosphere its proportional to its instantaneous mole fraction. That is,

$$\delta = X_{H_2O}\,\delta_{H_2O} + X_{salt}\,\delta_h$$

where X_{H_2O} and X_{salt} are the mole fraction in water structure and hydrated form. But this information does not give any way to ascribe hydration to the anion or cation independently. Many workers have speculated with the idea that there is a difference in the mode of bonding of water around anions and cations. From the point of view that affects our P.M.R. signals, if a proton might become embedded

in the electron cloud of the anion it becomes more shielded and resonates at a higher field relative to pure water as shown.

$$H^{+} \longrightarrow {}^{-}O_3N$$

Anions should have a greater effect on the P.M.R. signal than cations and possible bonds of cations and anions are screened by the oxygen atom. It is attempted in the present work to separate the hydration of cation and anion by the use of $(CH_3)_4NNO_3$, ascribing all hydrations to the nitrate group for reasons already stated in chapter two. Glueckauf (1955) first used this approach to separate specific hydration for the cation and the anion. The assignment of values for individual hydration numbers for cation and anions is shown in Table 3-25 and these values are based on Table 3-24.

Table 3-25

Salt	$M[NO_3^-]$	Total Hydration	Cation	Anion
$LiNO_3$	4.0	3.1	1.5	1.8
$NaNO_3$	4.0	3.0	1.2	1.8
$Ca(NO_3)_2$	3.0	7.3	4.0	3.3
	4.0	6.3	4.5	1.8

The values for Ca^{++} coincide quite well with those reported by Swift and Sayre (1965). That other effects take place here when applying the approach to determine hydration of cation and anion

individually, show that $(CH_3)_4NNO_3$ presents some unusual behaviour.

A controversial topic is the explanation of the magnitude of the shift observed in solution as the concentration of electrolye is varied. Shoolery and Alder (1955) stated that the shift magnitude is due to the combined effect of a) competition for water molecules, 2) change in polarization, 3) ion-pair or complexion formation. Pimentel and McClellan (1959) ascribe the P.M.R. shifts as a measure of the mean hydrogen bond energies. Luz and Yagil (1966) estimate that the main cause of these shifts in electrolyte solution is the variation of the direct interaction between ions and adjacent molecules as concentrations is changed. Polarization of water molecules by ions gives a decrease in chemical shift (Hindman, 1962). Maliknowski, Knapp and Feuer (1966) see the variation of the value of δ, as a measure of the different time a proton spends in the normal water structure (which consists of hydrogen bonded and non hydrogen bonded forms) and another fraction of its time as a part of water molecules complexed with the ions.

As a summary view, we may say that the proton exists in five environments given by pure water and the first and second hydration shell of cation and anion. But it seems reasonable to account for the magnitude of the bond shift as due to four effects which are very difficult to account independently: (1) bond breaking, (2) polarization, (3) non electrostatic effects, (4) structural effects.

IV SPECTRAL STUDIES OF NITRATE SOLUTIONS

Pure Salt Spectra

Introduction

Several authors have investigated the band structure of nitrate ions by infrared, Raman, ultraviolet and X-ray methods (McGlynn, 1956; Shutte, 1963). The results of these works are widely known: the nitrogen-oxygen bond has the character of a partial double bond. In spite of this, the structure has not been fully clarified. This also appears from the numerous forms of representation of the nitrate ions. Most widely used are the structures where it is shown that besides a σ bonding pair, a π electron pair exists in the ion.

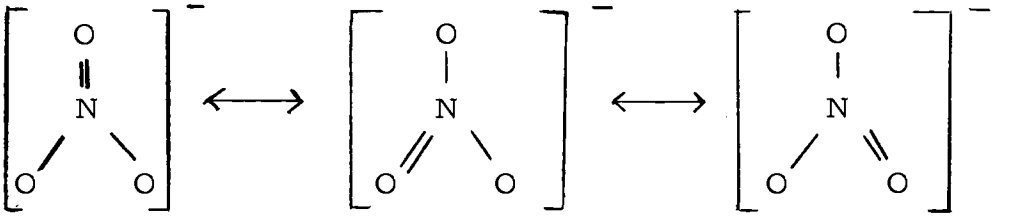

From the work of Orville-Jones and Thomas (1960) it is known that, using linear combination of atomic orbitals, parameter calculations can be made for molecules that have one heterogeneous atom. Strickler and Kasha (1964) give a detailed interpretation of the spectrum of nitrate ions based on the same method.

The spectrum of the nitrate ion in ionic medium has received much attention. The reason for the interest lies in the fact that the

spectrum is a function of the ionic environment, so that the nitrate-ion spectrum serves as an indicator of specific ionic interactions. In most cases metal nitrate interactions have not been characterized.

In dilute solution the system consists presumably of completely solvated spectral ions: $M^{+}_{aq} + NO^{-}_{3aq}$. From relaxation experiments the ions in this state are known to diffuse together with a rate predicted by the Debye theory and in agreement with solvent dielectric measurements, solvent viscosity, ionic strength in the continuum solvent model (Atkinson and Petrucci, 1966). The success of the Debye theory has been in the extreme low range of electrolyte concentration. Above a 10^{-2} M concentration in spite of much experimental or theoretical work nothing is known with certainty. It seems that at higher concentration the Van der Waal's forces become of equal or greater importance than the electrostatic forces in solution. Depolymerization effects in water by the ions seem to be a complicated problem not fully understood yet.

A number of investigators have previously interpreted the weak NO^{-}_{3} band in the near ultraviolet at 4.1 e.v. as a forbidden $n \rightarrow \pi^*$ band. McConnell (1952) first made this suggestion after comparing the spectra of derivatives of NO^{-}_{3}, CO^{-2}_{3} and CS^{-}_{3}. Walsh (1953) has also considered to be a $n \rightarrow \pi^*$ transitions on the basis of simple linear combinations of atomic orbitals. Many experiments have been carried out to find a general criterion for the type of transition involved,

mainly for organic compounds. Solvent effects were applied for this purpose and the property that $n \rightarrow \pi$ transitions shift to the blue as we increase the polarity of the solvent is generally accepted as a characteristic for this type of transition. In the case of $\pi \rightarrow \pi^*$ transitions a shift to the red serves to identify this other type of transition.

A transition that is forbidden as an electric dipole process can be observed only when the nitrate ion is suitably perturbed by vibrations or an asymmetric environment. Such vibrational perturbations may account for a change in the oscillator strength (f) and extinction coefficient when the concentration or solvent is varied. Since it is a weak band, if it is a singlet-singlet transition the high symmetry of NO_3^- (D_{3h}) must play an important part in fixing the selection tube. However McEwen's (1961) suggestion on theoretical grounds, that it may be $n \rightarrow \sigma$ is supported by Rothevi and Treinin (1965). It must be considered in this type of treatment that ion-pairs in solution are formed and the change in symmetry due to the deformation in the geometry of the ion-pair, is very difficult to account in this case. According to McEwens (1961) and Smith and Boston (1961) the 300 mμ band is due to excitation of the lone pair nonbonding electron in the oxygen into an antibonding π orbital (π^* orbital) of the NO_3^-.

The smaller the crystalline radius of a cation in a series the higher the solubility of the nitrate. But not much can be said about

the prediction of this higher limit of solubility, mainly due to the fact that the determination of the energies in a Born-Haber cycle is not possible (Russell, Drago and Purcell, 1965) and that energies of hydration and crystal lattice type do not provide all the information needed to account for a solubility limit in concentrated solutions.

Raman spectroscopy is capable of answering many interesting questions concerning the structure of solutions. The type of spectrum e.g., the number of lines, depolarization factors and mainly the frequency shifts can aid in the complete identification of a species in solution. The ratio of integrated intensities between two solutions is often equal to the ratio of concentrations of a Raman active substance in the two solutions. Results from Raman spectroscopic work will be used to compare and explain results obtained by studies in the ultraviolet region.

The refraction as well as the absorption does not change linearly with concentration (as it is the case in dilute solutions) and in concentrated solution the dispersion theory predicts that the refractive index will have a strong influence on the coefficient of absorption (Fajans, 1928). The value of the refractive index is a function of the nature of the media, the solute and the density of the solution. Interactions between ions in concentrated solutions such as the alkali metal nitrates apparently are responsible for the deviations of observed properties from properties predicted from theories which

assume complete dissociation. These deviations are described in terms of ion-pairs. Previous work on nitrates (Halban and Eisenbrand, 1928; Kortüm, 1944) ascribe the optical ultraviolet observations of nitrate solutions to the existence of ion-pairs and ions with different degree of solvatation. Darmois (1928) argued that the water shell in ion-pair would enhance interaction of cation and anion producing deformation of the NO_3^- molecule which may account for irregularities in the transition of nitrate solutions of intermediate concentration and up. Ion-pair considerations will be presented in this work and the approach used is purely operational in that we will ascribe some special effects to these ion-pairs. Nothing is known of their real nature but we will assume that its absorption is different from NO_3^- ion. The concept of ion-pair is well accepted in the literature (Robinson and Stokes, 1955; Hammer, 1959) but the actual definition of ion-pair varies among workers.

Experimental Part

Spectrophotometric measurements were carried out with a Cary 1501 spectrophotometer. Silica absorption cells were used of 10, 5, 1 and 0.5 cm. pathlength. A variable pathlength cell manufactured by Research and Industrial Instruments Company (England) Ser N^o 1846 was employed when pathlengths between 0.5 and 0.01 cm were necessary. This cell had CaF_2 windows fabricated by Beckman

(Fullerton, California). The pathlength of the cell was determined as indicated by Vandenbelt and Spurlock (1955) using a solution 8.22 10^{-4} M K_2CrO_4 that is 0.05 M in KOH. The extinction coefficient of such a solution is 4775 at 27.000 cm^{-1}. All the salts used were A.R. grade, filtered through sintered glass and recrystallized. The water used was triple distilled water from permanganate and dilute dichromate solution. Tetramethyl ammonium nitrate was made by adding a solution of Merck reagent silver nitrate to a solution of Eastman White Label tetramethyl ammonium iodide. These solutions were made from accurately weighed equivalent amounts of the two materials. The silver iodide was filtered off with a fine fritted glass filter, and the solution evaporated to obtain the tetramethyl-ammonium nitrate. This material was very difficult to recrystallize because of its very high water solubility and very low solubility in other solvents. The limit of accuracy of our measurements is about one percent. We did not correct our measurements for reflexion and dispersion losses. The expression for the oscillator strength is

$$f = 4.32 \cdot 10^{-9} \int \varepsilon(\gamma)\, d\gamma = 4.32\, 10^{-9}\, A$$

being ε molar absorption absorption coefficient, γ the wave number and A the area ($M^{-1} cm^{-2}$). This expression for oscillator strength would apply for homogeneous solutions where one specie is present. But in the absorption of an electrolyte where a solvent and a solute

are present the coefficient of absorption has to be considered as a function of the index of refraction of the media. The expression for oscillator strength becomes then

$$f = 4.32\ 10^{-9} \frac{n}{(n^2+2)^2} A$$

since the absorption coefficient is not pure ε but $\frac{\varepsilon \cdot n}{(n^2+2)^2}$ (Kortüm, 1955).

Results and Discussion

Spectral studies of nitrate solutions received much attention between 1920 and 1944 mainly in Germany due to Kortüm (1930, 35, 44). Halban and Eisenbrand (1928), Hantzsch (1939). Only two more modern publications have further studied this problem: Meyerstein and Treinin (1961) and Rotlevi and Treinin (1965). Work involving pure salt spectra of more concentrated solutions were reported for KNO_3 and $Ca(NO_3)_2$ by Halban and Eisenbrand (1928) and for $LiNO_3$ by Halban (1928).

$LiNO_3$ Solutions. We have taken pure salt spectra of $LiNO_3$ solutions as presented in Figure 4-1. The curves in Figure 4-1 a) decrease in height as the concentration increases b) shift to the blue at higher molarities and c) no isosbestic point is found.

Halban and Eisenbrand (1928) observed that Beer's law does not hold in concentrated $LiNO_3$ solutions (3M and up). This

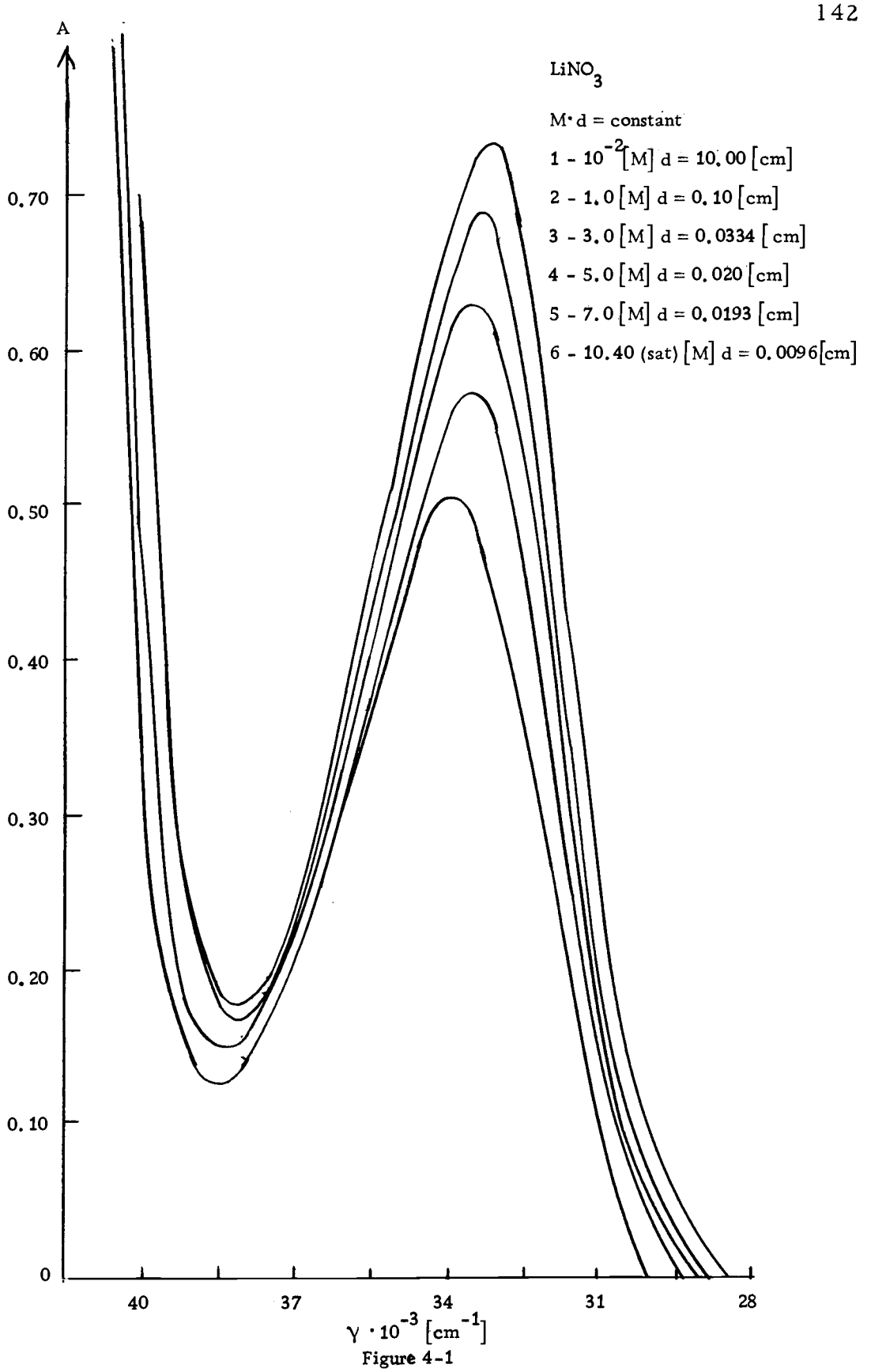
A
LiNO3
M·d = constant
1 - 10^-2 [M] d = 10.00 [cm]
2 - 1.0 [M] d = 0.10 [cm]
3 - 3.0 [M] d = 0.0334 [cm]
4 - 5.0 [M] d = 0.020 [cm]
5 - 7.0 [M] d = 0.0193 [cm]
6 - 10.40 (sat) [M] d = 0.0096 [cm]
0.70
0.60
0.50
0.40
0.30
0.20
0.10
0
40
37
34
31
28
γ · 10^-3 [cm^-1]

Figure 4-1

observation was initially discounted because it challenged the classical dissociation theory. They argued that ε values are decreased due to a) ion-pair formation at higher concentration removing a significant amount of the NO_3^- ions from the solution b) the NO_3^- is deformed in the electric field of the cations and this had as a consequence the alteration of the optical properties of the salt. The cation then would influence the light absorption of the anion if they are present in sufficient high quantity. In their work they determined an association constant for the $LiNO_3$ using ε values, the respective water partial pressures and extrapolating to zero ionic strength at concentrations beyween 3.9 and 8.5 M. They arrive at a K_{assoc} = 0.036. By conductivity (Davies, 1931) gives $K_{assoc} \leq 0.2$, studying solutions of $LiNO_3$ up to 0.1 M. More recent work for the determination of an association constant for nitrates is scarce. Kangro (1962) by partial pressure work reports a variable amount of dissociated $LiNO_3$ at higher concentration but not a K_{assoc} that holds in the whole molarity range.

Table 4-1

$LiNO_3$ Molarity	Kangro Dissociation %
1.88	99.1
5.20	92.4
8.60	66.8
9.80	56.0

It has been considered for a long time that hydrogen bonding effect may account for the form and decrease of our spectra as we go to more concentrated solutions but no quantitative assessment of this effect has been successfully worked out yet. The energy of the electronic transition is affected by H-bond formation. Any polarization effect on the solvent molecules H-bonded to the NO_3^- will therefore affect the observed spectra. We also do not have at this point any rigorous work showing that the change of spectra due to the dehydration of the anion is due to the hydration of the cation. As the nitrates become more concentrated it is not known exactly how the hydration of the cation varies in concentrated solution

Our data are presented in Table 4-2 for the $LiNO_3$ solutions:

Table 4-2

$LiNO_3$ Molarity	Moles H_2O per liter	Mole Fraction H_2O	f . 10^{-5}	ε_{max}	$\gamma_{max}[cm^{-1}]$
10^{-2}	55.35	0.996	14.34	7.21	33.400
10^{-1}	55.20	0.993	13.96	6.14	33.400
1	53.56	0.981	13.59	6.93	33.430
3	50.05	0.943	12.99	6.55	33.560
5	46.66	0.915	11.78	5.93	33.680
7	43.17	0.860	10.03	5.40	33.720
10.40	36.38	0.778	8.98	4.65	34.120

f oscillator strength

ε coefficient of molar absorption

γ wave number

In Figure 4-2 it is presented a plot of f and ε against concentration of $LiNO_3$ solution. The f value was calculated by the formula (Hart, 1957) for the Area = $1/3\ \Delta\gamma(\ 2\varepsilon_{extremes} + 4\varepsilon_{unpair\gamma} + 2\ \varepsilon_{pair\gamma})$

In the case of a 10^{-2} M $LiNO_3$ solution:

Unpair Values		Pair Values	
$\gamma[cm^{-1}]$	ε	$\gamma[cm^{-1}]$	ε
29.000	0.00	30.000	0.50
31.000	2.60	32.000	5.70
33.000	7.20	34.000	6.50
35.000	4.80	36.000	3.20
37.000	2.00	38.000	0.80

$$\text{Area} = \frac{1}{3}\,1000\ \{4\ 16.60 + 2\ \ 16.70\} = 3319.7$$

$$f = 4.32\ 10^{-9}\ 3319.7 = 14.34\ 10^{-5}$$

In Figure 4-2 the best assessment of the energy involved in the transition is given by the f values. The reason for it is that ε is a function of frequency and the transition takes place over a range of energies varying from 28.000 to about 40.000 cm^{-1} for the 300 mμ band of nitrates. The value of f takes into account the absorption at all wave numbers involved in the transition and not an isolated one, like ε does.

Figure 4-3 presents the shift of γ_{max} vs. concentration of

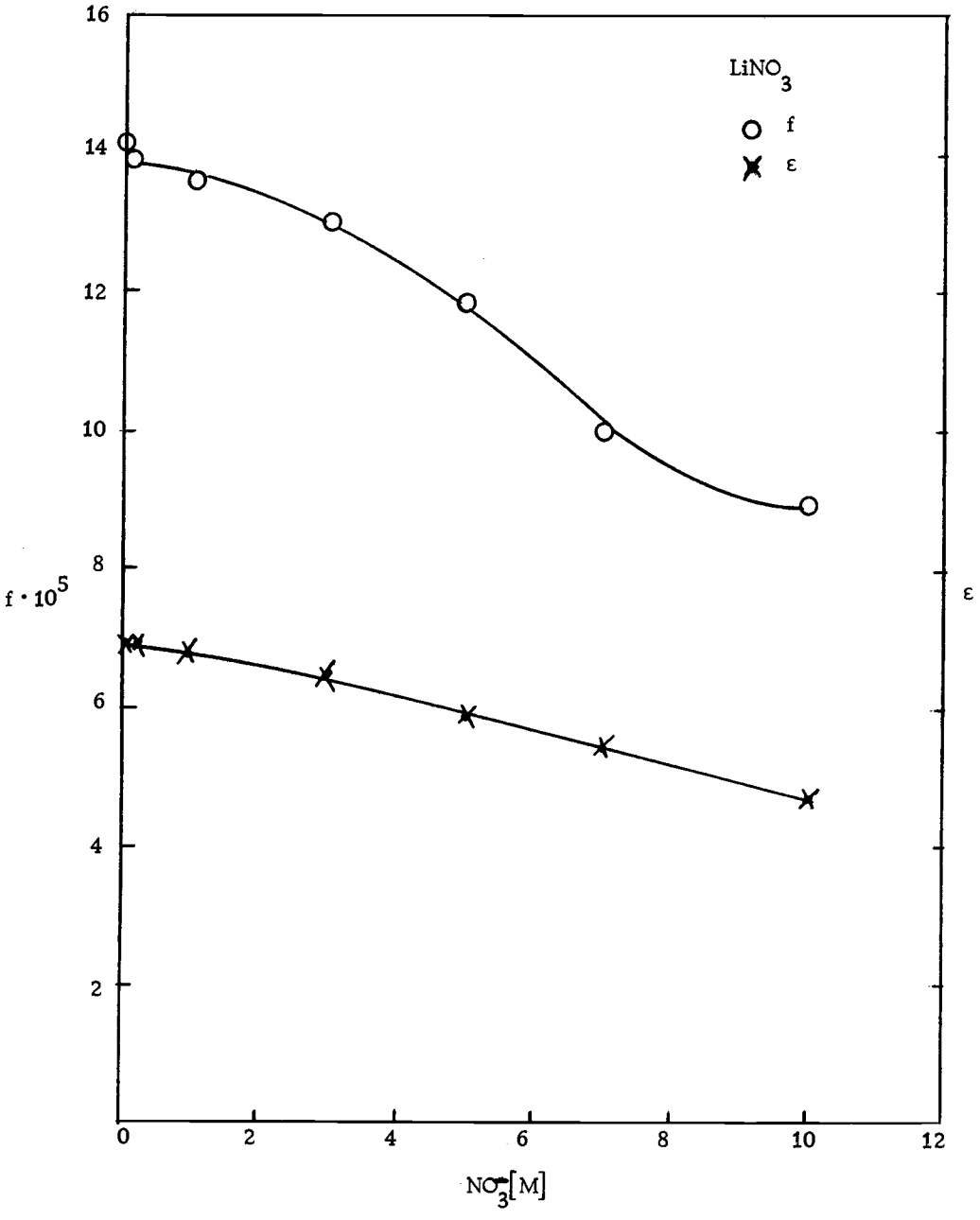

Figure 4-2

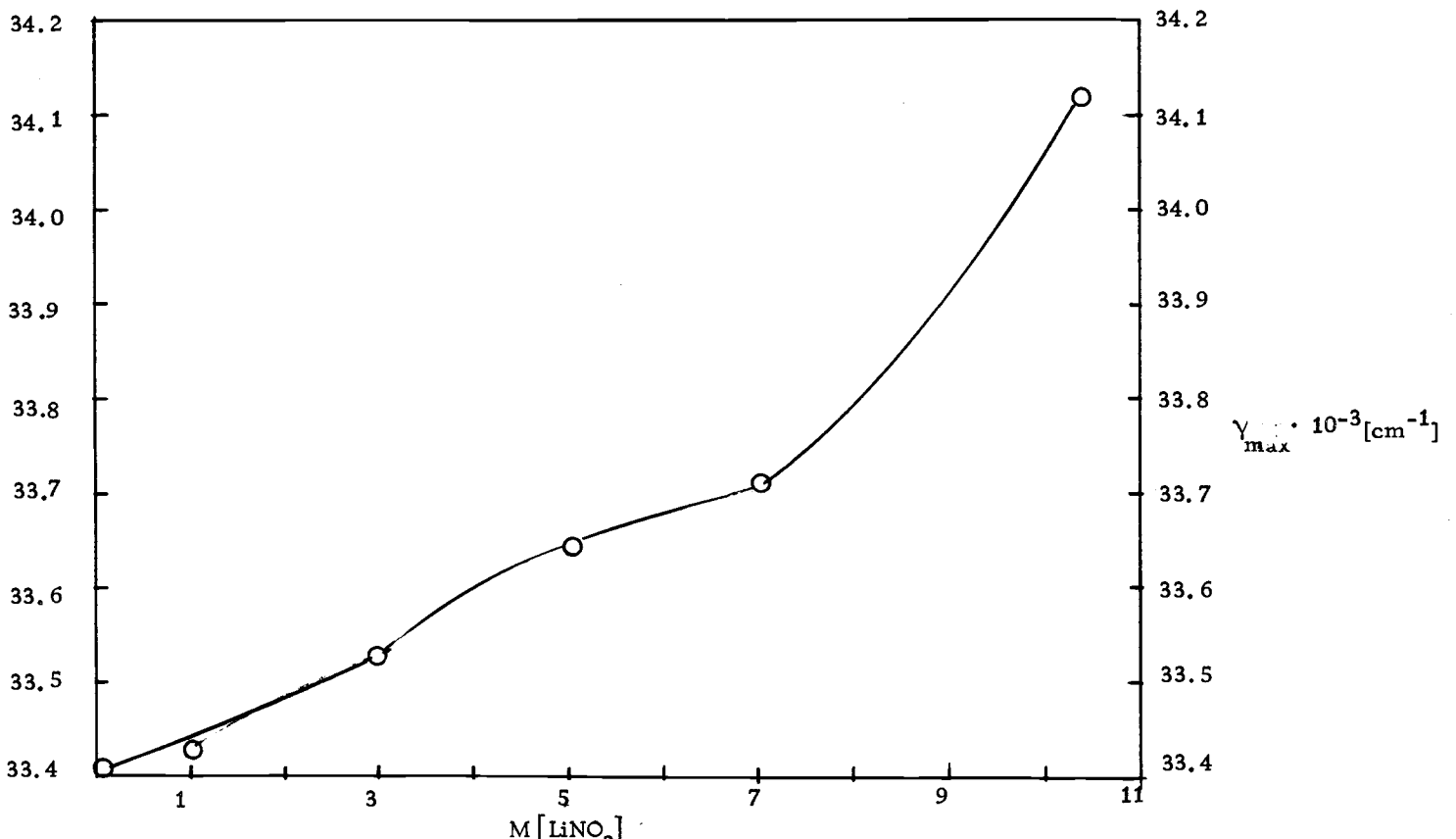
34.2
34.1
34.0
33.9
33.8
33.7
33.6
33.5
33.4
1
3
5
7
9
11
M [LiNO3]
$\nu_{max} \cdot 10^{-3}[cm^{-1}]$

Figure 4-3

$LiNO_3$. The method used to find this peak was the one of finite differences. Figure 4-4 presents this method for a 7 M $LiNO_3$ solution. This resolution is employed since it is assumed that the high energy transition does not affect the right hand side of the maximum in the lower energy transition shown in Figure 4-5. In this figure it is shown that if the points on the right hand side of the A axis are taken (the stripped segment), they will determine the maximum of the pure absorption band since the tail H-T of the high energy transition band affects the left portion of this low energy transition only. To interpret the general blue shift of Figure 4-3 there are two theories that we may attempt to explain our data. Boston and Smith (1961) postulated that during an $n \rightarrow \pi^*$ transition the molecular volume is expanded and antibonding levels of NO_3^- are occupied. Most of the expansion is localized the N atom. This has the effect that collisions between N atoms (of NO_3^-) and cations present are enhanced. But what produces a shift in the energy associated with the transition is that more overlap energy between cation and anion in the bonding and antibonding orbitals. The shift to the blue is due to more energy associated to the antibonding orbitals (repulsive energy). In the $LiNO_3$ solutions we observe a shift to the blue as we increase the concentration which agrees with this theory since having more salt present will enable to have more overlap between cation and N-atom which in turn will generate more repulsive overlap energy

7 M $LiNO_3$

$\gamma 10^{-3}[cm^{-1}]$	O. D.	$\Delta A \cdot 10^2$
32.8	580	-
33.2	611	+31
33.6	618	+7
34.0	601	-17
34.4	566	-35

$\gamma_{max} = 33720\ cm^{-1}$

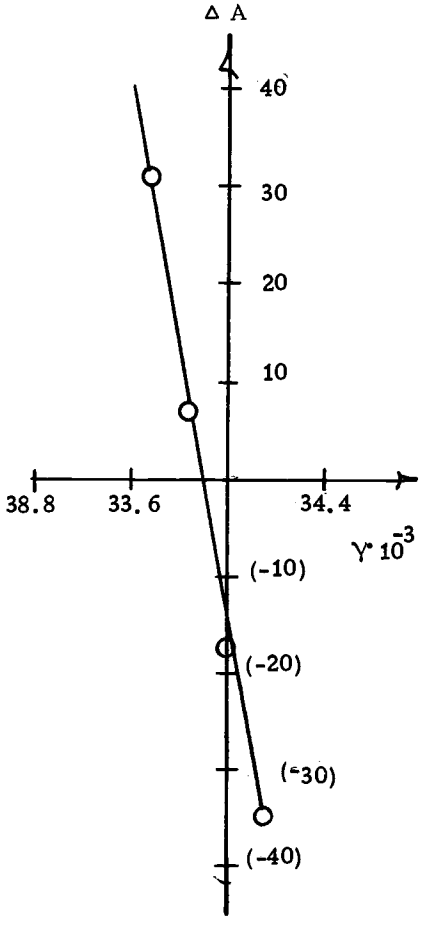

Figure 4-4

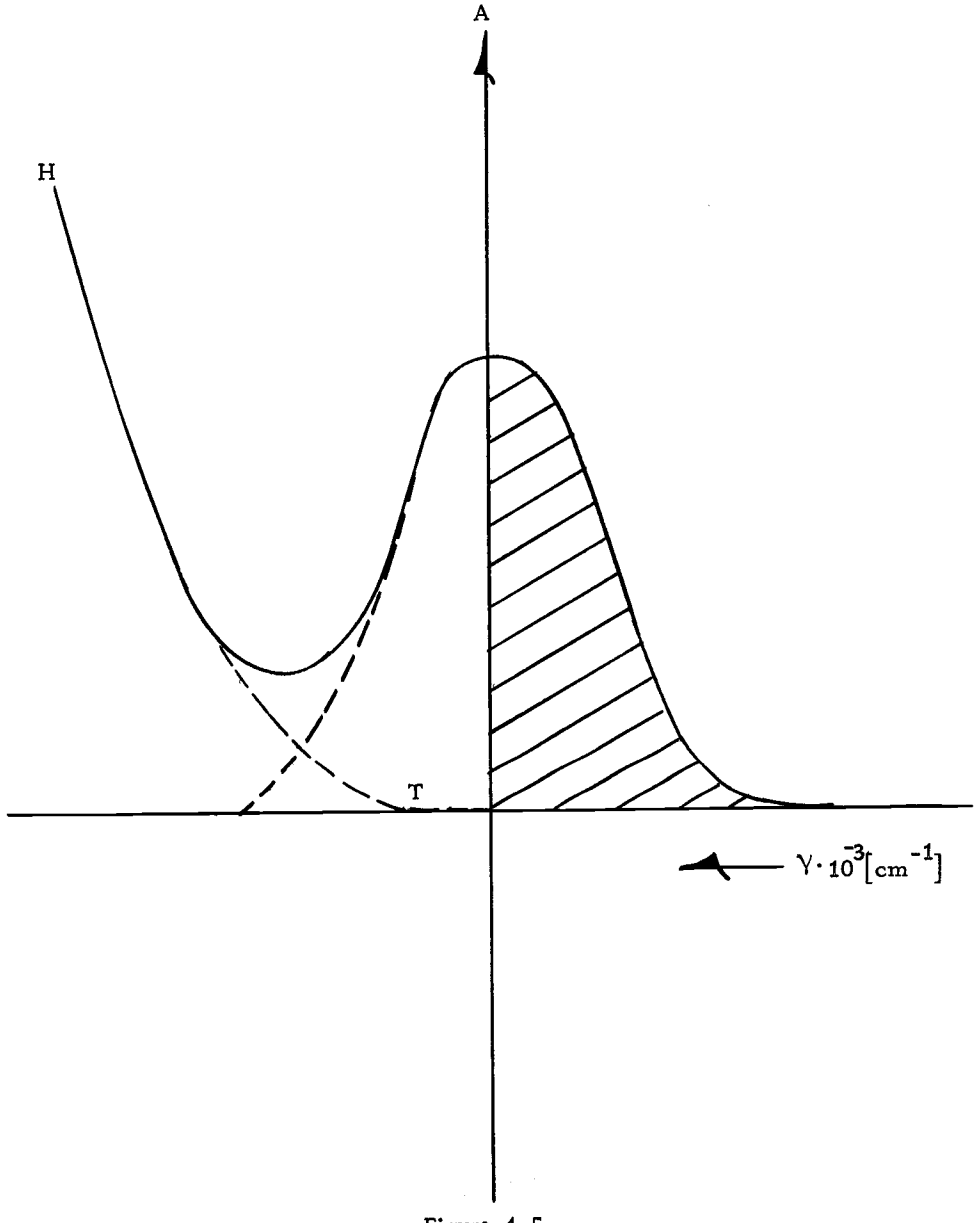

Figure 4-5

and produce a bigger shift.

Strickler and Kasha (1964) postulated that in an $n \rightarrow \pi^*$ transition, an electron from the ionic pair of the N-atom is smeared over the oxygen atoms present. This fact induces a higher electronic density in the oxygen atoms and they react more readily with the H atoms. When the electrons of the oxygen atom become involved in the formation of H-bonding they move the initial state of the electrons of the oxygen atom to a lower level of energy. Therefore their excitation process requires more energy and the $n \rightarrow \pi^*$ transition takes place at higher energies. Polar solvents (or that move readily from H-bonds) will then produce a blue shift. In $LiNO_3$ solutions blue shift takes place as concentration increases. We are not in the position to ascribe this shift to a higher polarity of our solvent since we do not have the experimental data for the dielectric constant $LiNO_3$ solutions in the concentration range. The explanation of Boston and Smith (1961) for the shift agrees with the observed phenomena. To account for Strickler and Kasha (1964) theory, not enough information is available. Therefore both approaches may be right, it may be a coparticipation of both or some other effect takes place to induce a blue shift as concentration is increased.

$NaNO_3$ Solutions. The spectra of different sodium nitrate solutions are presented in Figure 4-6. The data worked out for the different concentrations are presented in Table 4-3.

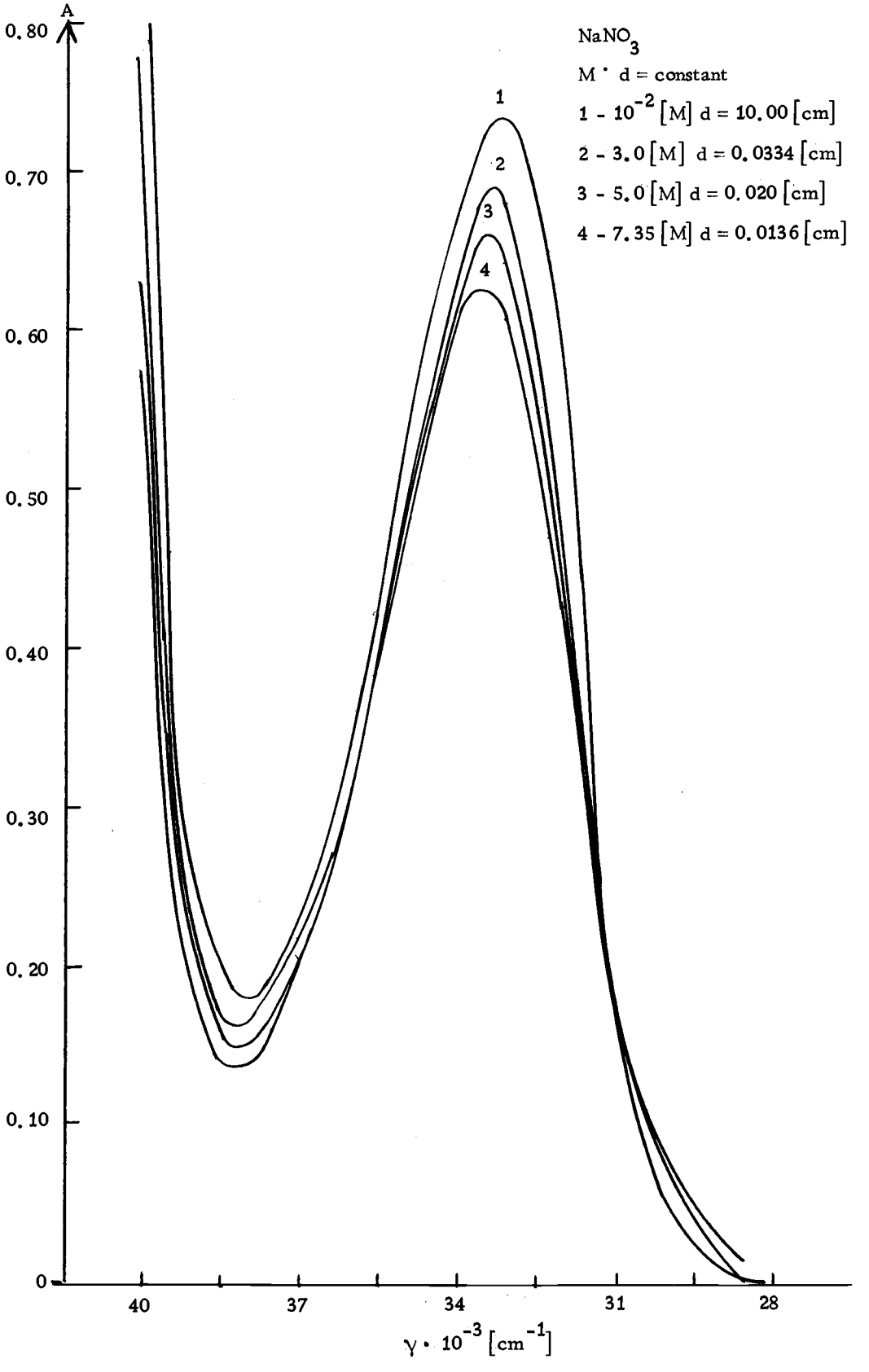
A
0.80
0.70
0.60
0.50
0.40
0.30
0.20
0.10
0
40
37
34
31
28
$\gamma \cdot 10^{-3}$ [cm^{-1}]
$NaNO_3$
M · d = constant
1 - 10^{-2} [M] d = 10.00 [cm]
2 - 3.0 [M] d = 0.0334 [cm]
3 - 5.0 [M] d = 0.020 [cm]
4 - 7.35 [M] d = 0.0136 [cm]
1
2
3
4

Figure 4-6

Table 4-3

$NaNO_3$ Molarity	Moles H_2O per liter	Mole Fraction H_2O	$f \cdot 10^5$	ε_{max}	$\gamma_{max[cm^{-1}]}$
10^{-2}	55.60	0.997	14.60	7.20	33.300
10^{-1}	57.70	0.995	14.00	7.13	33.320
1	53.61	0.982	13.79	7.00	33.350
3	49.89	0.943	13.49	6.70	33.430
5	46.11	0.902	12.84	6.43	33.480
7.35	42.50	0.852	11.58	6.11	33.570

f is the oscillator strength, being ε the coefficient of molar absorption and γ is used to designate wave number. A tentative K_{assoc} so calculated varies between values 0.020 and 0.102. Davies (1927) reports by conductivity measurements a K_{assoc} of 0.26 in studies of solutions ranging from 0.05 to 0.10 M $NaNO_3$. Robinson (1935) by isiopestic point determination obtained $0.31 \leq 0.5$ in solutions with concentrations ranging from 0.1 M to 1.44 M. More recent work by Kangro(1962) of the water vapor pressure type gives the dissociation as functions of concentration:

Table 4-4

$NaNO_3$ Molarity	Dissociation %
1.88	81.7
3.35	78.9
4.99	77.1
6.27	74.7
6.81	73.8

KNO_3 Solutions. The spectra of different potassium nitrate solutions are presented in Figure 4-7. The pertaining data are presented in Table 4-5.

Table 4-5

KNO_3 Molarity	Moles H_2O per liter	Mole Fraction H_2O	$f \cdot 10^5$	ε_{max}	ν_{max} cm^{-1}
10^{-2}	55.65	0.999	14.66	7.20	33.250
10^{-1}	55.33	0.997	13.99	7.13	33.270
1	53.01	0.981	13.77	7.00	33.300
2.1	50.44	0.960	12.81	6.56	33.320
3.18	47.61	0.937	12.01	6.20	33.360

The values for a K_{assoc} reported in the literature were: a) Robinson and Davies (1937) for molarities between 0.01 to 0.1 as 0.60 b) By partial pressure diverse authors (Robinson et al.) cite values ranging from 0.83 to 1.15 c) In a more recent work by Fuoss (1963) a $K_{assoc} = 1.64$ is reported by conductance studies carried out in KNO_3 solutions ranging from 0.002 to 0.10 M.

$CsNO_3$ Solutions. The extremes of the four spectra taken are presented in Figure 4-8. Only for the sake of clarity the lowest and the highest concentration are shown. The data related to the spectral observations are presented in Table 4-6.

Table 4-6

$CsNO_3$ Molarity	Moles H_2O per liter	Fraction Mole H_2O	$f \cdot 10^5$	ε_{max}	γ_{max} cm^{-1}
10^{-2}	55.36	0.999	14.18	7.20	33.250
10^{-1}	55.10	0.998	14.49	7.13	33.250
0.63	52.90	0.988	13.82	7.06	33.250
1.26	52.32	0.976	13.48	6.90	33.250

The values reported for a K_{assoc} of $CsNO_3$ are a) Nernst (1928) by lowering of freezing point of these solutions as 0.104 in 0.1 M solutions b) Davies (1931) reports a K_{assoc} of 0.01 for dilute solutions c) By partial pressure Robinson (1937) reports a value of around 1.3 for solutions up to 1.0 M. That γ_{max} is the same at all concentrations would enable us to say that H bonding or interaction cation anion is very weak since no shift is detected. This is strange in view of the fact that the overlap of orbitals between Cs^+ and NO_3^- ion should be enhanced due to the big size of Cs^+ and this property should be reflected in a spectral shift.

$Ca(NO_3)_2$ Solutions. The spectra taken are presented in Figure 4-9. The data containing the spectral observations is presented in Table 4-7. The values reported for K_{assoc} have been worked out by a) Righellato and Davies (1930) as 0.19 b) Hester and Plane (1967) using Raman spectroscopy in the range 2 to 13 M $Ca(NO_3)_2$ and obtaining a value of 0.12 to 0.17 for the K_{assoc} of an

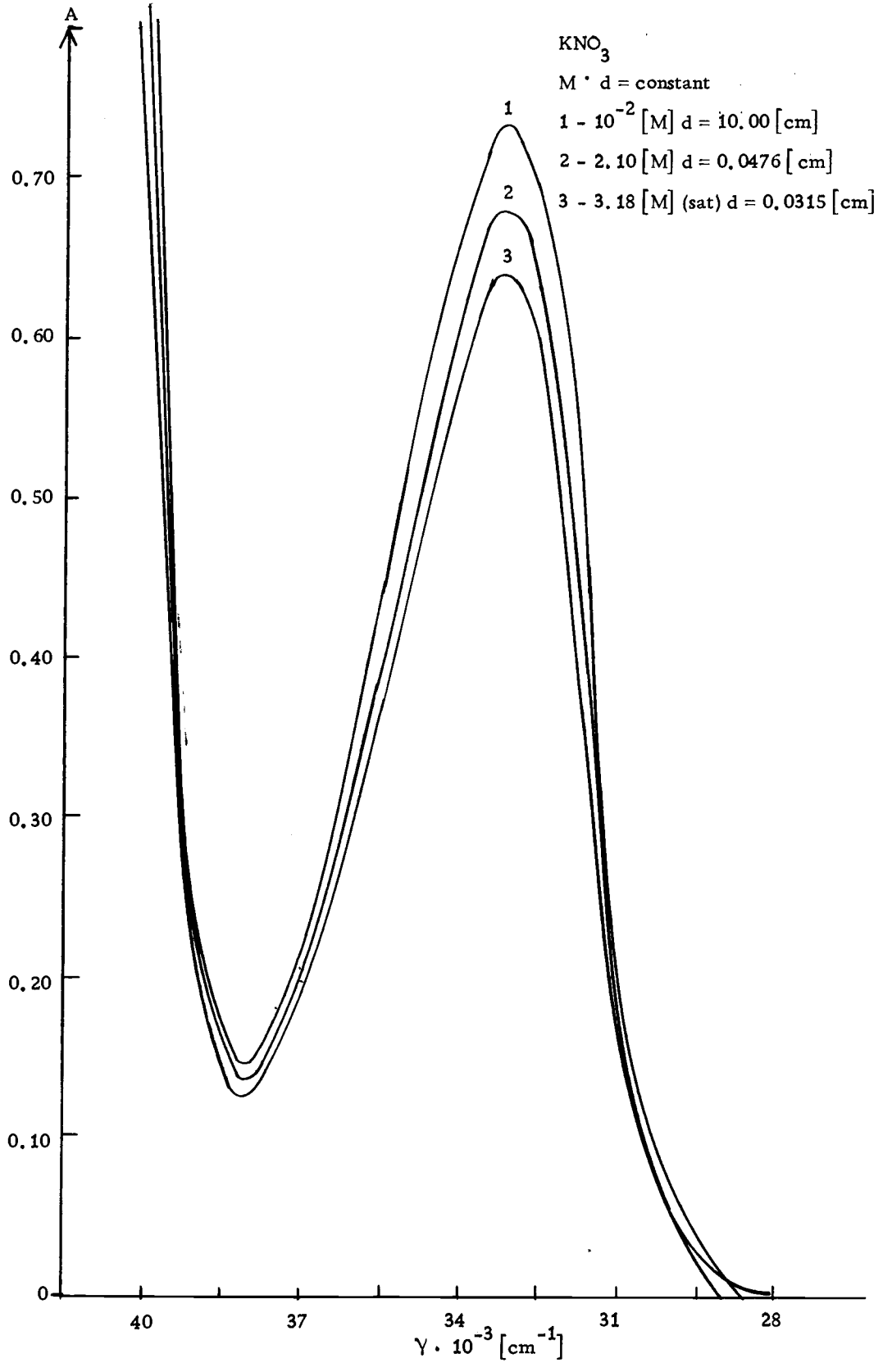
A
KNO3
M · d = constant
1 - 10^-2 [M] d = 10.00 [cm]
2 - 2.10 [M] d = 0.0476 [cm]
3 - 3.18 [M] (sat) d = 0.0315 [cm]
1
2
3
0.70
0.60
0.50
0.40
0.30
0.20
0.10
0
40
37
34
31
28
γ · 10^-3 [cm^-1]

Figure 4-7

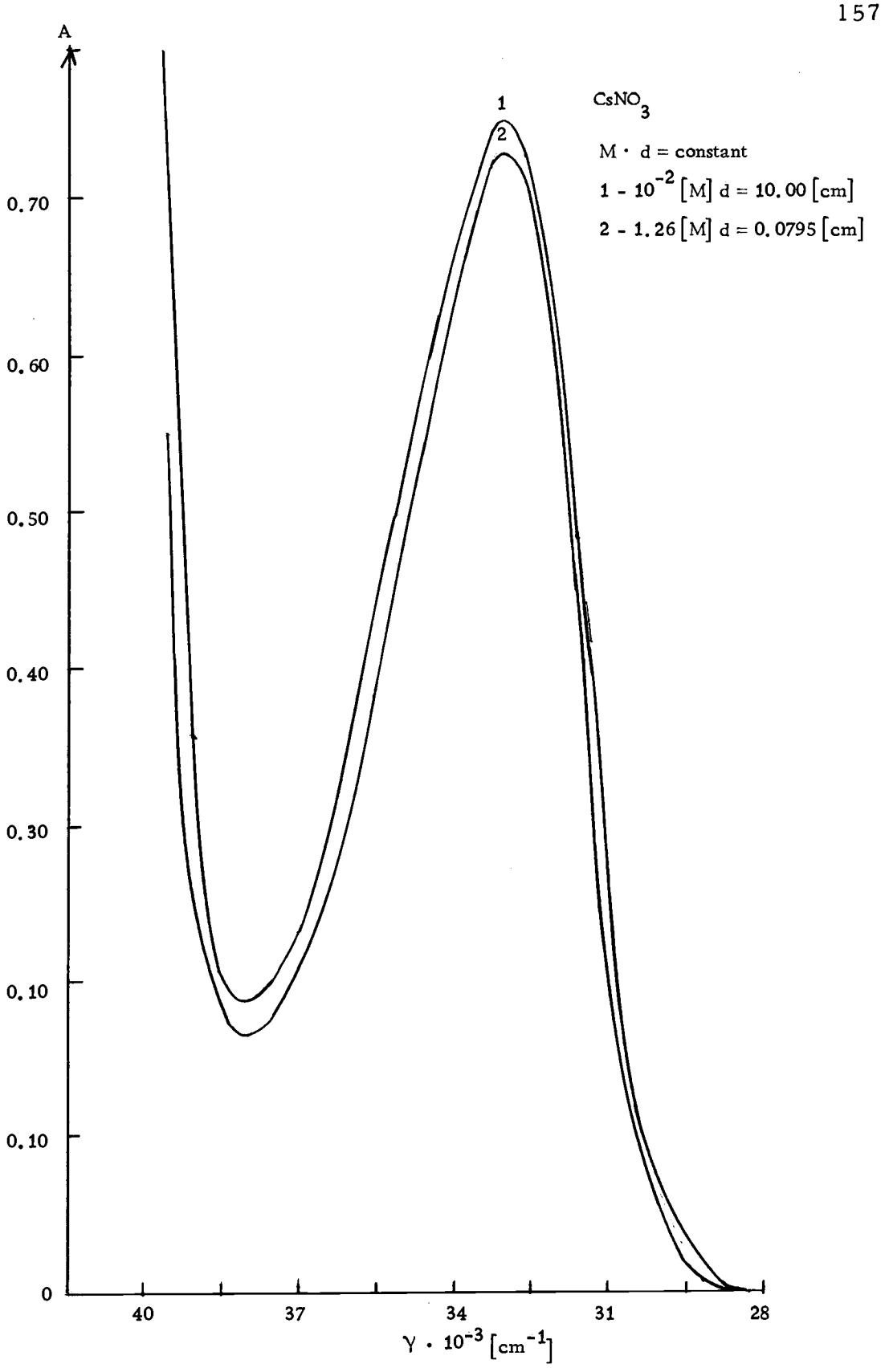
A
0.70
0.60
0.50
0.40
0.30
0.10
0.10
0
40
37
34
31
28
γ · 10⁻³ [cm⁻¹]
1
2
CsNO3
M · d = constant
1 - 10⁻² [M] d = 10.00 [cm]
2 - 1.26 [M] d = 0.0795 [cm]

Figure 4-8

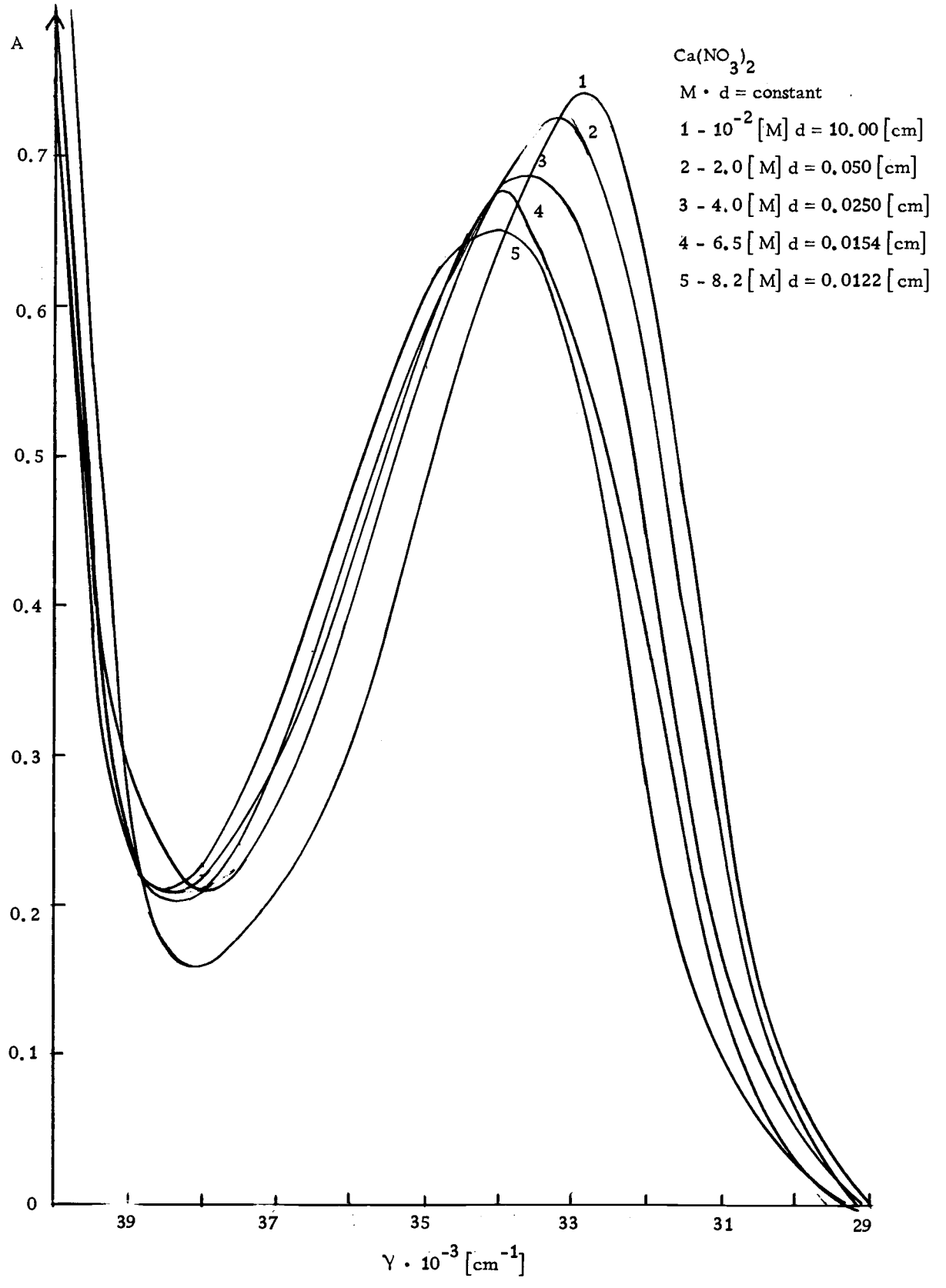
A
0.7
0.6
0.5
0.4
0.3
0.2
0.1
0
39
37
35
33
31
29
$\nu \cdot 10^{-3}$ [cm^{-1}]
$Ca(NO_3)_2$
M • d = constant
1 - 10^{-2} [M] d = 10.00 [cm]
2 - 2.0 [M] d = 0.050 [cm]
3 - 4.0 [M] d = 0.0250 [cm]
4 - 6.5 [M] d = 0.0154 [cm]
5 - 8.2 [M] d = 0.0122 [cm]
1
2
3
4
5

Figure 4-9

associated species that they assigned to the species $CaNO_3^+$. Further verification of an equilibria of two species in solution here would be $CaNO_3^+$ and the NO_3^- ion in equilibrium indicated by the isosbestic point in Figure 4-9.

Table 4-7

$Ca(NO_3)_2$ Molarity in NO_3^-	Moles H_2O per liter	Mole Fraction H_2O	$f \cdot 10^5$	ε_{max}	γ_{max} cm^{-1}
10^{-2}	55.40	0.999	14.40	7.20	33100
10^{-1}	55.20	0.998	14.18	7.10	33490
1.0	49.66	0.980	14.08	6.36	33700
2.0	43.60	0.456	14.19	6.85	33900
4.0	30.78	0.885	13.65	6.50	34250
6.0	16.72	0.736	12.99	6.30	34500
8.2	4.66	0.361	12.56	6.18	34780

$(CH_3)_4NNO_3$ Solutions. The spectra taken are presented in Figure 4-10. The data containing the spectral observations are presented in Table 4-8.

Table 4-8

$(CH_3)_4NNO_3$ Molarity	Moles H_2O per liter	Mole Fraction H_2O	$f \cdot 10^5$	ε_{max}	γ_{max} cm^{-1}
10^{-1}	no data available		14.33	7.07	33350
0.79	55.39	0.9859	13.55	6.80	33300
1.31	51.57	0.9751	12.58	6.40	33220
2.48	43.16	0.9460	12.41	6.20	33180
3.89	36.50	0.9130	11.53	5.85	33120

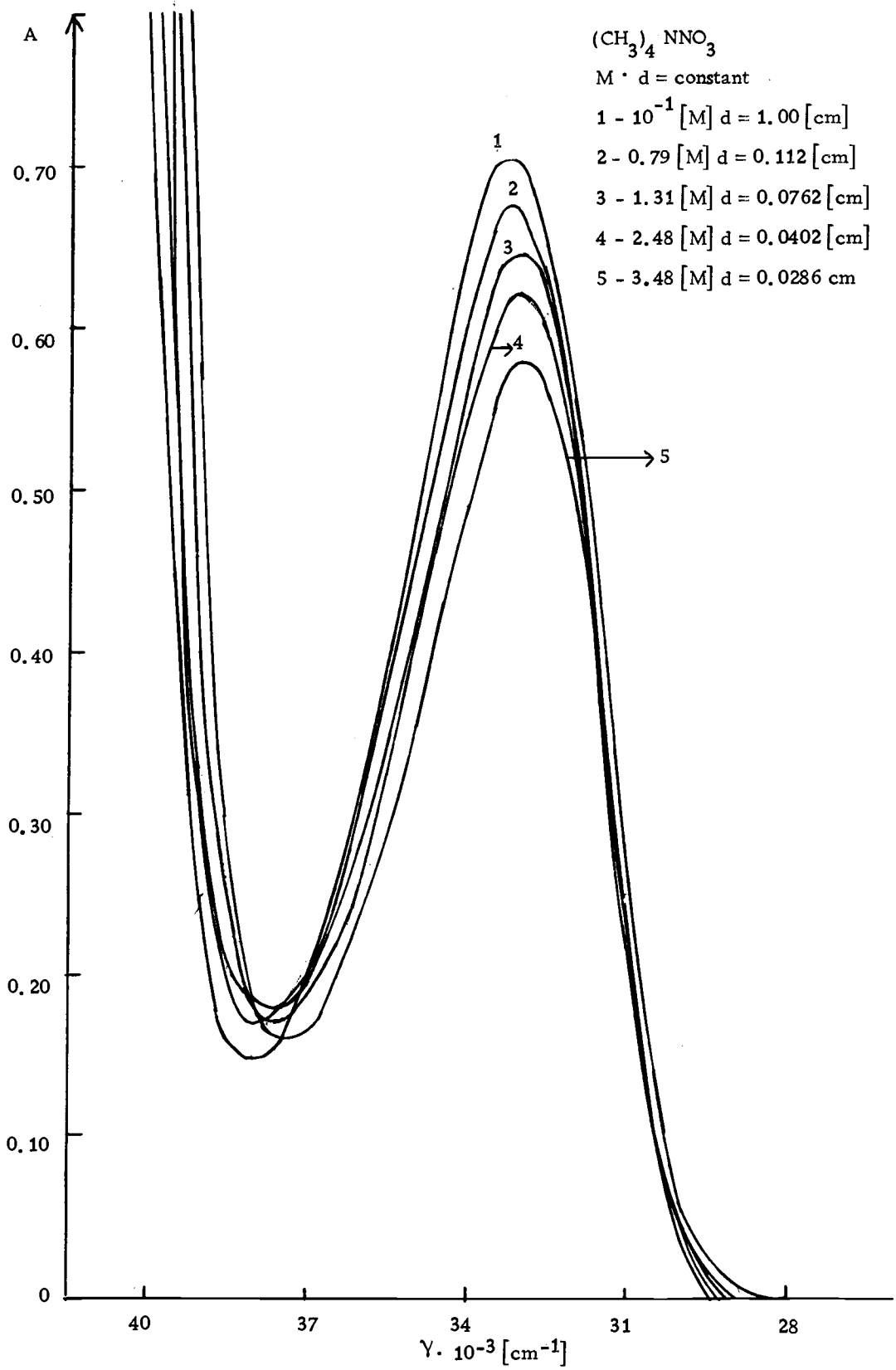
A
0.70
0.60
0.50
0.40
0.30
0.20
0.10
0
40
37
34
31
28
γ. 10⁻³ [cm⁻¹]
(CH3)4 NNO3
M · d = constant
1 - 10⁻¹ [M] d = 1.00 [cm]
2 - 0.79 [M] d = 0.112 [cm]
3 - 1.31 [M] d = 0.0762 [cm]
4 - 2.48 [M] d = 0.0402 [cm]
5 - 3.48 [M] d = 0.0286 cm
1
2
3
4
5

Figure 4-10

The study of $(CH_3)_4NNO_3$ was undertaken primarily to demonstrate that if dehydration of the solvated NO_3^- ion and not cation-anion interaction was responsible for the decrease in the shape observed, then in the salt we should also observe a decrease as the increase the concentration of $(CH_3)_4NNO_3$. It is widely accepted currently in the literature that the interaction between alkyl and anion group is smaller than metallic cation-anion, but this observation has to be taken only as an assumption without much experimental backing.

Tentative Assignment of Nitrate Resolved Spectra

Several procedures have been tried to account for the shape of these curves. The first fit attempted was of the Gaussian type. An expression for $LiNO_3$ solutions as given below was used

$$\varepsilon = \varepsilon_o e^{-\left(\frac{\gamma - \gamma_o}{S}\right)^2} \qquad (3)$$

where

E_o = molar absorption coefficient at the maximum

γ_o = frequency at which ε_o is maximum

S = adjustable width of the Gaussian to fit experimental profile.

The lower band has been separated from the high intensity band assuming the tail of the lost band as exponential, and using semilog paper to subtract one from the other. Such an approach did not fit

the experimental curves. This approach is shown in Figure 4-11. Next a Du Pont 310 Curve Resolver was used. This is instrument designed to generate Gaussians and it is useful to resolve a spectra into its components. It works as a modified analog computer. For each resolved individual distribution function we week a) the height b) position along x-axis c) the integrated area. No regular trend was found when resolving the experimental curves into two or three Gaussians that indicated the possibility of ascribing some physical meaning to them. Vandebelt and Heinrich (1953) point out that when assignments of this type are made, the parameters of one component spectrum have to be known. If not many possibilities that "confuse" a systematic assignment arise. Combining Gaussians and Lorentzian does not give a proper fitting either. A Lorentzian curve of the type

$$\varepsilon = \frac{\varepsilon_o}{\delta^2 - (\gamma - \gamma_o)^2}\,\delta^2$$

where δ is the half width at half height of one experimental curve (Petrakis, 1967), did not give a good fit either.

A skewed Gaussian distribution (Fraser and Suzuki, 1969) was used of the type

$$\varepsilon = \varepsilon_o \exp\left(-\ln 2 \cdot \{\ln[1 + 2b(\gamma - \gamma_o)/\delta]/b\}^2\right)$$

where ε, ε_o, γ, γ_o δ have the usual meaning and b is an adjustable parameter that has to be found by trial and error and that varies

between 0 and 1. Since no adequate fit was so obtained an attempt was made using Jørgensen's (1954) approach that two Gaussian with the same height ε_o and position of maxima γ_o but different half width δ values. The fit is poor particularly at the extremes of our observed spectra.

The mechanism for light absorption of nitrates has been postulated by many workers by three species a) the ion NO_3^- b) an ion-pair $M^+ \ldots NO_3^-$ c) a solvated hydrate of composition other than the simple hydrated NO_3^-. After examination of the nitrate solutions at different concentrations the conclusion is presented here that the shape of the spectral transition could be ascribed to two components a) A Gaussian distribution that represents the pure NO_3^- ion present in the solution b) A second portion corresponding to spectra of an hydrated cation-anion pair or an NO_3^- hydrate with defined optical absorption properties. A definite species will be present if it absorbs with a maximum at a certain wavelength γ_o, and the parameter to characterize the Gaussian σ/ε_o has a particular value characteristic of the species. σ is the width of the Gaussian (not necessarily at half height) and ε is the molar absorption at the maximum of γ_o. This view does not agree with the McCabe and Fisher (1970) idea that the Gaussian describing an individual species is described by the position of the maximum (γ_o) and the half band width, irrespective of the value of $\varepsilon(\gamma_o)$ of the Gaussian under consideration.

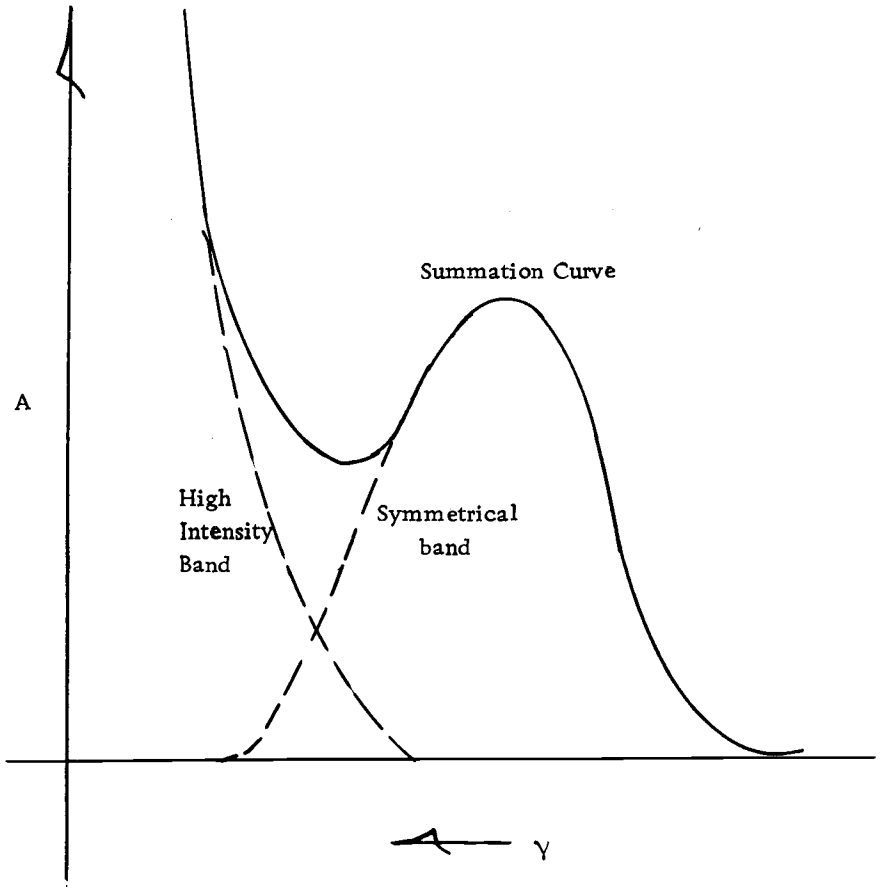

Figure 4-11

In concentrated nitrate solutions it is observed that 1) large deviations of Beer's Law occur. Beer's Law breaks down in the case as we have stated not because the assumptions it is based change in concentrated solutions, but due to the fact that high concentrations bring about changes in the internal constitution of the solution that are not known at the present time. Modern theories for strong electrolytes postulate validity of this law up to 10^{-2} M. 2) We observe small shifts in the wavelength of maximum absorption. We consider that at concentration the pure ion absorption can be separated from the total spectrum for a new species which possess optical properties similar to those of the solvated nitrate ion. This is in agreement with the ideas of Meyerstein and Treinin (1961). This approach allows to handle the experimental data regarding that the NO_3^- ion gives rise to a symmetrical band of fixed extinction coefficient at a defined wavelength. We call this Gaussian the "normal band" of the isolated NO_3^- group at each concentration. A description by this approach avoids the dominant idea of the work carried and on nitrate solutions between 1920 and 1944 which ascribed the observed shapes to a deformation of the anion in the field of the cation as the concentration is varied.

In Figure 4-12 a resolution of the spectrum of 10^{-2} M $LiNO_3$ is shown. At the right hand side a separated Gaussian band for the ion is presented. By subtraction of the low frequency Gaussian

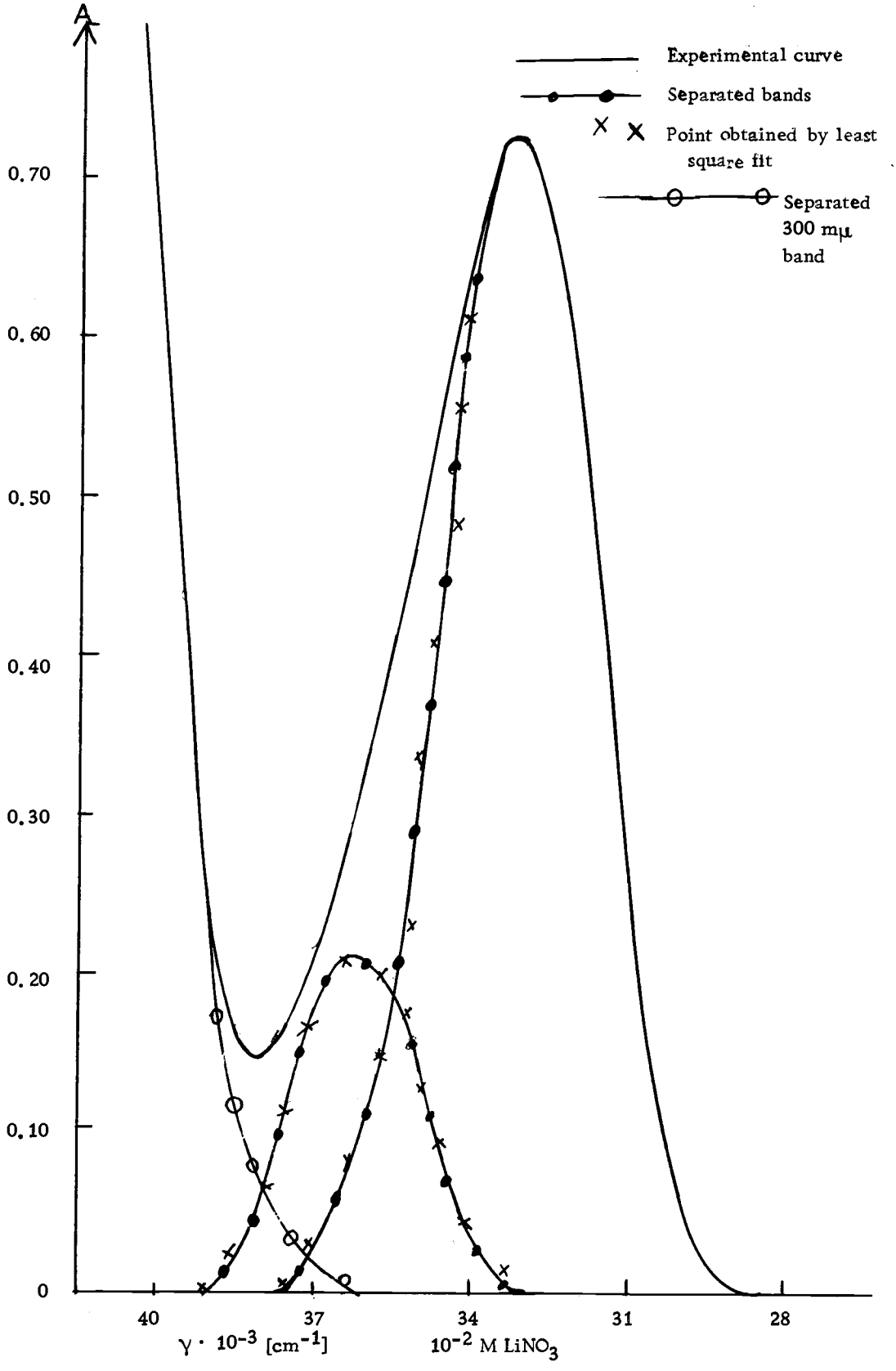
A
0.70
0.60
0.50
0.40
0.30
0.20
0.10
0
Experimental curve
Separated bands
Point obtained by least square fit
Separated 300 mμ band
40
37
34
31
28
γ · 10-3 [cm-1]
10-2 M LiNO3

Figure 4-12

from the complete separated band, a smaller Gaussian at the left hand side is plotted. The value of σ (width of Gaussian) that best fits both resolved curves has been found and this has been done with the help of the control Data Corporation 3300 computer, so that the error involved in the least square fit of σ could be minimized. The fit is good to about $\pm 1\%$ (using the σ so obtained) for the two separated Gaussians. The data is shown in Tables 4-9, 10, 11, 12, 13, and 14 for the nitrates under study. By inspection of the values of γ_o (position of the maxima) of the Gaussians in the low energy side, they do not present significant difference when the same molarities of different nitrates are considered. This is not the case for $Ca(NO_3)_2$ where the effect of double charged Ca^{++} ion probably solvates more water molecules in his first hydration shell, due to its higher electronic density when compared with the cations of the first group. The values of σ/ε vary in a regular way with molarity for the nitrates under consideration (in the margin of experimental error, for the value of σ) so that a pure nitrate ion that dehydrates as the concentration is increased may give a physical picture for the variation in the optical absorption of the band. The shift in the maxima γ_o is always to the blue with the exception of $(CH_3)_4NNO_3$ where the ionic solvation may be affected by the presence of the big $(CH_3)_4^+$ in the solvent media. The values of σ/ε increase when the concentration increase showing that the trend in this

Table 4-9
$LiNO_3$

	Low Energy Gaussian						High Energy Gaussian						
M	γ_1 [a]	σ_1 [b]	ε_1 [c]	$\sigma\%\varepsilon$ [d]	σ/ε	$f_1 \cdot 10^5$	γ_2	σ_2	ε_2	$\sigma\%\varepsilon$	σ/ε	$f_2 \cdot 10^5$	$\gamma_2 - \gamma_1$
10^{-2}	33130	2125 ±21.7	7.20	85.0	295	12.07	36150	1687 ±54.9	2.12	86.0	796	2.53	3020
10^{-1}	33200	2115 ±31.7	7.13	86.0	297	11.49	36300	1583 ±60.3	2.13	81.5	743	2.57	3100
1	33250	2189 ±31.3	6.92	89.0	316	11.25	36300	1559 ±56.4	1.94	87.5	803	2.31	3050
3	33300	2089 ±46.7	6.53	83.5	320	10.42	36250	1509 ±11.3	2.33	80.0	687	2.67	2950
5	33350	2072 ±40.6	5.92	88.0	350	9.36	36300	1482 ±40.6	2.24	78.0	662	2.53	2950
7	33500	2067 ±40.6	5.43	87.0	381	7.93	36500	1380 ±45.4	1.71	77.0	807	1.80	3000
10.40	33900	2222 ±43.4	4.64	89.0	479	7.87	36950	1351 ±40.0	1.29	84.5	1089	1.33	3050

Table 4-10
$NaNO_3$

	Low Energy Gaussian						High Energy Gaussian						
M	γ_1 [a]	σ_1 [b]	ε [c]	$\sigma\%\varepsilon$ [d]	σ/ε	$f_1 \cdot 10^5$	γ_2	σ_2	ε	$\sigma\%\varepsilon$	σ/ε	$f_2 \cdot 10^5$	$\gamma_2 - \gamma_1$
10^{-2}	33050	2041 ±24.3	7.20	86.0	283	11.22	36050	1049 ±4.04	2.32	87.0	847	3.43	3000
10^{-1}	33100	2156 ±30.1	7.10	87.6	301	11.66	36250	1550 ±61.6	2.12	88.1	731	2.51	3150
1	33200	2104 ±42.0	7.00	87.0	304	11.23	36150	1505 ±43.8	2.31	86.0	651	2.63	2950
3	33300	2202 ±21.8	6.72	86.5	328	11.29	36300	1538 ±40.3	1.92	84.5	666	2.24	3000
5	33400	2114 ±38.2	6.32	86.5	334	10.18	36350	1477 ±65.8	2.00	85.0	738	2.24	2950
7.85	33450	2171 ±28.6	6.00	85.1	362	9.95	36450	1457 ±44.6	1.62	84.5	899	1.80	3000

[a] γ_o position of the maximum in cm^{-1}

[b] σ width of Gaussian in cm^{-1}

[c] ε maximum molar absorption $M^{-1}cm^{-1}$

[d] height of σ as % of ε_{max}

Table 4-11

KNO_3

	Low Energy Gaussian						High Energy Gaussian						
M	γ_1 [a]	σ_1 [b]	ε_1 [c]	σ %ε	σ/ε	$f \cdot 10^5$	γ_2	σ_2	ε_2	σ %ε	σ/ε	$f_2 \cdot 10^5$	$\gamma_2 - \gamma_1$
10^{-2}	33100	2226 ±64.3	7.13	86.0	327	12.05	36300	2113 ±23.2	2.01	77.5	1051	3.04	3200
10^{-1}	33100	2112 ±23.2	7.01	83.0	301	11.30	36300	1736 ±71.3	2.00	91.0	868	2.64	3200
1.0	33150	2137 ±34.2	7.00	86.0	305	11.21	36350	1677 ±57.3	2.00	86.0	838	2.55	3200
2.1	33.200	2147 ±39.3	6.52	84.5	329	10.69	36400	1641 ±73.4	1.87	90.0	877	2.34	3200
3.18	33.200	2201 ±42.7	6.12	87.8	360	10.08	36.500	1745 ±71.5	1.61	82.5	1083	2.14	3300

Table 4-12

$CsNO_3$

	Low Energy Gaussian						High Energy Gaussian						
M	γ_1 [a]	σ_1 [b]	ε_1 [c]	σ %ε [d]	σ/ε	$f_1 \cdot 10^5$	γ_2	σ_2	ε_2	σ %ε	σ/ε	$f_2 \cdot 10^5$	$\gamma_2 - \gamma_1$
10^{-2}	33100	2058 ±22.5	7.20	90.0	286	11.33	36150	1695 ±30.9	2.10	84.0	807	2.72	3050
10^{-1}	33200	2132 ±23.1	7.14	84.0	296	11.61	36450	1610 ± 25.8	2.06	81.0	781	2.99	3250
0.63	33100	2126 ±36.3	7.10	86.0	299	11.22	36450	1523 ± 75.6	2.30	82.5	662	2.67	3350
1.252	33100	2074 ±32.6	6.90	88.0	300	10.93	36250	1538 ±34.9	2.10	82.5	732	2.46	3150

[a] γ_o positionof the maximum in cm^{-1} [b] σ width of Gaussian cm^{-1} [c] ε maximum molar absorption $M^{-1}cm^{-1}$ [d] Height of σ as % of ε_{max}

Table 4-13
$Ca(NO_3)_2$

Min NO_3^-	Low Energy Gaussian γ_1 [a]	σ_1 [a]	ε_1 [c]	σ % ε	σ/ε	$f_1 \cdot 10^5$	High Energy Gaussian γ_2	σ_2	ε_2	σ % ε	σ/ε	$f_2 10^5$	$\gamma_2 - \gamma_2$
10^{-2}	33150	2029 ±28.1	7.23	89.1	281	11.20	36050	1695 ±37.0	2.50	89.0	678	3.23	2900
10^{-1}	33200	2191 ±42.5	7.10	86.0	309	11.87	36500	1482 ±48.5	2.10	88.0	705	2.38	3300
1.0	33400	2161 ±33.0	6.90	89.0	313	11.38	36450	1578 ±65.6	2.37	87.5	666	2.67	3050
2.0	33350	2292 ±38.8	6.78	85.0	338	11.87	36700	1491 ±24.7	2.12	81.5	703	2.41	3350
4.0	33950	2289 ±40.7	6.28	86.0	364	10.28	37000	1705 ±15.9	2.08	86.5	820	2.70	3050
6.0	34150	2344 ±25.4	6.30	85.5	372	11.27	37100	1494 ±38.7	1.61	82.5	927	1.83	3050
8.2	34400	2327 ±27.4	6.20	85.0	375	11.02	37200	1405 ±42.6	1.50	87.0	936	1.61	3200

Table 4-14
$(CH_3)_4NNO_3$

M	Low Energy Gaussian γ_1 [a]	σ_1 [a]	ε_1	σ % ε	σ/ε	$f_1 \cdot 10^5$	High Energy Gaussian γ_2	σ_2	ε_2	σ % ε	σ/ε	$f_2 \cdot 10^5$	$\gamma_2 - \gamma_2$
0.13	33150	2171 ±26.7	7.10	84.5	306	11.77	36350	1461 ±116	2.30	89.0	635	2.56	3200
0.79	33100	2106 ±28.2	6.70	81.6	314	11.11	36050	1439 ±29.3	2.30	82.0	625	2.53	2950
1.31	33050	2146 ±35.4	6.30	84.0	341	10.13	36000	1473 ±44.1	2.00	86.0	736	2.25	2950
2.48	32950	2164 ±48.8	6.20	85.5	349	10.23	35850	1475 ±46.9	1.97	87.5	749	2.22	2900
3.89	32900	2016 ±37.2	5.60	88.0	360	8.62	35750	1982 ±45.4	1.88	80.0	1054	2.84	2850

[a] γ_o position of the maximum in cm^{-1} [b] σ width of Gaussian cm^{-1} [c] ε maximum molar absorption $M^{-1}cm^{-1}$ [d] Height of σ as % of ε_{max}

Gaussian is to widen and decrease in height at higher molarities. In the high energy band the values of γ_2 show a trend to the left. The difference $|\gamma_1 - \gamma_2|$ remains about the same for all molarities in different nitrates, giving a further indication that a two band assignment is possible. No regular trend was observed in the value of σ/ε as concentrations are varied. Different values for the same concentration of individual nitrates may signify an interaction between cation and anion in these bands. Since the value of ε_2 decreases with molarity in all cases and the characteristics of the absorption of an cation-anion hydrated pair located next to the absorption of the pure NO_3^- absorption itself (the pair has the same anion), we postulate this high energy Gaussian represents some sort of ion pairing—not knowing at the present time the intrinsec value of ε_2 for this band—but considering that such an absorption must have optical properties not too different from the low energy Gaussian. Added salt studies where by excess cation the equilibria is shifted towards complex formation may verify the ion-pairing or complexing ascribed to the low energy band. If the shift in the spectra are analogous it gives a further indication of ion pairing. By excess cation the association taking place would be

$$M^+ + NO_3^- \rightarrow (MNO_3)_{complex}$$

Boston and Smith (1961) have presented the only work in which a quantitative analysis of the $n \rightarrow \pi^*$ band has been reported. They worked in molten nitrates (which for many investigators resemble a solution 4 M and up where no more bulk water exists) and give the values shown in Table 4-15.

Table 4-15

Melt	T°C	ε_{max} [M^{-1} cm^{-1}]	λ_{max} [mμ]
$LiNO_3$	367	16.70	309.5
$NaNO_3$	365	8.38	298.8
KNO_3	405	4.87	326.1
$CsNO_3$	425	5.12	330.1

The values of λ_{max} and ε_{max} (this last one with exception of $LiNO_3$) are somewhat close to the values reported in this work for the same solutions at high concentration.

Added Salt Studies

A) $LiNO_3$ Solutions

Studies have been carried out in which the equilibria of dilute nitrate solutions (10^{-1} M) is displaced by adding a large excess of common cation

$$MNO_3 + MX \longrightarrow (MNO_3)_{complex} + M^+ + X^-$$

A complex may be formed when MX is added in concentrations 20 to 120 times in excess of the concentration of MNO_3. A shift in the position of the spectra or a change in height may give the clue for complex formation. We do not have a direct way to identify the new species so formed and responsible for the shift. In some cases the addition of excess cation produces one or two isosbestic points. In the case of $LiNO_3$ by adding LiCl we notice one isosbestic point in Figure 4-13. If two species have absorptions bands that overlap, there will be some wavelength at which the molar absorption of the two species are equal. If the concentration of two species is constant at a certain wavelength there will be no change in absorbance of this wavelength as the ratio of the two materials is varied. The invariant point so obtained is called the isobestic point. In the $LiNO_3$ + LiCl solutions we have two species presumably NO_3^- and $(LiNO_3)_{complex}$ absorbing in solution. The equilibria is reflected at the isosbestic

$$Li^+ + NO_3^- \leftrightarrow (LiNo_3)_{complex}$$

point. There are two absorbing species with different molar absorbivities and at the isosbestic point the molar absorbivities of the two species are equal. In such a case the equilibrium constant may be worked out by the method of Rose and Drago (1959) and Drago et al. (1961).

In an equilibria like $M^+ + NO_3^- \rightarrow (MNO_3)_c$, C_c being the

concentration of complex, $C^{o}_{NO_3^-}$ is the initial concentration of NO_3^-, and $C^{o}_{M^+}$ the initial concentration of M^+, then the total absorptivity is given by:

(1) $A = \varepsilon_c C_c + \varepsilon_{NO_3^-} C_{NO_3^-}$ at equilibrium,

being A the absorption at any wavelength, $C_{NO_3^-}$ concentration of NO_3^- at equilibrium and ε_c molar absortivity of the complex. The equilibrium condition is given by

$$(2)\quad K_c = \frac{C_c}{(C^{o}_{NO_3^-} - C_c)(C^{o}_{M^+} - C_c)}$$

(3) $C^{o}_{NO_3^-} = C_c + [NO_3^-]$ being $[NO_3^-]$ concentration at equilibrium

From (1) and (3) $A = C_c(\varepsilon_c - \varepsilon_{NO_3^-}) + \varepsilon_{NO_3^-} \cdot C^{o}_{NO_3^-}$

We also have (4) $A^o = \varepsilon_{NO_3} \cdot C_{NO_3^-}$

After simplifying in equations (1) (2) (3) and (4)

$$(5)\quad K^{-1} = \frac{A - A^o}{\varepsilon_c - \varepsilon_{NO_3^-}} - C^{o}_{M^+} - C^{o}_{NO_3^-} + \frac{C_{M^+} \cdot C_{NO_3^-}}{A - A^o}(\varepsilon_c - \varepsilon_{NO_3^-})$$

K^{-1} and ε_c are not known in equation (5). By trial and error, values of $(\varepsilon_c - \varepsilon_{NO_3^-})$ are arbitrarily assigned to give K^{-1} values at a certain wavelength. If this is done for three different molarities of added salt and at two wavelengths we get an intersection of lines corresponding to the molarities thus is the value of the association constant. The treatment of the data so indicated has not given any intersection and therefore not a K_{assoc} value for $LiNO_3$ solutions.

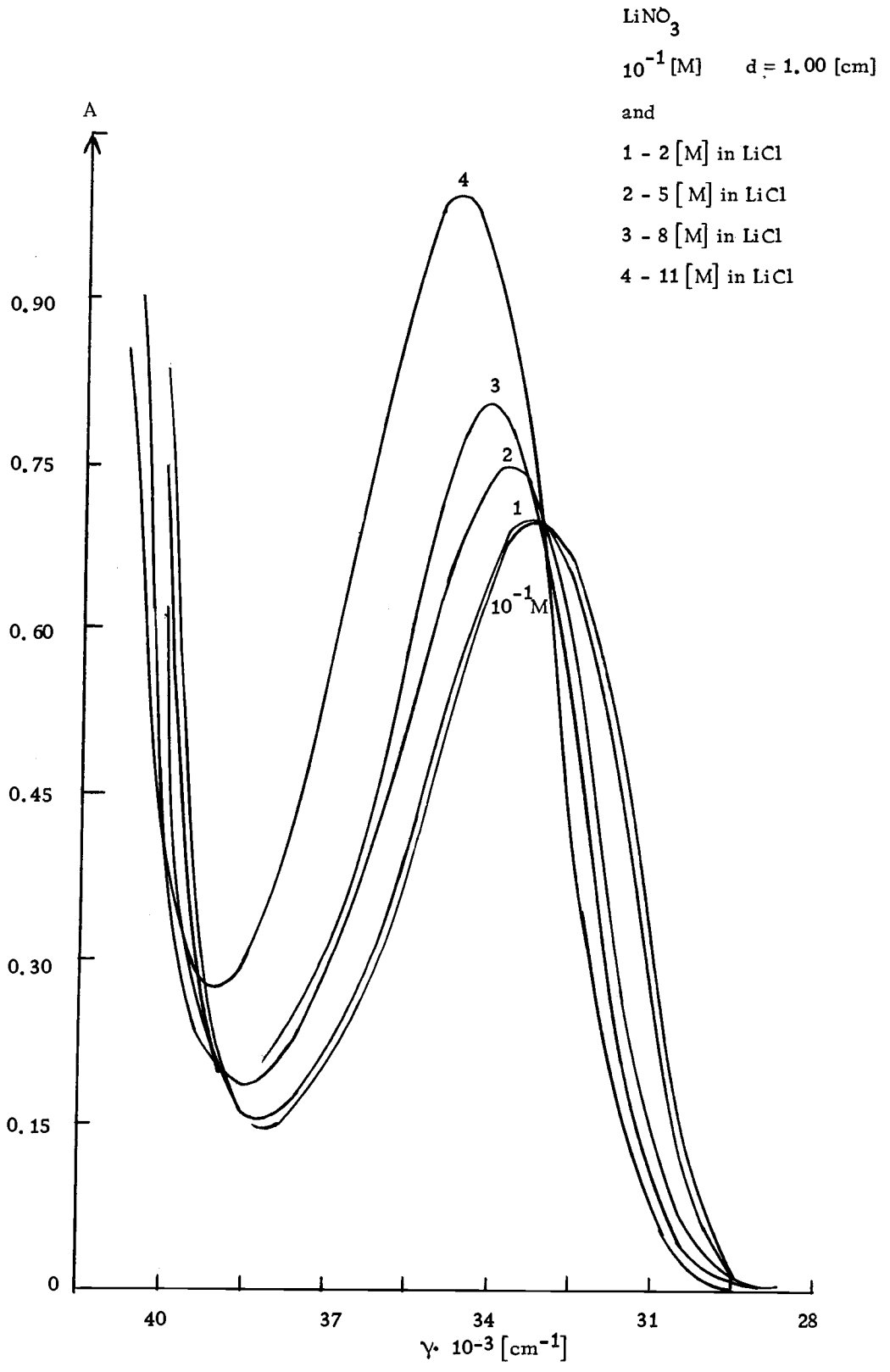
LiNO3
10-1 [M] d = 1.00 [cm]
and
1 - 2 [M] in LiCl
2 - 5 [M] in LiCl
3 - 8 [M] in LiCl
4 - 11 [M] in LiCl
A
0.90
0.75
0.60
0.45
0.30
0.15
0
4
3
2
1
10-1M
40
37
34
31
28
γ· 10-3 [cm-1]

Figure 4-13

That the Li^+ cation added produces a spectral shift as well as change in the 10^{-1} M $LiNO_3$ solution has been described in a non quantitative way by the work of Halban (1928) who added LiCl to dilute KNO_3 solution, observing spectral shift in the latter one. Halban postulated a contact ion-pair formed between Li^+ and NO_3^- when LiCl is added. Kortüm (1944) ascribes the formation of the isosbestic point to an asymmetric deformation of the nitrate in the strong field of the Li^+ with small radius and therefore high electrostatic density. A better explanation is yet to be found.

B) $NaNO_3$ Solutions

Spectral observations are presented in Figure 4-14 and 4-15. These observations have been carried out to primarily show that the effect of the anion has a significative importance in the spectral shift and shape in added salt spectra studies. This aspect was considered in very little detail in the work carried out between 1928-1944 in nitrate solutions. The change of acidity or basicity of the media and of added ions resulted in very little change in the nitrate spectra and this effect was rationalized as being due to the big size of the anions (an therefore low electric density) so that the dipole type interaction with the cation was small. The rationalization for the fact that $NaNO_3$ solutions do not show an isosbestic point when NaCl, $NaClO_4$ or CH_3COONa are added was attempted by Kortüm

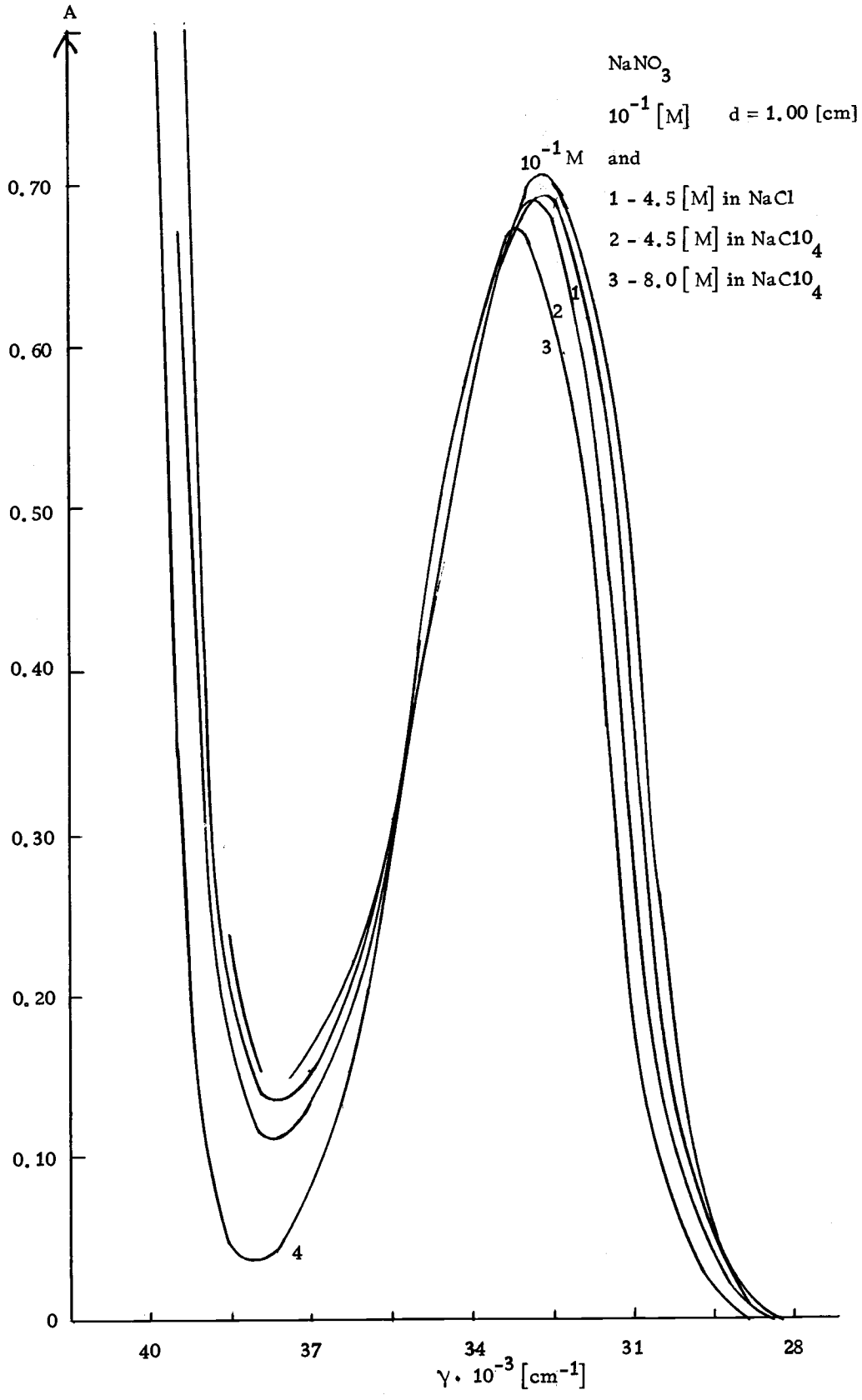
A
0.70
0.60
0.50
0.40
0.30
0.20
0.10
0
40
37
34
31
28
γ · 10^-3 [cm^-1]
NaNO3
10^-1 [M] d = 1.00 [cm]
10^-1 M and
1 - 4.5 [M] in NaCl
2 - 4.5 [M] in NaClO4
3 - 8.0 [M] in NaClO4
1
2
3
4

Figure 4-14

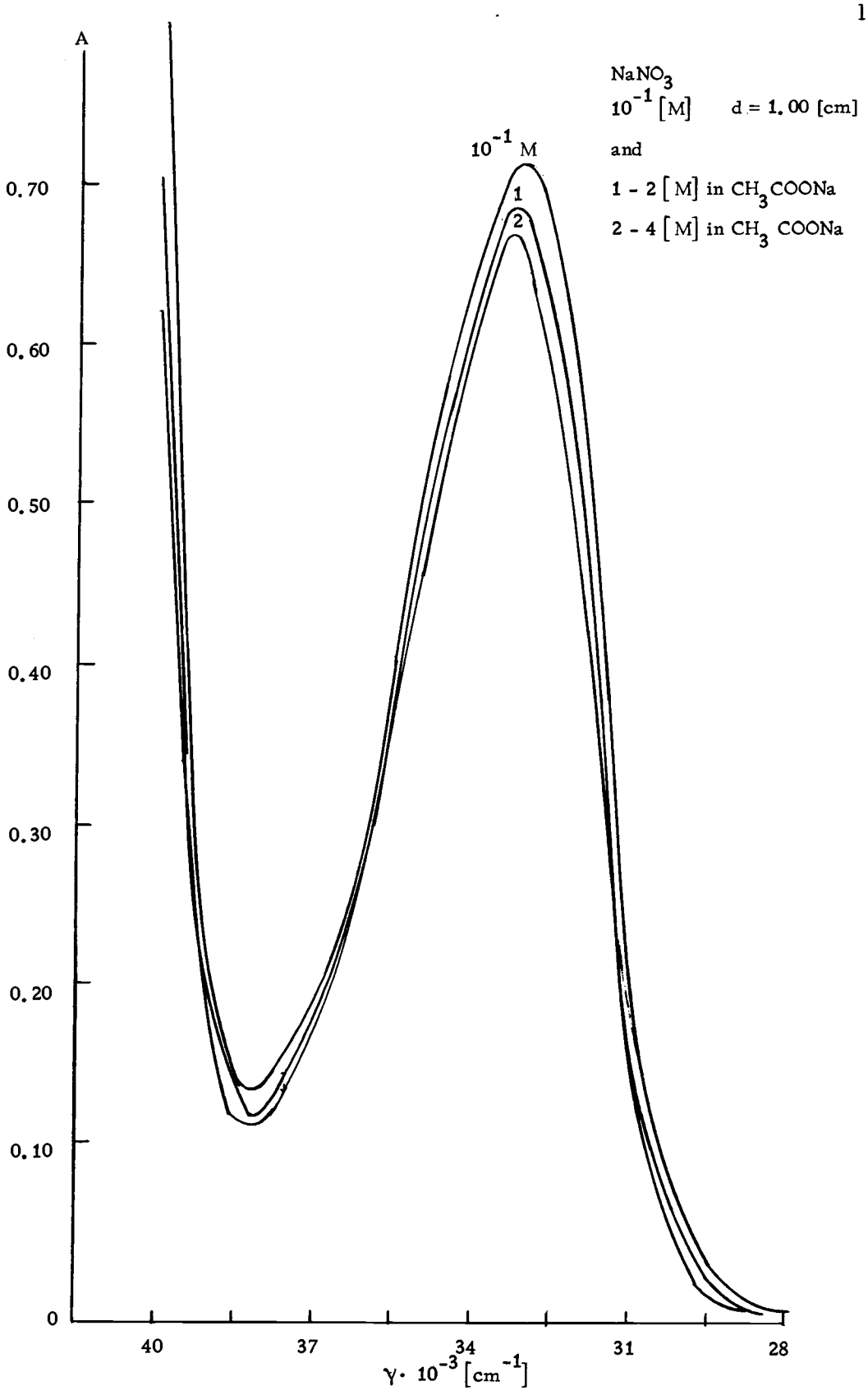
A
0.70
0.60
0.50
0.40
0.30
0.20
0.10
0
40
37
34
31
28
γ· 10^-3 [cm^-1]
NaNO3
10^-1 [M] d = 1.00 [cm]
and
1 - 2 [M] in CH3COONa
2 - 4 [M] in CH3 COONa
10^-1 M
1
2

Figure 4-15

(1944) saying that a uniform deformation of the electronic cloud in the nitrate leads to a complex that is symmetric in space. The addition of NaCl to 10^{-1}M $NaNO_3$ seems to prevent ion-pair formation which is reflected in the unusually low value of the absorption in Figure 4-14 (labeled 4). The value of this lower shoulder is A = 0.05, instead of 0.12 for pure NO_3^- hydrated ion.

C) KNO_3 Solutions

In Figures 4-16 and 4-17 there are shown several added salt spectra to a 10^{-1} M KNO_3 solution. These results deserve the same comment cited for the $NaNO_3$ solutions in part B and essentially constitute a more systematic search for a complex formation sought by spectroscopic means for KNO_3 solutions. The shape and shift of these spectra has yet to be explained.

D) $Ca(NO_3)_2$ Solutions

The spectra taken when $CaCl_2$ is added to a solution 10^{-1} M of $Ca(NO_3)_2$ is shown in Figures 4-18 and 4-19. Similar results were obtained by von Halban (1928). A quantitative analysis has been carried out since for our data. To a 10^{-1} M solution of $Ca(NO_3)_2$ in a 1.00 cm cell it has been made 2, 4, 6, 8, 10, 11.5 M in $CaCl_2$. Isosbestic points are observed at 34.050 cm^{-1} and 33.260 cm^{-1}.

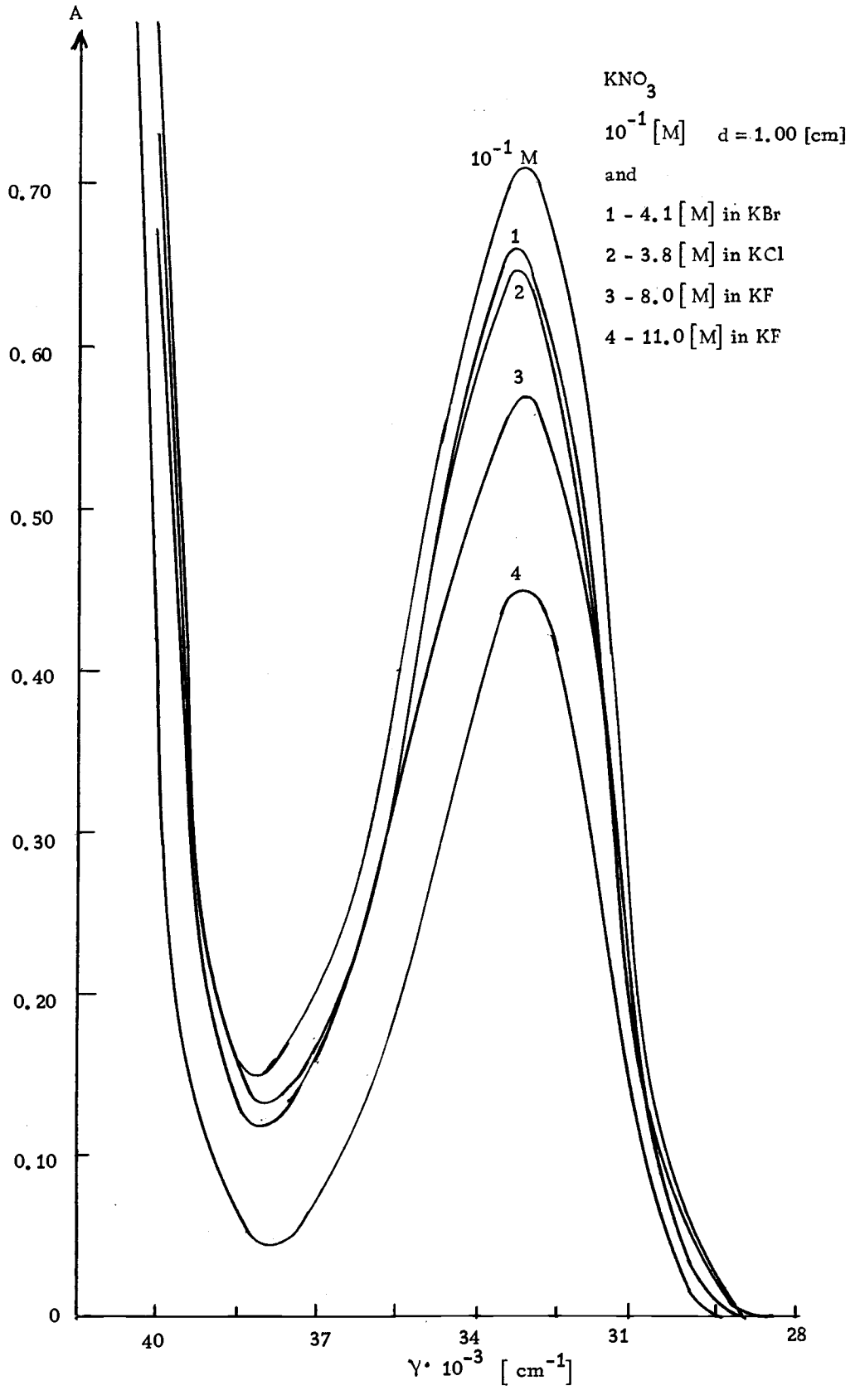
A
0.70
0.60
0.50
0.40
0.30
0.20
0.10
0
40
37
34
31
28
$\gamma \cdot 10^{-3}$ [cm^{-1}]
KNO_3
10^{-1} [M] d = 1.00 [cm]
and
1 - 4.1 [M] in KBr
2 - 3.8 [M] in KCl
3 - 8.0 [M] in KF
4 - 11.0 [M] in KF
10^{-1} M
1
2
3
4

Figure 4-16

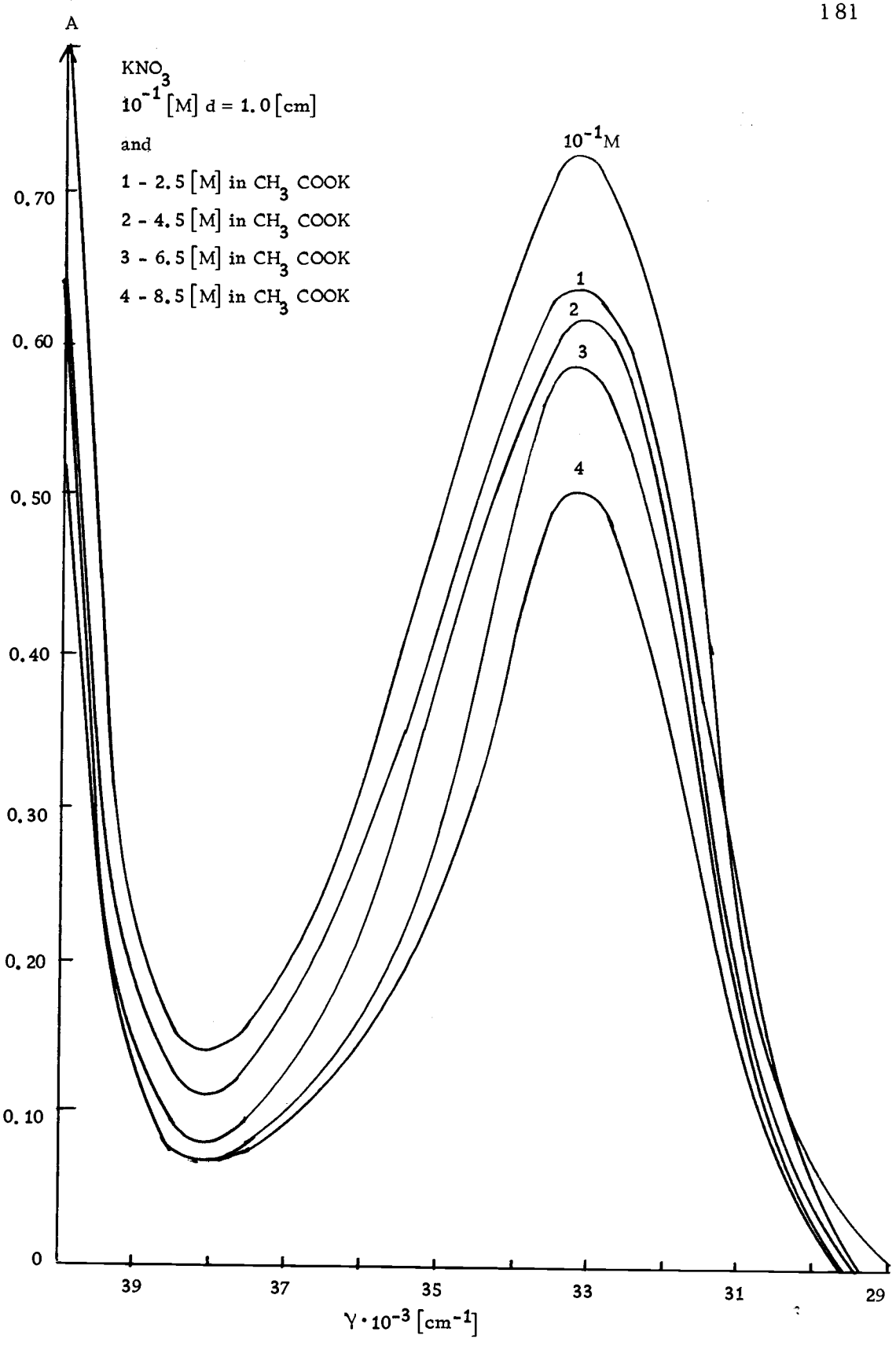
A
KNO3
10-1 [M] d = 1.0 [cm]
and
1 - 2.5 [M] in CH3 COOK
2 - 4.5 [M] in CH3 COOK
3 - 6.5 [M] in CH3 COOK
4 - 8.5 [M] in CH3 COOK
10-1M
1
2
3
4
0.70
0.60
0.50
0.40
0.30
0.20
0.10
0
39
37
35
33
31
29
ν·10-3 [cm-1]

Figure 4-17

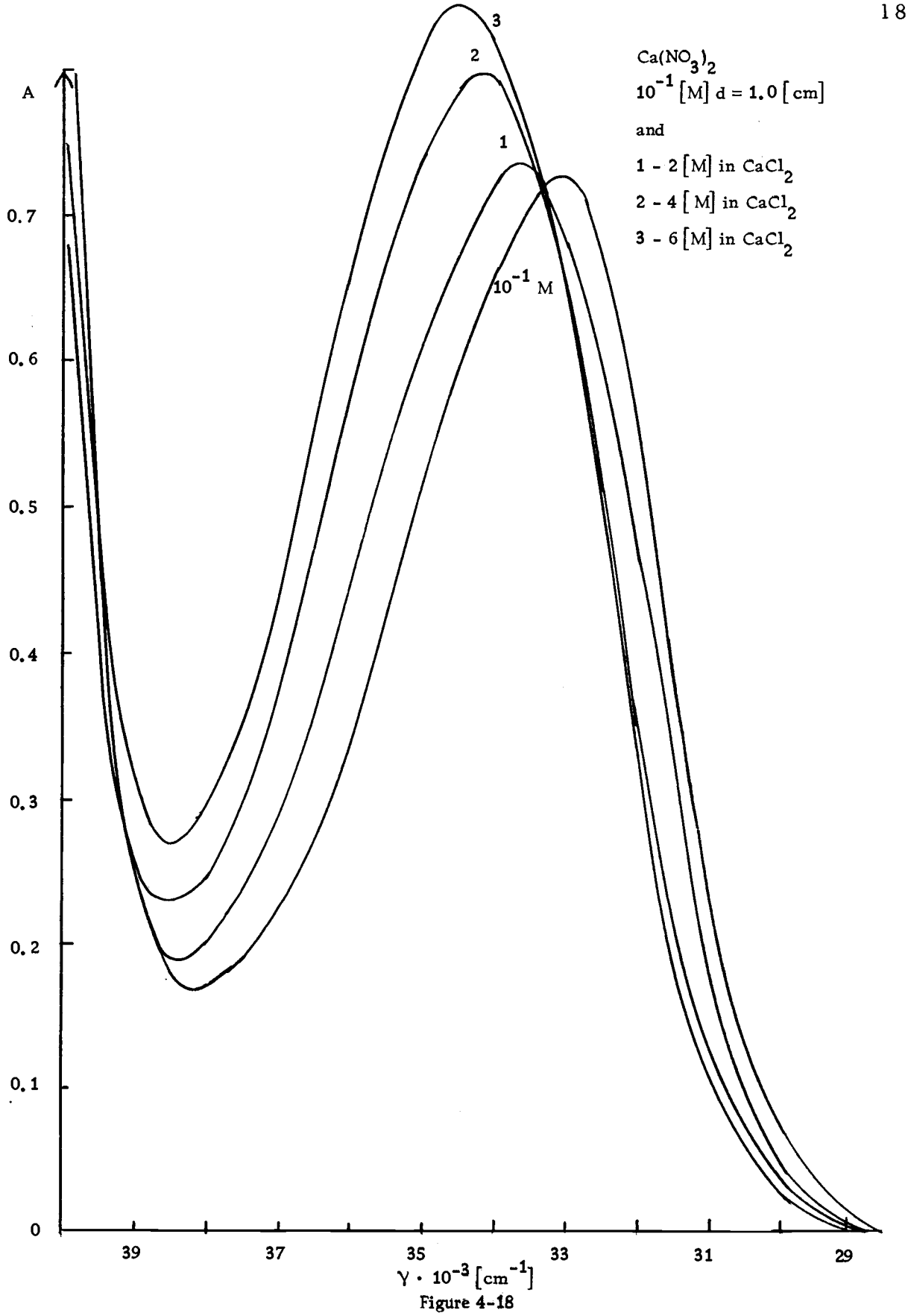
A
0.7
0.6
0.5
0.4
0.3
0.2
0.1
0
39
37
35
33
31
29
$\gamma \cdot 10^{-3}$ [cm^{-1}]
3
2
1
10^{-1} M
$Ca(NO_3)_2$
10^{-1} [M] d = 1.0 [cm]
and
1 - 2 [M] in $CaCl_2$
2 - 4 [M] in $CaCl_2$
3 - 6 [M] in $CaCl_2$

Figure 4-18

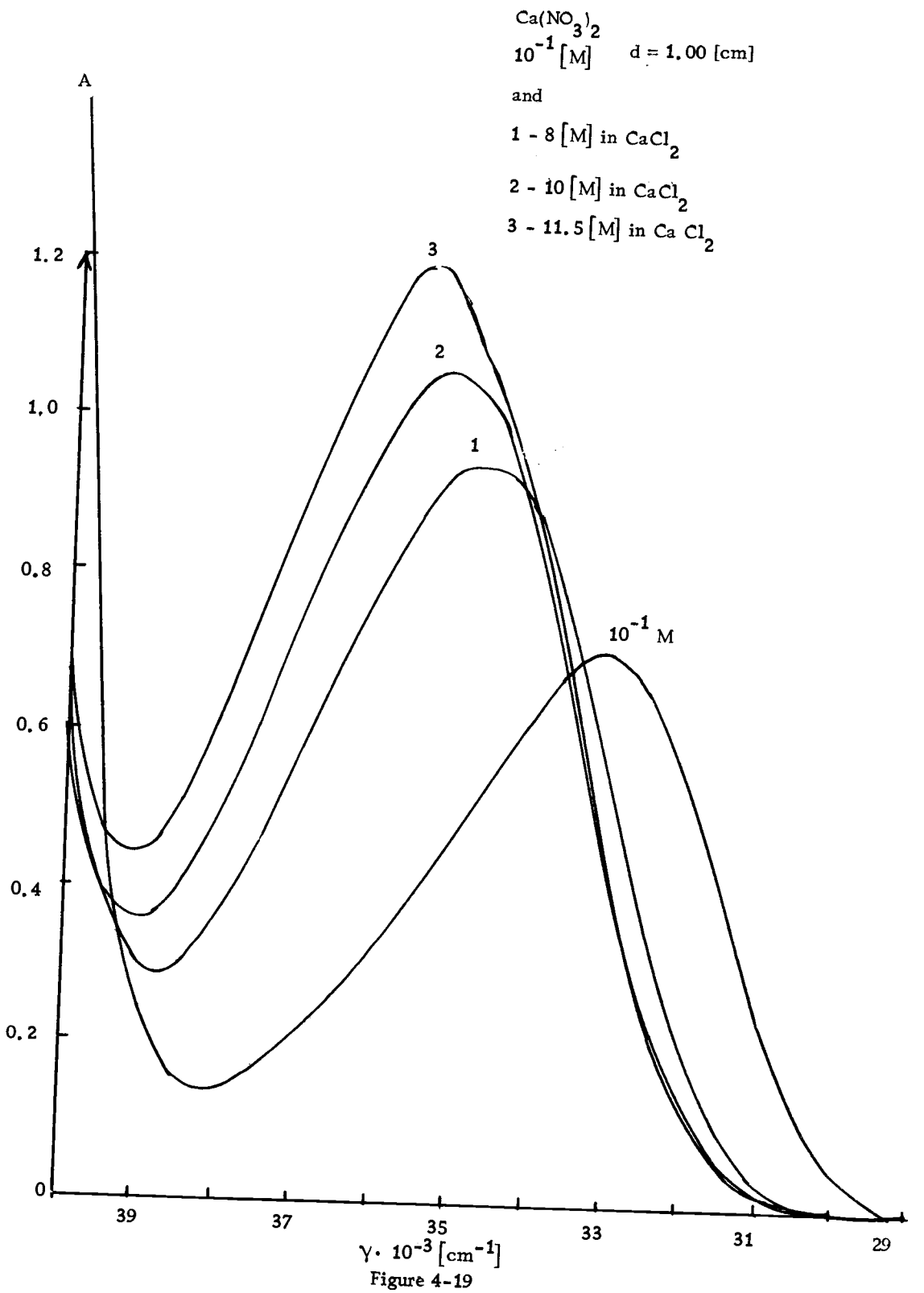
Ca(NO3)2
10-1 [M] d = 1.00 [cm]
and
1 - 8 [M] in CaCl2
2 - 10 [M] in CaCl2
3 - 11.5 [M] in Ca Cl2
A
1.2
1.0
0.8
0.6
0.4
0.2
0
3
2
1
10-1 M
39
37
35
33
31
29
γ· 10-3 [cm-1]

Figure 4-19

The two isosbestic points obtained are indicative of different species in equilibria. These isosbestic points are analyzed according to Rose and Drago (1959) treatment and they lead to the following tabulation of data at 32000[cm^{-1}] for concentrations added of 2, 4, 6, [M] $CaCl_2$ ($inCl^-$) 2 M $CaCl_2$ added:

$$C^o_{Ca^{++}} = 1[M] \text{ (from } CaCl_2) + 0.05 \text{ M[from } Ca(NO_3)_2]$$

$$C^o_{NO_3^-} = 0.1\,[M]$$

In this expression

$$K^{-1} = \frac{A - A^o}{\varepsilon_c - \varepsilon_{NO_3^-}} - C^o_{M^+} - C^o_{NO_3^-} + \frac{C_{M^+} \cdot C_{NO_3^-}}{A - A^o}(\varepsilon_c - \varepsilon_{NO_3^-})$$

from Figure 4-19 substituting the values

$$K^{-1} = \frac{0.034}{m} - 1.15 - \frac{0.105}{0.034}\,m \qquad\qquad m = \varepsilon_c - \varepsilon_{NO_3^-}$$

and giving ourselves values of m we end up with:

m	K^{-1}
1	1.88
3	8.12
4	11.29
5	14.35
6.5	17.60

In the same way operate at 32000 cm^{-1} with 4 and 6[M] $CaCl_2$ added.

The three lines obtained are shown in Figures 4-20 and 4-21

$K^{-1} = 9.3$ or $K = 0.11$ $(32000\ cm^{-1})$

$K^{-1} = 12.6$ or $K = 0.08$ $(34500\ cm^{-1})$

so that K_{assoc} for isosbestic point at 33680 cm^{-1} has a value $0.11 < K_{assoc} < 0.08$. This treatment is repeated for added $CaCl_2$ concentrations of 8, 10 and 11.5 molar. The plots are shown in Figures 4-22 and 4-23. The K_{assoc} arrived:

$K^{-1} = 7.5$ or $K = 0.13$ $(32000\ cm^{-1})$

$K^{-1} = 8.4$ or $K = 0.12$ $(34500\ cm^{-1})$

so that the K_{assoc} for the isosbestic point at 34160 cm^{-1} has a value $0.12 < K_{assoc} < 0.13$. These values compare well with the values obtained by Hester and Plane (1963) by Raman spectroscopy, which reported a value of K_{assoc} ranging between 0.12 and 0.17 for a complex that they assigned as $CaNO_3^+$. We have two isosbestic points and therefore we can postulate two equilibria, such as:

1 $\quad Ca^{++} + NO_3^- \rightarrow Ca\,NO_3^+$

2 $\quad CaNO_3^+ + Ca^{++} \rightarrow [CaNO_3Ca]^{+3}$

but it is not possible to elaborate with certainty about the species involved at this point.

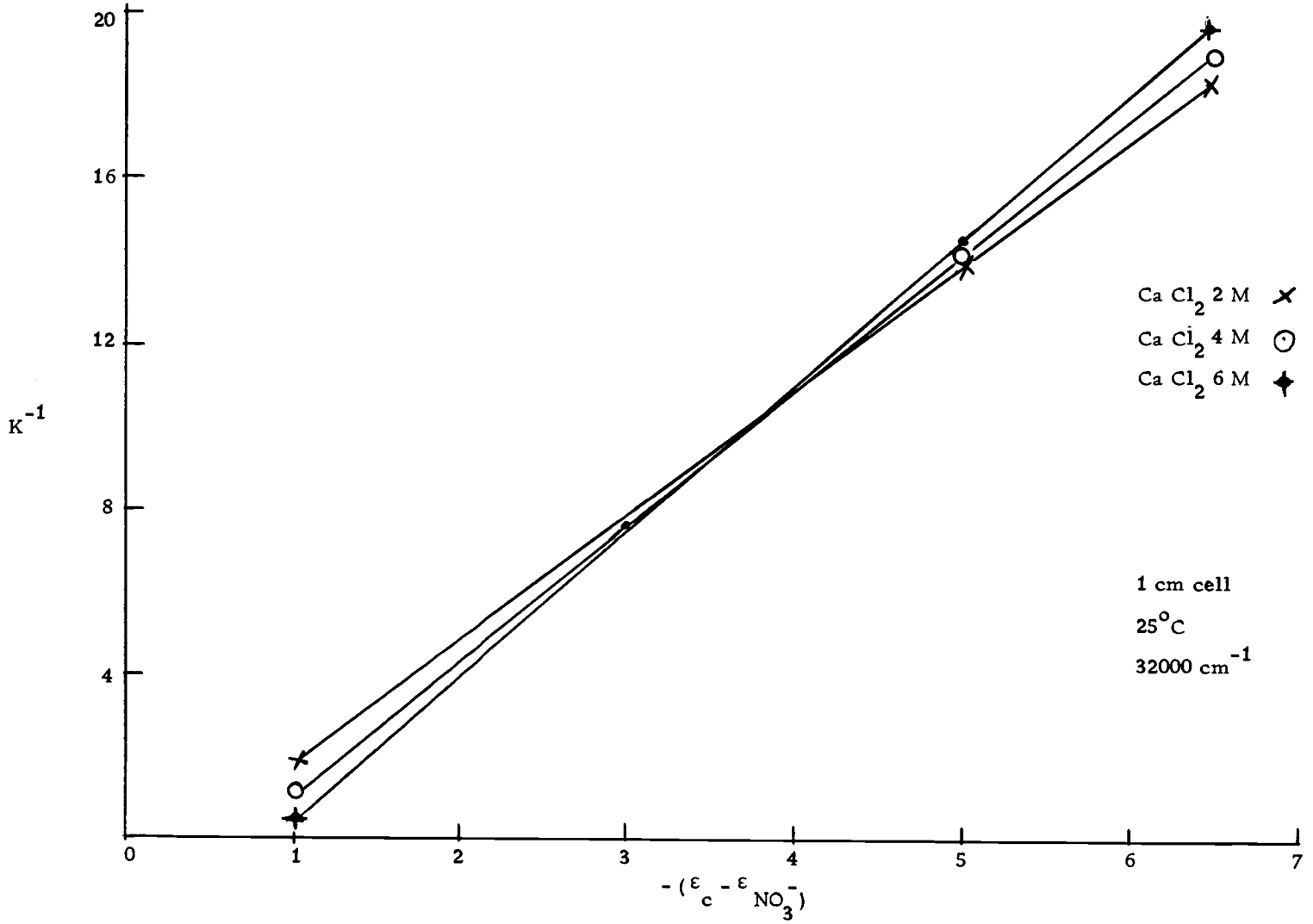
20
16
12
8
4
K^{-1}
0
1
2
3
4
5
6
7
$-(\varepsilon_c - \varepsilon_{NO_3^-})$
Ca Cl_2 2 M
Ca Cl_2 4 M
Ca Cl_2 6 M
1 cm cell
25°C
32000 cm^{-1}

Figure 4-20

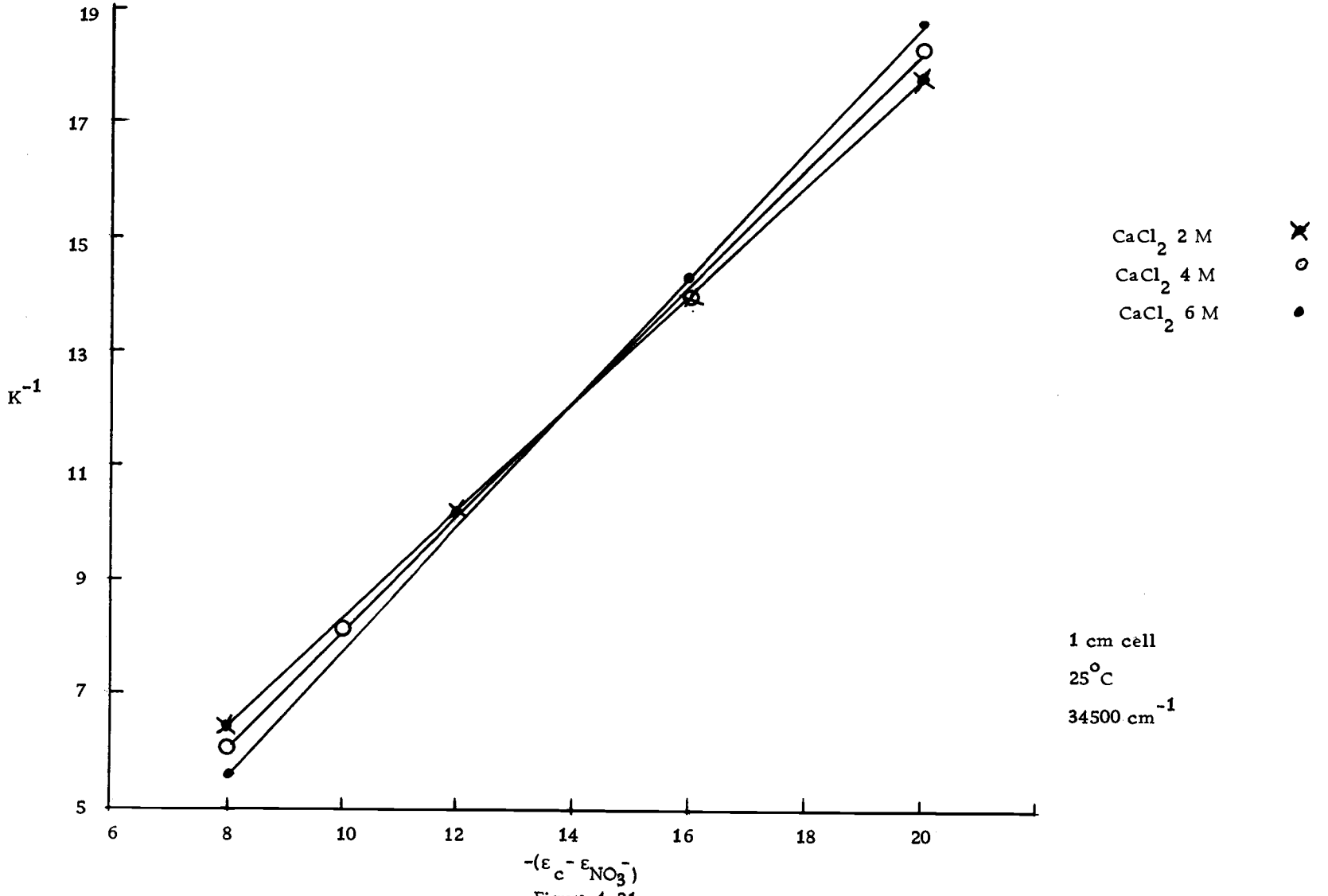
19
17
15
13
11
9
7
5
K^{-1}
6
8
10
12
14
16
18
20
$-(\varepsilon_c - \varepsilon_{NO_3^-})$
$CaCl_2$ 2 M
$CaCl_2$ 4 M
$CaCl_2$ 6 M
1 cm cell
25°C
34500 cm^{-1}

Figure 4-21

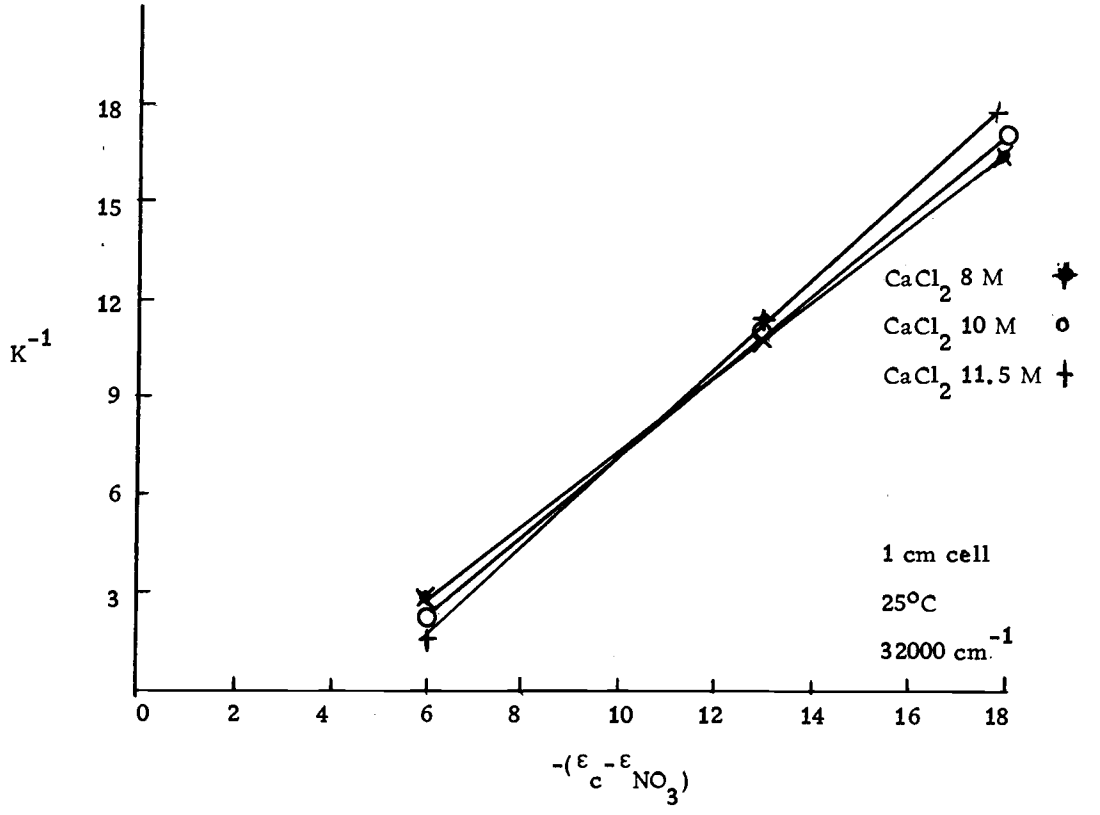
18
15
12
9
6
3
K^{-1}
0
2
4
6
8
10
12
14
16
18
$-(\varepsilon_c - \varepsilon_{NO_3})$
$CaCl_2$ 8 M
$CaCl_2$ 10 M
$CaCl_2$ 11.5 M
1 cm cell
25°C
32000 cm^{-1}

Figure 4-22

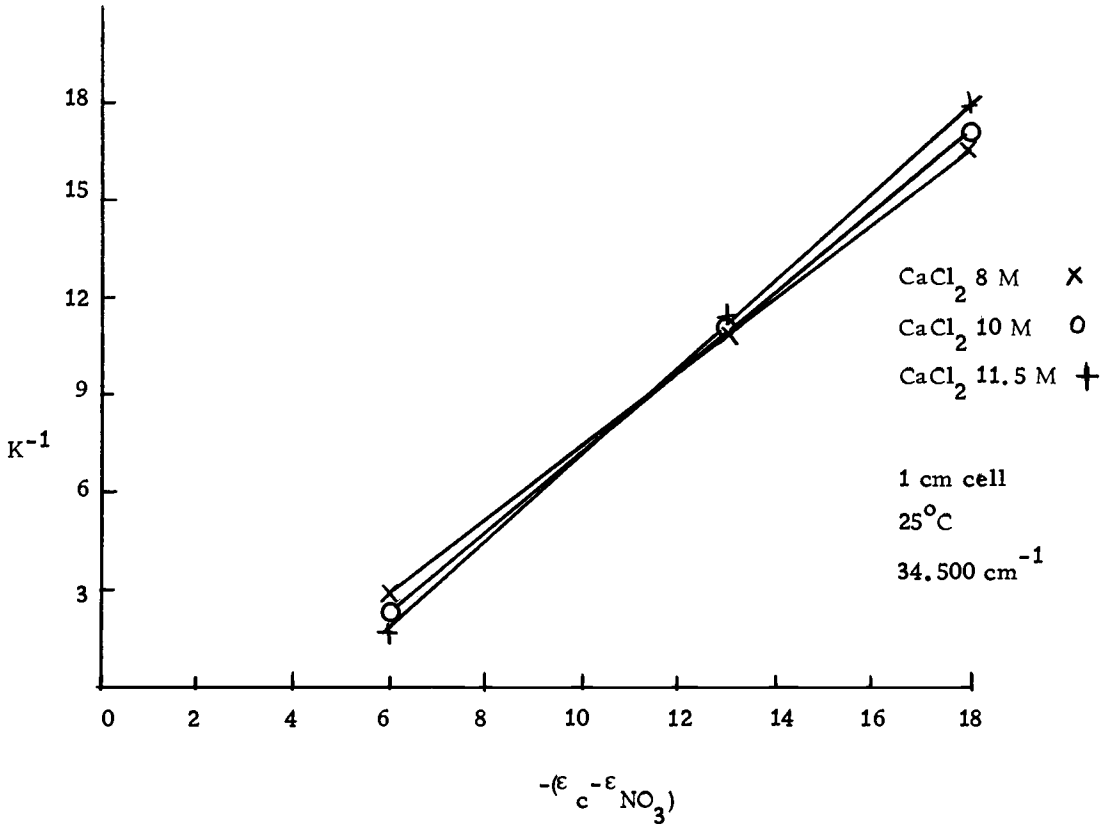
18
15
12
9
6
3
K^{-1}
0
2
4
6
8
10
12
14
16
18
$-(\varepsilon_c - \varepsilon_{NO_3})$
$CaCl_2$ 8 M
$CaCl_2$ 10 M
$CaCl_2$ 11.5 M
1 cm cell
25°C
34.500 cm^{-1}

Figure 4-23

Study of Nitrate Solutions Using the Method of Continuous Variations

Previous work attempts to discuss behaviour on basis of 1:1 complex. Present studies describes attempts to characterize complexes. This can be ascertained from photometric studies by the method of continuous variations attributable to Job (1928) and modified by Vosburgh and Cooper (1941). The method of formation of complex ions can in general be represented by the equation

$$M + nA \longrightarrow MA_n$$

in which M is a metallic ion and A is an anion. If M and A react as described then mixing solutions of A and B in varying proportions should give some variation in the optical density and in this way a suitable property to detect complexation of the resulting solutions should be attained. We have chosen to determine a constant for association when the sum of cation anion in $LiNO_3$, $NaNO_3$, KNO_3 and $Ca(NO_3)_2$ is 5 M.

$LiNO_3$ Solutions

Solution of NH_4NO_3 (11.1 M) and LiCl (12.0 M) were mixed and diluted with water to vary continuously the proportion of cation and anion in the constant sum $\Sigma\ Li^+ + NO_3^- = 5$ M. Data was taken at 290 mμ. The NH_4^+ and Cl^- ions do not absorb in solution at 290 mμ

so that all the absorption is ascribed to the NO_3^- ion. Therefore the equilibria of interest is

$$Li^+ + NO_3^- \leftrightarrow (LiNO_3)_c$$

and the optical density A as a function of the fraction of NO_3^- present ($f_{NO_3^-}$) may follow a type of relation where it is assumed that the absorption of an arbitrary wavelength (290 mμ) near the isosbestic point is due only to NO_3^- hydrated ion present and its decrease is due to some sort of association of this ion.

$$A_{290\ m\mu} = k \cdot f_{NO_3^-} = k \frac{NO_3^-}{Li^+ + NO_3^-}$$

where k is a proportionality constant that relates the absorption A to the free hydrated NO_3^- which undergoes electronic transition. A plot of A vs. $f_{NO_3^-}$ is shown in Figure 4-25 for $LiNO_3$. If we invert the relation, namely

$$\frac{1}{A_{290}} = \frac{1}{k} \frac{Li + NO_3^-}{NO_3^-} = K \frac{Li^+ + NO_3^-}{NO_3^-}$$

and K then a proportionality constant for the association constant of anion and cation over the nitrate concentration range.

The data for the $LiNO_3$ solutions is shown in Table 4-16.

Table 4-16

$A_{290\ m\mu}$	$\frac{NO_3^-}{NO_3^- + Li^+}$	$\frac{1}{A_{290\ m\mu}}$	$\frac{Li^+ + NO_3^-}{NO_3^-}$
0.15	0.1	6.65	10
0.28	0.2	3.56	5
0.41	0.3	2.44	3.33
0.53	0.4	1.88	2.50
0.65	0.5	1.54	2.00
0.75	0.6	1.33	1.66
0.85	0.7	1.18	1.43
0.95	0.8	1.05	1.25
1.02	0.9	0.98	1.11

The data is plotted out in Figure 4-24 and a K value of 0.66 is obtained. The purpose of this study is to compare a K_{assoc} so obtained for concentrated solutions with the K_{assoc} found by this method for the other nitrates and establish this way a relative comparison for the association in these solutions. It is not possible to identify the associated spectra.

$NaNO_3$ Solution

Solutions of NH_4NO_3 (11.1 M) and $NaClO_4$ (8.93 M) were mixed and a value for the K_{assoc} = 0.96 was obtained. The data is shown in Table 4-17 and plotted out in Figure 4-25.

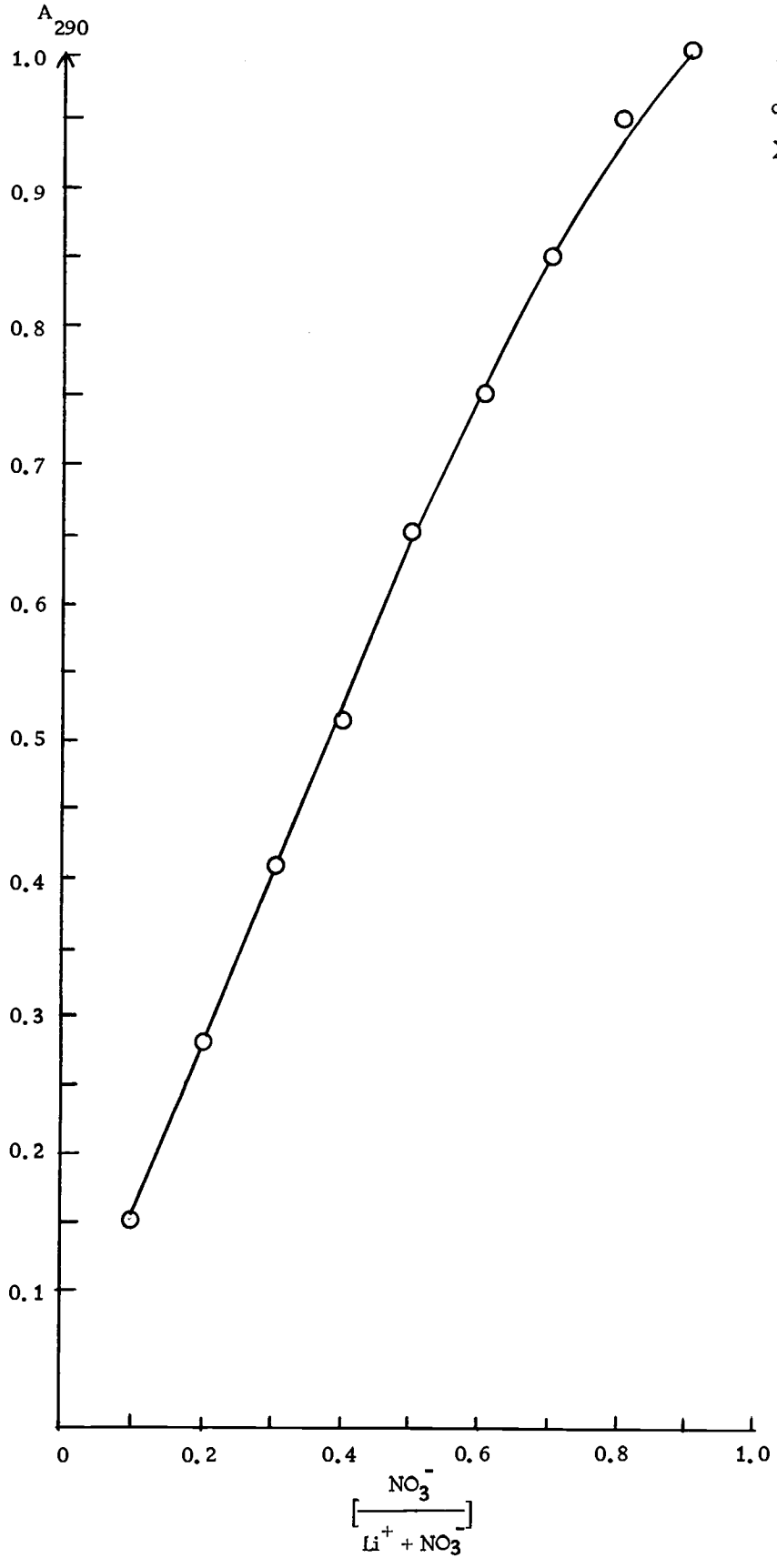
A290
1.0
0.9
0.8
0.7
0.6
0.5
0.4
0.3
0.2
0.1
0
0.2
0.4
0.6
0.8
1.0
[NO3- / Li+ + NO3-]
LiNO3
d = 1.00 [cm]
ΣLi+ + NO3- = 5 M

Figure 4-24

$LiNO_3 = 0.66$ ×
$NaNO_3 = 0.96$ +
$KNO_3 = 1.67$ o
$Ca(NO_3)_2 = 0.48$ •

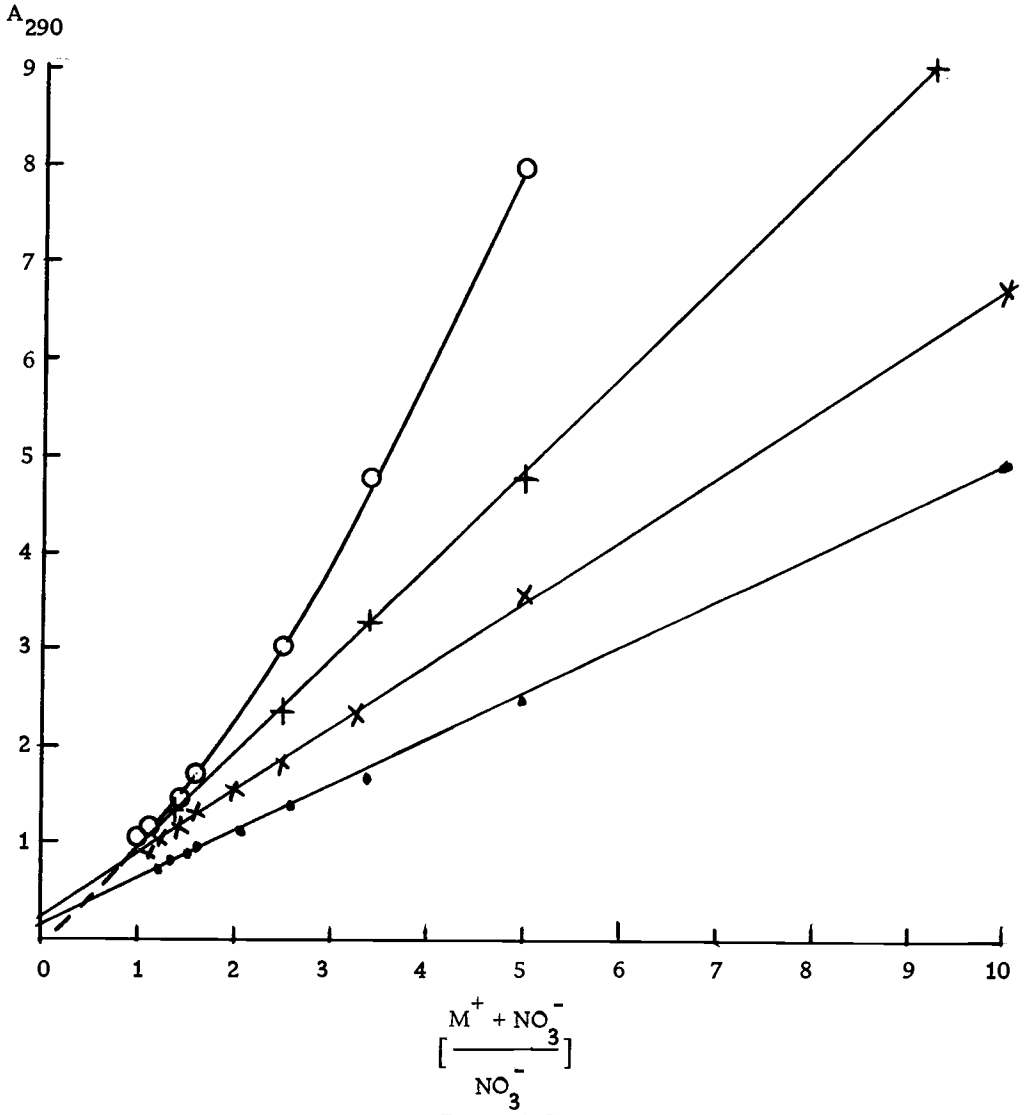

Figure 4-25

Table 4-17

A_{290}	$\frac{NO_3^-}{Na^+ + NO_3^-}$	$\frac{1}{A_{290}}$	$\frac{Na^+ + NO_3^-}{NO_3^-}$
0.10	0.1	10	10
0.21	0.2	4.76	5
0.31	0.3	3.22	3.33
0.43	0.4	2.34	2.50
0.55	0.5	1.82	2.00
0.68	0.6	1.47	1.66
0.80	0.7	1.25	1.43
0.88	0.8	1.14	1.25
0.98	0.9	1.02	1.11
1.09	1.0	0.91	1.0

KNO_3 Solution

Solutions of CH_3 - COOK (9.37 M) and NH_4NO_3 (11.10 M) are mixed and a K_{assoc} 1.67 was obtained. The data is shown in Table 4-18 and plotted out in Figure 4-25.

Table 4-18

A_{290}	$\frac{NO_3^-}{K^+ + NO_3^-}$	$\frac{1}{A_{290}}$	$\frac{K^+ + NO_3^-}{NO_3^-}$
0.07	0.1	14.3	10
0.125	0.2	8.0	5
0.21	0.3	4.76	3.33
0.33	0.4	3.0	2.50
0.47	0.5	2.13	2.00
0.59	0.6	1.69	1.66
0.73	0.7	1.37	1.43
0.83	0.8	1.20	1.25
0.93	0.9	1.08	1.11
1.01	1.0	0.99	1.0

The value for K_{assoc} is 1.67. That this value is higher than the similar one for $LiNO_3$ and $NaNO_3$ solution may be due to the fact that the limit of solubility of KNO_3 is 2.98 M at 20°C and we work in a range of supersaturated solution.

$Ca(NO_3)_2$ Solution

Solutions of $CaCl_2$ (12.7 M in Cl^-) and NH_4NO_3 (11.1 M) were mixed and a K_{assoc} = 0.48 was obtained. Data as shown in Table 4-19 and plotted in Figure 4-25.

Table 4-19

A_{290}	$\frac{NO_3^-}{Ca^{++} + NO_3^-}$	$\frac{1}{A_{290}}$	$\frac{Ca^{++} + NO_3^-}{NO_3^-}$
0.19	0.1	5.15	10.0
0.34	0.2	2.94	5.0
0.47	0.3	2.12	3.33
0.62	0.4	1.61	2.50
0.77	0.5	1.30	2.00
0.84	0.6	1.20	1.66
0.93	0.7	1.08	1.43
1.00	0.8	1.00	1.25
1.03	0.9	0.97	1.11

It seems that the species $CaNO_3^+$ is present as reported in Raman studies by Hester and Plane (1964). A Job's analysis in 5 M $Ca(NO_3)_2$ solutions was carried out by Irish and Walrafen (1966) using Raman spectroscopy in the 740 cm^{-1} band. They suggested a complex with more than one Ca^{++} ion associated with each NO_3^- ion in the region of high concentration, but no definite identification of species was

conclusively reported. In Figure 4-25 the intercept may give some indication that the ions are associated even at very low molarities. This agrees with Irish et al. (1969) that using Raman spectroscopic measurements concluded that cation and anion have a strength of interaction independent of concentration, extrapolating to low concentrations work carried out at higher molarities. This method, is based on incorrect notions concerning the dependence of activity coefficients on composition. Molarities and not activities of ions were used for estimates of concentrations of species like $CaNO_3^+$ which actually do not exist in appreciable amounts.

Study of Nitrate Solutions by Variation of the Solvent

To study the shape and characteristics of the spectra of the nitrate solutions it seems that theoretical difficulties exist related to properties of the liquid media such as dielectric constant, polar moment, viscosity or refractive index. Since several factors seem to be present here, the variation of these properties by added solvents seems to be a way to solve the problem. It is the intention to carry out experiments in solvent media to discover the trend of properties that influence the shape of the spectra. These independent solvent spectra observations should give a better insight in the molecular forces of the electrolytes and through this to the structure of these solutions.

In Figures 4-26 and 4-27 $LiNO_3$ 10^{-1} M spectra are presented taken in ion cell in different solvents. The results are tabulated in Table 4-20.

Table 4-20

$LiNO_3$ 10^{-1} M Solution

Solvent	Solvent Dielectric Constant 25°C	Solvent Dipole Moment Debyes	Viscosity c.p.	$f \cdot 10^5$	$\varepsilon_{max} M^{-1} cm^{-1}$	$\gamma_{max}[cm^{-1}]$	Refractive Index $n_D^{20°}$	1 cm cell u.v. cutoff mμ
H_2O	78.54	1.87	0.890	13.96	7.14	33400	1.3416	190
CH_3OH	32.60	1.66	0.445	12.45	6.80	32800	1.3285	202
C_2H_5OH	24.30	1.69	1.08	12.48	6.59	32720	1.3594	200
nC_3H_7OH (-prop)	18.30	1.65	2.004	12.98	7.00	32600	1.3834	203
H $CON(CH_3)_2$(DMF)	37.61	3.82	0.796	8.05	4.10	32100	1.4269	270
HCO NH_2 (F)	109.5	3.73	3.302	13.20	7.20	33100	1.447	260
$H_2CCO_2NH_2$ (0.875 M) glycine	98.03			11.35	6.66	33320		
$H_2CCO_2NH_2$ (2.50 M glycine)	134.50			12.98	8.02	33600		
CH_3CN	37.50	3.37	0.325	9.99	5.02	32400	1.3416	190
$HO(CH_2)_2OH$ glycol	39.00	2.2	13.55	12.10	7.20	32800	1.4302	190

Note in Figure 4-28 the vibrational levels that appear in the spectra of $LiNO_3$ 10^{-1} M when DMF is used as a solvent. In the work out of this type of spectra the cutoff of the solvent is a factor that has to be taken into consideration before running the spectra. Any solvent that had a cutoff above 260 mμ (38000 cm^{-1}) was rejected. This consideration excluded most of the available organic solvents that were used previously to attain a smooth variation of the dielectric constant in the solutions investigated. The refractive index here

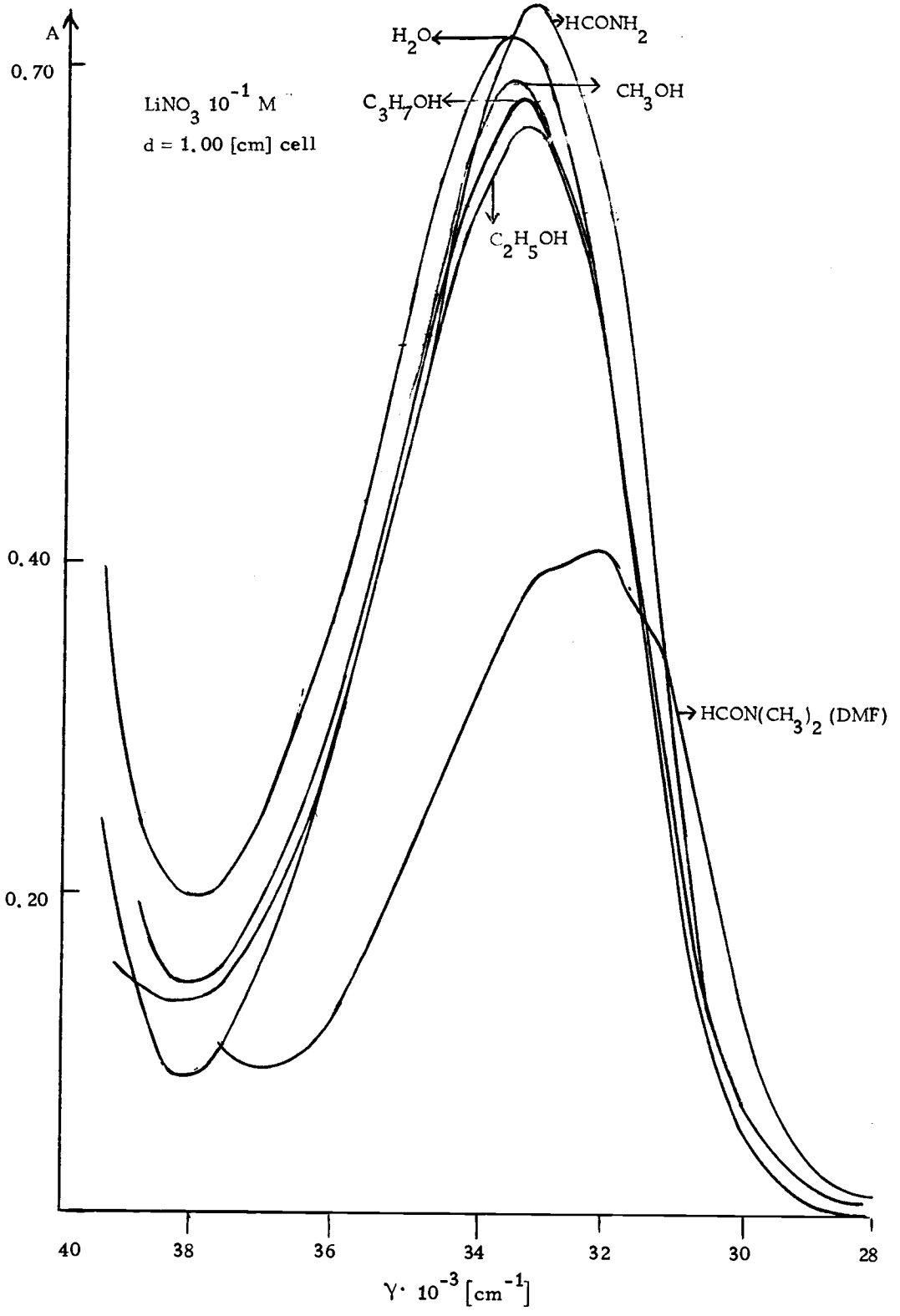
A
0.70
0.40
0.20
LiNO3 10-1 M
d = 1.00 [cm] cell
H2O
HCONH2
C3H7OH
CH3OH
C2H5OH
HCON(CH3)2 (DMF)
40
38
36
34
32
30
28
γ· 10-3 [cm-1]

Figure 4-26

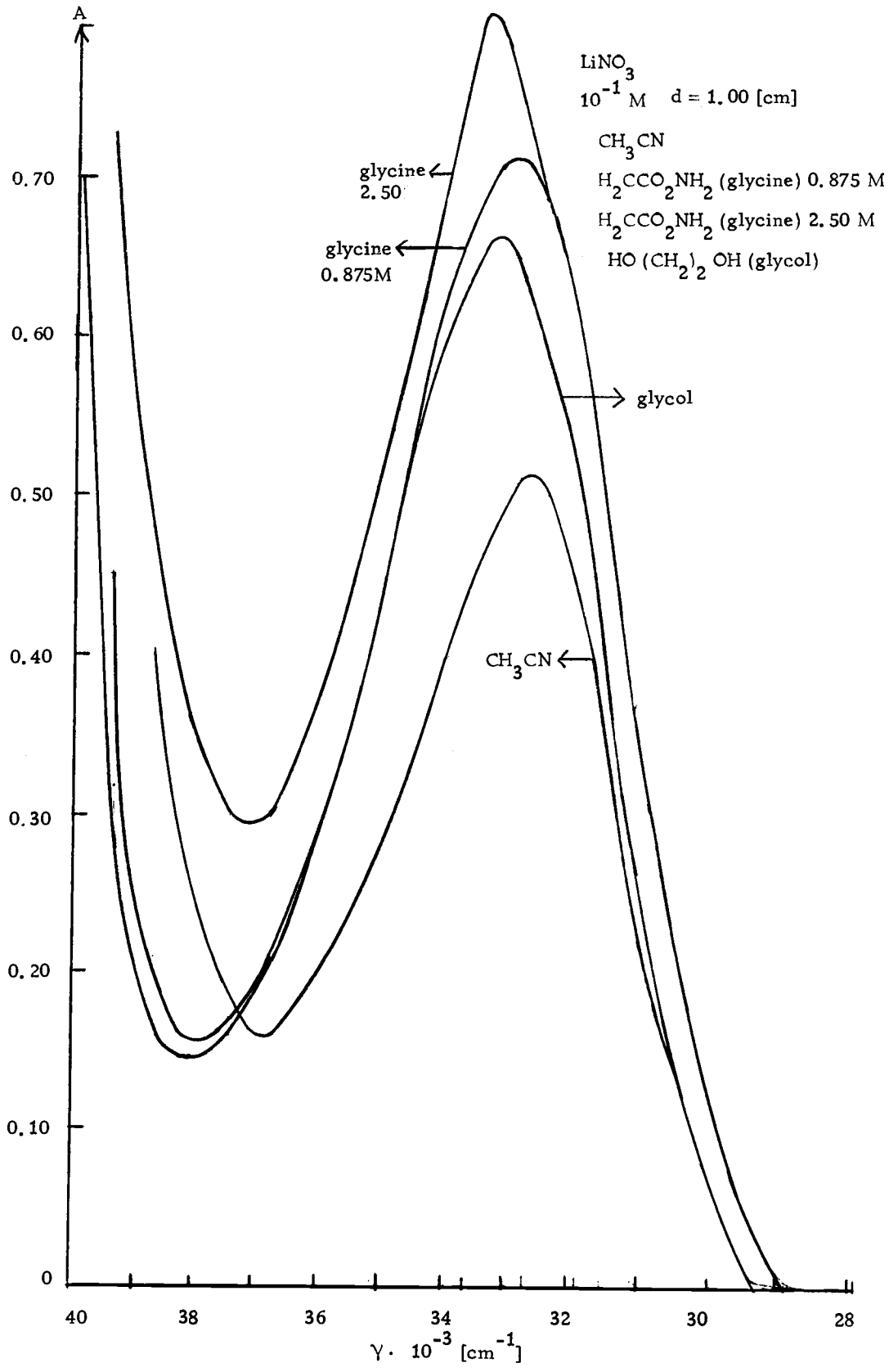
A
0.70
0.60
0.50
0.40
0.30
0.20
0.10
0
40
38
36
34
32
30
28
γ · 10^-3 [cm^-1]
LiNO3
10^-1 M d = 1.00 [cm]
CH3CN
H2CCO2NH2 (glycine) 0.875 M
H2CCO2NH2 (glycine) 2.50 M
HO (CH2)2 OH (glycol)
glycine 2.50
glycine 0.875M
glycol
CH3CN

Figure 4-27

should give an estimate of the refractive losses due to the solvent at 5893 A^o (the Na line). Water itself at 4046.6 A^o has an n_D^{20} = 1.34348 and at 3000 A^o the value for n_D^{20} is 1.35884. The variation is small for values of the refraction index at 300 mμ compared with those determined at 5893 A^o. The estimate for the scattering is calculated by the Kronick-Kramer relations. Refraction indexes for the solutions as such are not available at 300 mμ and the refractive loss factor that could account for the decrease in ε and f value of the transition is not calculated at the present time. The viscosity values of the solvent have been brought into the picture to get an "a priori" physical description of the shapes observed without positive results. The values found for f, ε and γ_{max} agrees with the values reported by Rotlevi and Treinin (1965).

Strickler and Kasha (1964) postulated that the n → π* transition energy increases as a function of the amount of H bonding formed between oxygen of the NO_3^- ion and the H atoms of the solvent. Solvents with more polarity form more readily a H bond and a blue shift will then take place at a higher energy.

In Figure 4-28 we plot γ_{max} vs. polar moment of different solvent used. This is not the polar moment of the solution but it will be useful to assess an experimental verification of Strickler and Kasha's theory. Large deviation for such a postulated behaviour are present in water, acetonitrile and dimethyl formamide. The

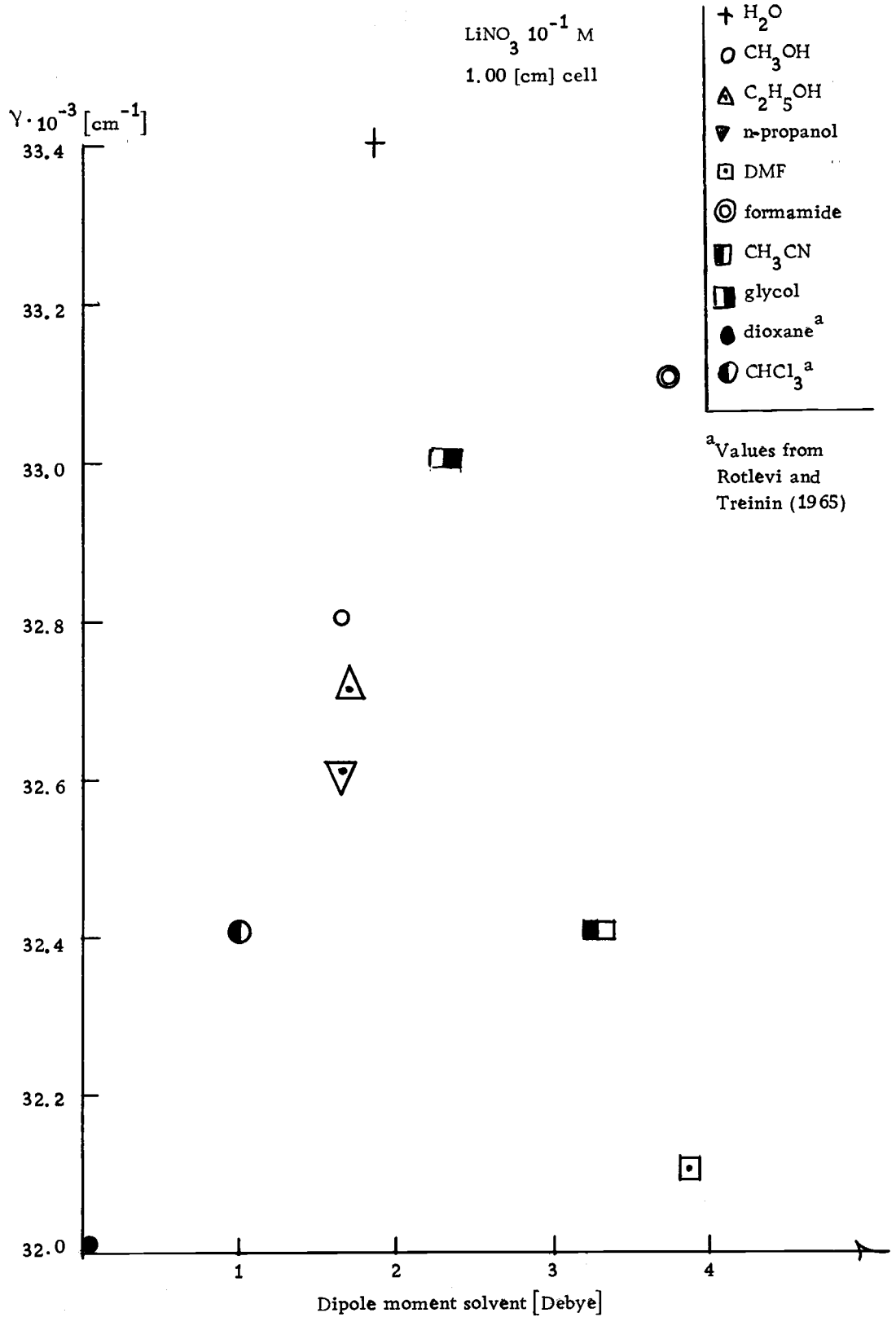
LiNO3 10-1 M
1.00 [cm] cell
H2O
CH3OH
C2H5OH
n-propanol
DMF
formamide
CH3CN
glycol
dioxane a
CHCl3 a
a Values from Rotlevi and Treinin (1965)
γ·10-3 [cm-1]
33.4
33.2
33.0
32.8
32.6
32.4
32.2
32.0
1
2
3
4
Dipole moment solvent [Debye]

Figure 4-28

other values follow some trend as indicated by the theory. It is clear that more specific effects take place and the first to consider would be the shape in Figure 4-29 of a plot of γ_{max} vs. dielectric constant of the solvent (not solution!). It is observed a scattering around an increasing value for γ_{max} for ascending values of the dielectric constant. It means that the H bonding is enhanced by a bigger dielectric constant in the solvent media. A blue shift in nitrate solutions is due to a higher amount of H bonding present that is a consequence of a bigger dipole moment and dielectric constant in the solvent media. The low values of γ_{max} for CH_3CN and DMF as function of solvent dipole moment (Figure 4-28) could be explained by the fact that both solvents are dipolar aprotic according to Parker (1962), and cannot donate labile hydrogen to form H bond.

Spectral Studies of Nitrates in Mixed Solvents

Dioxane-water mixtures as solvent for our nitrates was used to further verify the influence of the dielectric constant on the H bonding formation and how this H bonding variation influences the shape of the spectra of nitrates solution. Since it has been stated in our solvent studies that the H bonding formation is apparently due to the dielectric constant of the media and/or its dipole moment, if this argument is correct this should hold when more than one solvent is used as well. The solvatation of the NO_3^- ion should then proceeds

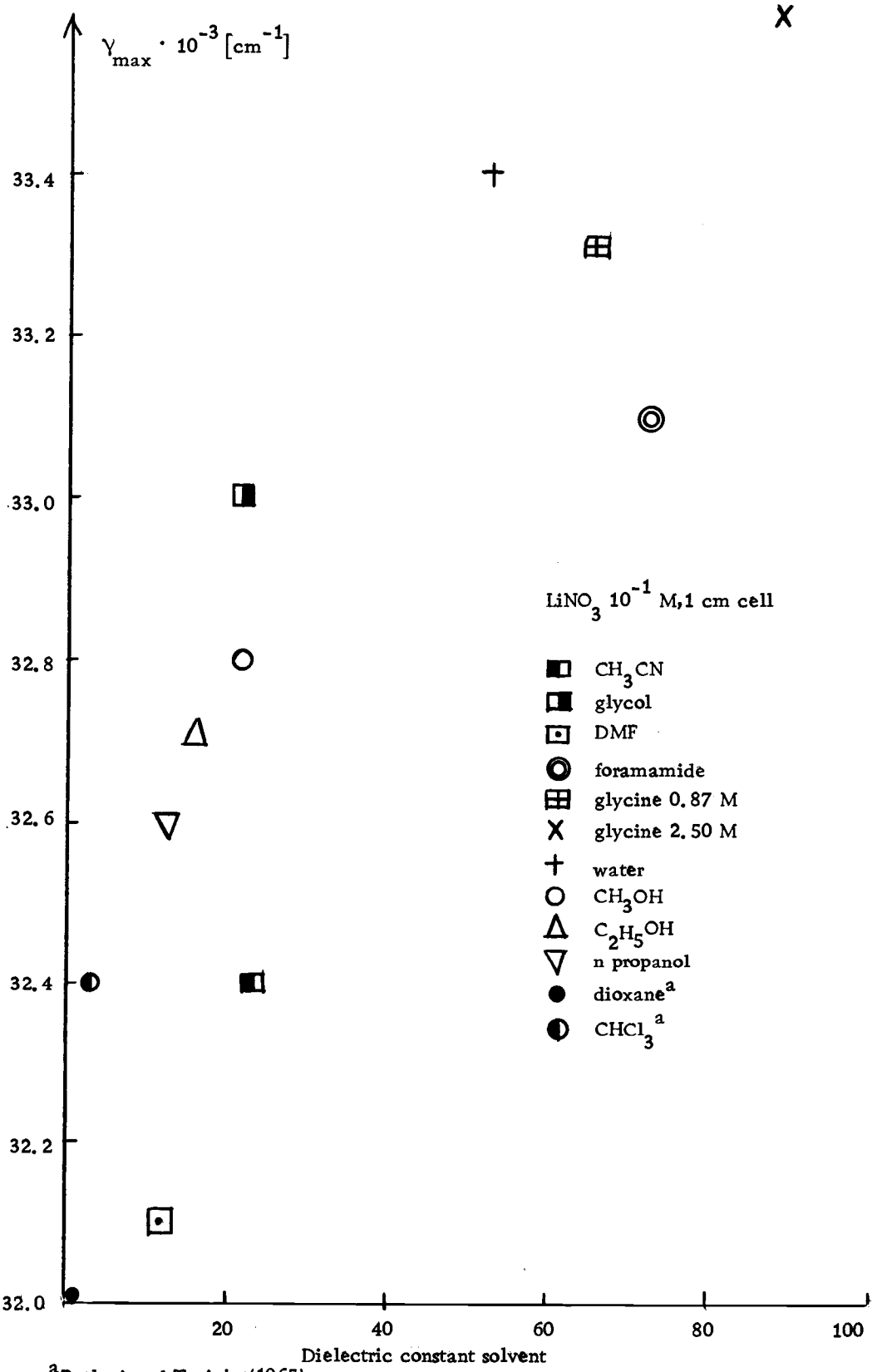

[a]Rotlevi and Treinin (1965)

Figure 4-29

through H bonding influenced by the two parameters already stated also in this three component system. Water-dioxane mixtures were selected because its dielectric constant has been determined by Fuoss (1933) as presented in Table 4-21.

Table 4-21

Dioxane wt %	Water wt %	Dielectric Constant
100	0.00	2.20
98.76	1.24	2.60
95.99	4.01	3.50
93.63	6.37	4.40
90.50	9.50	5.80
85.05	14.95	9.00
79.77	20.23	12.00
47.00	53.00	37.00
0.00	100.00	78.60

From this table is calculated the dielectric constant for mixtures in volume of dioxane and water used. Table 4-22 contains the data for the $LiNO_3$-H_2O-dioxane system. The spectra shows a shift to the red as more dioxane is present and the ε_{max} as well as f value decrease. The Figure 4-30 presents the $LiNO_3$-H_2O dioxane system.

Table 4-22

Solvent by Volume	$f \cdot 10^5$	ε_{max}	$\gamma_{o\ max}$ [cm^{-1}]	Dielectric Constant
H_2O only	14.00	7.16	33.400	78.60
H_2O 90%	13.32	6.93	33.300	77.30
H_2O 80%	12.45	6.70	33.200	57.90
H_2O 50%	11.40	6.29	33.050	33.10
H_2O 20%	11.04	6.09	32.800	10.80
H_2O 10%	10.70	5.89	32.750	5.20
Dioxane only	1.99	0.80	--	2.20

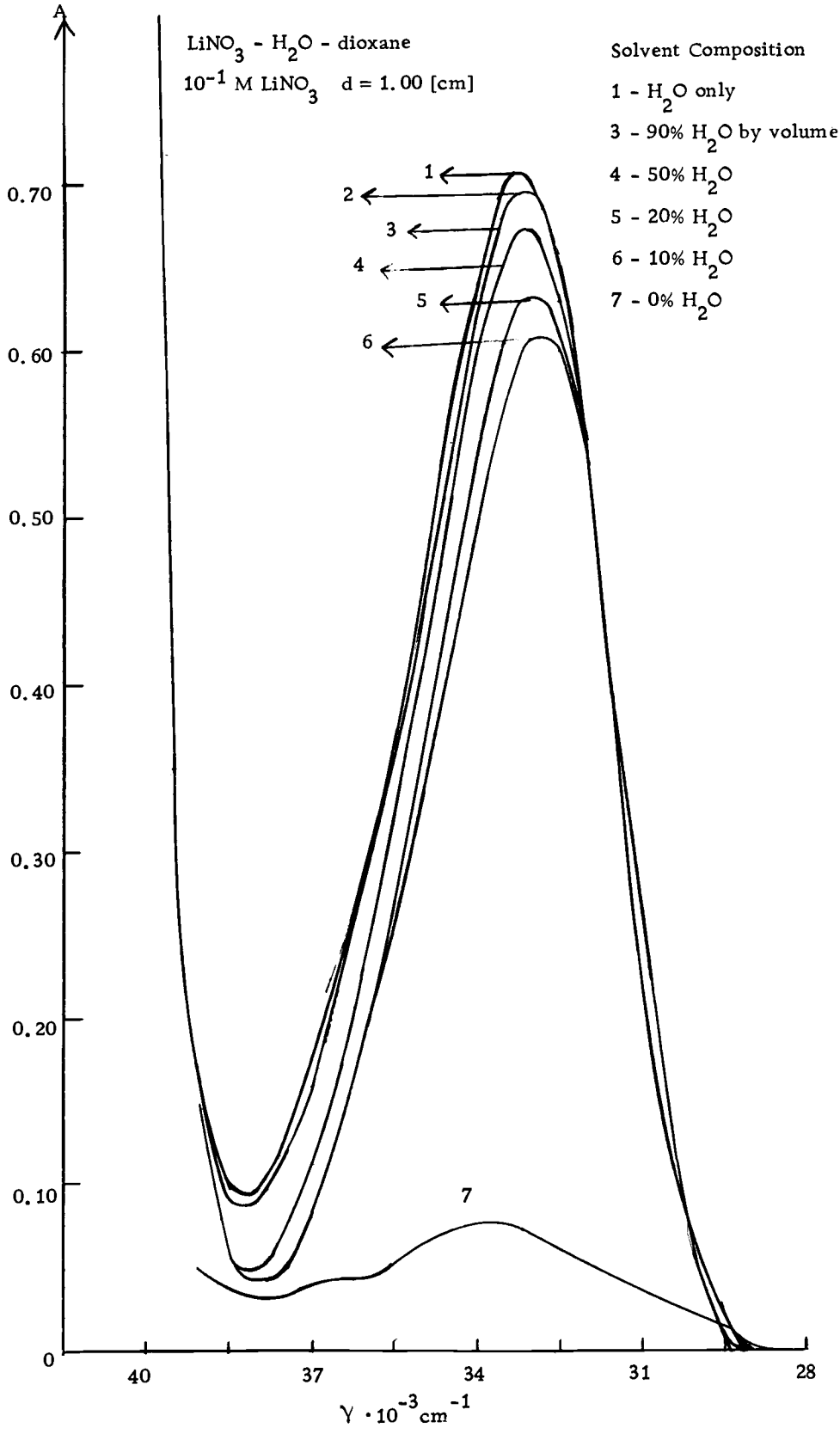
A
$LiNO_3$ - H_2O - dioxane
10^{-1} M $LiNO_3$ d = 1.00 [cm]
Solvent Composition
1 - H_2O only
3 - 90% H_2O by volume
4 - 50% H_2O
5 - 20% H_2O
6 - 10% H_2O
7 - 0% H_2O
1
2
3
4
5
6
7
0.70
0.60
0.50
0.40
0.30
0.20
0.10
0
40
37
34
31
28
$\nu \cdot 10^{-3}$ cm^{-1}

Figure 4-30

The solvatation effect of dioxane is practically non-existent in these 10^{-1} M $LiNO_3$ solutions, to which we attribute in conjunction with low dielectric constant the low ε_{max} in pure dioxane. A simple relationship was sought for dielectric constant, decrease as dioxane is more abundant in the mixture and oscillator strength or molar absorption coefficient. It was not found. It seems that the changing refractive index and viscosity play an important role here but no information was available for these parameters in water dioxane mixtures. The same trend as in the $LiNO_3$ -water-dioxane system holds in $NaNO_3$-water dioxane, KNO_3-water-dioxane and $Ca(NO_3)_2 \cdot 4H_2O$-water-dioxane mixtures.

The data for the $NaNO_3$-dioxane-water system is shown in Table 4-23.

Table 4-23

Solvent by volume	$f \cdot 10^5$	ε_{max}	γ_{max} [cm^{-1}]	Dielectric Constant
H_2O only	14.00	7.20	33.300	78.60
H_2O 90%	13.77	7.00	33.250	77.30
H_2O 80%	13.53	6.91	33.200	57.90
H_2O 50%	12.67	6.60	33.060	33.10
H_2O 20%	11.80	6.13	32.950	10.80
H_2O 10%	10.53	5.57	32.900	5.20
Dioxane only	1.22	0.07	--	2.20

The data for the KNO_3-dioxane-water system is shown in Table 4-24.

Table 4-24

Solvent by volume	$f \cdot 10^5$	ε_{max}	$\gamma_{max}[cm^{-1}]$	Dielectric Constant
H_2O only	13.99	7.08	33.250	78.60
H_2O 90%	13.61	6.80	33.150	77.30
H_2O 80%	13.33	6.65	33.100	57.90
H_2O 50%	13.08	6.38	33.000	13.10
H_2O 20%	12.43	6.00	32.850	10.80
H_2O 10%	10.73	0.08	32.750	5.20
Dioxane only	1.30	0.06	--	2.20

The data for the $Ca(NO_3)_2 \cdot 4H_2O$-dioxane-water system is shown in Table 4-25.

Table 4-25

Solvent by volume	$f \cdot 10^5$	ε_{max}	$\gamma_{max}[cm^{-1}]$	Dielectric Constant
H_2O only	14.15	7.10	33450	78.60
H_2O 90%	12.60	7.00	33420	77.30
H_2O 80%	12.17	6.95	33280	57.90
H_2O 50%	10.95	6.90	33250	13.10
H_2O 20%	8.83	6.89	33750	10.80
H_2O 10%	9.31	6.65	33900	5.20
Dioxane only	8.25	4.10	34200	2.20

The $(CH_3)_4 NNO_3$ system present the same general trend as seen for the inorganic nitrates in water dioxane mixtures. This substance is so hygroscopic that determinations only up to 10% H_2O were carried out.

Table 4-26

Solvent by volume	$f \cdot 10^5$	ε_{max}	$\gamma_{max}[cm^{-1}]$	Dielectric Constant
H_2O only	14.15	7.10	33.380	78.60
H_2O 90%	13.70	6.95	33.280	77.30
H_2O 80%	12.35	6.15	33.100	57.90
H_2O 75%	11.22	5.96	33.00	53.20
H_2O 10%	10.54	5.36	32.780	2.20

Optical opalescence occurs in solutions with 10% or less of water content in nitrate-dioxane-water systems. The $NaNO_3$-Dimethyl formamide-H_2O system shows the same trend as the H_2O-dioxane solutions already investigated. Figure 4-31 shows the KNO_3-DMF-H_2O system. The data is presented in Table 4-27.

Table 4-27

Solvent by volume	$f \cdot 10^5$	ε_{max}	$\gamma_{max}[cm^{-1}]$	Dielectric Constant
H_2O only	14.15	7.10	33300	78.60
90% H_2O	12.60	6.80	33200	not available
80% H_2O	12.17	6.70	33150	not available
50% H_2O	10.95	6.15	32900	not available
20% H_2O	9.83	5.45	32650	not available
10% H_2O	9.31	5.25	32400	not available
DMF only	8.25	4.15	32100	37.61

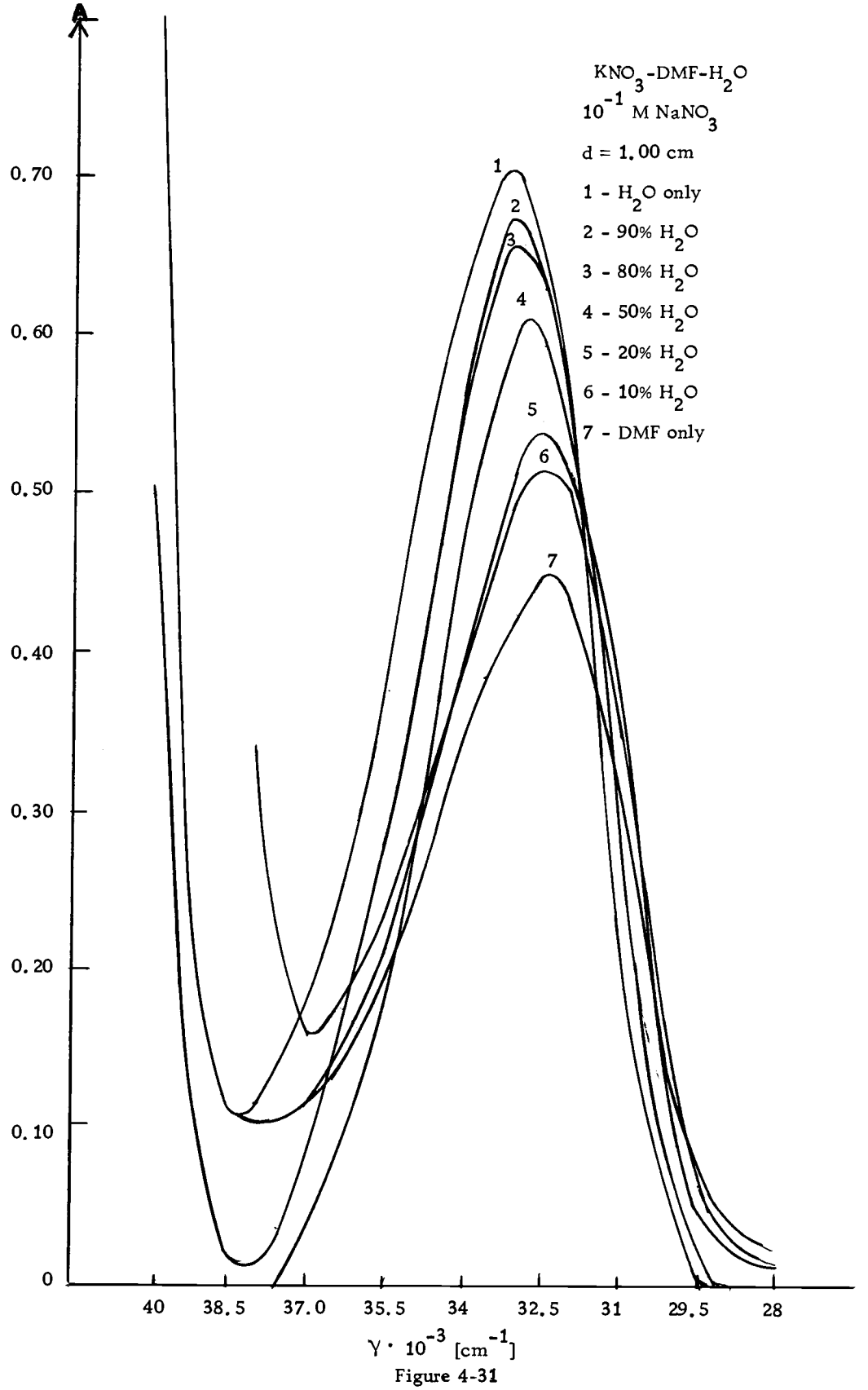
A
0.70
0.60
0.50
0.40
0.30
0.20
0.10
0
KNO3-DMF-H2O
10-1 M NaNO3
d = 1.00 cm
1 - H2O only
2 - 90% H2O
3 - 80% H2O
4 - 50% H2O
5 - 20% H2O
6 - 10% H2O
7 - DMF only
1
2
3
4
5
6
7
40
38.5
37.0
35.5
34
32.5
31
29.5
28
ν · 10-3 [cm-1]

Figure 4-31

V RADIOLYSIS OF CONCENTRATED NITRATE SOLUTIONS

Introduction

Some agreement exists for the mechanism of radiolysis in dilute solutions, but in concentrated solutions very little is known. What complicates any kinetics of concentrated solutions is that non-homogeneous scavenging kinetics takes place in such a type of solution and a more simplified treatment is only a big approximation. Values of $G(NO_2^-)$ and $G(H_2O_2)$ have been reported by Daniels and Wigg (1967) for $NaNO_3$ solutions. Values for $G(O_2)$ and $G(H_2)$ for these solutions have been reported by Mahlman (1961). These are the four products formed by γ-radiolysis in nitrate solutions. As a consequence of the work on the sodium salt the $G(NO_2^-)$ values have been explained by Daniels (1968) in Figure 5-1 showing that the overall mechanism of radiolysis in concentrated solution for $NaNO_3$ is: $NO_3^- \rightarrow NO_2^- + 1/2\ O_2$ using the electronic fraction model. This method assumes that all electrons are equally effective in energy absorption when leading to the products observed in radiolysis. Studies of the radiolysis of nitrate solutions indicated that more nitrite is produced that can reasonably be accounted for by an indirect radiolysis mechanism based on radical products of radiolized water. Increase of nitrite yield with nitrate concentration occurs in a way that suggests that a reaction of H atoms with nitrate ions is responsible for the observed H_2 and some NO_2^- yields.

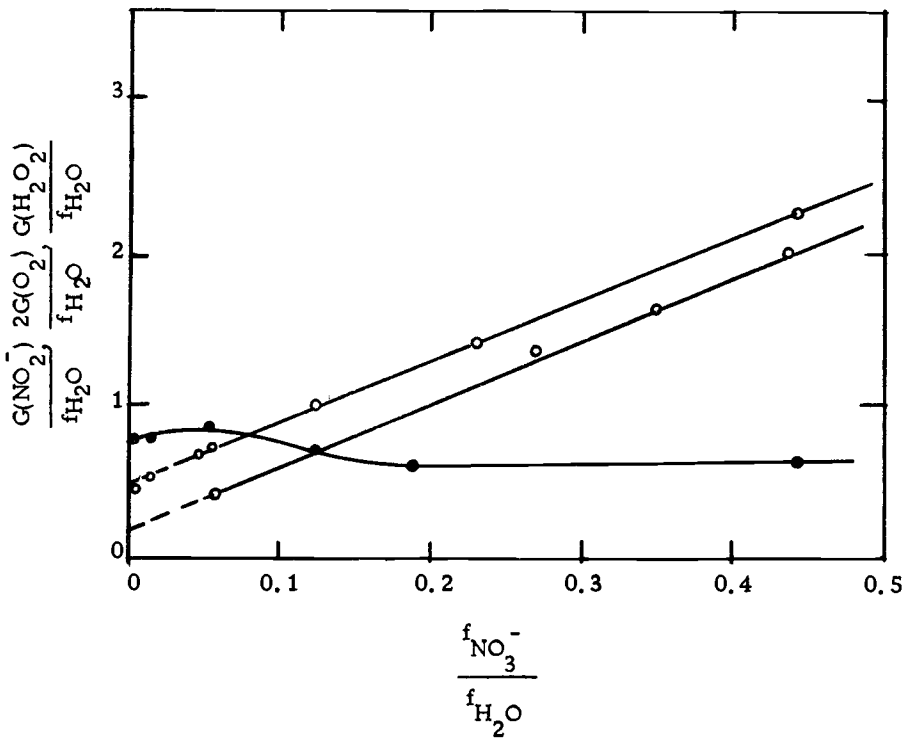

$G(NO_2^-)$, corrected for spur scavenging of H_2 by nitrate

$G(O_2)$, data of Mahlman (1961)

$G(H_2O_2)$

Figure 5-1. Dependence of $G(NO_2^-)$, $G(O_2)$, and $G(H_2O_2)$ on electron fractions

The need to work out our experimental data to postulate a mechanism for nitrate radiolysis is due to the fact that $G(H_2)$ at different nitrate concentrations has only been reported for $NaNO_3$. The irradiation yield of nitrite vs. nitrate concentration has been reported for gamma irradiation at different nitrate solutions, but it is necessary to work out our own values for two reasons. 1) Not all values of $G(NO_2^-)$ vs. nitrate concentration have been reported up to saturated solutions of Li, Ki, Cs, Ca-nitrate as higher limit of experimental observations. 2) The analytical method used by Mahlman and Schweitzer (1958) used Ce IV ion in solution during irradiation and this may induce secondary and back reactions in the system. Ce IV (H_2O) + (NO, NO_2, NO_2^-) → Ce III (H_2O) + NO_3^-. Also the Ce IV is in a 0.4 M sulphuric acid media and Ce III was calculated by difference. The introduction of this acid media complicates even more the situation.

A problem in more concentrated solutions is that the constitution of the solutions is not what we encounter there in terms of ions in a continuum solvent media. Association exists and more information for this phenomena is necessary as shown in Chapters II, III and IV. In more concentrated solutions the energy is absorbed by a two electron component system; the salt and the water. Radicals from both sources affect the system. Daniels (1966, 1969) working with neutral $NaNO_3$ solutions above concentrations of 0.5 M, assigned

a species produced by pulse radiolysis as NO_3.

Experimental Part

Dosimetry

Dosimetry on cells shown in Figure 5-2-a was carried out using the Fricke dosimeter as described by Spinks and Wood (1964), page 106. Cells used were 2.8 cm in diameter and 9 cm long, containing about 30 cm^3 of solution. In the dosimetry vessel all the secondary electrons, formed by the beam passing through the system, must have transferred their full amount of energy to the medium; this condition is satisfied if the diameter of the irradiated cell is larger than the maximum free path of the secondary electrons in the dosimeter. Weiss (1952) showed that for dosimeters based on Co^{60}-γ irradiation acting on aqueous solutions the minimum internal diameter of the glass cell should be about 8 mm. or about twice the maximum free path of secondary electrons. The cells were positioned in the lower chamber of the Co^{60} γ source as shown in Figure 5-2-b. In this way at one irradiation time four different doses have been received by the samples since the dose depends on the geometry of the cells in the radiation chamber. Position 1 is vertical and the other three are horizontal. The reaction involved in the Fricke dosimeter is the oxidation of an acid solution of ferrous sulphate to the

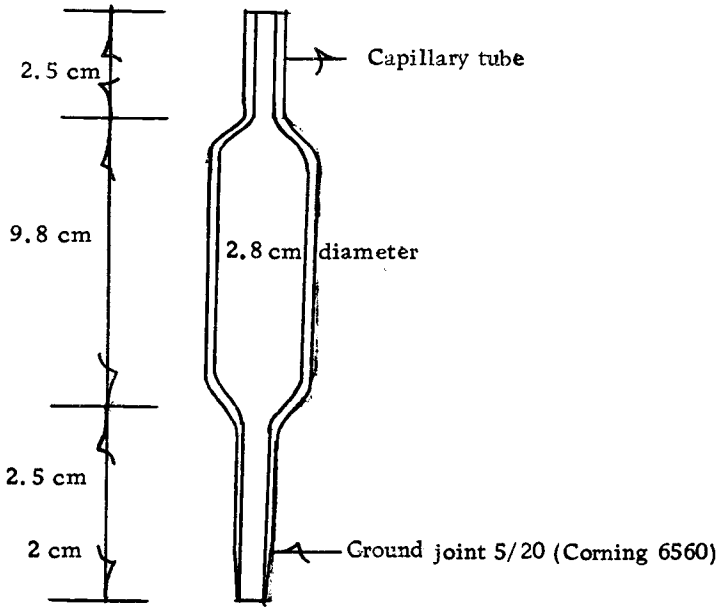

Figure 5-2a. Irradiation Cell for Co^{60} γ Source

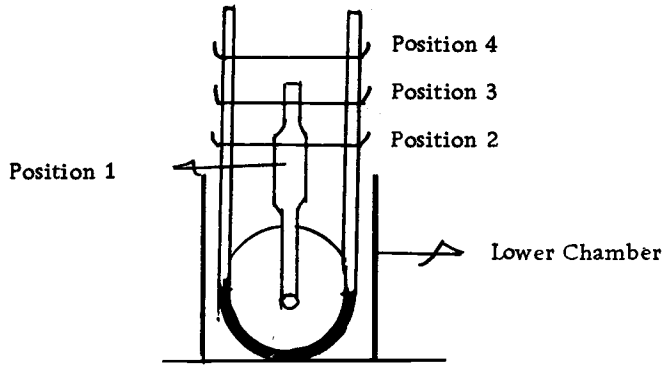

Figure 5-2b. Irradiation Positions in Co^{60} - γ Source

ferric salt, in the presence of oxygen and under the influence of radiation. $G(Fe^{+3})$ is 15.5. The amount of Fe^{+3} produced is read at 304 mμ in the Zeiss PM-Q II spectrophotometer, to determine the dose at each position. The dosimetry solution was made out of 2 g $Fe(NH_4)_2(SO_4)_2 \cdot 6(H_2O)$, 0.3 g NaCl and 110 ml H_2SO_4 98% in a 5 liter solution. The number of electrons per liter of such a solution was calculated in 3.413×10^{26}. The results of the latest dosimetry are shown in Table 5-1 and calculated from the value of the tangent over the time of irradiation in Figure 5-3. These values have been taken in 1968, 1969 and 1970 and are in agreement with a 5.26 years half life for Co^{60}. Errors in the dosimetry are generally due to a) impurities in the Co^{60} when its initially installed due to other isotopes present b) Different positioning or geometry vessels used c) cleanliness of the cells used. To clean our glassware from any grease impurity we used the muffle during five hours at 500°C.

Table 5-1

Position	Dose rate	(January 18, 1971)
1	$1.70\ 10^{20}$	[ev/lt/min]
2	$0.84\ 10^{20}$	
3	$0.48\ 10^{20}$	
4	$0.25\ 10^{20}$	

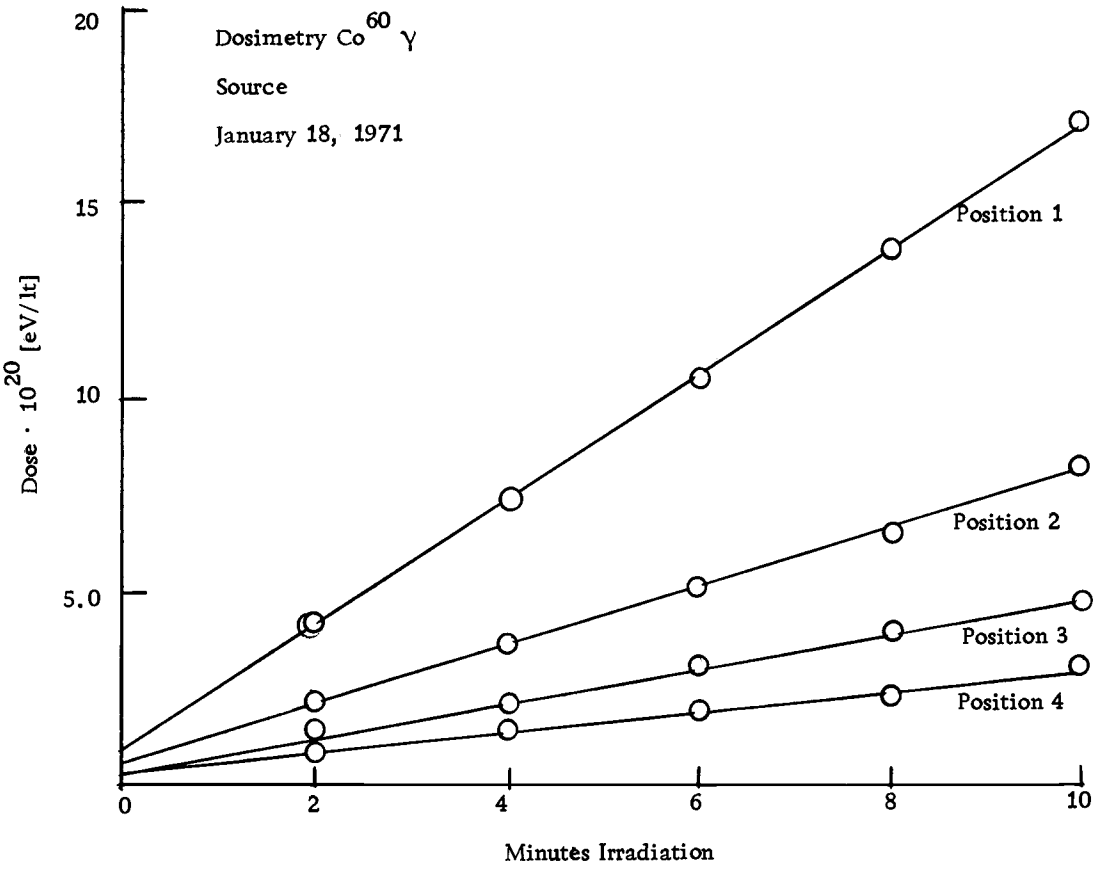
Dosimetry Co^{60} γ
Source
January 18, 1971
Position 1
Position 2
Position 3
Position 4
Dose · 10^{20} [eV/lt]
20
15
10
5.0
0
2
4
6
8
10
Minutes Irradiation

Figure 5-3

The Co^{60} γ source has to be lifted to irradiate the samples. This fact introduces a certain "in and out" dose that has to be kept constant through all the irradiations. This is attained by means of a metronome (that we set at 112 c.p.m.) when lifting or lowering the source attaining always the same final position. The in and out dose (January 18, 1971) were: a) for position 1, $0.54\ 10^{20}$ eV/lt b) for position 2, $0.33\ 10^{20}$ eV/lt c) for position 3, 0.18 eV/lt d) for position 4, 0.12 eV/lt. A correction has to be introduced for solutions with a number of electrons per liter different than the one of the Fricke dosimeter. The correction factor for electrolyte solutions is based on the assumption that all electrons in a certain microscopic volume are equally effective in energy absorption. The correction factor is given by the ratio of the electrons per liter of solution and the ones found in the Fricke dosimeter.

Determination of Nitrite Yields

The Shinn (1941) method was used to determine micromolar quantities of nitrites produced by irradiation. The reagent was made out of a) 0.5% sulfanilamide solution b) 0.1% Coupling reagent solution (N-1-Naphtyl-ethylenediamine-dihydrochloride) c) 1:1 HCl. All reagents and solutions to be irradiated were made from double distilled water to avoid organic impurities. Dust was kept out by means of oxygen in the distillation system. The double distilled water uses

$KMnO_4$ in its first stage and K_2CrO_4 in the second stage to eliminate organic material. From each sample 5 cc was poured into a 25 cc flask, adding 5 cc of sulfanilamide and 1 cc of HCl 1:1 in this order. After 5 minutes, 1 cc of coupler was added and the volume completed to 25 cc. The [μM] of NO_2^- present in solution are given by the following expression:

$$\mu M[NO_2^-] = \frac{A}{5.19 \cdot 10^4} \frac{25}{\text{aliquot sample}} \qquad (1)$$

being A the absorption of the solution in a 1.00 [cm] cell. In the analysis of nitrite no correction was allowed for the dependance of the nitrite reported on nitrate concentration. This amounts to around 4% as reported by Daniels and Wigg (1969)

Determination of Hydrogen Peroxide Yields

The $G(H_2O_2)$ values obtained in the nitrate solution are read from calibration plots like the one shown in Figure 5-4 for the yields of H_2O_2 in KNO_3 solutions. The calibration has to be done due to changes in the refractive index of the electrolyte solution that perturb the absorption. The lower limit of detection was 1.5[μM] concentration of H_2O_2. The H_2O_2 used was standardized with K_2CrO_4 using ferroin as indicator. The reaction for H_2O_2 follows the Hochanadel (1952) method. Immediately before using, equal volumes of a) 66 g. KI, 2 g NaOH, 0.2 g $(NH_4)\,Mo_7O_{24} \cdot 4H_2O$ b) 20 g

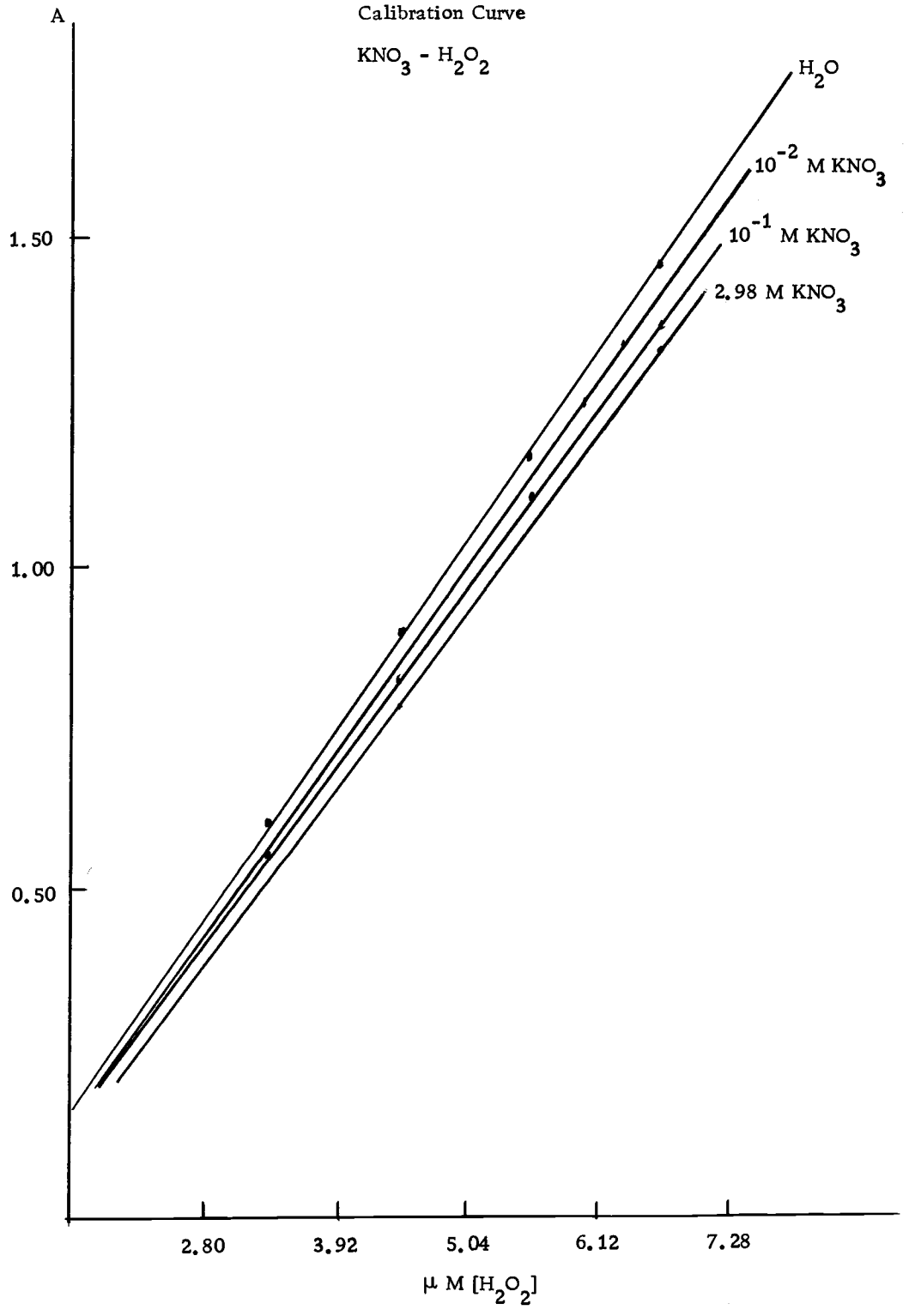
A
Calibration Curve
KNO3 - H2O2
H2O
10-2 M KNO3
10-1 M KNO3
2.98 M KNO3
1.50
1.00
0.50
2.80
3.92
5.04
6.12
7.28
μ M [H2O2]

Figure 5-4

K-biphthalate per liter were used. The absorption of the solutions is read at 350 mμ where the I_3^- formed has an ε value between 25900 and 26400. Ten centimeter cells were used since the optical densities are generally low. These values were taken in the Shimadzu spectrophotometer.

Determination of Oxygen and Hydrogen

To carry out these gas determinations where only micromoles of gas are involved we have primarily to degass the initial nitrate solutions. Cells used were shown in Figure 5-2a. A modification in the lower stem was necessary. The ground joint used here are interjoints manufactured by California Glass Co., mounted on a 1 mm capillary 3 cm long. To degass the solutions and fill the cells we use an injector device as shown in Figure 5-5. A cold trap is inserted between the injector and the oil pump to condense the impurities coming from the pump. The pump attains a vacuum of about 10^{-3} mm Hg. Running for 10 minutes this is enough to provide a degassing of 10 mμ of gas in the initial solution. Cells were filled by shaking and inversion of the injector. After radiolysis the cells are immersed in liquid nitrogen in such a way that the lower stem is frozen without touching the body since the freezing affects the union point of the stem and the body. The frozen cells are placed in a degassing bottle that is attached to the vacuum line as shown in Figure 5-6a. A

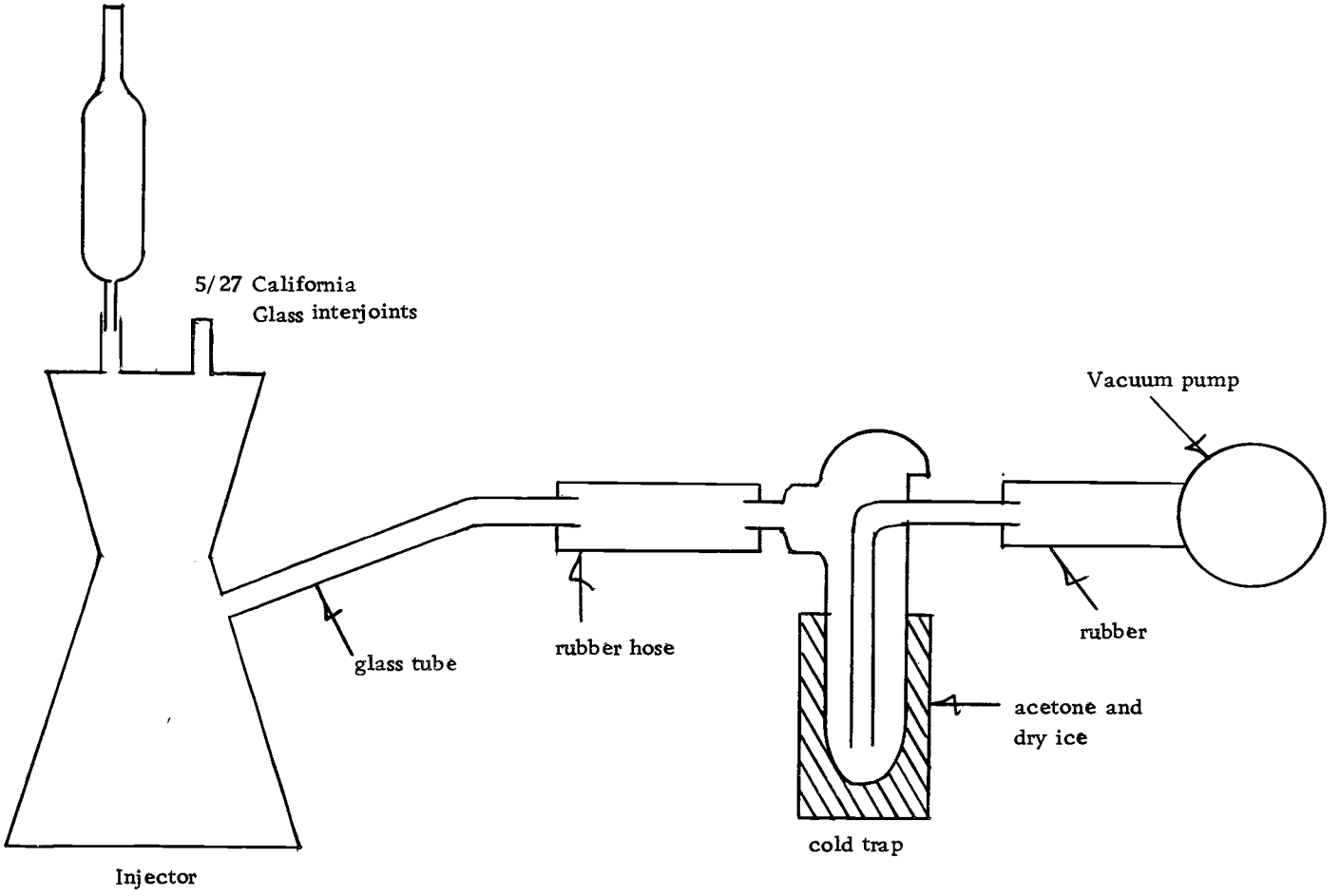

Figure 5-5. Injector Device for Degassed Solutions

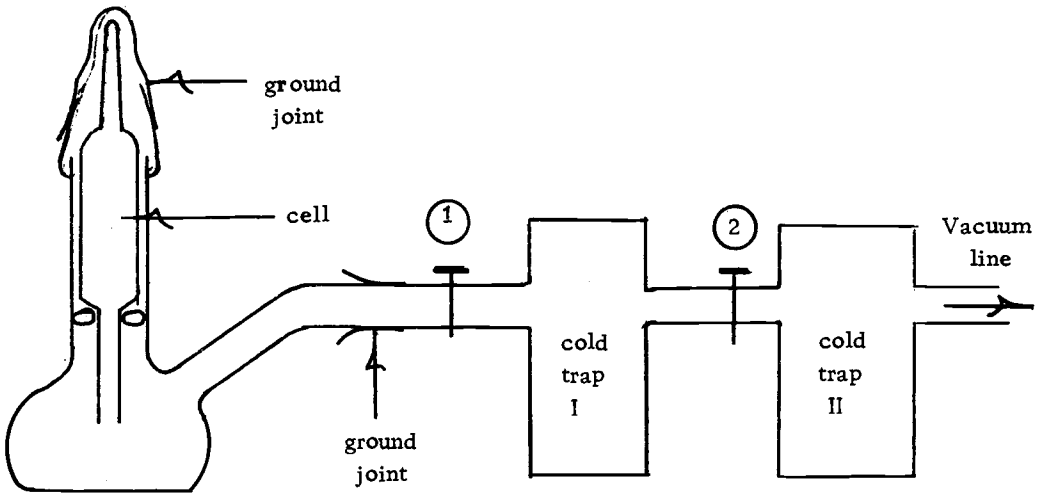

Figure 5-6a. Gas collection system in vacuum line

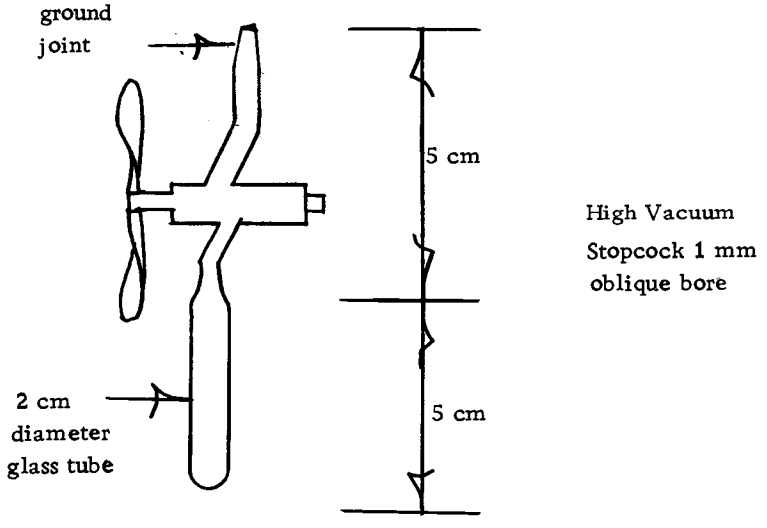

Figure 5-6b. Gas collection cell of the vacuum line

degassing of this bottle is done bypassing the mercury pump in the vacuum line. The Pirani Gauge shows about 300 micron and at this point the mercury pump is used to bring the vacuum in the system to about 20 microns. Then the high vacuum stopcock (Eck and Krebs) in Figure 5-6a, 1 mm oblique bore with vacuum cup is closed and an infrared light is used to melt the nitrogen in the stem. High vacuum Dow Corning silicone grease is used in stopcocks and joints to avoid organic contamination. The gas is then collected from the liquid by means of a Toepler pump (DS-7030) manufactured by Delmar Scientific Glass (Illinois). These pumps are used for the quantitative transfer of gases. They work with a slight excess of mercury and diminish by one half the gas left after every recycling. Usually after nine recyclings no more variation in the product PV of the gas collected is observed and about 0.1% of initial gas is not collected. By pressure difference with the mercury in the capillary, the pressure of the observed gas is measured and the volume is read in a burete calibrated at 0.01 cc intervals. This is the lower limit of our detection for gases in the line. Before starting to collect the gas, the mercury levels in the burete and capillary have to be the same to insure that no gas is initially in the line. From a 1 M $NaNO_3$ solution 0.11 cc are collected at 7.7 cm Hg, then by the relation $PV = nRT$ and putting the values for R and T

$$n = \frac{7.7\ \ 0.11}{1.88\ \ 10^{6}} = 0.45\ 10^{-6}\ [\text{moles}]$$

collected from 31 cc solution. It means $\frac{0.45\ \ 1000}{31} = 14.5\ 10^{-6}\ [\mu M]$ or 14.5 μM gas collected. The gas collected is pushed by the mercury to fill a gas cell like shown in Figure 5-6b. This gas cell is analyzed in the Picker Nuclear MS-10 mass spectrometer. Once the gas is injected in the MS-10, the ion-gauge (VC-10) is supposed to read the pressure of the gas. This ion gauge is not accurate enough for these measurements, and the total pressure will be the one given by the sum of the component gases in the mixture. In the Instruction Manual Picker Nuclear MS-10 (1967, page 44) the partial pressure of each gas is given by the expression

$$\text{Partial pressure gas} = \frac{\text{Recorder reading x Sensitivity factor machine x } 10^{-13}}{\text{Sensitivity each gas in m}\mu\text{/torr}}\ [\text{torr}] \qquad (2)$$

To get the percentage of gas in the mixture we add the partial pressures and the ratio of each individual pressure to the total will give the percentage composition of the mixture. The gases encountered in our work commonly were H_2, CH_4, (H_2O) vapor, N_2, O_2, A, CO_2 with masses 2, 16, 18, 28, 32, 40 and 44 respectively. But the sensitivities for the gases change after baking out. To determine sensitivity factors, pure H_2, CH_4, N_2, H, CO_2 and O_2 gases are injected in the machine and the reading of the ion gauge pressure

(P_2) and meter reading (I_2) are inserted in the formula

$$\text{Sensitivity gas} = \frac{I_2 - I_1}{P_2 - P_1} 10^{-11} \text{ amp/torr} \qquad (3)$$

P_1 and I_1 being the pressure and meter reading before injection to get our sensitivity value for a gas in a straight line fit. For water vapor this is not possible and a value is used of 1.18 relative to N_2 as reported in page 100 of the mass spectrometer instruction manual. To determine the sensitivity factor for the oxygen an approximation had to be used. It was observed, that when the ion gauge filament was on, the readout of the oxygen decreased by 12 to 15% as shown in the recorder reading. Since this filament provides the measurement for P_2 in the equation for the sensitivity of the gas and it had to be on to determine these sensitivities, the values of P_2 read were multiplied by a factor of 1.15. The value for the sensitivity changes after each baking. What is maintained is the ratio between them, usually taken respect to N_2. This is why no sensitivity factors are mentioned in this chapter. As an example to determine the percentage composition in a mixture usually the seven gases present were found in the following way: the recorder reading shows as in Figure 5-7, the peaks of the gases under consideration. The first gas scanned (from left to right) is H_2. We had an experimentally determined sensitivity factor of $2.93\ 10^{-5}$. The partial pressure by equation (2)

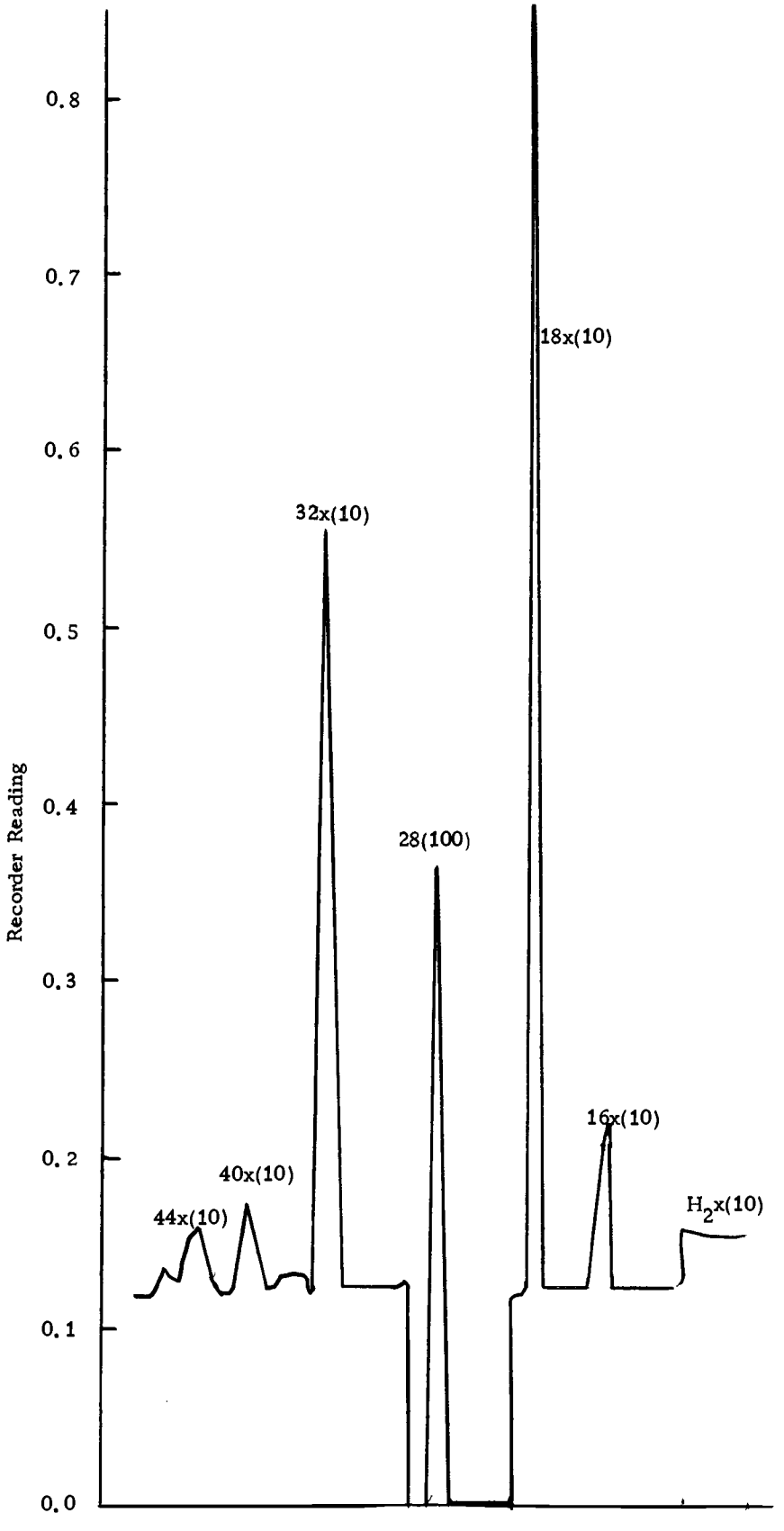

Figure 5-7. Typical Mass Spectrometric Scan. Sensitivity machine in parenthesis.

is then:

$$\text{Partial pressure of } H_2 = \frac{0.15 \times 100 \times 10^{-13}}{2.93 \quad 10^{-5}} = 5.15\ 10^{-8}\ [\text{torr}]$$

being 100 the sensitivity factor of the machine used to get the peak. The partial preserver of the seven peaks 16 (CH_4), 18(H_2O), 28(N_2), 32(O_2) 40(A), 44(CO_2) are added and the total pressure found. In this way the percentage of each gas in mixture is known, and the number of moles already measured in the vacuum line is partitioned to get the molar concentration of each gas. The precision in our mass spectrometer determinations were about 2 %. The lowest limit of detection is $5 \cdot 10^{-6}$ standard cc of gas.

Results

Experimental values for $G(NO_2^-)$, $G(H_2O_2)$, $G(O_2)$ and $G(H_2)$ are presented for solutions of $LiNO_3$, $NaNO_3$, KNO_3, $CsNO_3$ and $Ca(NO_3)_2$ in Tables 5-2, 5-3, 5-4, 5-5 and 5-6. The correction factor mentioned in these tables is the ratio of the electronic density of the solution to the one of the Fricke dosimeter. For $LiNO_3$, KNO_3, $CsNO_3$ and $Ca(NO_3)_2$ solutions the values of $G(O_2)$, $G(H_2)$, $G(NO_2^-)$ and $G(H_2O_2)$ have been worked out experimentally. For $NaNO_3$ solutions the values of $G(NO_2^-)$ were taken from Daniels and Wigg (1967), and $G(H_2)$ and $G(O_2)$ values were cited from Mahlman (1961). We have tried to reproduce the results of Mahlman, at 1 M and 5 M.

Table 5-2

Experimental Data for the Radiolysis of $LiNO_3$ Solutions

Molarity	Correction factor[a]	$G(NO_2^-)$	$G(H_2O_2)$	$G(O_2)$	$G(H_2)$
0.010	0.981		0.59		
0.011	0.973				
0.038	0.975	0.77			
0.13	0.982		0.69		
0.17	0.980	0.89			
0.38	0.984	1.07			
0.76	1.000	1.30			
0.80	1.001		0.64		
1.00	1.026	1.41		0.33(1)	0.15(1)
2.00	1.036			0.50(1)	0.088(1)
2.10	1.037		0.55		
2.90	1.074	1.56			
3.00	1.076		0.40	0.56(1)	0.048(1)
3.30	1.081		0.40		
4.60	1.117	1.63			
5.00	1.129			0.96(1)	0.045(1)
5.40	1.134		0.33		
7.00	1.183			0.70(2)	0.029(2)
7.20	1.187	1.75	0.30		
9.00	1.237		0.26	0.45(1)	0.014(1)
9.65)	1.240	1.94			
10.80	1.292			0.28(1)	0.003(1)

(1)(2) Number of experimental points

[a]Correction factor is the relative electronic density respect to the Fricke dosimeter.

Table 5-3

Experimental Data for the Radiolysis of $NaNO_3$ Solutions

M	Correction Factor	$G(NO_2^-)$[a]	$G(H_2O_2)$	$G(O_2)$[b]	$G(H_2)$[b]
0.01	0.977	0.45	0.67		0.38
0.05					
0.10	0.967	0.57	0.74		0.24
0.50	1.001		0.79		0.15
1.00	1.023	1.00	0.75	0.21	0.096
2.00		1.20		0.31	0.059
3.00	1.102	1.31	0.56	0.42	0.095
5.00	1.187	1.47	0.39	0.56	0.035
6.00		1.56		0.63	0.029
7.00				0.70	0.025
7.35	1.298		0.23		

[a] Daniels and Wigg (1967)

[b] Mahlman (1961)

Table 5-4

Experimental Data for the Radiolysis of KNO_3 Solutions

Molarity	Correction Factor	$G(NO_2^-)$	$G(H_2O_2)$	$G(O_2)$	$G(H_2)$
2.98	1.108	1.38	0.57	0.67(3)	0.030(3)
2.00	1.070	1.31	0.65	0.50(2)	0.056(2)
1.00	1.028	0.98	0.75	0.32(2)	0.13(2)
0.50	0.968	0.80		0.22(3)	0.20(2)
0.10			0.75		
0.05	0.983	0.72			
0.01	0.974		0.66		
0.01	0.979		0.62		

(2) (3) Number of experimental points

Table 5-5

Experimental Data for the Radiolysis of $CsNO_3$ Solutions

M	Correction Factor	$G(NO_2^-)$	$G(H_2O_2)$	$G(O_2)$	$G(H_2)$
10^{-3}	0.979	0.54	0.49		
10^{-2}	0.977	0.58	0.52		
10^{-1}	0.988	0.74	0.63		
0.56	1.029	0.97	0.63	1.46(1)	0.54(1)
1.12	1.114	1.21	0.67	0.64(1)	0.016(1)

(1) Number of experimental points

Table 5-6

Experimental Data for the Radiolysis of $Ca(NO_3)_2$ Solutions

Molarity	Correction Factor	$G(NO_2^-)$	$G(H_2O_2)$	$G(O_2)$	$G(H_2)$
0.001	0.981		0.59		
0.010	0.986		0.62		
0.037	0.990	0.64			
0.10	0.984		0.67		
0.29	0.983	0.88			
0.34	1.001				
0.37	1.003	0.95			
0.46	1.006				
0.60	1.022				
0.73	1.023	0.99			
1.00	1.033		0.71	0.62(2)	0.29(2)
1.61	1.053	1.28			
2.00	1.080		0.57		
3.00	1.115			1.07(2)	0.11(2)
3.40	1.143	1.53	0.48		
5.00	1.209		0.27	0.79(2)	0.014(2)
6.00	1.239	1.66			
7.00	1.293			0.62(2)	0.010(2)
8.00	1.329		0.11		
9.00	1.395			0.50(2)	0.010(2)
10.50	1.535				
11.00	1.547	1.46	0.08		
12.00	1.682			0.34(2)	0.004(2)

(2) Number of experimental points

The results at 1 M coincide well with Mahlman's work. At 5 M our value somewhat lower for oxygen was obtained namely 0.45 against 0.56 reported in the previous work. The values for $G(H_2O_2)$ of $NaNO_3$ were reported previously by Daniels and Wigg (1967). But the values reported in Table 5-3 may add to the precision of the former ones, since 10.00 cm cells were employed in these measurements. The experimental values obtained are plotted in Figures 5-8, 5-9, 5-10, 5-11, and 5-12. The emphasis is on the concentration values 10^{-1}[M] and up in these semilog plots. Values have been reported for $G(NO_2^-)$, $G(H_2O_2)$, $G(H_2)$ and $G(O_2)$ for various concentrated nitrate solutions. More work is needed for the gas yields since one or two point determinations for them were obtained and G values are usually reported with more experimental points. To study the "direct effect", data for a fractionation model is presented in Table 5-7 for $LiNO_3$ solutions. In this table $G(NO_2^-)_c$ means the values of $G(NO_2^-)$ corrected as we go up in concentration due to two reasons (assuming that all the H radical present comes only from the water) 1) In the indirect radiolysis at low concentrations of NO_3^- a process takes place $H + NO_3^- \rightarrow HNO_3^- \rightarrow NO_2^-$ so that NO_2^- will also be produced by an "indirect effect" 2) As we go up in concentration less H will be produced since less water fraction is present. The correction factor leads to an expression

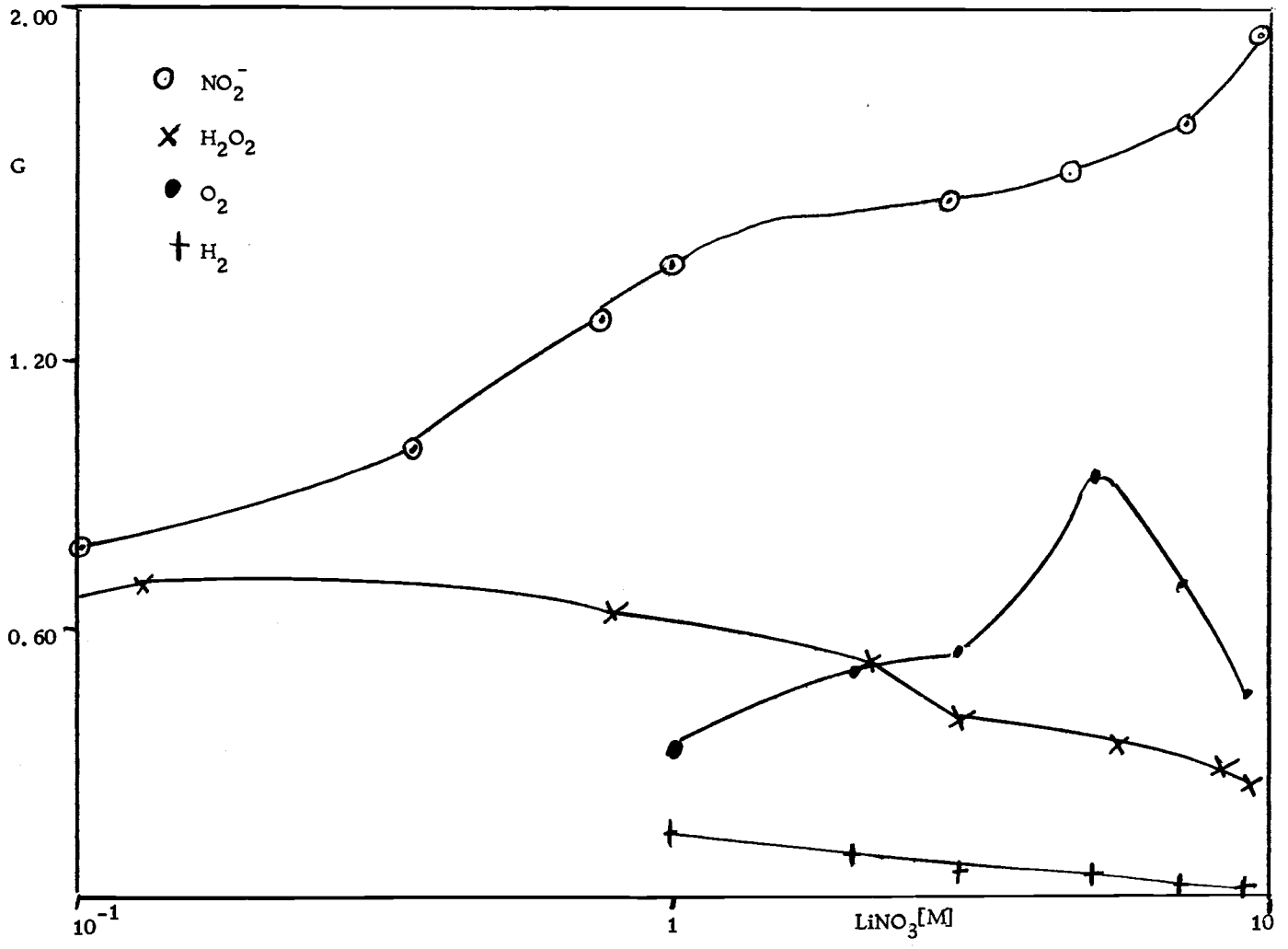

Figure 5-8

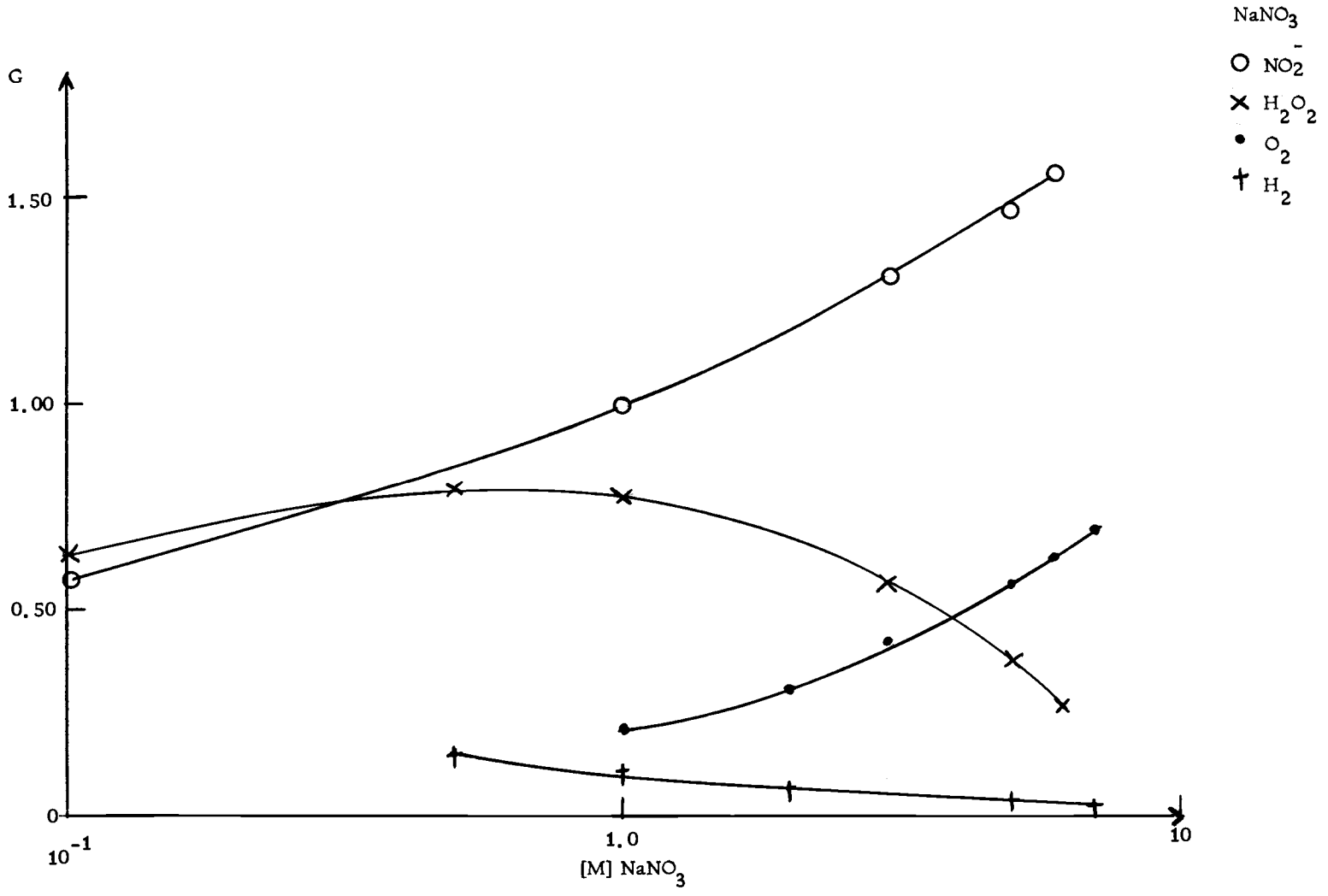

Figure 5-9

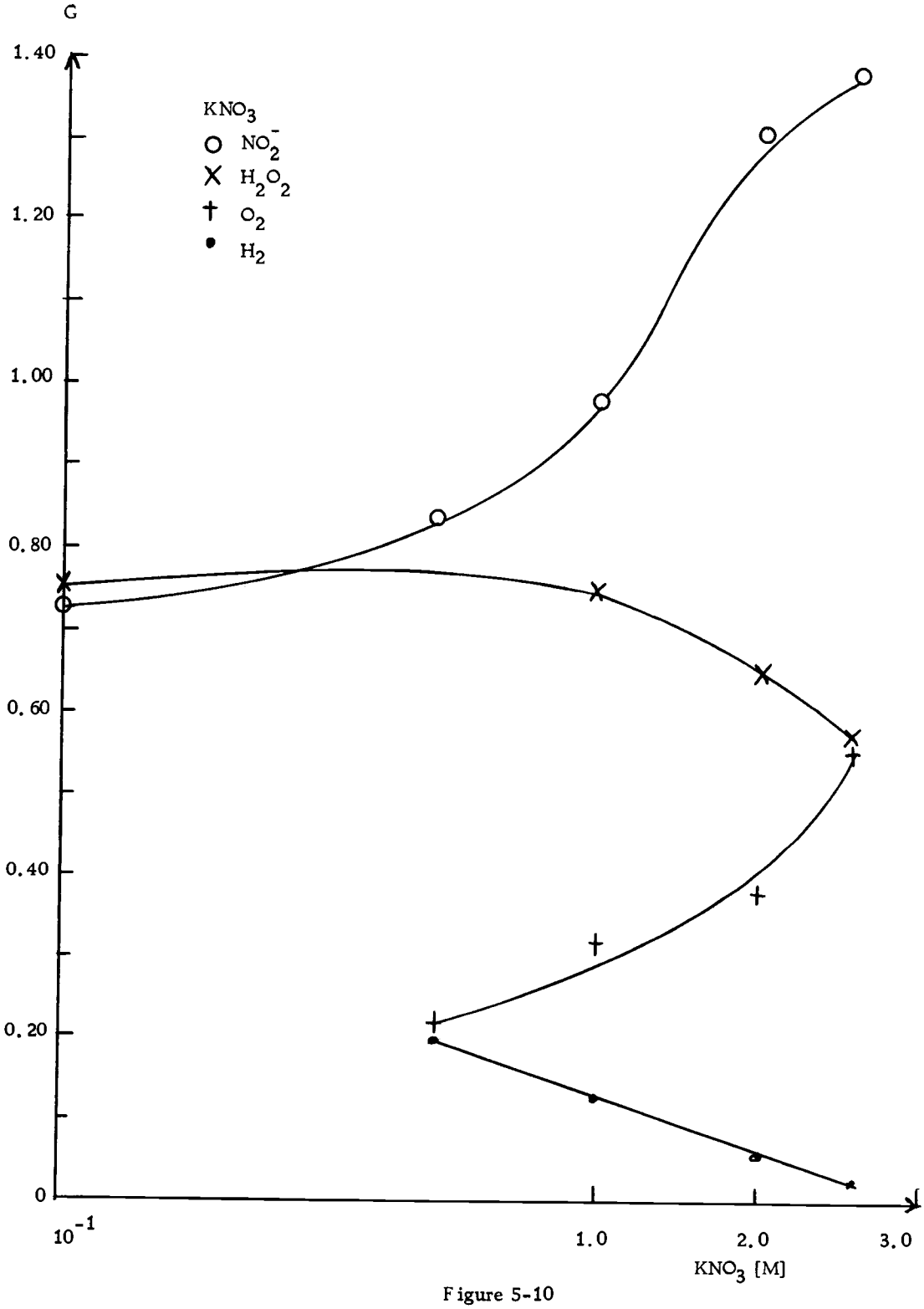
G
1.40
1.20
1.00
0.80
0.60
0.40
0.20
0
KNO3
NO2-
H2O2
O2
H2
10-1
1.0
2.0
3.0
KNO3 [M]

Figure 5-10

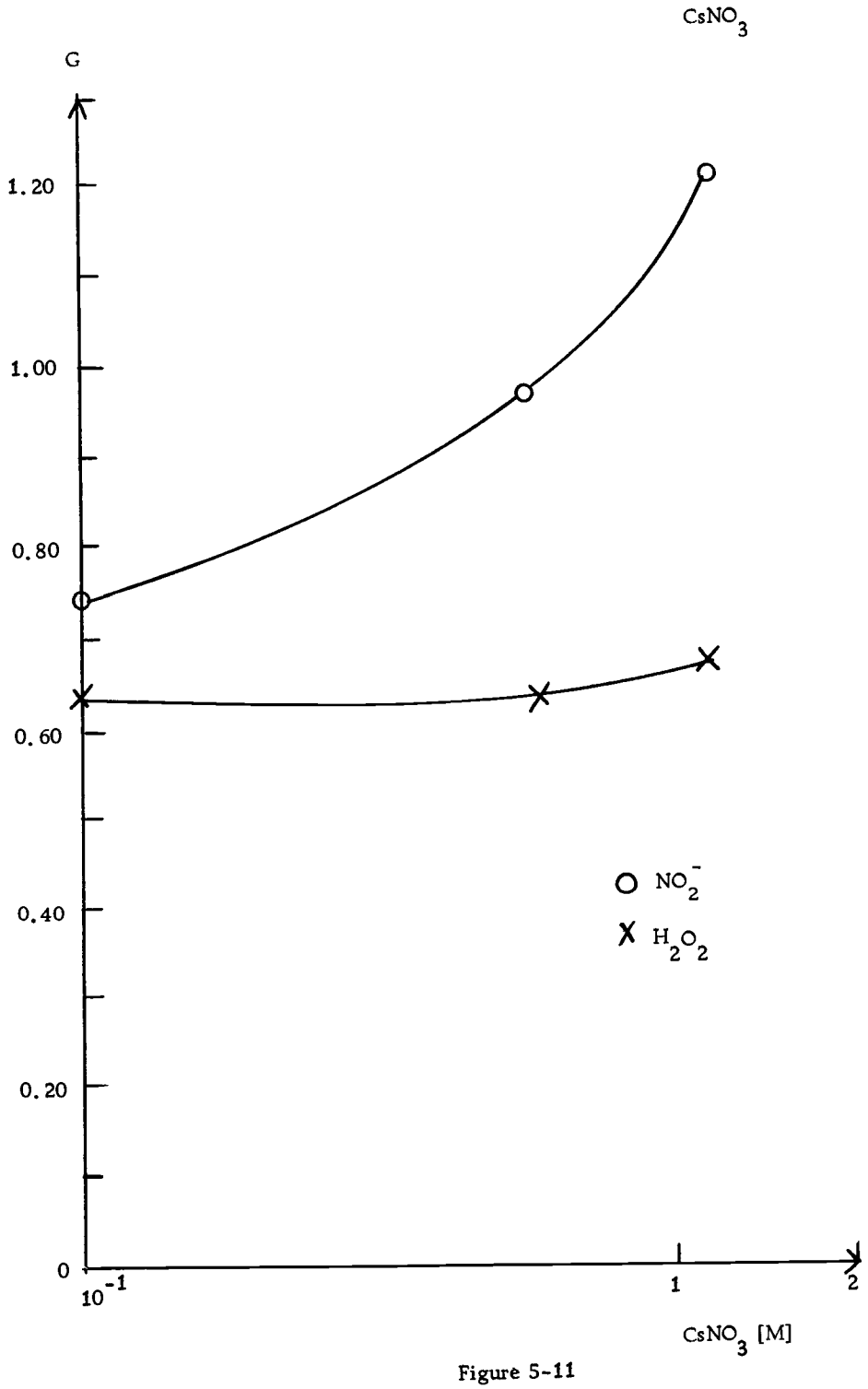

Figure 5-11

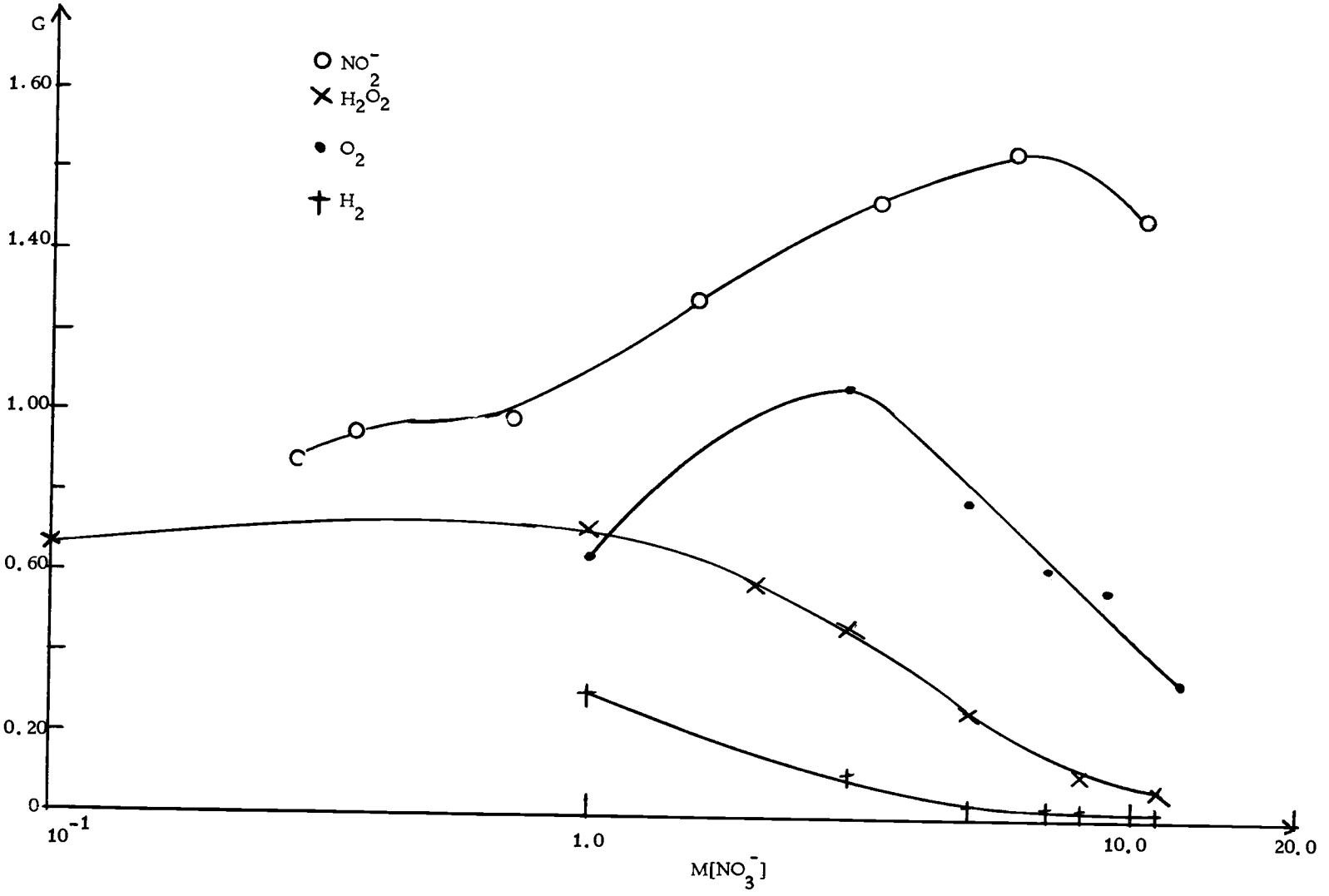

Figure 5-12

$G(NO_2^-)_c = G(NO_2^-)_{obs} - [f_{H_2O} \cdot G(H_2)^o - G(H_2)_{obs}] G(H_2)^o$ and $G(H_2)_{obs}$ being the yields of hydrogen in pure water and nitrate solutions of different concentrations respectively. A successful account by Daniels (1968) for the "direct effect" (considered as chemical transformation in a solute due to its energy absorption) with the assumption that indirect and direct effect modes of radiolysis are independent leads to the relation:

$$G(\text{Product}) = G(\text{Product})_{H_2O} \cdot f_{H_2O} + G(\text{Product})_{NO_3^-} \cdot f_{NO_3^-}$$

Dividing this equation by f_{H_2O}, a plot like Figure 5-1 for $NaNO_3$ solutions is found. The direct effect may account for the products of radiolysis like NO_2^- and O_2 at concentrations above 0.5 M. There is not so far any procedure by which electronic fractions could be calculated from theoretical principles. The correct account for the observed yields using this method is the best proof available for the electronic fractionation approach. In Tables 5-8 and 5-7 the values for an electronic fractionation approach are given for KNO_3 and $LiNO_3$ respectively. In Figures 5-13, 5-14, and 5-15 the plots for these electronic fractionation model for $LiNO_3$, KNO_3 and $Ca(NO_3)_2$ are shown.

Table 5-7

Calculated Data for the Energy Fractionation Model of $LiNO_3$ Solutions

M	$G(NO_2^-)_c$[a]	$f_{NO_3^-}$	f_{H_2O}	$\frac{f_{NO_3^-}}{f_{H_2O}}$	$\frac{G(NO_2^-)_c}{f_{H_2O}}$	$\frac{G(O_2)}{f_{H_2O}}$	$\frac{G(H_2O_2)}{f_{H_2O}}$
1.0	1.11	0.055	0.941	0.058	1.18	0.352	0.63
2.0		0.109	0.884	0.123		0.573	
2.9	1.23	0.153	0.837	0.183	1.47		
3.0		0.155	0.832	0.186		0.673	0.48
4.6	1.33	0.231	0.750	0.310	1.77		
5.0		0.261	0.740	0.353		1.297	
5.4		0.269	0.714	0.377			0.46
7.0		0.332	0.646	0.514		1.083	
7.2	1.48	0.342	0.635	0.541	2.33		
9.0		0.411	0.537	0.767		0.838	0.48
9.6	1.80	0.441	0.535	0.825	3.36		
10.8		0.473	0.498	0.94 7		0.562	

[a] $G(NO_2^-)_c$: is the corrected yield of NO_2^-.

Table 5-8

Calculated Data for the Energy Fractionation Model of KNO_3 Solutions

M	$G(NO_2^-)_c$	$f_{NO_3^-}$	f_{H_2O}	$\frac{f_{NO_3^-}}{f_{H_2O}}$	$\frac{G(NO_2^-)_c}{f_{H_2O}}$	$\frac{G(O_2)}{f_{H_2O}}$	$\frac{G(H_2O_2)}{f_{H_2O}}$
0.05		0.0029	0.992	0.0029			
0.10			0.991	0.0078			0.76
0.50	0.56	0.0292	0.984	0.0297	0.57	0.22	0.77
1.00	0.60	0.054	0.911	0.0607	0.66	0.35	0.77
2.00	0.99	0.105	0.835	0.126	1.18	0.60	0.78
2.98	1.06	0.146	0.775	0.189	1.37	0.81	0.74

Table 5-9

Calculated Data for the Energy Fractionation Model of $Ca(NO_3)_2$ Solutions

M	$G(NO_2^-)_c$	$f_{NO_3^-}$	f_{H_2O}	$\frac{f_{NO_3^-}}{f_{H_2O}}$	$\frac{G(NO_2^-)_c}{f_{H_2O}}$	$\frac{G(O_2)}{f_{H_2O}}$	$\frac{G(H_2)}{f_{H_2O}}$	$\frac{G(H_2O_2)}{f_{H_2O}}$
0.010		0.0002	0.999	0.0002				
0.037		0.0040	0.945	0.0041				
0.10		0.0056	0.993	0.0057				
0.37		0.0202	0.972	0.0208				
0.73	0.87	0.0394	0.953	0.041	1.09			
1.00		0.053	0.928	0.057		0.67	0.31	0.77
1.61	1.11	0.084	0.889	0.094	1.25			
2.00		0.101	0.866	0.117				
3.00		0.143	0.812	0.176		1.32	0.14	0.66
3.40	1.27	0.164	0.782	0.209	1.62			0.61
5.00		0.221	0.708	0.313		1.12	0.020	0.38
6.00	1.37	0.264	0.655	0.403	2.26			
7.00		0.290	0.608	0.477		1.02	0.015	
8.00		0.330	0.566	0.583				0.18
9.00		0.355	0.532	0.667		0.94	0.012	
10.50		0.377	0.504	0.748				0.16
11.00	1.34	0.391	0.485	0.808	7.76	0.70	0.010	
12.00		0.393	0.472	0.833				

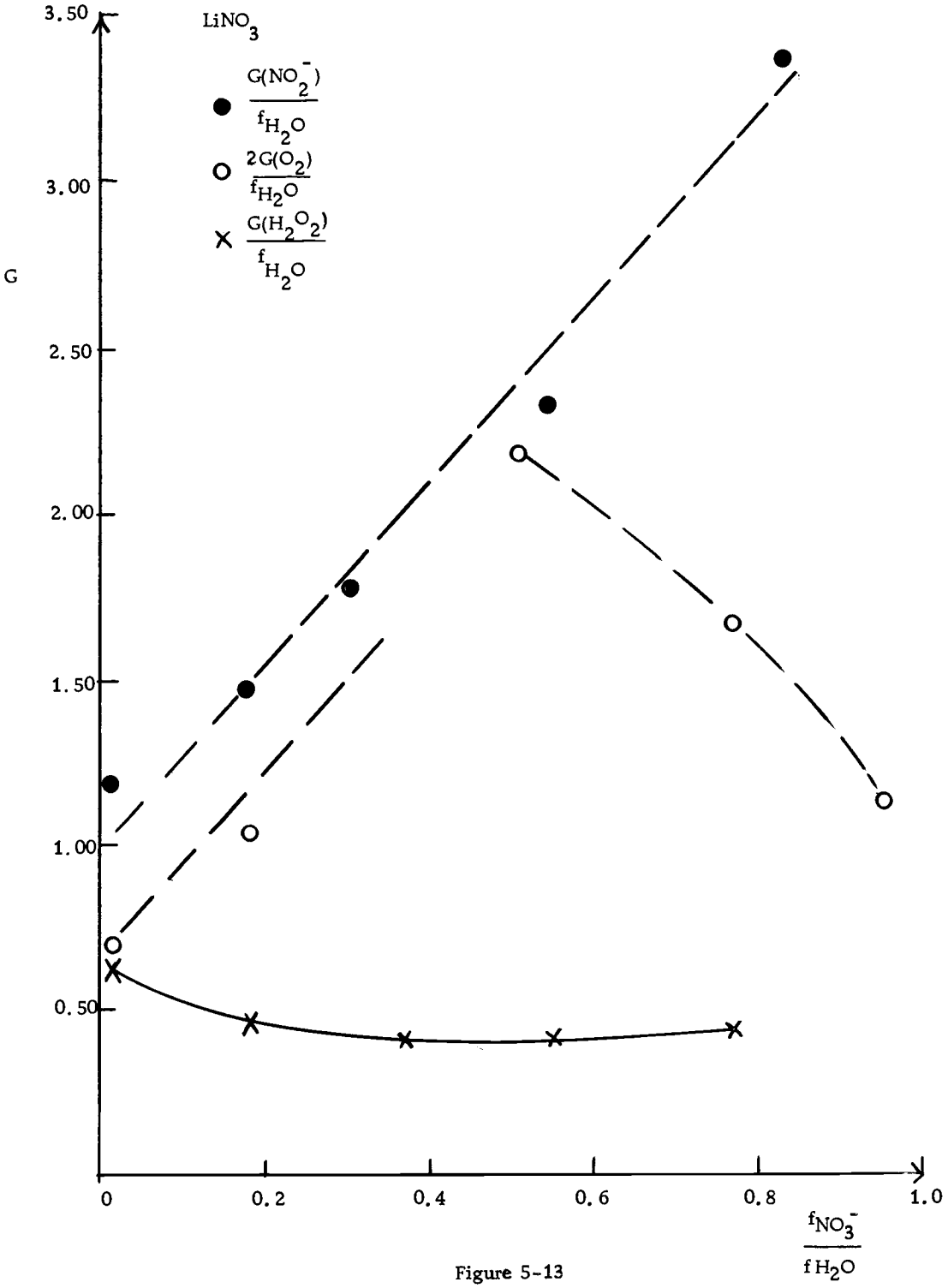
LiNO3
G(NO2-)/fH2O
2G(O2)/fH2O
G(H2O2)/fH2O
G
3.50
3.00
2.50
2.00
1.50
1.00
0.50
0
0.2
0.4
0.6
0.8
1.0
fNO3-/fH2O

Figure 5-13

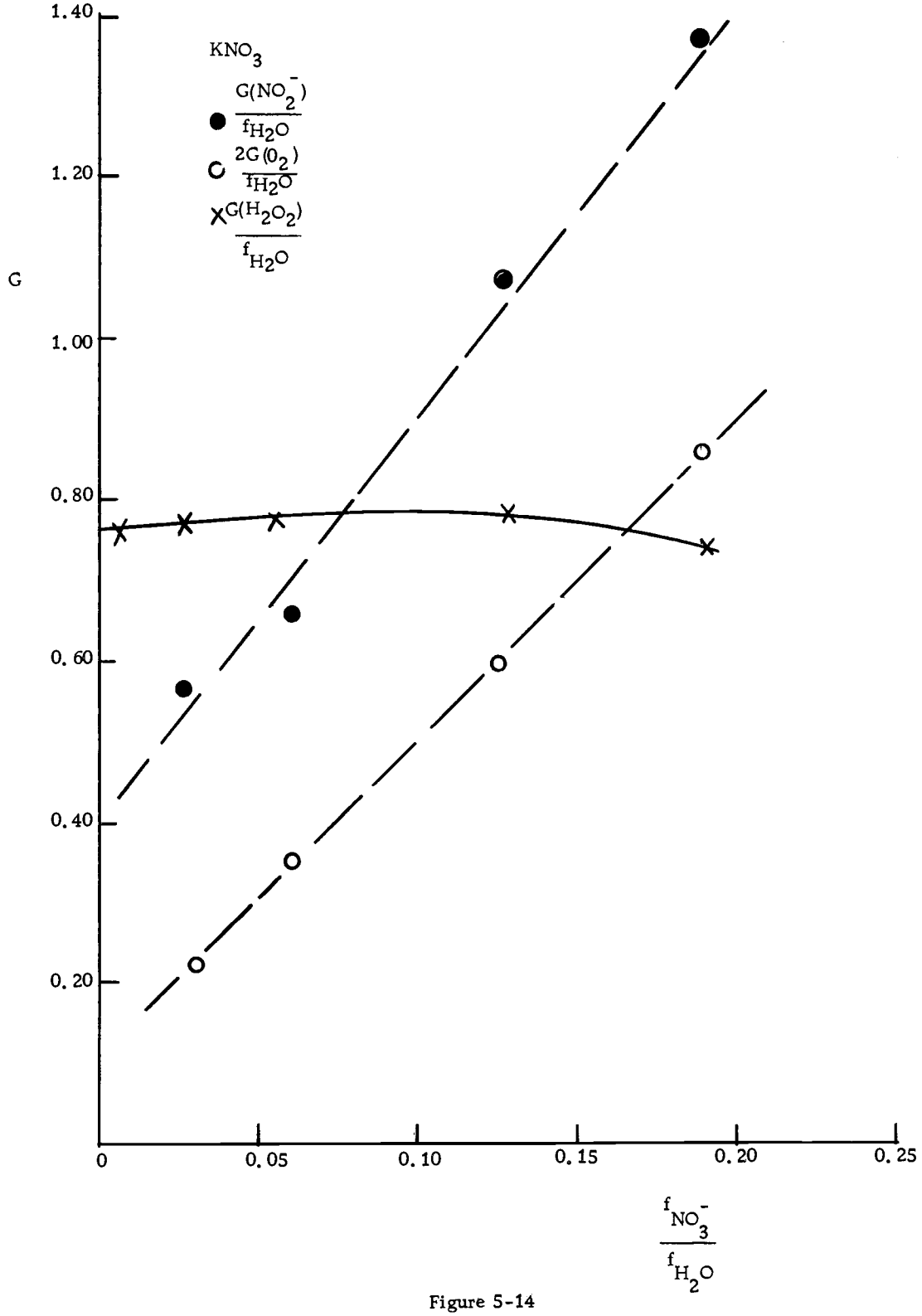
1.40
1.20
1.00
0.80
0.60
0.40
0.20
G
KNO3
G(NO2-)/fH2O
2G(O2)/fH2O
G(H2O2)/fH2O
0
0.05
0.10
0.15
0.20
0.25
fNO3-/fH2O

Figure 5-14

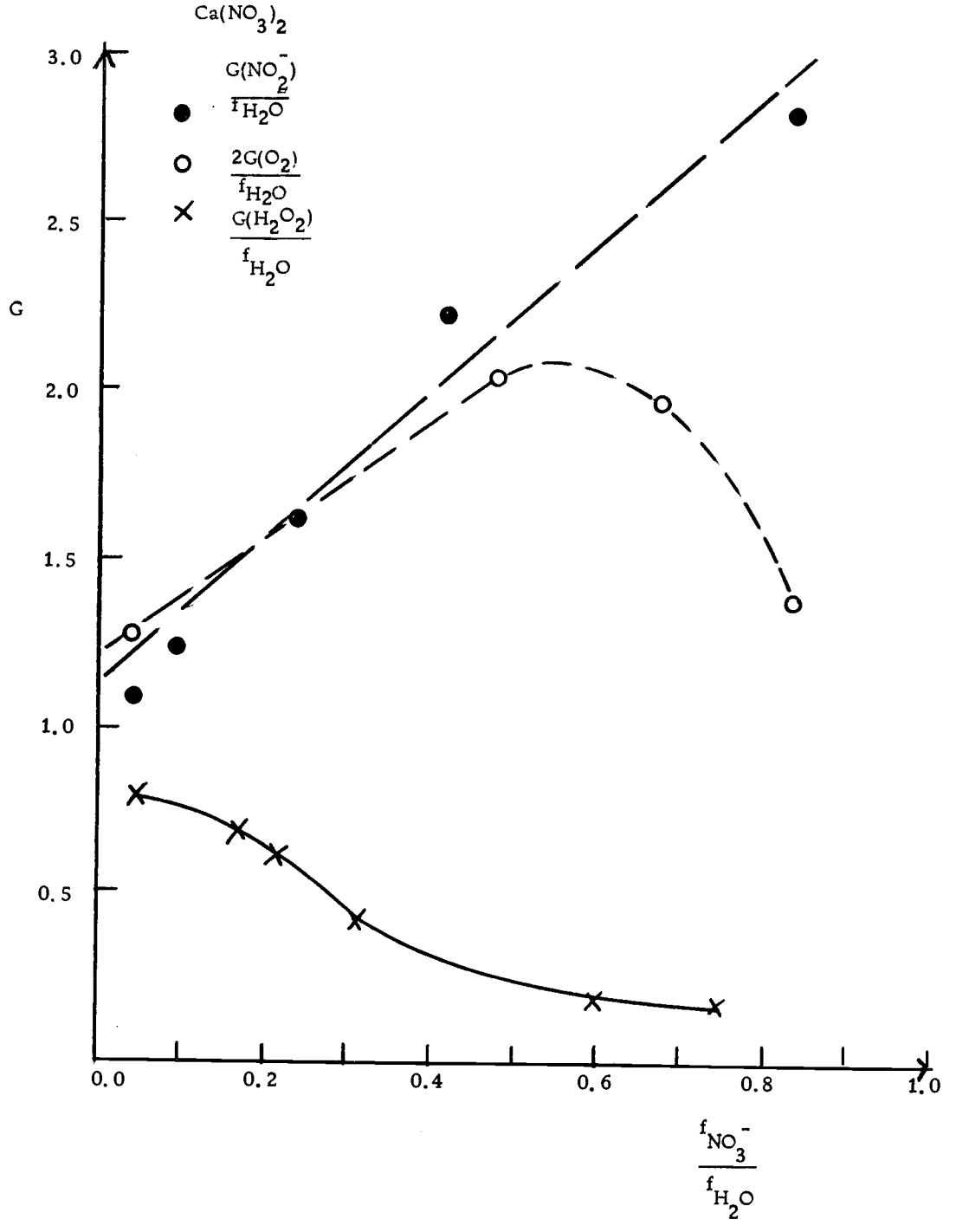
Ca(NO3)2
3.0
2.5
2.0
1.5
1.0
0.5
G
G(NO2-)/fH2O
2G(O2)/fH2O
G(H2O2)/fH2O
0.0
0.2
0.4
0.6
0.8
1.0
fNO3-/fH2O

Figure 5-15

Discussion

In Figure 5-9, the $G(NO_2^-)$ values of $NaNO_3$ increase as the concentration increases up to 7 [M] concentration. At the same time that $G(O_2)$ values also increase. The stoichiometry is $NaNO_3 \rightarrow NaNO_2 + \frac{1}{2}O_2$ and has already been shown by Daniels (1968) in the electron fraction plot of Figure 5-1. The H_2 values go down with increasing concentration in the nitrates and the scavenging is a process of the type: $H + NO_3^- \rightarrow HNO_3^- \rightarrow NO_2 + OH^-$ seems to explain the shape of these $G(H_2)$ curves. Some relation exists between the precursors of NO_2^- and H_2O_2 in $NaNO_3$, $LiNO_3$, KNO_3 and $Ca(NO_3)_2$ solutions, since generally as one goes up, the other goes down at higher concentrations of nitrate. In the $LiNO_3$ case the values of $G(NO_2^-)$ go up with concentration, but the shape after the plateau at 2 M (Figure 5-8) increases in an irregular way. Evidence for complexation of $LiNO_3$ at high concentrations has been obtained in Chapter IV and fact together with the evidence for less hydrated ions reported in Chapters II and III (for high concentrations of nitrate) may explain the shape of the curve in the limit of saturation. The diffusion of the species formed in the spurs must be different in the case of oxygen and nitrite formation of $LiNO_3$ at high concentrations. In Figure 5-8 it is seen that the $G(O_2)$ values begins to decline after 5 M, but NO_2^- values continue to increase. The viscosity, for solutions

above 8 M in $LiNO_3$ and $Ca(NO_3)_2$ cases increases sharply. This fact is particularly noticed in the $Ca(NO_3)_2$ solutions where above 7 M a decrease of the $G(NO_2^-)$ value is observed. This fact can also be tied up with the $CaNO_3^+$ species formed in calcium nitrate solutions that shows the association existing in those solutions. The oxygen seems not to be affected by this association and dehydration of ions at higher molarities in the same way that NO_2^- values do, since it begins to decrease around 3 M and a different mechanism may originate the O_2 produced. A reason for the observed low yields may be, that the precursors of oxygen are not free to diffuse in concentrated solutions. In Table 5-5, $G(O_2)$ values reported for $CsNO_3$ go down as the concentration is increased. This observation may indicate association of $CsNO_3$ at the solubility limit (1.12 M). The values for $G(O_2)$ and $G(H_2)$ are point experimental results, and more experimental evidence is needed as well as work in other molarities to account for any model to be applied. Experiments were not repeated here due to the high cost involved and will have to be delayed to a later date. In the electronic fractionation plot like Figure 5-1 the yields of O_2 and NO_2^- are separated. $G(P)_{NO_3^-}$ is the value of the slope and $G(P)_{H_2O}$ the one of the intercept in the relation $G(P) = G(P)_{NO_3^-} \cdot \frac{f_{NO_3^-}}{f_{H_2O}} + G(P)_{H_2O}$. The "direct effect" is given by the value of the slope P is (O_2 or NO_2^-) and the intercept is

a measure of the "indirect" effect due to radicals produced in water radiolysis. The comparative "indirect" and "direct" effects are shown in Table 5-10 (the values for the intercept and slope are taken from Figures 5-1, 5-13, 5-14 and 5-15).

Table 5-10

Salt	$G(O_2)_{NO_3^-}$	$G(O_2)_{H_2O}$	$G(NO_2^-)_{NO_3^-}$	$G(NO_2^-)_{H_2O}$
$LiNO_3$ [a]	1.51	0.64	2.80	0.94
$NaNO_3$ [b]	2.00	0.23	4.00	0.50
KNO_3 [a]	1.85	0.12	5.40	0.40
$Ca(NO_3)_2$ [a]	1.67	1.20	2.20	1.11

[a] This work

[b] Daniels (1968)

Note that the values for the slope are one-half of the reported in the Figures 5-1, 5-13, 14, 15 since there $\frac{2G(O_2)}{fH_2O}$ is on the vertical axis for oxygen. The initial portion up to 5 M reveals that the value of the stoichiometry in $LiNO_3$ is the same as the one reported by Daniels (1968) for the direct effect in $NaNO_3$. Then the decomposition proceeds $LiNO_3 \rightarrow LiNO_2 + \frac{1}{2}O_2$. For the $G(O_2)$ parameters of $Ca(NO_3)_2$, only the initial portion of the curve was taken. Values of $G(O_2)$ at 3 and 5 M $LiNO_3$ have not been presented in Figure 5-13. The same has been done with 3 and 5 M $Ca(NO_3)_2$ values. The values were so big that they had to be rejected if this model was to be applied

to the other values. Initial evidence has been presented here that different cations modify the yields of radiolysis interpreted by an electronic fractionation model. The role of the cation has yet to be studied in nitrate radiolysis. The results for the $G(H_2O_2)$ values of different nitrates are summarized in Table 5-11.

Table 5-11

Salt	$G(H_2O_2)$ 10^{-2} M	$G(H_2O_2)^a$ maximum	$G(H_2O_2)^b$ minimum	$\frac{G(H_2O_2)}{f_{H_2O}}$ lower concentration	$\frac{G(H_2O_2)}{f_{H_2O}}$ high concentration	Δ^c
$LiNO_3$	0.59	0.70(0.1)	0.26(9)	0.63	0.48	0.15
$NaNO_3$	0.67	0.80(0.7)	0.23(7.3)	0.85	0.60	0.15
KNO_3	0.66	0.75(0.5)	0.57(3)	0.78	0.76	0.02
$CsNO_3$	0.52					
$Ca(NO_3)_2$	0.62	0.73(0.8	0.08(11)	0.77	0.18	0.59

[a] In parenthesis is molarity of NO_3^- at this $G(H_2O_2)$ value

[b] In parenthesis is molarity of NO_3^- at this $G(H_2O_2)$ value

[c] $\frac{G(H_2O_2)}{f_{H_2O}}$ (low concentration-high concentration of NO_3^-)

$G(H_2O_2)$ for water has a value of 0.75. The values at low concentration (even 10^{-3} M) are lower than 0.75. No explanation is known for this fact. At low concentrations the main process of H_2O_2 formation is $OH + OH \rightarrow H_2O_2$. As we increase concentration (around 0.5 M) NO_3^- seems to scavenge the H radical. The reaction H + OH does not take place and the OH undergoes recombination increasing the values of $G(H_2O_2)$. As we go to higher concentrations, $G(H_2O_2)$ has lower

values. A "direct effect" for the formation of H_2O_2 seems to be responsible for the H_2O_2 observed. Therefore the value of $\frac{GH_2O_2}{f_{H_2O}}$ at low concentrations, would be a sort of "indirect effect" with a mechanism close to the one observed in pure water for H_2O_2 formation. The difference between indirect and direct effect (Δ) is not the same for the different nitrates. These observations lead to the consideration of the nature of the mechanism for H_2O_2 scavenging by the radicals produced. This is not known at the present time.

BIBLIOGRAPHY

Anbar, A. and D. Meyerstein. 1968. Isotopically substituted water in the investigation of the primary radiolytic processes. In: Radiation Chemistry of aqueous Systems ed. by G. Stein. Jerusalem. Weizmann Science Press. 241 p.

Atkinson, G. and S. Petrucci. 1970. Ion association of magnesium sulfate in water. Journal of Physical Chemistry 70:3122-3128.

Bockris, J. 1949. Ionic solvation. Quarterly Reviews. London. 3:173-180.

Bockris, J. 1964. Modern aspects of electrochemistry. New York. Academic Press. 394 p.

Cabrera, B. und H. Fahlenbrach. 1933. Diamagnetismus von Wasser bei verschiedenen Temperaturen I. Zeitschrift für Physik 82: 753-764.

Chapman, T. and J. Newman. A compilation of selected thermodynamic and transport properties of binary electrolites in aqueous solutions. University of California Press. UCRL 7767. 257 p.

Conway, E. and J. O'M Bockris. 1954. Modern aspects of electrochemistry. London. Butterworths and Co. 351 p.

Cotton, A. and G. Wilkinson. 1966. Advanced inorganic chemistry. New York. Interscience Publishers. 1135 p.

Creeckmore, R. and C. Reilley. 1969. Nuclear magnetic resonance determination of hydration numbers of electrolytes in concentrated aqueous solutions. Journal of Physical Chemistry 73: 1563-1568.

Cunningham, J. 1962. Radiation chemistry of ionic solids. II. Journal of Physical Chemistry 66: 779-787.

Daniels, M. 1963. Radiation Chemistry of the aqueous Nitrate System. III. Journal of Physical Chemistry 73:3710-3717.

Daniels, M. 1966. Pulse radiolysis of the aqueous nitrate system. Formation of NO_3 in concentrated solutions and the mechanism of "Direct Action". Journal of Physical Chemistry 70:3022-3024.

Daniels, M. 1968. Radiolysis and photolysis of the aqueous nitrate system. In: Radiation Chemistry. I. ed. by F. Gould. Washington, D. C. American Chemical Society. Advances in Chemistry Series 81. 396 p.

Daniels, M. and E. Wigg. 1967. Radiation Chemistry of the aqueous nitrate system. I. γ-radiolysis of dilute solutions. Journal of Physical Chemistry 71:1024-1033.

Daniels, M., R. Meyers and E. Belardo. 1967. Photochemistry of the aqueous nitrate system. I. Excitation in the 300-mμ band. Journal of Physical Chemistry. 72:389-399.

Darmois, E. 1928. Effet des sels neutres sur la puvoir rotatoire de l'acide tartrique et des tartrates, Annales de Physique 10: 70-115.

Davies, C. 1927. The extent of dissociation of salts in water. Transactions of the Faraday Society. 23:351-356.

Davies, C., W. Banks, and E. Righellato. 1931. The extent of dissociation of salts in water. III. Transactions of the Faraday Society 27:621-627.

Douglass, D. and A. Fratiello. 1963. Volume magnetic susceptibility measurements by N.M.R. Journal of Chemical Physicis 39:3161-3162.

Drago, R., R. Carlson, N. Rose, and D. Wenz. 1961. Thermodynamic data for the Dinoethylacetamide-iodine system, Journal of the American Chemical Society 83:3572-3575.

Dyer, R. 1965. Nuclear magnetic resonance spectroscopy, New York, Prentice Hall, 147 p.

Eisenberg, D. and W. Kauzmann. 1969. The structure and properties of water. Oxford University Press. London. 296 p.

Fabricand, B. and S. Goldberg. 1961. Proton resonance shifts in alkali halide solutions. Journal of Chemical Physics 34:1624-1628.

Fajans, K. 1928. Die eigenschaften salzartiger verbindungen und atombau. Zeitschrift fur Kristallographie 66:321-353.

Frank, H. 1963. Single ion activities and ion solvent interactions in dilute aqueous solutions, Journal of Physical Chemistry 67: 1554-1558.

Frank, H. and S. Wen. 1957. Ion solvent interaction. III. Discussions of the Faraday Society 24:133-140.

Franks, F. 1969. Effects of solutes on the hydrogen bonding in water. In: Hydrogen - Bonded Solvent Systems. ed. by Covington, A. and P. Jones. London. Taylor and Francis Ltd. 295 p.

Franks, F. and D. Ives. 1966. The structural properties of alcohol-water mixtures, Quarterly Reviews, London, 20:1-44.

Fraser, R. and Suzuki. Resolution of overlapping bands: Functions for simulating band shapes. Analytical Chemistry 41:37-40.

Frei, K. and H. Bernstein. 1962. Method for determining magnetic susceptibilities by N.M.R. Journal of Chemical Physics 37: 1891-1892.

Fuoss, M. 1969. Conductance of electrolytes. Petroleum Research Bulletin 15:72.

Fuoss, M. and C. Krauss. 1933. Properties of electrolytic solutions. I. Conductance as influenced by the dielectric constant of the solvent medium. Journal of the American Chemical Society 55:21-36.

Glew, D., H Mak and N. Rath. Aqueous non electrolyte solutions. Part VII. In: Hydrogen- Bonded Solvent Systems. ed. by Covington, A. and P. Jones. London. Taylor and Francis. 295 p.

Glueckauf, E. 1955. The influence of ionic hydration on activity coefficients in concentrated solutions. Faraday Society Transactions. 51:1235-1244.

Gmelin. 1966. Handbuch der anorganischen chemie. Heinheim. Verlag Chemie. G.M.B.H. Volume 21. p. 1363.

Goto, S. 1964. Studies of the hydration and the structure of the water and their roles in protein structure I. Chemical Society of Japan Bulletin. 37:1685-1689.

Griffiths, T. M. Symons. 1960. Ionic interactions in solutions of electrolytes as studied by ultraviolet spectroscopy. Molecular Physicis 3:90-102.

Halban, V. H. and J. Eisenbrand. 1928. Zur kenntniss des Zustandes Stärker elektrolite in konzentrierter lösung. Zeitschrift für Physikalische Chemie A. 132:401-432:433-455.

Halban, V. H. 1928. Die lichtabsorption der starken elktrolyte. Zeitschrift für Elektrochemie 34:489-497.

Halliday, J. R. Richards, and R. Sharp. 1969. Chemical shifts in nuclear resonances of caesium ions in solutions. Proceedings of the Royal Society of London 313:45-66.

Hammer, W. 1959. The structure of electrolytic solutions. New York. John Wiley and Sons. 495 p.

Harned, S. and B. Owens. 1958. Physical Chemistry of electrolytic ionic solutions. New York. Reinhold Publishing Co. 809 p.

Harris, F. and O'Konski, T. 1957. Dielectric properties of aqueous ionic solutions at microwave frequencies. Journal of Physical Chemistry. 61:310-319.

Hart, W. 1957. Analytic Geometry and Calculus. Boston, Heath and Co. 716 p.

Hester, R. and R. Plane. 1964. A Raman spectrophotometric comparison of interionic association in aqueous solutions of metal nitrates, sulfates and perchlorates. Inorganic Chemistry 3:769-770.

Hester, R. and R. Plane. 1964. Raman spectrophotometric study of complex formation in aqueous solutions of calcium nitrate. Journal of Chemical Physics 40:411-414.

Hertz, G. Professor. 1970. Institut für Physikaliche Chemie. Universitaet Karlsruhe. Personal Communication. Karlsruhe. Germany.

Hertz, G. and M. Zeidler. 1964. Kernmagnetische Relaxions zeitmessungen zur frage der hydration unpolaren gruppen in wässriger lösung. Zeitschrift der Bunsengesellschaft für Physikalische Chemie. 68:829-837.

Herzberg, G. 1945. Infrared and Raman spectra of polyatomic molecules. New York. Van Nostrand 612 p.

Hindman, J. 1962. Nuclear magnetic resonance effects in aqueous solutions of 1-1 electrolytes. Journal of Chemical Phisicis 36: 1000-1015.

Hindman, J. 1966. Proton resonance shift of water in the gas and liquid states. Journal of Chemical Physicis. 44:4582-4592.

Hochanadel, J. 1952. Effects of Cobalt γ-radiation on water and aqueous solutions. Journal of Physical Chemistry. 56:587-594.

Inglefield, P. 1971. Assistant Professor, Clark University, Department of Chemistry. Personal Communication. Worcester, Massachusetts.

Irish, D. and G. Walrafen. 1966. Raman and infrared studies of aqueous calcium nitrate solutions. Journal of Chemical Physics 46:378-384.

Irish, D., Davis, and R. Plane. 1969. Types of interaction in some aqueous metal nitrate systems. Journal of Chemical Physics 50:2262-2263.

Job, P. 1928. Recherches sur la formation de complexes mineraux en solution, et sur leur stabilite, Annales de Chimie 9:8-103.

Jørgensen, K. 1954. Studies of absorption spectra. Acta Chemica Scandinava 8:1495-1501.

Journet, G. and J. Vadon. 1955. Mise au point. Societe' Chimique de France. 5:593-607.

Kabakchi, A. 1958. Radiolysis of nitrate solutions. In: Proceedings of the First all Union Conference on Radiation Chemistry. Moscow. 175 p.

Kangro, W. 1962. Konzentrierter wässrige losungen. II. Zeitschrift für Physikaliche Chemie Neue Folge 32:273-295.

Kappusami, J. and S. Suryanarayana. 1968. Dependance of viscosity and conductance of aqueous ammonium nitrate solution on the internal pressure. Indian Journal of Pure and Applied Physics. 7:532-534.

Klemm, W. 1941. Uber Ionendimagnetismus II. Zeitschrift für Anorganische und Allgemeine Chemie 264:347-362.

Klotz, I. 1965. Role of water structure in macromolecules. Federation Proceedings. American Societies of Experimental Biology. 24:S24-S33.

Kolthoff, I., D. Stosesoca, and T. Lee. 1953. Acid strength of iodine monochloride, antimony trichloride and picric acid with reference to the bases pyridine and aniline in nitrobenzene, Journal of the American Chemical Society 75:1834-1839.

Kortüm, G. 1935. Das optiche verhalten gelöster ionen und seine bedeutung die struktur elektrolyticher losungen. Zeitschrift für Physikaliche Chemie 30:317-355.

Kortüm, G. 1944. Uber die structur konzentrierter wässriger salzlösungen. Zeitschrift Elektrochemie 50:144-149.

Kortüm, G. 1955. Kalorimetrie und Photometrie. Berlin. Springer Verlag. 312 p.

Latimer, W., K. Pitzer and C. Slansky. 1939. The free energy of hydration of gaseous ions, and the absolute potential of the normal calomel electrode. Journal of Chemical Physics 7: 108-111.

Leclaire, A. and J. Monier. 1970. Calcium structure of calcium nitrate tetrahydrate. Paris. Academie des Sciences Ser. C. 271:1557.

Luz, Z. and G. Yagil. Water ^{17}O nuclear magnetic shift in aqueous solutions of 1:1 electrolytes. Journal of Chemical Physics 70:554-561.

Mahlman, A. 1961. The OH yield in the Co ^{60} γ-radiolysis of HNO_3. Journal of Chemical Physics 35:936-939.

Mahlman, A. and G. Schweitzer. 1958. Radiation induced nitrate formation from concentrated nitrate solutions. Journal of Inorganic and Nuclear Chemistry 5:213-218.

McCabe, W. and H. Fisher. 1970. A near-infrared spectroscopic method for investigating the hydration of a solute in aqueous solution. Journal of Physical Chemistry 74:2990-2998.

McCabe, W. and W. Fisher. 1965. Measurement of excluded volume of protein molecules by differential spectroscopy in the near infrared. Nature. 207:1274-1276.

McEwen, L. Electronic structure and spectra of mitromethane and nitrogen dioxide. Journal of Chemical Physics 32:1801-1814.

McGlynn, S. and M. Kasha. Interpretation of the lowest frequency electronic absorption band of inorganic molecules of type XO as $n \rightarrow \pi^*$ transitions. Journal of Chemical Physics 24:481-482.

Malinowski, E. P. Knapp and B. Feuer. 1966. Nuclear Studies of Electrolytes Solutions. I. Journal of Chemical Physics 45: 4274-4279.

Mellor's Th. 1967. Treatise in inorganic and theoretical chemistry. New York. John Wiley and Sons. Volume 8. Supplement II. 679 p.

Meyerstein, D. and A. Treinin. 1961. Absorption spectra of NO_3^- ion in solution. Faraday Society Transactions 57:2104-2112.

Mujerkee, P. 1966. Ionic partial molal volumes and electrostriction in aqueous solution. Journal of Physical Chemistry 120: 2708.

Muller, N. 1965. Concerning structural model for water and chemical shifts data. Journal of Chemical Physics. 43:2555-2556.

Orville-Thomas, W. and W. Jones. 1960. First-order hyperconjugation in cyanamide, diazomethane and ketene. Zeitschrift für Elektrochemie 64:714-717.

Padova, J. 1964. Ion-solvent interaction. III. Partial molar volume and electrostriction: a thermodynamic approach. Journal of Chemical Physics 39:1552-1557.

Parker, J. The effects of solvation on the properties of anions in dipolar aprotic solvents. Quarterly Reviews. London 16: 163-187.

Petrakis, L. 1967. Spectral Line Shapes. Journal of Chemical Education 44:432-436.

Plmental, G. and L. McClellan. 1960. The hydrogen bond. San Francisco. Freeman and Co. 390 p.

Pople, J. 1951. Molecular association in liquids. II. A theory of the structure of water. Royal Society of London Proceeding 205:163-178.

Pople, J., W. Schneider and H. Bernstein. 1959. High resolution nuclear magnetic resonance spectroscopy, New York, McGraw-Hill Co. 501 p.

Popov, H. and R. Humphrey. 1959. A study in the absorption spectra of ion-pairs. Journal of the American Chemical Society 81:2043-2047.

Prue, J. 1966. Ionic equilibria. In: The international encyclopedia of physical chemistry and chemical physics. Oxford. Pergamon Press. 112 p.

Redlich, O. and D. Meyer. 1964. The molal volumes of electrolytes. Chemical Reviews. 64:221-227.

Reilly, C., M. McConnell and R. Meisenheimer. 1955. Nuclear magnetic resonance spectra of annular samples. Physical Review 98:263-265.

Rhodes, E. and R. Ubbenholde. 1959. Effect of thermal transformations of ionic crystals on their ultraviolet absorption. Royal Society of London Proceedings. A. 251:156-171.

Robinson, R. 1937. The osmotic and activity coefficient data of some aqueous salt solutions from vapor pressure measurements. Journal of the American Chemical Society 59:84-90.

Robinson, R. 1935. The activity coefficients of alkali nitrates, acetates and p-toluensulfonates in aqueous solution from vaport measurements. Journal of the American Chemical Society 57:1165-1168.

Robinson, R. and R. Stokes. 1955. Electrolyte solutions. London. Butterworths and Co. 559 p..

Rose, N. and R. Drago. 1959. An absolute method for the spectroscopic determination of equilibrium constants. Journal of the American Chemical Society 83:6138-6145.

Rotlevi, E. and A. Treinin. 1965. The 300 mμ band of NO_3^-. Journal of Physical Chemistry 69:2645-2648.

Russel, M. R. Drago and B. Purcell. 1965. Thermochemistry of solutions. In: Non aqueous solvent systems. ed. by C. Waddington. New York. Academic Press. 408 p.

Samoilov, O. 1957. A new approach to the study of hydration of ions in aqueous solutions. Discussions Faraday Society. 29: 141-146.

Schneider, W. Bernstein and Pople. 1958. Proton magnetic resonance chemical shift of free and associated hydride molecules. Journal of Chemical Physics 28:601-607.

Selwood, P. 1956. Magnetochemistry. New York Interscience. 496 p.

Senior, A. and W. Thomson. 1965. Assignment of the infrared and Raman bands of liquid water. 205:170.

Shinn, M. 1941. Colorimetric method for determination of nitrate. Journal of Industrial and Engineering Chemistry. Analytical Edition. 13:33-34.

Shoolery, J. and B. Alder. 1955. Nuclear magnetic in concentrated aqueous solutions. Journal of Chemical Physics 36:805-811.

Smith, P. and C. Boston. 1961. $n \rightarrow \pi^*$ electronic transition in pure alkali nitrate melts. Journal of Chemical Physics 34: 1396-1406.

Smith, M. and R. Symons. 1957. The effect of environmental changes upon the ultraviolet spectra of solvated ions. Discussions Faraday Society 24:206-215.

Spanier, R., T. Vladimiroff, and E. Malinowski. 1966. Bulk magnetic susceptibility determined by NMR spinning sidebands using coaxial cells. Journal of Chemical Physics 45:4355-4356.

Spinks, J. and R. Woods. 1964. An introduction to radiation chemistry. New York. John Wiley and Sons. 477 p.

Strickler, S. and M. Kasha. 1964. Electronic structure and absorption spectra of the nitrate ion. In: Molecular Orbitals in Chemistry, Physics and Biology. A tribute to R. S. Mulliken. New York Academic Press. 412 p.

Suhrmann, R. and F. Breyer. Untersuchung in ultraroten absorptionsspectrum über die änderung des lösungsmittels durch die gelösungsmittels durch die gelöste substanz. Zeitschrift für Physikalische Chemie 23:193-212.

Swift, T. and W. Sayre. 1965. Determination of the hydration number of cations in aqueous solutions by means of proton N.M.R. Journal of Chemical Physics 54:178-181.

Sworski, T. 1965. Kinetic evidence that excited water is precursor of intraspur H_2 in the radiolysis of water. In: Solvated Electron. p. 73, Washington, D.C., American Chemical Society Publications. 289 p.

Tamura, K. and Sasaki, T. 1963. Ionic hydration in an aqueous electrolyte solution and its parameter. Chemical Society of Japan. Bulletin 36:975-980.

Tietz, T. 1959. The variation of the diamagnetic susceptibility of water with temperature in the Thomas-Fermi model. 31:274-275.

Timmermans, J. 1955. Physico-chemical constants of pure organic compounds. New York. Elsevier. 693 p.

Vandebelt, J. Spurlock. 1955. Collaborative study on the performance of the Cary spectophotometer. Journal of the Optical Society of American 45:967-970.

Vandebelt, J. and C. Henrich. 1953. Spectral anomalies produced by the overlapping of the absorption bands. Applied spectroscopy. 7:171-176.

Verwey, E. 1942. The interaction of ion and solvent in aqueous solutions of electrolytes. Recueil des Travaux Chimiques des Pays-Bas. 61:127-141.

Vogrin, F., P. Knapp, W. Flint, A. Anthon, G. Highberger and E. Malinowski. 1971. N.M.R. studies of electrolyte solutions. IV. Journal of Chemical Physics. 54:178-181.

Vosburgh, W. and G. Cooper. 1941. The identification of complex ions in solution by spectrophotometric measurements. Journal of the American Chemical Society 63:437-442.

Walsh, A. 1953. The electronic orbitals, shapes, and spectra of polyatomic molecules. Journal of the Chemical Society. Pt. 4: 2260-2332.

Wang, J., C. Robinson and I. Edelman. 1953. Self diffusion and structure of liquid water. III. Journal of the American Chemical Society. 75:466-470.

Weiss, J. 1952. Chemical dosimetry using ferrous and ceric sulfates. Nucleonics. 10:28-31.

Wen, W. and S. Saito. 1965. Activity coefficients and molal volumes of two tetraethanol ammonium halides aqueous solutions at 25°C.

Wirth, H. 1967. Equilibria in solutions of tetraalkylammonium bromides. Journal of Physical Chemistry 71:2922-2929.

Zana, R. and E. Yaeger (1966). Ultrasonic vibration potentials and their use in the determination of ionic partial molal volumes. Journal of Physical Chemistry 71:521-536.

Zimmerman, J. and M. Foster. 1957. Standardization of N.M.R. high resolution spectra, Journal of Physical Chemistry 61:282-289.

Zundel, G. 1969. Hydration and intermolecular interactions. New York. Academic Press. 312 p.